The detection of hydrogen induced cracking in welded and seamless steel pipes using acoustic emission and ultrasonic techniques

C.A. Raine

THE DETECTION OF HYDROGEN INDUCED CRACKING IN WELDED AND SEAMLESS STEEL PIPES USING ACOUSTIC EMISSION AND ULTRASONIC TECHNIQUES

by

C A Raine, F.Inst. NDT.TEng (CEI)

A Thesis Submitted to the University of Durham in Candidature for the Degree of Master of Science

November 1986

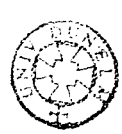

To Wyn

ABSTRACT

THE DETECTION OF HYDROGEN INDUCED CRACKING IN WELDED AND SEAMLESS STEEL PIPES USING ACOUSTIC EMISSION AND ULTRASONIC TECHNIQUES

George Alan Raine, F.Inst. NDT. T.Eng (CEI)

The detection and location of hydrogen induced cracks in steel pipes is unreliable and time consuming because of the unpredictable nature of the defect and the lack of sensitivity of conventional non destructive testing techniques.

Determination of the susceptibility of steels to the formation of hydrogen induced cracking by attack from a sour gas environment has always been based on laboratory testing of small samples where the samples are subjected to attack from all sides. This is unrealistic compared to the in-service situation and a single sided exposure test is more realistic.

In this thesis the subject literature is reviewed. Experiments on small samples show that seamless steel is the least susceptible to hydrogen induced cracking, whereas electric welded unidirectionally formed pipe is the most susceptible. The susceptibility of submerged arc welded pipe depends on the metallurgical form of the pipe but is always less susceptible than the electric welded pipe.

Ultrasonic techniques have been used to detect the location of hydrogen induced cracks but manual techniques are labour intensive and unreliable.

Four complete pipes were subjected to a sour gas environment from one side, one of which was seamless and one electric welded. These pipes were monitored using a passive non destructive testing technique, acoustic emission.

A mechanised ultrasonic scanner was used to examine the last two pipes found to be susceptible to cracking using a specially selected ultrasonic transducer.

The acoustic emission data collected was used to detect and locate areas of high acoustic activity produced by the formation of hydrogen induced cracking.

These areas were examined metallographically and shown to include several forms of hydrogen induced cracking.

The mechanised ultrasonic technique failed to detect near surface (<1 mm) cracks, but was able to resolve mid wall affected areas.

The seamless steel pipe was unaffected, whereas the electric welded pipe was severely affected by the sour gas environment.

The automatic welded pipes suffered varying degrees of attack. This supports laboratory based experiments on small samples reported previously by other workers.

ACKNOWLEDGEMENTS

The work contained in this thesis was conducted at the Engineering Research station of British Gas, Newcastle, England and the laboratories of the Independent Testing Laboratories, Searcy, Arkansas, USA and I am indebted to both these organisations for the provision of the laboratory facilities.

I would like to acknowledge the collaboration obtained from Mr D Williams of I.T.L. during my stay at the I.T.L. Laboratories during which we were able to resolve the metallurgical problems posed from the results obtained, to Mr P Kyle, I.T.L. who gave guidance during the acoustic emission analysis and to Dr L Jones who gave direction during the metallurgical literature survey. I would also like to acknowledge the guidance and encouragement provided Dr B K Tanner who suggested that I embark upon this project and had the confidence that I would succeed.

CONTENTS

CHAPTER 1

INTRODUCTION TO THE MECHANISMS OF HYDROGEN INDUCED CRACKING

Transmission pipelines are used for the carriage of gas and petroleum products at high pressures and as long as the pipeline material has sufficient resistance to corrosion and the transmitted material is correctly treated failure should not occur. During the life of the pipeline the condition of the transmitted material may change and its severity of corrosion may increase.

The main cause of this change is the hydrogen sulphide which, when its partial pressure exceeds 0.05 psia and the total pressure exceeds 65 psia, the gas or oil carrying product changes its classification from sweet to sour. The effect of the hydrogen sulphide is increased by the presence of water and salt, and it has been noted that water must be present before cracking can occur[1,2].

Gas supplied from offshore wells normally is salt bearing and due to condensation of the moisture from the gas also carries water, satisfying the necessary conditions. The condensation of the hydrogen sulphide and the water produces hydrosulphuric acid, resulting in cracking.

Hydrogen induced cracking is not a predictable type of defect in that it is not always located at one particular position in the pipeline i.e. at the weld line, or the six o'clock position and it can occur

anywhere along the length or the circumference of the pipeline. However, recent tests have suggested that in very high yield steels preferential attack will occur near the seam weld heat affected zone.

Although the phenomenon is classed as hydrogen induced cracking it is also described in the following terms:-

Hydrogen induced cracking (HIC)

Hydrogen induced blister cracking (HIBC)

Blistering

Blister crack array

Hydrogen pressure cracking (HPC).

It has the following features:-

1) The cracks are parallel to the surface.
2) The parallel cracks are often linked together in the form of steps.
3) It tends to occur at the sites of inclusion clusters such as elongated sulphide or aluminates, and in areas of 'hard' metallurgical structures such as martensite or bainite.
4) It can occur in the absence of stress and under compressive stress.
5) It has been suggested that it generally affects steels with a yield strength less than 5.50 MPa.
6) It was also suggested that hydrogen induced cracking resulted in delamination, porosity and leakage rather than catastrophic

failure. The results of recent tests on X70 pipeline steel have been catastrophic failure.

The reason for the interest in this mode of failure is that at present 2300 miles of under sea pipe have been in service since 1967 using steel grades X52-X65, although since 1975 all of the steels have been X60-X65 and represent 90% of the total length of pipe in service. Since 1951 failures of pipelines have occurred[3,4], but the failure of a submarine pipeline in 1972[5,6] increased attention to this form of failure. Although fourteen examples of failures have been reported[3,4,5,6,7], it is interesting to note that seven of the failures occured in unidirectionaly rolled non-heat-treated steels i.e. electric and spirally welded pipe.

These failures occurred in steels which had both high and low strength values having various metallographic structures varying from ferrite/pearlite to heat treated controlled rolled structures. Examination of the failures showed elongated planar cracks parallel to the surface associated with lenticular manganese sulphides, oxide clusters and areas of lamination. In some cases these planar cracks were connected by stepwise cracks linking the various layers and propagating through the pipe wall, leading eventually to failure. An example of stepwise cracking is shown in Figure 1. HIC failures and damage have only been recorded in welded pipeline steels of the submerged arc, electric resistance and spiral welded type, but have never been recorded in seamless pipe[8], this may be due to the production process of the seamless pipe being a forging hotwork

process and producing a preferential form of non-metallic inclusion and metallurgical structure.

At the present time the common test applied to pipeline steels for the evaluation of resistance to sour gas has been single-sided immersion tests, followed in some cases by a simple form of ultrasonic scan. The initial tests were based on the BP/Cotton tests([9]), but because of the number of variations which have been produced having various specimen configurations and environmental conditions, it was thought that there was a need for a standard test. A NACE([10]) task group was formed to produce a standard test([11]) which could be applied to all steel types which could possibly operate in a sour environment.

This and other tests are laboratory based tests and only cover a very small area which is the same philosophy that is used for mechanical testing. In the case of mechanical testing the samples are always selected from standard locations in the pipe, plate, casting forging or component that is to be tested so that results can be related back to a standard. However, as has already been stated earlier, HIC is not a predictable defect and thus these laboratory tests only give an indication of the susceptibility of the steel. What is required is a macro test and an evaluation technique which can be applied during this test which can detect the initiation of the HIC, the location and the rate of growth with time in terms of both area and through wall propagation.

A mechanised ultrasonic scanner having the correct scanning pattern, probe type, level of sensitivity and resolution and the ability to store and analyse the data will give the rate of growth with time but only if it is located in an area which is known to have HIC or which is known to be susceptible to HIC. Not all ultrasonic systems are suitable for this purpose and have to be carefully selected and evaluated in terms of the above, i.e. resolution and sensitivity and also if to be used repeatedly on the same sample, reproducibility.

In order to detect the initiation of HIC, a more global macro technique would have to be used, such as acoustic emission, which would detect the acoustic emissions transmitted through the steel from crack tip opening during the formation of HIC. Acoustic emission could also be used to locate the area of emissions and measure the rate of increase in acoustic activity during a test.

This combination of a mechanised ultrasonic scanning system and an acoustic emission system used during a sour gas test on full size pipe would produce more information than a single-sided smallscale laboratory test.

Mechanism of Hydrogen Induced Cracking

In any gas or oil pipeline operating in a sour environment the hydrogen sulphide reacts with any water present and hydrolyses, forming a weak hydrosulphuric acid:

$$H_2S \rightleftharpoons HS^- + H^+$$

$$H_2S \rightleftharpoons 2H^+ + S^{2-}$$

Reactions then take place between these ions and the steel to form corrosion and ferric ions at the anode sites

$$Fe \rightarrow Fe^{2+} + 2e$$

These electrons combine with the hydrogen ions to form atomic hydrogen which migrates into the steel:

$$2H^+ + 2e \rightarrow 2H$$

$$Fe^{2+} + S^{2-} \rightarrow FeS$$

$$2H \rightleftharpoons H_2$$

The atomic hydrogen then precipitates at voids to form molecular hydrogen in the steel, resulting in high pressure at these sites([12]). It is these sites which cause propagation of the HIC in the steel matrix. These sites may take many forms but are mainly associated with inclusions, shrinkage voids and laminations produced during the production process and surrounded by voids. Keisling([13]) describes the preferential inclusion type resulting in void formation. Although all inclusions and discontinuities are possible sites for the initiation of HIC, the more angular and sharp edged are preferable, i.e. the elongated Type II manganese sulphides and aluminates compared with the lenticular globular sulphides or rare earth treated steel types. This may give one of the reasons for the non susceptibility of

seamless pipe. Carbide cementite-matrix metallographic structures provide more resistance than banded or controlled rolled structures.

As stated earlier, hydrogen induced cracking may take two forms. The most common method of propagation is in a linear manner, while the other is a more dramatic stepwise cracking propagation through the pipewall. Central segregation normally found in the plates produced from the top portion of ingots or found in the majority of continuously cast steels produces bands of non-metallic and elongated bands of untempered martensite and bainite which are ideal sites for HIC propagation and thus can form extensive lamellar cracking. Stepwise cracking is a separate phenomenon and finite element analysis has been applied to determine the stresses and strain produced around the sites during the development of these stepwise cracks([14]). The results of the analysis produced the following deductions about the mechanism of hydrogen induced cracking:

1. The formation of molecular hydrogen produces pressure and results in the separation between the inclusions and the metallurgical structure accompanied by plastic deformation of the crack tip.

2. These plastic regions become embrittled by the hydrogen.

3. The cracks propagate through this embrittled region in a direction normal to the tensile stress (i.e. normal to the planar HIC).

Three examples of the creation of stepwise cracks are shown in Figure 2.

Present Test Procedures

The present test procedures are based on small laboratory samples typically 20 mm x 100 mm x Δt (plate thickness) and these are immersed in de-aerated hydrogen sulphide saturated synthetic sea water for 96 hours. The samples are then sectioned at the quarter, half and three-quarter position along the axis of the sample and any cracks present are measured on three metallographically prepared surfaces. This is the basis of the BP/Cotton test. After metallographic examination the susceptibility of the steel is presented in terms of ratios of total lengths and widths of HIC and the length and width of the sample.

Three crack indices are determined:

a) Crack length ratio (CLR), representing the total crack length in the rolling plane.

b) Crack thickness ratio (CTR), representing the amount of cracking in the through thickness direction of the plate or pipe.

c) Crack sensitivity ratio (CSR), derived from the product of (CLR) and (CTR) and representing the crack area.

These three crack indices are represented in Figure 3. Various modifications have been made to this test, in some cases side coating of the samples has occurred and the use of more severe testing conditions have been applied as improved steels having greater resistance to HIC have been developed. Twenty-seven varieties of the BP/NACE test have been produced by various oil and gas companies, all having different acceptance criteria, and because of this NACE have produced a standard test([15]), which can be used for comparison purposes only, as acceptance or rejection criteria are not included.

In all cases the results of a company's test can only be compared with their own results on other steels, as any variation in the test piece preparation, the conditions of the test, and the form of evaluation can completely alter the final result obtained.

NACE Test

The NACE test requires samples to be removed from the pipe with the longitudinal axis of the specimen parallel to the longitudinal axis of the pipe. If welded pipe is used, the specimen should also be parallel to the weld. Weld area samples are removed perpendicular to the weld. The specimens are 100 mm long by 20 mm wide and must be from the full thickness of the pipe. For each pipe, three specimens are removed. If the pipe is welded, one is from across the weld and the remaining two at 90° and 180° away from the weld. If the pipe is seamless the three samples are taken 120° apart around the circumference. The specimens are then immersed in the NACE solution

of synthetic seawater saturated with hydrogen sulphide at a pH in the range of 4.8 - 5.4 for 96 hours. At the completion of the test the samples are sectioned and examined transversely microscopically and their CSR, CLR and CTR ratios determined.

Other Test Methods

No matter which test is used, the HIC severity still has to be assessed and the method normally applied is metallographic. The first main problem, is that the HIC occurs randomly, so that in some cases the sections may have more or less severe defect areas in relation to the remainder of the sample. The other problem is that, depending on the crack separation criteria used, different values of crack sensitivity ratio (CSR) are obtained, Figure 4([16]).

Ultrasonic techniques have also been used as an aid to metallography in order to determine both those areas affected by HIC and to ensure that sections are selected from the worst areas. The technique has also been used in its own right as a replacement for metallography and results have been compared with both CLR and CSR. The results are shown respectively in Figures 5 and 6([17]) and although the relationship between CLR and areas defined by ultrasonics is quite good, the results for CSR show a large amount of scatter and suggest a critical value of CSR has to be achieved before any ultrasonic data is obtained.

An example of the results obtained using attenuation techniques([18]) is shown in Figure 7 where a C-scan presentation is produced with time.

One further problem that affects the result of the smallscale test is the orientation of the sample itself. Work carried out by Kowaka et al([19]) has shown that crack susceptibility in samples sectioned parallel to and examined in the rolling direction, is greater than those taken transverse to the rolling direction. The location of the samples is shown in Figure 8 and it would appear that the orientation of the samples, together with that of the rolling direction and the preferred orientation of the non-metallic inclusions, plays an important role in the final result obtained.

There have been many comments made on the attributes and value of the smallscale test, but the general comment is that whereas it would appear that the single-sided test is more representative of service conditions, the results obtained suggest that the uncoated specimen overestimates the HIC susceptibility of the steel whereas the coated specimen underestimates HIC susceptibility([20]). Results showed that crack lengths obtained during standard HIC tests were double those obtained during single-sided fullscale tests([21]).

The point has also been made([22]) that the hydrogen content of the mid wall in a real situation will only be half that of the affected surface because of differences at the outer wall, whereas in a fully immersed test a state of hydrogen equilibrium will be produced throughout the specimen. Figure 9 illustrates this effect and shows

that a single-sided tested specimen is as close as possible to actual pipe conditions.

The Effect of Metallurgical Variations on HIC Susceptibility

Metallurgical variations such as steel production route, forming and heat treatment all have some effect on the HIC susceptibility properties of steel.

Production Route:-

The two main production routes of ingot and continuously cast steel both affect the production of HIC in relation to the most susceptible areas in the final rolled product. The shape, in terms of length and width of the initial ingot, determines the freezing rate and thus dendrite formation. It also determines the final metallurgical structure and preferential segregation pattern. These are important factors in that they affect the location of and number of the non-metallics in the ingot. These create sites for HIC formation and the creation of hardened microstructures such as martensite or bainite leads to areas where crack propagation and growth may occur. The top centre core of fully killed ingot steels have always been known for their high degree of segregation whereas the bottom core of negative segregation is completely opposite. Similarly, the rim of the ingot near the skin is known to be relatively free of adverse inclusions and hard crack forming metallographic structures. Thus, sampling plays an important part when identifying the most

susceptible areas([7]) and Figure 10 illustrates the location of these areas([23]). Figures 11 and 12 also demonstrate the points made above relating to ingot bottom and edge location. These findings were also confirmed by other workers([24]) who also selected their samples from these susceptible areas. It has been suggested that only submerged arc welded (SAW) pipe produced from the bottom of the ingot will be HIC free([8]) and that pipe areas opposite the weld from the top third of the ingot will be the most susceptible to HIC. The effect reduces as the pipe body approaches the weld. (This will only apply to pipe produced from plate rolled length for length or for pipe produced from coiled strip rolled directly from the slab stage i.e. electric welded or spirally welded pipe.) If, on the other hand, the plate had been cross rolled from slab, then the most susceptible areas would reach from opposite the weld up to the weld area but would not extend along the total length of the pipe. The effect will decrease towards the ends. Because of this variability it has been suggested that samples are taken at 120° to each other from the end of the pipe to attempt to resolve this problem especially if the rolling direction is not known([25]).

Continuous casting practice tends to produce a line of central segregation concentrating sulphides and other non-metallic inclusions in a band. The width of this can vary depending on the speed of casting, cooling rate affecting the solidification pattern and the tundish deoxidation additions. If these conditions are incorrect then hard metallographic structures may also form caused by high proportions of alloying additives. If ideal conditions occur then

this would produce a very acceptable product and is to be recommended[26,27]. On the other hand there may be a predominance of linear cracking compared to stepwise cracking. Small ingots have been used in the forging and tyrecord industry for many years to produce high quality steel free from harmful segregation patterns[28,29] and seamless tube tends to be produced from small ingots which may be one of the reasons why they tend to have a low susceptibility to HIC[12,14,30]. Samples of linepipe examined have shown greater susceptibility to HIC in the centre of a 2-4 m plate than in the quarter width location[31]. Whereas other workers have confirmed this, they found that the location varied from the ingot top to the ingot bottom when calcium additions were made to the steel[32]. The effect of calcium additives is to modify the inclusions and reduce harmful segregation patterns. The stage following that of casting is deoxidation and this can take place in the ladle or in the ingot/concast stage by deoxidant injections. Fully killed steels are those deoxidised using silicon or aluminium, whereas semi-killed are those classed as ladle balanced where the deoxidation practice is performed in the ladle. There appears to be a higher sensitivity to HIC in fully killed steels than semi killed steels. The result of fourteen samples of both steels subjected to BP solution confirmed this[7] and a good correlation was obtained with aluminium content, thus giving an indication of the level of deoxidation.

The predominant inclusions in fully killed steels are aluminate and Type II manganese sulphides which tend to be formed because the sulphides are the last to solidify and are caught between the grain

boundaries and dendrites. They form thin films which elongate during rolling and result in thin sharpended inclusions. The inclusions in the semi killed steels are primarily silicates, globular Type I sulphides and formable duplex sulphide silicates.

The degree of susceptibility to HIC of fully killed steels as compared to semi killed steels is shown in Figure 13([23]) and Figure 14([17]). Note that rimming steel which is a soft and ductile clean steel, free from deoxidants has a low susceptibility even though produced from a undirectional rolling production route.

The production route and the deoxidation practice chosen are the overriding factors in the type of non-metallic inclusions produced in the final product, whether it be welded pipe seamless tube or plate to be used in further fabrication.

Many pipes which have failed because of hydrogen induced cracking have been subject to both optical and scanning electron microscopy investigations ([7,12,21,29-36]).

The common findings of all of these examinations were as follows:

1. Type II elongated sulphides were predominant in all of the failed tubulars. This suggests that steels having these present have a greater susceptibility to HIC then those steels containing the lenticular Type I sulphides.

2. Steel having elongated thin oxides and sulphides present sites for crack propagation which then follow lines of stress to join up the independant inclusions.

3. Inclusions containing alumin ᵅ calcium and silicon (i.e. the constituents of fully killed steels), promote the formation of HIC.

4. Voids or cracks produced around non deforming non-metallics([13]) act as sites for molecular hydrogen.

5. Examination of fracture surfaces showed a predominance of elongated manganese sulphides, glassy silicates and aluminates.

6. Subsurface alumin ᵅ clouds were located in pipe produced from continuously cast steel([37]).

The above suggests that if very low sulphide content steels could be produced HIC could be eliminated. As this is not always possible, the elimination and reduction of elongated sulphide inclusions would improve the steel susceptibility to HIC. This can be achieved by modifying the shape of the sulphides by the addition of rare earth metals such as cerium, Figure 15([38]). Although the reduction and the modification of the sulphides decreases the susceptibility it will only be limited if aluminate and glassy silicate inclusions are still present. Thus an effort is required to reduce these levels also.

One problem does arise if HIC prevention is being attempted by examining the pipe, tube or plate before use. Whereas alumina clusters or large areas of non-metallics can be detected using ultrasonic techniques, sulphides are completely homogeneous with the steel and are invisible to ultrasound([39]). Many techniques have been used to determine inclusion content using ultrasound based on an attenuation measurement or noise level techniques but none have been conclusive. ASTM performed a number of 'round robin' tests on high quality ball bearing steels([40]) and BSC([41],[42]) repeated a number of tests on tyre cord steel but were not able to define levels of attenuation that could be correlated with results obtained from sulphur printing or metallographic inclusion assessments.

Before leaving the subject of steel production routes and the susceptibility to HIC, the final stage of the rolling or forming process must be discussed. The mechanical properties required for a plate may be produced by rolling the plate to the required dimensions and then subjecting the plate to a heat treatment process such as normalising or quenching and tempering. An alternative method is to roll the plate to some fixed reduction ratio and then hold the partially reduced plate until the temperature is reduced sufficiently such that the plate can be finally rolled at a temperature between 700-950°C. This is known as controlled rolling and produces a 'stiffer' plate than that produced by conventional rolling practices. The controlling factors are the reduction ratio and the hold temperatures used.

If the plate is subjected to a normal rolling practice then steel will be deformed at high temperatures i.e. 1000°C and the steel will flow around the 'hard' non-metallics i.e. aluminates or glassy silicates. This will not produce any voids to act as nucleation sites. Under controlled rolling conditions the steel is finish rolled at much lower temperatures which does not allow the steel to flow around the non-metallics. Two routes can then be followed. Either the brittle non-metallics fracture, leaving voids or voids are produced at either end of the non-metallics producing sites for molecular hydrogen to propagate.

Controlled rolling also tends to produce elongated Type II manganese sulphides([7]) which increase the sensitivity to HIC([30]). Thus normalised and quenched and tempered steels should have a better resistance to HIC([21]).

The above argument may contain the reasons why more failures of pipes occur in welded pipe than seamless as controlled rolled plate is being increasingly used for the production of pipe, whereas seamless pipe production is a forging process. Forging the pipe from blooms at high temperatures (1300°C) with resultant high finishing temperatures of about 1000°C allows the steel to deform much more easily.

Investigations carried out on hot strip showed it to have even higher susceptibility to HIC than controlled rolled plate and a greater tendancy to stepwise cracking([30]). The reason for this could not be explained but it is thought that it could be caused because of the

unidirectional rolling route and the higher reduction ratio used when rolling the slab to thin strip which could be in the order of 20:1 inducing stresses on any non-metallic present and the adjacent material. This could also be the reason for the number of HIC failures occuring in electric welded and spirally welded pipes.

The structure produced by these routes will be metallographically different. The normalised pipe and seamless type have a more uniform structure producing greater resistance to HIC, whereas the controlled rolled and coiled strip may have a predominantly orientated grain structure prevalent to crack propagation.

CHAPTER 2

NON-DESTRUCTIVE TESTING TECHNIQUES FOR THE LOCATION AND DETECTION OF HYDROGEN INDUCED CRACKING

The preceeding sections have described the hydrogen induced cracking problem and have shown that, because of factors such as the production route, the deoxidation practice carried out on the steel and the rolling direction of the semi-finished product, HIC will appear to occur randomly. Thus selection of samples and performance of laboratory tests may not predict the susceptibility of the material or indicate the rate of growth of hydrogen induced cracks. When a pipe or pressure vessel is placed in service the problem is even more accentuated and techniques such as repeated checking of one particular area using ultrasonics is a regularly used technique. It has been suggested that there is no other cost effective method([43]). The previous sections describing the laboratory tests have indicated that ultrasonic techniques have been used and are able to detect HIC. This is acceptable if the area that is affected is known, and from then on a piece of plant from that area can be monitored using a mechanical scanning device. There has been some development of these scanning devices but the results obtained are variable and in some cases do not produce the data in an easily usable fashion. Part of this thesis will describe the evaluation of such ultrasonic mechanised scanners and report the results of investigations using such a scanner. Remote global monitoring, if it could be used, would be able to detect areas

of initiation of HIC and locate the position that ultrasonic techniques could be applied. One such technique is acoustic emission.

ACOUSTIC EMISSION

Acoustic emmision is a passive non destructive testing technique. Whereas the majority of techniques interrogate the defect, acoustic emission relies on the defect producing a signal which can be detected. This suggests that AE will only detect growing defects such as propagating cracks, but this is not so. Defects producing such emissions are known as primary sources, but secondary sources can also be produced and detected. These secondary sources can be caused by adjacent fracture faces rubbing together or crushing corrosion products. It is usually quite easy to differentiate between a primary and secondary source as the former has a high amplitude and fast rise time and short duration, whereas a secondary source has low amplitude, slow rise time and long duration. Acoustic emission is known by many terms such as:

stress wave emission
micro seismic activity
emission
elastic waves

and is described as the phenomenon when a rapid release of energy from an isolated source generates a transient elastic wave within a material([44]). This rapid release of energy can be produced by crack growth or plastic deformation in the material. The wave generated will then travel through the material, the distance will depend on the attenuation of the wave by the material, until it is detected by a transducer coupled to the material Figure 16. This transducer will be a piezo electric transducer of a known frequency which will respond to the wave producing a weak electrical signal. Although the technique has been known for a long time AE was not used in NDT until the 1950's and 1960's([45]) but since then it has been used to monitor spot welding([46],[47]), leak detection([48-51]), loose part detection([52-54]), bearing inspection([55-58]) tool wear([59-61]), ceramic testing([62-64]), fibre reinforced plastic vessels([65-67]), composite structures([68],[69]), pressure vessels([70-73]), pipelines([74]) and offshore structures([75-88]).

Standards have been written so that acoustic emission can be applied reliably in the majority of the above applications([89-91]). This was done because initial claims that the technique could detect locate, identify and determine the increase of the rate of growth of flaws were in some cases unfounded. It is now accepted that the technique can detect flaws but cannot identify them.

AE is able to detect microscopic and submicroscopic changes and because of this can be used to monitor changes other than flaw detection, that may be occurring within the material. Such changes as creep, strain hardening and phase transformation may be studied in this manner.

The greatest advantage that AE has is that it is able to locate structural discontinuities or flaws without using some scanning or grid pattern examination of the structure. The other main non-destructive testing techniques such as radiography, ultrasonics, magnetic particle inspection and eddy currents will only give information about a structure at one particular site and that information will be limited to the technique used. Radiography will only provide information on embedded defects, while magnetic particle inspection and eddy currents are limited to surface breaking flaws. Depending on the procedure used, ultrasonics can give localised information on either embedded or surface breaking flaws. When applied correctly, AE can provide information on embedded or surface breaking flaws, although there is a limitation that if the flaw is embedded in very thick material, problems on acoustic location may occur. Nevertheless, the technique has been used on pressure vessels having wall thickness of 100 mm([92]). AE can provide complete information in real time on the flaw location and initiation over the entire volume of the structure. When an acoustic emission pulse is produced, the signal is amplified and the waveform captured for analysis Figure 17. The waveform shown in the figure is known as an event, the total time that the event exists is called the duration.

The time taken from the first cycle cutting a predetermined threshold to maximum amplitude of the signals is called the rise time. The number of cycles cutting the threshold level are classed as ringdown counts. Thus each event can be analysed in terms of rise time amplitude, duration and counts, and discrimination can be made between primary and secondary emissions from this data. The value of the threshold level is important in eliminating noise originating from bubbling or the passing of gas or liquid through a pipeline.

A computerised system is usually required to analyse the large amount of data produced during monitoring and this is used to produce activity histograms from each transducer, listing plots of events, amplitude distribution and location plots. Large numbers of transducers can be used together; up to 144 have been used on the monitoring of the domes on blast furnaces stoves([93]). To use these transducers, geometric configurations have to be used, and these may be cylindrical or multiple arrays.

The cylindrical array comprises four sensors arranged as in Figure 18 with a circumferential spacing of 90°. This form of array deals well with a cylindrical form and combines versatility with transducer economy. It can detect and locate a defect within a cylindrical array but can also locate sources within and outside the boundaries of the array. There is a limitation to the distance between the sensors because of signal loss due to atenuation, and the longitudinal spacing

is twice the circumference of the cylinder, whereas in the y direction sources can be located upto 3.25 times the circumference.

The multitriplet set is shown in Figure 19 and is made up of interlocking triangular arrays.

An algorithm is used to locate an event with the array using the Δt values (the differences in arrival times from the source) from the three sensors in the array. If more than one array is hit, the one with the smallest range of Δt is used, thus producing a greater location accuracy. The maximum error introduced on location is about 5% of the longest side. The triangular array arrangement may produce locations which are outside of the arrays because of ambiguous Δt values, the multi triplet array algorithm will always return the location of the source within the triangle.

Once a source of activity has been located, it can be monitored and a record of maximum amplitude, duration rise time and counts can be made. Analysis of this data gives an indication of the activity of the source. A record of events against time is shown in Figure 20 and an example of a location plot is shown in Figure 21.

It is only recently that large computerised systems have been available and the majority of investigations were carried out using simple AE systems with up to three transducers. Early work on the detection of stress corrosion cracking([102]) clearly detected increased activity in terms of cumulative counts until the pipe failed and an

increase in the number of events when leakage was detected Figures 22 and 23.

Although AE has been used to detect leaks in pipelines both within nuclear installations on the secondary and primary cooling loop[94,95] a large 9 Km pipeline[96] and to detect flaws in pressure vessels during hydro or pressure testing[97,98] until recently it had never been successfully used to detect hydrogen induced cracking in pipelines or pressure vessels. Initial trials were performed by a major oil company on a pressurised pipe but were not successful.

The mechanism of HIC described earlier involves atomic hydrogen migrating to voids around non-metallics caused by lack of formation of the non metallic and already stressed. This produces molecular hydrogen and introduces even greater pressure, eventually leading to crack propagation through the steel. Such a process is ideal for detection by acoustic emission, which relies on crack extension emitting waves of mechanical energy due to the release of elastic energy stored at the crack tip. This mechanical energy is transformed to electrical energy at the site of an acoustic emission transducer.

Chapter 4 will describe an acoustic emission technique that will detect the initiation and location of HIC.
Acoustic emission technology can be applied in a number of ways during the investigation of HIC.

a) Detection of micro cracking and macrocracking.

b) Separation of diffusion controlled crack advancement from incremental stable crack advancement in burst activity.

c) Definition of primary and secondary incubation times for cracking processes.

d) Time resolved records of crack advancement activity.

e) Definition of the optimum time to stop and test prior to failure.

f) Determination of performance of on-line real time monitoring of full scale structures to establish level of HIC activity and determination of areas where damage is occurring.

It is hoped to illustrate some of these applications through the investigations carried out.

Ultrasonic Testing

Whereas acoustic emission has been described as a passive inspection technique, ultrasonics is the complete opposite and relies on the interrogation of a material and the interpretation of the response to determine the integrity of that material. The ultrasonic technique uses the piezo electric effect, to convert high frequency voltage

pulses into ultrasonic waves which then propagate into the material under test until they are reflected, converted or diminish in intensity with distance. In the case of normal probes and transducers these waves are normal to the crystal surface([99],[100]). The ultrasound then travels through the material and is reflected from the opposite face to that of the transmitting face and returns to the transducer where it is converted back to an electrical signal. The time between the transmission pulse and the received pulse can be measured and is called the transit time. This method, using both intensity and transit time, is called pulse transit time or pulse echo and is one of the oldest ultrasonic techniques in use. It had been used since the first world war([101]) for locating objects under water such as submarines or icebergs, but it was not until 1940([102]) that its application to non-destructive testing was recognised as a technique for the location of flaws.

The pulse echo technique can be applied in many ways, but the two most common are those using longitudinal and transverse waves. Hydrogen induced cracking is a lamellar defect located parallel to the pipe surfaces although these lameller cracks can combine to form step wise cracks. For the detection of the most common form of hydrogen cracking a normal pulse echo technique is suitable but it may also be possible to detect the step wise cracking using a shear wave technique.

The pulse echo technique can be applied to any object having parallel faces. That is why it is applied especially in the steel industry for

the inspection of semi finished products such as steel blooms, billet, plates and forgings([103]). Depending on the thickness of the material and its metallurgical condition([104]), probes of varying diameter and frequency can be used. The probe or transducer selected depends on two main parameters, the wave length of the sound produced and the near zone of the probe. The wave length gives some guidance to the resolution of the transducer, i.e. the limiting detectable defect size and a rule of thumb guidance is that the resolution of a transducer is equal to half the wavelength value. So from the formula

$$C = f\lambda$$

C = velocity of sound

f = frequency

For C ≃ 6000 m/s for longitudinal waves and a 4 MHz transducer

$$\lambda = \frac{c}{f} = \frac{6{,}000}{4} = 1.5 \text{ mm}$$

Theoretically that transducer should be able to detect a defect 0.75 mm diameter.

The beam which emerges from a transducer into a medium of infinite length can be separated into two zones, one of which the near zone has a length N. The length of the near zone depends on the diameter of the transmitter, the wavelength of the ultrasonic radation, the frequency and the speed of the ultrasonic energy in the medium.

$$N = \frac{0.25\ D^2\ f}{V}$$

$$N = \frac{0.25\ D^2}{\lambda} = \frac{D^2}{4\lambda}$$

When N = near zone λ wavelength

D = diameter of the transducer e.g. 24 mm

Therefore, $N = \frac{D^2}{4\lambda}$

$$= \frac{24 \times 24}{4 \times 1.5}$$

$$N = \underline{96 \text{ mm}}$$

In this area of the sound beam it is difficult to perform defect sizing. Krautkramer([104]) has produced a relationship between distance in terms of near zones, amplitude of defect echo and ratio of defect to transducer diameter which is used to determine the size of defects located. This AVG diagram also known as DGS (Distance, Gain, Size) is used to size defects in plate, castings and forgings although the relationship only becomes linear after a distance of one zone is reached.

The other main parameter is the dead zone of the transducer which is related to the ringing time of the crystal selected. Depending on the damping used in the construction of the transducer the crystal could ring continuously. The use of a damping medium such as calcium tungstate not only directs the sound into the material to be tested but also damps the crystal and reduces the ringing time, consequently reducing the size of the dead zone. This dead zone can be up to 12 mm in length in which no defects can be detected. One solution to this problem is the use of twin crystal transducers, one crystal acting as a transmitter and the other as a receiver. If these transducers can be set back from the probe housing face, the dead zone is reduced and also the defect search area will be outside the near zone of the transducers. This technique is used to detect small defects in thin section plates.

Figures 25 and 26 show examples of the separate A-scan ultrasonic traces produced by a single crystal transducer and a twin crystal transducer using a stand-off.

A transducer had to be selected to detect hydrogen induced cracks that had high sensitivity and good near surface resolution. Transducer suppliers produce DGS diagrams for specific transducers and several were examined([105]) but none met the requirements thought to be necessary, namely that of being able to detect a 1 mm diameter hole 3 mm from the outside surface of the pipe. Thus sensitivity curves had to be produced of the type described by Raine([106]) to determine the most suitable probe type Figures 27-29 . Twin crystal probes

have been used to detect laminations in plates 7 mm thickness([107]) with success, using small diameter focussed probes and it was thought that this would be the correct transducer to be used to detect hydrogen induced cracking. Earlier references have stated that the use of attenuation techniques would give an indication of the presence of hydrogen induced cracks, but it has already been stated that these should be associated with non-metallic inclusions. Investigations have been carried out in the past with little success([108]) and it was suggested then that the volume or area of inclusions present was more important than the number and that a minimum value had to be present before a relationship began to exist ([17]). Attenuation techniques were suggested as a method for the selection of steels for sour gas in order to determine their freedom from sulphide inclusions but investigations carried out by BSC([41]) revealed that even extreme sulphide segregation in steel did not produce definitive indications so that this technique could not be used prior to service. Thus, it was suggested that pulse echo ultrasonic techniques using a twin crystal high frequency small diameter probe should be used for the detection of hydrogen induced cracking.

Because hydrogen induced cracking occurs around the whole circumference and along the length of the pipes, it would be very labour intensive manually to scan ultrasonically the whole surface area of the pipe. Trials carried out in the past have shown that it takes two man-days to examine 1 metre of 500 mm diameter pipe affected with hydrogen induced cracking. There is thus a need for a mechanised

ultrasonic scanner to be used to scan the circumference of the pipe in such a manner as to cover effectively the whole area of the pipe surface. During this scanning, a large volume of data will be collected and this will require storage in such a manner that it can be retrieved for viewing and analysis. The majority of mechanised ultrasonic scanners have been developed for the examination of welds, with one exception, a unit developed by Det Norske Veritas([109]) from a system produced by the Danish Welding Institute (SVC)([110],[111]). Other mechanised scanners have been produced by Ultra Image([112]) and RTD([113]), Voest Alpine([114]) South West Institute([115]) and others([116]) for the inspection of welds. Ultra Image, RTD and SVC have also developed instruments to scan pipework and perform corrosion mapping. It was concluded that corrosion mapping was not too dissimilar to the detection of wall thinning caused by the presence of lamellar defects such as hydrogen induced cracking and it was decided that this route should be investigated in order to define a mechanised scanner which would have the following attributes.

(a) The scanner should have a variable scanning pattern in the longitudinal and transverse direction in terms of incrementation of the scanner and variable scanning speed.

(b) It should have good reproducibilty and be able to return to the same detection point repeatedly.

(c) It should have the capability of storing all of the data in its base form, suitable for further analysis in order to use a variable sensitivity threshold.

(d) It should be able to produce in real time, an image of the data being collected by the ultrasonic transducer and give an indication of the rate of growth of the defect in terms of increased area and through wall penetration.

(e) The transducer used should have the sensitivity and resolution which would enable it to detect lamellar hydrogen induced cracking before it penetrates further than half the through wall thickness.

In Chapter 3 a number of mechanised ultrasonic scanners are evaluated and one selected for use on the pipes selected for sour gas evaluation. Its effectiveness in meeting the above criteria is examined.

CHAPTER 3

EVALUATION OF MECHANISED SCANNING SYSTEMS TO DETECT LOCATE AND CHARACTERISE HYDROGEN INDUCED CRACKING

The hydrogen induced cracks are usually laminar and are interlinked by stepwise cracking. Whereas stepwise cracks are difficult to detect, they can be located using shear wave 45° angle probes, but the examination is very laborious and requires skillful ultrasonic operators, the detection being made more difficult because of interference by the laminar cracking. The laminar hydrogen induced cracks can be detected more easily using compression probes which can be scanned over the surface quite quickly, but because of the large areas involved in pipe inspection, and the time required to delineate the defects, the task is still time consuming. The practical requirement is for a mechanised ultrasonic scanner which can scan the total circumference of the pipe with the required scanning resolution to detect hydrogen induced cracks and using a selected transducer with the required sensitivity, can detect the defect. It should have sufficient near surface resolution to locate defects near to the outer surface of the pipe.

The object of this section of the study was to examine a limited number of ultrasonic units which combined the use of mechanised scanners and a circumferential tracking system which enabled an area

of the pipe surface to be scanned, the hydrogen induced cracking to be detected and located and to produce an image of the data collected.

MECHANISED SCANNING SYSTEMS

There are few non dedicated mechanised ultrasonic systems, the majority being produced for a specific purpose to a strict specification, designated by the end user. There are available a limited number of mechanised systems developed to detect the onset of corrosion in pipework. It was decided to examine these systems to see if they met the criteria specified in Chapter 2.

The systems quoted were those produced by Ultra Image, RTD, SVC and the DNV adapted SVC unit. The difference between these latter two is that the DNV system was specifically adapted for use underwater for the examination of risers and pipelines, and used a specially adapted mechanised scanner that had a pivoting scanning arm and a magnetised probe holder to cope with undulating pipe surfaces. Another feature of this system was that it utilised a non contacting focussed probe fixed 10 mm away from the surface of the pipe; the basic SVC system using a contact probe and a scanner to be used for above water use only.

Although Chapter 2 specified the minimum requirements of a mechanised ultrasonic scanner, because the equipment would be needed to operate on a large diameter pipeline a more restricted specification was required. This is given in Table I. The above scanners were

investigated using this specification to compare their relative properties.

ULTRA IMAGE

The Ultra Image mechanised ultrasonic scanning unit was designed as a modular system, based on four modules consisting of:

a) A manual scanner which is attached to a band which encircles the pipe diameter, Figure 30.

b) A data acquisition unit which recorded the data collected from the scanner transducer with locations identified by the scanner's optical encoders. The data can be stored in memory and can then be transferred to floppy disc for permanent storage. The data can be manipulated, processed and analysed with this unit.

c) A digital pulser probe receiver unit converts the analogue data to digital for rapid acoustic data recording.

d) A data presentation and video module displays the analogue A-scan of the pulses received as described in Figure 25 and is also used to display the resultant C-scan of the pipe area scanned. A typical C-scan of three flat-bottomed holes, 1 mm, 2 mm and 3 mm diameter is shown in Figure 31. This being a plan view of the flat bottomed holes viewed from the top of the sample

A Schematic of the unit is shown in Figure 32.

RTD PRIMSCAN

The RTD Primscan is based on their girth weld inspection system, the Bandscan, consisting of four modules:

a) A fully automated ultrasonic probe scanner able to scan in both X and Y direction around the pipe, producing positional feedback using optical shaft encoders and having a scanning increment of 1 mm minimum in both the X and Y directions, Figure 33.

b) A basic ultrasonic module used to collect the A-scan data depth location which is transferred in its analogue form to an X-Y recorder, together with the scanner positional information.

c) An X-Y plotter which produces a pseudo 3D format, Figure 34.

d) A control unit for the mechanised scanner.

SVC P-SCAN

The SVC P-scan is a fully computerised modular mechanised ultrasonic system which consists of:

a) A fully mechanised ultrasonic scanner capable of scanning in both the longitudinal and transverse direction, using mechanised encoders to give location information. The scanner is able to carry both gap scanning and contact scanning transducers, Figures 35 and 36.

b) A pulser receiver unit converting the analogue data to digital.

c) A microprocessor unit for storage of data prior to manipulation and analysis.

d) A dual cassette unit for the master and storage tapes.

e) Twin visual display units producing the A-scan presentation and the P-scan presentation (Projection Image Scanning). The P-scan is a C-scan image of the area scanned and a side view of the image showing the location of the defect with depth, Figure 37. This system has been fully described by Iverson([110]) and Neilson([111]).

f) A scanner control unit.

The whole system in use is shown in Figure 38.

DNV CORROSCAN

This unit is an adaption of the P-scan as it has been specially

developed for use underwater for the detection of corrosion in pipelines and risers. The electronic units are the same as for the P-scan but the scanner is a new development, Figure 39, having an independent power source to be used underwater and a pivoting arm to cope with the possible undulations on the pipe surface, Figure 40. The system also uses a focussed non-contacting probe as shown in Figure 41 although during the evaluation a contact probe was used.

EVALUATION OF THE SCANNING SYSTEMS

The most important item in any mechanised ultrasonic scanner is the transducer selected to detect the defect. No matter what form of advanced manipulation or analysis of the data is used, if the initial data is poor or sub-standard due to the fact that the transducer does not have the near surface resolution or sensitivity to enable detection of the defect, then enhancement will still not reveal the defect. Metallurgical investigations have suggested that a 3 mm disc would be the equivalent to a laminar hydrogen induced crack that could be tolerated to exist in a steel pipeline, any cracking smaller than this would be acceptable except when they exist in a cluster. It was then essential to select the correct transducer which would enable the detection of a 3 mm disc at the midwall location.

In order to comply with this requirement a twin crystal focussed transducer was selected, the focal point being at the midwall position or in the area of interest. Three transducers were acceptable for this purpose. The Krautkramer MSEB4H had a focal length of 6-10 mm

and thus could be used on a 12.5 mm wall thickness pipe; the MSEB4T was an immersion probe, suited for use with mechanised systems, which had a focal length of 4-6 mm, and finally the SEB5KF3, usually used for thin wall thickness measurement, which had a focal length of 3 mm. It is essential that this parameter is known as a very small spherical reflector delivers a maximum echo when focussed and thus extra amplification of the echo may be required to permit efficient detection of defects located outside the position. DGS diagrams for the transducers are shown in Figures 42-44 showing the focal point and the ability to detect a 3 mm disc.

These probes were used where possible with the above scanners during the evaluation. A 600 mm diameter 12.7 mm wall thickness pipe was used during the evaluation. Slots and notches, 1 mm, 2 mm and 3 mm width and diameter respectively were machined in the inner surface at 1 mm increments from 3 mm from the outer surface to 6 mm from the outer surface (Figures 45-46, Table 2).

The four mechanised scanners were then used to examine the pipe over a number of runs and the results are presented in Tables 3-15 and Figures 47-62.

RESULTS

As can be seen from the results, not all of the transducers were used with all of the mechanised scanners.

The Ultra Image scanner and electronics were designed to operate only with a single crystal transceiver and thus could not be used with any of the twin crystal focussed transducers, with the result that although the minimum size flat bottomed holes and notches could be detected, all of the depth measurements were overestimated.

The DNV Corroscan was developed for underwater application and the transducer holder was designed only to be used with the MSEB4T transducer. During the evaluation it was not able to detect the 1 mm flat bottomed holes or notches, possibly because of the lower frequency, i.e. 4 MHz compared with the Ultra Image 8 MHz probe.

The Primscan was used with all three transducers and the SVC P-scan was evaluated using the MSEB4T and the SEB5KF3.

DISCUSSION

The results show that all of the mechanised scanners were able to detect a 3 mm hole at a minimum distance of 3 mm from the outer surface of the pipe using all of the various transducers, although there was a variation in the ability of the systems to detect the 1 mm flat bottomed holes.

The Ultra Image system using the single crystal 8 MHz transducer was able to detect all of the flat bottomed holes and notches, but because of a wide initial transmission pulse, it was difficult to accurately measure the transit time to the flat bottom hole echo which created an

inaccuracy when measuring depths. Figure 63 shows the transducer characteristics in relation to depth showing no resolution below 3 mm because of the transmission pulse width.

The Primscan system was not able to detect any of the 1 mm diameter flat bottomed holes even though the characteristic curves for the transducers show they are able to detect holes of that dimension. The SVC P-scan and the DNV corroscan also had difficulty detecting the 1 mm flat bottomed holes. This suggests that although the transducers are capable of detecting these small holes, the electronic equipment does not have the capacity to resolve them. This is a function of the amplifier bandwidth. High frequency amplifiers of the broad band type, 1-10 MHz range, have the advantage that short pulse transducers having wide frequency bands pass through with little distortion. But the amplifier noise limits the amount of amplification available. This noise is proportional to the square root of the amplifier band width so that a narrow band width permits higher amplification and low noise. The short pulse results in a shorter decay time between the pulses resulting in better resolution. Thus a wide band width amplifier will produce better resolution, whereas the narrow bandwidth will give better amplification. It would appear that both the Primscan and the SVC systems have narrow band width amplifiers whereas the Ultra Image is known to have a band width of 1-10 MHz. Both systems produced better results with the SEB5KF3 transducer in terms of determining the depth below the surface, this is as expected as the transducer was of a higher frequency, i.e. 5 MHz instead of 4 MHz.

In terms of detection and resolution all of the mechanised scanners were capable of detecting hydrogen induced cracking but some of the practical problems precluded some of them from use.

The Ultra Image scanner was manually operated and did not have automatic indexing, relying on total 'colouring in' of the video monitor to ensure full coverage of the pipe section. This made the scanning rate very slow and uneconomic. The unit could only be used with a single crystal transducer which had a dead zone of 3 mm and finally did not have automatic acoustic coupling, couplant having to be applied to the surface prior to inspection.

The Primscan unit did not have any storage capacity for data collected to be used in post test analysis. Interpretation of data was difficult due to the pseudo 3D print-out and the scanning speed was slow. All measurements of defect depth had to be performed manually from the X-Y recording.

The D.N.V. Corroscan had been developed for underwater application and was purpose-built for this application having a separate power supply for the scanner, which only moved in one direction, thus making it impossible to return to its original index point.

The S.V.C. P-scan with the Corroscan software had a fully mechanised scanner able to move in the clockwise anti clockwise and transverse directions. It had automatic couplant control and was able to carry

the twin crystal transducer. The computer had data storage facilities for post test analysis and threshold levels could be adjusted after the test and the data reanalysed. A permanent copy of the data could be produced with direct readout of the penetration of the hydrogen induced crack.

A final check was performed on a test block as shown in Figure 64 and the results compared with a C-scan image produced using a 10 MHz focussed probe scanning the plate in an immersion tank, Figures 65 and 66. The holes appear to be rectilinear because of the stepped scanning increments.

The S.V.C. P-scan mechanised system using the Corroscan software was thus the unit selected for examination of the pipes subjected to a sour gas environment in that it was able to characterise the area of hydrogen induced cracking by producing C-scan images of the areas affected and measurements of propagation through the pipe wall thickness.

CHAPTER 4

EXPERIMENTAL PROCEDURE FOR THE EXPOSURE OF PIPE STEEL TO A SOUR GAS ENVIRONMENT

Materials

Four pipe sections 48 inches long were prepared for the investigations, details of the pipe dimensions and chemical analyses are given in Table 16. It should be noted that one of the pipe sections selected was of seamless pipe. This sample was chosen as it is generally thought that pipe produced by the seamless route is less susceptible to hydrogen induced cracking than welded pipe because the pipe forming process is complete at a higher temperature producing less elongated non metallic inclusions and a more uniform metallographic structure.

All of the pipes were cleaned and degreased prior to testing. The sections were then installed vertically and end caps attached using rubber seals to facilitate removal of the end fixtures and acoustically isolate the sample. The pipes were then filled to 36" with the recommended NACE solution of 5% sodium chloride NaCl and 0.5% acetic acid CH_3 COOH to give an initial pH value of 4.8-5.4. Hydrogen sulphide H_2S was then bubbled into the pipe at a rate of 100cc/minute to obtain saturation producing a pH value of less than 4. These are the same conditions that small scale NACE samples are subjected to, except that all sides of the samples are affected which would be an

unreal situation. The pipes were then left under test for at least 96 hours as per the NACE requirements. No pressure was exerted in the pipe sample.

The experimental system is shown in Figure 67 and it can be seen that this is a fair representation of what would occur in a real situation and not the unrealistic aggressive conditions applied during small scale laboratory trials. It can also be seen that the hydrogen content determined at the centre of the pipe wall will only be half the value found at the surface in contact with the sour gas environment because of escaping hydrogen from the outside surface which would not be in the case of the immersed sample. Other workers[21,22] had concluded that pipe samples exposed to hydrogen sulphide from both surfaces suffered greater damage from hydrogen induced cracking than those exposed from one side only. Thus the experimental procedure selected for the laboratory trials simulated more closely actual field conditions and also assisted the use of the acoustic emission technique.

ACOUSTIC EMISSION PROCEDURE

A Dunegan/Endevco model 1032D acoustic emission system was used during all of the tests. The system had 32 channels available and with the 1032D computer was able to perform two dimensional locations of the sources of acoustic energy and record all of the acoustic tests on floppy diskettes. Two location algorithms were used during the test.

Cylindrical location was used on the first pipe and the remainder were monitored using an interlocking triangular method called multi-triplet. The two configurations are shown in Figures 68 and 69. The difference between the two algorithms is that with a cylindrical array ambiguous results may be obtained producing locations which may be outside the triangular array, with the multi-triplet algorithm the location will always be returned within the triangle.

The two figures 68 and 69 show the sensor location and the corresponding computer projection of the pipe sections, four sensors being attached to each pipe. A sensor preamplifier combination was used to give a frequency range of 100-350 KHz and the sensors were mounted on the pipe section using magnetic clamps. Because of a lack of knowledge it was not known what the amplitude threshold of the hydrogen induced cracking would be so that a low threshold of 30 dB (reference 0 dB = 1 microvolt at the sensor) was used during the tests. This low threshold caused a large amount of data to be recorded which required filtering increasing post-test analysis time.

A typical example of unfiltered data is shown in Figure 70 showing the location of windows required to analyse extraneous noise. The windows were arranged to cover 10% of the surface area and include a minimum of 10 events. All four parameters of rise time, amplitude, duration and acoustic emission counts were measured and the values used to filter extraneous noise such as bubbling from the remaining incoming data. An example of post analysis filtering is shown in Figure 71.

The procedure in the experiment was to install the sensors just below the liquid level and as near to the base as possible and measure the attenuation in the material to ensure adequate coverage by the sensors. In this case because of the small size of the sample, i.e. 48" long by 12" diameter this was not a problem.

The velocity was measured and a simulated source was used to determine the location accuracy, Figure 72. Passage of an inert gas was then used to simulate the bubbling noise which would occur during the test and the parameters measured. The experiment then commenced using the hydrogen sulphide gas.

Pipe Test Section 1 - Automatic Welded Mild Steel Pipe

Figures 73-80 are the computer plots from the acoustic emission data collected during the testing of pipe section 1 and as can be seen a large amount of data was collected using four discs. With acoustic emission it is always preferable to collect all the data, then discard that which is unnecessary during analysis. Figure 73 shows the first unfiltered location plot revealing a heavily concentrated C shaped area of acoustic activity in the centre of the plot. The left hand bottom corner of the plot has a medium density area of activity just slightly more dense than the activity in the remainder of the pipe. This was background noise generated by the hydrogen sulphide gas bubbling into the pipe. Figure 74 shows the same location plot after applying the window technique analysing the data within the windows to characterise the data and using the software package to remove the

extraneous noise. The concentrated area in the centre of the pipe location plot remained showing that it was valid data. Seventeen hours later the central area of activity had decreased leaving two areas at the extreme ends of the 'C' with some increase in general noise, Figure 75. Three hours later the central active source had increased its activity together with a build up of the background noise, Figure 76.

Thirteen hours later the central area of the pipe was still emitting acoustic events but the remainder of the 'C' area had virtually disappeared, Figure 77. This suggests that once the hydrogen cracking had occurred the stress concentration around the crack tip had been relieved preventing further emissions and new areas of cracking had appeared creating the latter areas of acoustic activity. At this stage the experiment was halted and the test pipe drained and ultrasonically examined. The S.V.C. Corrosan was not available for this first experiment so that ultrasonic examination had to be applied manually. Two areas produced laminar indications and these were identified for subsequent metallographic examination. Further areas which indicated acoustic activity but did not produce ultrasonic echo responses were also identified together with areas having no acoustic activity present, Figure 78.

Figures 79 and 80 reveal the amplitude distribution plot obtained from the two areas of high acoustic acitivy. These showed an amplitude range of 40-50 dB for area S0 and 40-55 dB for area S1. A history plot of event rate for the first ten hours of the test is given in

Figure 81 and shows an event rate of 3 events/minute for some periods of time, and if this is compared to the history plot of amplitude against time, amplitudes of 60 and 70 dB can be seen, Figure 82. At the latter stage in the experiment a second array of sensors S1 was placed on the area of suspected cracking and the location plot produced from this array is shown in Figure 83. This was produced at the same time as the location plot in Figure 77. The two amplitude history plots are shown in Figures 84 and 85, the amplitude history plot for array S1 being the more concentrated. The event rate for both these arrays is much greater than that measured at the beginning of the test suggesting that crack growth was continuing and that the steel was highly susceptible to hydrogen induced cracking, Figures 84(a) and 85(a).

Monsanto Chemical Company have an evaluation criteria which they place on metal pressure vessels under test. Two of the criteria are that there should be no high amplitude events greater than 65 dB and that the event rate should not increase during a test. If the criteria had been applied to this test then extreme cracking would have been predicted.

The areas identified after the ultrasonic inspection were removed for metallographic examination.

The general structure was that of ferrite and pearlite grains containing numerous non metallic inclusions, the majority being manganese sulphide. Four main types of defects were located. A central laminar crack was detected in area SO, Figure 86, and these

cracks were associated with transgranular non-metallic inclusions, Figure 87. The second type of cracking located in areas of high acoustic activity but which did not produce an ultrasonic response is shown in Figure 88. This crack was within 1 mm from the inner wall surface and would probably not have been detected solely by ultrasonics because any echo response would have been confused by the backwall echo. There were a number of these cracks and they lay in a band 0.41 mm to 1.27 mm from the inner wall surace. An area of banding can also be seen at the top of the metallographic section.

The third type of defect located was classical stepwise cracking, Figure 89. This again was close to the inner surface.

A fourth type of defect was located in the area S1, and although this being mainly parallel to the surface, it also propagated to the inner wall, Figure 90. This crack was 3.81 mm long and 2 mm from the inner wall. One of the planar defects was 7.7 mm long and 1.27 mm from the inner wall and had not been detected by manual ultrasonic inspection, which suggests that either the far wall resolution was not adequate to separate the defect echo from the back wall or the defect was missed during the scanning pattern.

Sections removed for examination from areas which did not give acoustic emission indications revealed no crack areas.

Pipe Section 2 - Seamless Steel Pipe

The multi-triplet array was used on pipe section 2, manufactured from seamless steel material. This pipe was tested for 200 hours because over the first 100 hours there were no positive areas of acoustic activity. Figure 91 shows the unfiltered location plot and as can be seen the acoustic activity was of very low level and diverse with no dense clusters apparent, similar to the effect produced by the bubbling of the hydrogen sulphide gas. The same software filter used during pipe 1 test was applied and virtually removed all traces of acoustic activity, Figure 92. An amplitude distribution plot for the pipe section revealed a range from 35-45 dB, the majority of events having amplitudes in the 35 dB region, Figure 93.

Careful ultrasonic examination of the pipe surface revealed no evidence of cracking. Because of the lack of hydrogen induced cracking, it was decided that an extensive metallographic examination should be performed. Sections were removed from around the whole circumference and apart from internal corrosion, no deterioration of the pipe was noted. The material had a much finer grain size than Pipe 1 and a lower population of non metallics, no elongated inclusions being present in the samples examined, Figures 94 and 95.

The fact that the pipe was seamless rather than welded is the reason for the lack of attack by the sour environment confirming the evidence of earlier work referred to in Chapter 1([12,14,30]).

Pipe Section 3 - Automatic Welded Mild Steel Pipe

Because of the uncertainties produced during the examination of Pipe Section 2, the procedure for Pipe Section 3 was slightly altered. The mechanised ultrasonic scanner was used to examine the whole area of the pipe prior to the test to see if there was any evidence of lamination or large non-metallic inclusions present. The pipe was then subjected to the same environment as the previous two pipes.

Figures 96 to 98 show the location plots for the test pipe. Initially the plot revealed scattered diverse acoustic activity with only a small number of clusters being detected by the computer. After applying filters only two regions remained. The two areas opposite being produced from the same source. A series of location plots produced from the pipe nine days later produced the same indications even after filtering, Figures 99-101.

The mechanised ultrasonic scanner was used to examine the pipe and produced indications in the same area as the acoustic emission events, Figure 102. Metallographic sections were removed in an attempt to validate the ultrasonic and acoustic emission indications.

A large sub surface crack was revealed, Figure 103, propagating towards the surface of the pipe in a stepwise manner similar to that detected in pipe section 1. Clusters of non-metallics could be seen associated with the stepwise section of the crack, Figure 104, and

fine cracking could be seen at the tip of the main crack, Figure 105. The structure was heavily banded, Figures 105-107.

Pipe Section 4 - Electric Welded Steel Pipe

Pipe section 4 was electric welded pipe known to be susceptible to hydrogen induced cracking. The pipe was scanned prior to commencement of the experiment using the mechanised ultrasonic scanner, and this revealed no internal discontinuities.

The pipe became active soon after the commencement of the test and produced wide areas of acoustic activity even after filtering. Figures 108-110, a further four discs were filled with data and after filtering extensive areas of high acoustic activity could be seen, Figures 111-119. Because of the large amount of acoustic activity the experiment was stopped after 96 hours and the pipe scanned using the mechanised ultrasonic scanner.

The ultrasonic data produced is shown in Figure 120, confirming the presence of defects from the areas of acoustic emission. Several areas which had emitted a large number of events did not reveal any ultrasonic discontinuities, but as earlier pipe tests have revealed, this could be due to near surface laminar cracks.

Metallurgical sections were removed from areas showing acoustic activity, some of which had been confirmed by ultrasonic examination. Further sections were removed from those areas not showing any acoustic activity.

Gross examples of hydrogen induced cracking were revealed, in one case delamination of the pipe had occurred, Figure 121. This section also revealed the presence of vertical sulphide stress corrosion cracking propagating from the inner pipe wall. These cracks had been produced from the internal stresses caused by gross lamellar hydrogen induced cracking.

One of the areas of hydrogen induced cracking detected was a duplicate of the area detected in pipe sections 3 and 1, confirming that these defects detected had indeed been hydrogen induced cracks.

All of the control metallographic samples removed were free from defects.

CHAPTER 5

COMMENTS

By subjecting four types of pipe to a sour gas environment and monitoring the pipe sections with an acoustic emission system, it has been demonstrated that acoustic emission has been able to detect and locate areas of acoustic activity that were confirmed by ultrasonic and metallographic examination to contain hydrogen induced cracks. Areas of acoustic activity that on examination by ultrasonics did not produce defect indications were shown also to contain hydrogen induced cracks, but these were within 1 mm from the inner surface of the pipes and probably outside the limitations of resolution of current dynamic or manual ultrasonic examination. There were no instances of areas examined metallographically that revealed hydrogen induced cracking that had not been detected by acoustic emission or ultrasonic examination. It is also true to say that all areas examined that did not indicate acoustic activity were shown to be free from hydrogen induced cracking.

The initial experiment on an automatic welded steel pipe 1 revealed in location plots, Figures 73-80, that the acoustic emission system did detect large areas of acoustic activity, but it was only after applying a technique to analyse the various clusters that it was possible to determine that some areas were different to others and were a source of background noise, caused by bubbling of the hydrogen sulphide gas through the pipe. Once this was identified it was possible to measure

the various parameters such as amplitude, rise time and duration and by applying these in the form of a software filter, remove this extraneous noise. This filter was then applied to each new disc of data obtained from the test.

The hydrogen induced cracking signals had amplitudes in the range 40-55 dB with short rise times and duration typical of a primary source, as indeed crack propagation is, whereas bubble noise is a secondary acoustic source and had long duration and rise times. It was these factors that enabled analysis and filtering to be performed. More information is required to characterise fully the hydrogen induced crack source in acoustic emission terms, and it has been stated recently "that acoustic emission is one technique where the practical application development and use are in advance of the fundamental research([11,93]).

Location plots were produced during all of the trials for each pipe but there are limitations in the accuracy that can be obtained. A common figure quoted is that acoustic emission can locate to within 100 mm of the defect source, but this depends on the acoustic measurement of the transducer position and the algorithm used to locate the source. The majority of algorithms have been produced from flat plate analysis, whereas in the majority of cases they are applied to curved surfaces producing inaccuracies. In this case it was hoped to produce locations to within 7.5 cm^2 of the hydrogen induced cracking site, considering the above errors involved in the locating ability of the acoustic emission system. In fact, results obtained

showed that the accuracy was within 6.5 cm^2 (1 square inch). Detection was the main objective of these trials but the location plots proved invaluable as the metallographic examinations became more extensive.

During pipe experiment 1 the concentrated 'C' broke up and became more diffuse suggesting completion of hydrogen induced cracking in that particular area and a relief of local internal pressure. As the experiment continued other areas became active, suggesting new growth and cracking, which indicate that acoustic emission can be used for recording the progress of cracking. The pipe was subjected to no other form of internal pressure except the static head of the NACE solution and any residual stress remaining from forming and fabrication, so that no secondary emissions were expected from the hydrogen induced cracking due to fracture faces fretting together or corrosion products being crushed. Thus once cracking had completed its growth cycle there was no reason for further activity to be expected from that source. This is a point to remember during large scale long term tests, that active sites can become quiet.

The microphotographs produced from the pipe revealed hydrogen induced cracking in the pipe section. It was always thought that hydrogen induced cracking would occur in the central band of the pipe walls, in areas of central segregation where the steel would be more susceptible to the presence of manganese sulphides and other non metallic inclusions producing sites for nucleation and growth of the hydrogen induced cracks. In fact, most of the cracks were found within 1 mm

from the inner pipe wall, the majority being within 0.5 mm. This would account for the difficulty in detection encountered when using the ultrasonic techniques. This depth of defect corresponds to a through wall of 7.8% which in certain material types could be classed as critical.

This may make invalid the suggestion that by applying mechanised ultrasonics as a method of condition monitoring to pipeline or plant susceptible to hydrogen induced cracking, advanced warning of failure would be obtained.

The crack shown in Figure 90 was 3.81 mm long and 2 mm from the inner wall, equivalent to a 32% through wall crack. If the pipe had been subject to any form of internal pressure, failure would have occurred. Fortunately this defect was detected by manual ultrasonics, giving some confidence to the requirements originally specified of being able to detect a 3 mm defect at the mid-wall location.

A central laminar hydrogen induced crack was also located, Figure 86, using manually applied ultrasonics. This was a classical hydrogen induced crack, located in the mid-wall, the tips of the cracks associated with lenticular non metallics. Four types of hydrogen induced cracks were detected in the pipe section examined, the three described above, two laminar at the inner surface and mid-wall, one at the inner surface but also propagating in a stepwise manner to the surface, and finally stepwise cracking formed by linking up of short laminar cracks, Figure 89.

The steel itself was subject to heavy banding and clusters of elongated non metallics, making it readily susceptible to attack and the production of hydrogen induced cracking. The location of the cracking did not suggest that the location could have been predicted.

Acoustic emission of the welded steel pipe 1 proved to be an effective and sensitive method of hydrogen induced cracking detection, detecting the cracks, at what appeared from metallographic investigation, at an early stage of growth. The acoustic emission detected these areas of acoustic activity at an early part of the test. Properly instrumented, a pipeline could be monitored using this application.

As can be seen from the results of welded steel pipe 1, the hydrogen induced cracks occurred randomly, and if ultrasonic or metallographic examination had been applied in the conventional manner of a grid pattern, the cracking could have gone undetected and produced a false indication of the condition of the pipe. This argument also applies to the selection and use of coupon testing, where the result will depend on the site chosen for examination. Acoustic emission in this case has proven to be an effective volumetric test.

The results of the seamless pipe 2 were very convincing even though no acoustic emission activity was detected. The pipe material was seamless steel and the literature survey([8]) had predicted that seamless pipe was not susceptible to sour gas attack and the initiation of hydrogen induced cracking. The test was extended from

the initial 100 hours by a further 200 hours because no significant acoustic activity had occurred; still with no response from the pipe, Figure 92. The amplitude distribution from the pipe showed only low amplitude values of around 35 dB's, lower than that obtained from the hydrogen induced crack signature, Figure 93. An extensive metallurgical examination was carried out on the pipe section revealing a fine grained clean steel structure with no evidence of hydrogen induced cracking, although internal corrosion had taken place.

The main differences between pipe sections 1 and 2 were the fact that pipe section 2 was produced from seamless steel and was much cleaner and fine grained.

The lack of acoustic activity from the pipe was confirmed by the results of the metallurgical investigation.

The results from the automatic welded pipe 3 were again different from those of the two previous pipes. Only two regions of activity were noted during the whole test. As before, because the acoustic activity produced was small the test was extended, monitoring on a limited basis. The same two regions remained active, Figures 99-101. The pipe had been fully examined using a mechanised ultrasonic scanner prior to the test and no defects had been detected. Post test examination of the pipe revealed an area of cracking in the same area as the acoustic emission system had predicted, Figure 102. Metallographic sections were removed from the pipe in the area

predicted by the mechanised scanner and in other areas. Hydrogen induced cracking of the type seen in pipe section 1 was revealed in Figure 103. There was some discussion as to whether the defect could have been a sub-surface lamination which had propagated during the test, but the pretest ultrasonic examination had shown that the pipe was defect free proving that the defect had occurred during the attack from the sour gas environment, and the usefulness of pretest scanning.

Pipe section 4 had been produced from electric welded pipe known because of its directional production route to be susceptible to attack from hydrogen induced cracking. This pipe started to emit acoustic emission signals from the commencement of the test, resulting in the production of a large amount of data, Figures 110-119. Filtering of the data showed tht the acoustic activity and presumably the severity of the cracking was increasing. The test was halted and the pipe section ultrasonically examined resulting in large areas of cracking being located, Figure 120.

The worst example of hydrogen induced cracking was revealed during the metallurgical examination of this pipe, that of a complete delamination of the pipe wall, Figure 121, an extreme form of hydrogen induced cracking. In the same sample evidence of sulphide stress corrosion cracking was found propagating at 90° to the inner surface.

The use of a mechanised ultrasonic system prior to and after the testing of the pipes proved useful in that it was possible to compare

the number of defects produced during the experiment. In both instances when it was applied the pipes were defect free before the experiment and thus helped to confirm that the one defect produced during pipe test 3 was a hydrogen induced crack. The limitations of the ultrasonic technique were also illustrated by the number of near surface hydrogen induced cracks revealed by metallographic examination from areas having a high level of acoustic activity. These were not detected by either manual or mechanised scanning of the pipes and would not have been detected if ultrasonic examination had been the only detection method used to locate the hydrogen induced cracks after the pipes had been subjected to the sour gas environment. Metallurgical sectioning alone would probably have missed a number of these cracks and could possibly have missed all of them depending on the frequency of sampling.

CONCLUSIONS

1. It has been demonstrated that acoustic emission can be used to detect and locate hydrogen induced cracking in full size pipe sections.

2. Acoustic emission showed that it could tell the degree of severity of attack by hydrogen induced cracking on the pipe section, where and when it was occurring in real time.

3. Acoustic emission showed its ability to detect and locate hydrogen induced cracking at an early stage (cracking near the inner surface).

4. A software filter was successfully used to identify extraneous noise caused by bubbling of the hydrogen sulphide gas and filter it from the acoustic emission emanating from the hydrogen induced cracks.

5. The acoustic emission data produced from the pipe was identified as hydrogen induced cracking following metallographic sectioning.

6. The hydrogen induced cracking occurred near to the inner surface of the pipe sections, as it would in a real situation rather than in the case of coupon testing when the sample is subjected to the environment from all sides.

7. The near surface (1 mm or less) hydrogen induced cracks were not detected by either manual or mechanical scanning techniques, probably because of lack of far distance resolution suggesting that ultrasonic procedures used here cannot be relied upon to give an early indication of hydrogen induced cracking attack.

8. The hydrogen induced cracking was associated with non metallic inclusions and occurred in areas of central segregation in pipe sections.

9. The acoustic emission data together with the metallographic evidence suggests that the seamless steel pipe offers the greatest resistance to sour gas attack.

10. The acoustic emission data with metallographic evidence suggested that the electric welded pipe offered the least resistance to the sour gas emission, producing delamination of the pipe wall.

11. Stress corrosion cracking was found to occur in areas of pipe subject to heavy attack by hydrogen induced cracking.

12. Acoustic emission has proved to be a reliable form of volumetric non destructive testing that can be applied to large sections of pipe, relative to the normal coupon size, in order to detect and locate areas of high acoustic activity caused by the initiation and growth of hydrogen induced cracking.

REFERENCES

1. Frazer, J P And Treseder R S. Corrosion 8 342, 1952.

2. Coldren, A P and Tither, G. Metallographic Study of Hydrogen Induced Cracking in Linepipe Steels. Climax Molybdenum Report Nov 5th 1975.

3. Parades, F and Mize, W W. The Oil and Gas Journal. Vol 53, No.12 p99, (1954).

4. Class 1, Report on Investigation of Sulphide Stress Corrosion Cracking of Steels Particularly of Steels of Low Tensile Strength. Second International Conference on Metallic Corrosion. March 11-15 1963 New York.

5. Mason, D W and Baker, J J. Fulmer Research Institute Report E146-21 October 1972.

6. Irving, R R. Iron Age Vol 217 No6 p43 (1974)

7. Moore, E M and Warga, J J. Materials Performance June 1976 pp 17-33.

8. Moore, E H. Hydrocarbon Induced Damage in Sour Wet Crude Pipelines Middle East Oil Technical Conference of SPE, Morama Bahrain March 14-17 1983.

9. SANDT Annual Lecture December 1985 - Prof H C Cotton.

10. National Association of Corrosion Engineers.

11. Nace Standard T-IF-20 Testing of Metals for Resistance to Sulphide Stress Corrosion Cracking at Ambient Temperatures. July 1977.

12. Wilde, B E, Kinn, C D and Phelps, E H. International Conference on Corrosion 80 Paper 107.

13. Keisling - Non Metallic Inclusions in Steel Pts I-IV 1978.

14. IKeda A, Morita Y, Terasoki F, and Tokeyama, N. Second International Congress on Hydrogenin Metals Paper No 4A7 Paris 1977.

15. NACE Standard T-IF-20 Draft 8, Evaluation of Pipeline Steels for Resistance to Stepwise Cracking 1982.

16. Development of Linepipe Steels for Sour Gas Service, Nippon Steel Corporation Report, February 1981, 1102, Sour 02-81-0.

17. Nakai, Y, Kurahashi, H Emi, T and Haida, O. Development of Steels Resistance to Hydrogen Induced Cracking in a Wet Hydrogen Sulphide Environment. Kawasaki Steel Corporation Report, January 1978.

18. Taira, T and Kobayashi, Y. Study of the H.I.C. Testing Method. Technical note for the T-1F-20 SWC. Task Group, March 3-7 1980, Chicago, 1-6, 1980.

19. Kawaka, M Terasaki, F Nagata, S and Ideda, A. The Sumitomo Search No.14 November 1975 p 36-50.

20. Taira, T and Kobayashi Y. Int. Conference Corrosion 81, Paper No 183.

21. Taira, T, Tsakada, K, Kobayashi, U, Inagaki, H and Watanabe, T. Corrosion 37 (1), 5,(1981)

22. Ikeda, A, Kaneko, T and Terasaki, F. International Conference Corrosion 80 paper No.8.

23. Ikeda A, Terasaki F Takeyama M, Tokeuchi I, and Nara, Y. International Conference Corrosion 28 Paper 43.

24. Nakai, Y, Kurahashi, H, Emi, T and Haido O. 94th ISIJ Meeting October 1977 Trans ISIJ19 P401, 1979.

25. Moore, E M and Hansen D A. Trans ASME 104, pp 134-141 June 1982.

26. Herbsleb G, Poepperling P K, and Schwenk W. Corrosion 36, (5), pp247-256 (1981).

27. Herbsleb, G Poepperling, P K, and Schwenk, W. Int. Conf. Corrosion 80 Paper No.9 March 1980 Chicago.

28. Robinson J L. The Welding Institute Research Bulletin, 18 (5) May 1977 pp121-126.

29. Ikeda A, and Kowaka M. Chemical Economy and Engineering Review 10 (5-6) pp12-22, 1978.

30. Miyoshi, E, Tanaka, T, Terasaka, F and Ikeda, A. ASME Publication Paper No 75-Pet-2(1975).

31. Inagaki, H, Tanimura, H, Matsushima, I and Nishimura, T. Trans Iron and Steel Inst Japan 1978, 18 No.3 pp149-156.

32. Taira T, Tsukada, K Kobayashi, Y, Tarimura, M, Inagaki, H and Seki, N. NKK Tech Report Overseas, No.31 1981.

33. Nauman F K and Spies F. Practische Metallographic 10 (8) pp475-480 1973.

34. Coldren, A P and Tither, G. Metallographic Study of Hydrogen Induced Cracking in Line pipe Steels. Climax Molybdenum. Report Nov 5th 1975.

35. Coldren, A P and Tither, G. Journal of Metals 5 May 1976.

36. Taira T, Kobayashi Y, Matsumato, K, Matsumoto, S. Terunuma, T and Arikata, K. Hydrogen Problems in Steels ASM Metals Park O.H. p173 1982 Ed. Interrante C.G. and Pressonyre, G.

37. Brown, A and Jones, C L. Hydrogen Induced Cracking in Pipeline Steels Int.Conference Corrosion 1983 Anaheim April 1983 Paper 155.

38. Parrini, C and DeVito A. Micon 78 Optimisation of Processing Properties and Service Performance Through Microstructural Control Houston Texas, 3-5 April 1978.

39. Detection of Lamination in Plate, Raine, G A. BSC Symposium on Non Destructive Testing Corby July 1970 MMS/250/70.

40. ASTM Round Robin Exercise for Determinations of Steel Cleanlines by an Ultrasonic Technique, 1968.

41. Raine, G A. The Ultrasonic Detection of Central Unsoundness in Billet Mill Slabs, MMS/261/70, 26 August 1970.

42. Investigation into the use of Ultrasonic Attenuation Measurements as a Means of Steel Cleanlines Assessment. EM69/11 Raine G A October 1979.

43. Timmins, P F. Assessing Hydrogen Damage in Sour Service Lines and Vessels as a Key to Plant Inspection Technology. Oil and Gas Journal Nov 1984.

44. ASTM Definitions to Terms Relating to Acoustic Emission "ASTM Standard E610-82, Vol 303 p691 (1983).

45. Kaiser, J. Erkenntnisse and Folgerungen aus der Messing von Gerauschen bei Zugbeansprunchung von Metallischen Werstoffen (Conclusions and Results from Sound Measurement in Tensile Stressing of Metals), Archiv fur das Eisenhuttenwesen Vol 24 No 1-2 p43 (1953).

46. Vahauiolos, S J et al. Adaptive Spot Weld Feedback Control Loop via Acoustic Emission, Physical Acoustics Corporation Technical Report TR-23 1981.

47. Drouillard, T F and Glenn, T G. Production Acoustic Emission Testing of Brazed Joints, Air Force DARPA Review of Progression Qualitative NDE, University of Colarado, Boulder, Colarado, August 2-7 1981.

48. Koemer, R M, Lord, Jnr, A E and Diesher, J N. Acoustic Emission detection of Underground Gasoline Tank Leaks, American Society of Non Destructive Testing Spring Conference, March 28-30 1977, Columbus, Ohio.

49. Koemer, R M, Lord, Jnr, A E and Deisher, J N. Acoustic Emission Stress and Leak Monitoring to prevent spills from Buried Pipeline, National Conference on Control of Hazardous Material Spills, 1976, New Orleans.

50. Lord, Jn, A E, Diesher, J N and Koemer, R M. Materials Evaluation Vol 35 No 11 p49 1977.

51. Parry, D L. Proceedings of the 1st International Conference on Structural Mechanics in Reactor Technology, EUR 4820, Vol 4 1972.

52. Pekrul, P J. On-Line Vibration and Loose Parts Monitoring of Nuclear Power Stations as a Preventative Maintenance Tool. Materials Evaluation, Vol 34, No 7, p154, 1976.

53. Finding Foreign Particles as Small as a Grain of Salt. Quality Assurance, Vol 8, No 2, p36 1969.

54. Selig, B J, Runde, H A and Kosky, R P. N-Plant Monitoring Improves Reliability, Electrical World, Vol 181, No 10, p44, 1974.

55. Taylor, R R. Predict Bearing Failures with Portable "Checkers", Hydrocarbon Processing, No 1, p88, 1982.

56. Balderston, H L. The Detection of Incipient Failure in Bearings, Materials Evaluation, Vol 27, No 6, p121, 1969.

57. James, R. Predictive Maintenance System Improved at Exxon Chemical Plant, Oil and Gas Journal, Vol 74, No 5, p59, 1976.

58. Sato, Y et al. Rotating Machinery Diagnosis with Acoustic Emission Techniques, Journal of Acoustic Emission, Vol 2, No 1-2, p1, 1983.

59. Umezawa, K, Ajima, T and Houjohm H. An Acoustic Method to Predict Tooth Surface Failure of In-service Gears, NDT International, Vol 16, No 4, p201, 1983.

60. Yee, K W and Blomquist, D S. An On-Line Method of Determining Tool Wear by Time-Domain Analysis, Society of Manufacturing Engineers Technical Paper MR 82-901, 1982.

61. Skubis, J. Partial Discharge Detection in Bushings by an Acoustic Emission Method, Journal of Acoustic Emission, Vol 2, No 4, p267, 1983.

62. Carlos, M F and Jon, M C. Detection of Cracking During Rotational Soldering of a High Reliability and Voltage Ceramic Capacitor, 28th Electronic Components Conference, 1978, Paper No17.

63. Kahn, S and Miller, D. Acoustic Emission Detection: Part II - Detecting Ceramic Substrate Cracking During Thermocompression Bonding, The Western Electric Engineer, October 1979.

64. Evans, A G et al. Thermal Fracture Studies in Ceramic Systems using an Acoustic Emission Technique, Journal of Materials Science, Vol 10, No 9, p1608, 1975.

65. Bunsell, A R. Acoustic Emission for Proof Testing of Carbon-Fibre Reinforced Plastics, NDT International, Vol 10, No 1, p21, 1977.

66. Dean, D S and Dernidge, L A. An Immersion-Technique for the Detection of Acoustic Emission in Carbon-Fibre Reinforced Plastics Pressure Vessels, NDT International, Vol 9, No 5, p233, 1976.

67. Mitchell, J R. FRP Storage Tank Testing with Acoustic Emission, Managing Corrosion with Plastics, Vol 5, p45, 1983.

68. Anderson, R T and DeLacy, T J. Non-Destructive Testing of Advanced Composites, Metal Progress, Vol 102, No 2, p88, 1972.

69. Hagemaier, D J, McFaul, H J and Parks, J T. Non-Destructive Testing Techniques for Fiberglass, Graphite Fiber, and Boron Fiber Composite Aircraft Structures, Materials Evaluation, Vol 28, No 9, p194, 1970.

70. Green, A T. Detection of Incipient Failures in Pressure Vessels by Stress Wave Emission, Nuclear Safety, Vol 10, No 1, p4, 1969.

71. Harris, D O and Dunegan, H L. Acoustic Emission - 5: Applications of Acoustic Emission to Industrial Problems, Non-Destructive Testing, Vol 7, No 3, p137, 1974.

72. Davis, R J and Peacock, M J. Acoustic Emission Monitoring of a Butane Storage Tank during Hydrotest, ERS Dunegan Endevco Service Report.

73. Hartman, W F and Kelly, M P. June 1984 IOMA Broadcaster AE Testing of Pressure Vessels and Storage Tanks and Gas Cylinders.

74. Dane, Harvey E and Hyatt, R W. Final Report on Acoustic Emission Evaluation (PR3-119), May 1980, PRC AGA.

75. Arrington, M. In-Situ AE Monitoring of a Selected Node on an Offshore Platform. Japanese Conference on AE, 1985.

76. Webb, M J M. Offshore, April 1982.

77. Monitoring Offshore Structures by Means of Acoustic Emission, Batelle Aktuell, September 1983.

78. Acoustic Emission for Offshore Platforms, Dr P Jax, EWGAE, Conference 12-14 October 1981.

79. Application of Acoustic Emission Analysis to the Integrity Monitoring of Offshore Steel Production Platforms - Hansen-Webbon-Materials Evaluation, August 1980.

80. Experimental Study of Acoustic Emission Monitoring of Crack Propagation on Offshore Steel Tubular Joint Demousseau-Laffort, Thebault OTC 1979.

81. Attenuation and Background Noise Measurements on the Dan Field 'B' Oil Production Platform, Webbon-Rogers UIC Tech Report 1030/3.

82. Conoco Viking B Platform Trial - Rogers-Webbon UIC Tech Report 1020/2.

83. Fatigue Tests on T Joint Specimens in the Sea - Rogers-Webbon UIC Tech Report 1020/3.

84. Offshore Focus - Acoustic Emission for Offshore Inspection, Issue 13, June 1979.

85. Offshore Focus, Listening for Cracks, Issue 10, November 1978.

86. Offshore Focus, Fatigue Crack Detection and Measurement, Issue 6, March 1978.

87. AE A Test for Offshore Structural Monitoring 0 Forli, June 1980, DNV Report.

88. Draft Revision to the Guidance Notes on Design and Construction Pt 1 Section 2 Surveys and Inspection, Dept of Energy Petroleum Engineering Division, August 1981.

89. ASTM E 569-76 AE Monitoring of Structures During Controlled Stimulation.

90. AE Examination Location of Sources Discrete Acoustic Events EWGAE Code, October 1979.

91. Standard Practice for AE Examination of Fibreglass Reinforced Plastic Resin (PR), ASTM E 1067-85, 1985.

92. Jax, P. EWGAE Meeting, Milan, 1983.

93. Fowler, T. One Day Presentation on the MONPAC System, September 1986.

94. Votavae, K W U. EWGAE Meeting, Milan, 1983.

95. Parry, D L and Robinson, D L. Elk River Leak Detection Tests. Reactor Technology, May 1970.

96. Discontinuity and Leak Analysis - Gas Pipelines - Butano AE Int Report 1981.

97. McElroy, J W. AE Monitoring of Pressurised Systems, ASTM STP 697 W F Hartman, J W McElroy eds, 1979, pp47-59.

98. Fowler, J T. Experience with AE Monitoring of Chemical Process Industry Vessels, 11th WC NDT, 1986.

99. Krautkramer J H, Ultrasonic Testing of Metals, 1969.

100. Filipczynski, L, Paulowski, Z and Weir, J. Ultrasonic Methods of Testing Materials, 1966.

101. Ultrasonic Flaw Detection in Metal, Banks, Oldfield, Rawding, 1982.

102. Behr, A. Metallurgica 23, 7 November 1940.

103. Desch, C H, Sproule, D O and Dausen, W J. Iron and Steel, Int 1 319, 1946.

104. Krautkramer, J U H. Ultrasonic Non Destructive Testing of Materials, 2nd Edition, 1961.

105. Krautkramer, J U H. Probe Data Sheets, 1980.

106. Raine, G A. The Sensitivities and Characteristics of Ultrasonic Probes in Use at Consett, EM70/1 January 1970.

107. Raine, G A. The Use of SE Probes for the Ultrasonic Testing of Thin Plate MMS/23/70, January 1970, Consett Iron Co Report.

108. Blanchard, F and Saurdillan, D. Second International Congress on Hydrogen in Metals, Paris, France, 1977. Paper 4A8.

109. Forli, O. Internal Corrosion Monitoring Corroscan, Dev Norske Veritas, 1980.

110. Iversen, S E. Recent Advances in the Documentation of Ultrasonic Weld Inspection, SVC Document 82.39, 1982.

111. Nielsen Niels, P Scan, System for Ultrasonic Welds.

112. Grills, R H. New Images Born to the Electronic Age, Materials Evaluation 40, January 1982.

113. De Sterke, A. Automatic Ultrasonic Inspection of Pipeline Welds, NDT International, December 1980.

114. Rose, J C, Ganglbauer et al. 11th International WC NDT. USA p1260.

115. Mechanised Equipment for Non Destructive Evaluation, South West Research Institute, Bulletin 1986, 11th WC NDT Conference USA.

116. Newman, R K, Barbian, O A and Boln, H. Recent Developments of NDT Equipment from the IZFP for Industrial Applications, Demands, Solutions, Examples, 11th WC NDT, Las Vegas, November 1985.

TABLE 1

ULTRASONIC SCANNER REQUIREMENTS

Scanning Mechanism

Remote Operation
Forward and Reverse Strokes
Minimum Scan Increment 2 x 2 mm (x x y)
Minimum Scan Width 300 mm
Maximum Scan Time 60 mins/band
Universal probe holder to accept Krautkramer MSEB4T, and SEB5kF3
Low probe wear rate
Acoustic coupling via thin (0.25 mm) water gap

Ultrasonic Performance

Minimum near surface resolution 3 mm
Single or twin crystal probe operation
Bandwidth 1 - 10 MHz
PRF to give 1 pulse/mm at maximum scan rate
Depth measurement to $\pm$ 0.5 mm

Display

C-scan mapping of corroded areas, approximately A4 size with minimum resolution 2 mm x 2 mm
Data display during scan to monitor performance
Depth information in zones according to material thickness
Identification of minimum depth of cracking in given area

TABLE 2

DIMENSIONS OF ARTIFICAL DEFECTS IN THE TEST PIPE

ARTIFICIAL DEFECTS IN TEST SAMPLE			
IDENTIFICATION	TYPE OF DEFECT	CONFIGURATION AND DIMENSIONS, mm	REMAINING WALL THICKNESS, mm
1	Flat Bottom Hole	Diameter Ø 1.0	3.0
2	Flat Bottom Hole	Diameter Ø 2.0	3.0
3	Flat Bottom Hole	Diameter Ø 3.0	3.0
4	Axial Notch	Length 20.0 Width 1.0	3.0
5	Axial Notch	Length 20.0 Width 2.0	3.0
6	Axial Notch	Length 20.0 Width 3.0	3.0
7	Flat Bottom Hole	Diameter Ø 1.0	4.0
8	Flat Bottom Hole	Diameter Ø 2.0	4.0
9	Flat Bottom Hole	Diameter Ø 3.0	4.0
10	Axial Notch	Length 20.0 Width 1.0	4.0
11	Axial Notch	Length 20.0 Width 2.0	4.0
12	Axial Notch	Length 20.0 Width 3.0	4.0
13	Flat Bottom Hole	Diameter Ø 1.0	5.0
14	Flat Bottom Hole	Diameter Ø 2.0	5.0
15	Flat Bottom Hole	Diameter Ø 3.0	5.0
16	Axial Notch	Length 20.0 Width 1.0	5.0
17	Axial Notch	Length 20.0 Width 2.0	5.0
18	Axial Notch	Length 20.0 Width 3.0	5.0
19	Flat Bottom Hole	Diameter Ø 1.0	6.0
20	Flat Bottom Hole	Diameter Ø 2.0	6.0
21	Flat Bottom Hole	Diameter Ø 3.0	6.0
22	Axial Notch	Length 20.0 Width 1.0	6.0
23	Axial Notch	Length 20.0 Width 2.0	6.0
24	Axial Notch	Length 20.0 Width 3.0	6.0

TABLE 3

RESULTS OBTAINED WITH THE ULTRA IMAGE SYSTEM

MINIMUM DEPTH MEASURED ON TEST SAMPLE

EQUIPMENT : ULTRA IMAGE

PROBE + SERIAL : 0.25" Ø 8MHz GD

DEFECT TYPE : FLAT BOTTOM HOLES OF DIAMETER Ø mms

DEFECT NO	Ø mms	DEPTH converted from 1/1000" to mms					
		NOMINAL	ACTUAL	RUN No 1.1-1.8			
1	1.0	3.0	3.25	4.47			
7	"	4.0	4.01	5.18			
13	"	5.0	5.49	-			
19	"	6.0	5.97	-			
2	2.0	3.0	3.23	4.27			
8	"	4.0	4.12	4.98			
14	"	5.0	4.98	5.89			
20	"	6.0	6.10	-			
3	3.0	3.0	3.13	4.27			
9	"	4.0	4.12	4.78			
15	"	5.0	5.03	5.79			
21	"	6.0	6.15	6.91			

TABLE 4

RESULTS OBTAINED WITH THE ULTRA IMAGE SYSTEM

MINIMUM DEPTH MEASURED ON TEST SAMPLE

EQUIPMENT : ULTRA IMAGE

PROBE + SERIAL : 0.25" Ø 8MHz GD

DEFECT TYPE : NOTCHES OF WIDTH W mms

DEFECT No.	W mms	DEPTH mms					
		NOMINAL	ACTUAL	RUN NO.			
				1.1-1.8			
4	1.0	3.0	3.05	4.27			
10		4.0	4.04	5.18			
16		5.0	5.08	5.99			
22		6.0	5.97	6.71			
5	2.0	3.0	3.08	4.27			
11		4.0	4.14	5.18			
17		5.0	4.98	5.69			
23		6.0	6.22	7.11			
6	3.0	3.0	3.33	4.27			
12		4.0	4.19	5.18			
18		5.0	5.13	5.79			
24		6.0	5.92	6.50			

TABLE 5

RESULTS OBTAINED WITH THE D.N.V. CORROSCAN

MINIMUM DEPTH MEASURED ON TEST SAMPLE

EQUIPMENT: CORROSCAN U/W

PROBE AND SERIAL: MSEB4T

DEFECT TYPE: FLAT BOTTOM HOLES OF DIAMETER ϕ mms

DEFECT NO.	ϕ mms	DEPTH mms							
		NOMINAL	ACTUAL	RUN NO.					
				7.2	8	9	24	25	24.5
1	1.0	3.0	3.25	6.2	*	*	*	*	*
7	"	4.0	4.01	*	*	*	*	*	*
13	"	5.0	5.49	*	*	*	*	*	*
19	"	6.0	5.97	*	*	*	*	*	*
2	2.0	3.0	3.23	4.2	4.2	3.8	4.2	4.2	3.6
8	"	4,9	4.12	5.2	5.2	4.8	4.8	4.8	5.2
14	"	5.0	4.98	5.6	5.6	5.6	5.8	5.8	5.8
20	"	6.0	6.10	6.4	6.4	6.4	6.6	6.6	6.8
3	3.0	3.0	3.13	4.4	4.2	4.2	4.2	4.2	3.8
9	"	4.0	4.12	4.4	4.4	4.4	4.8	4.2	4.4
15	"	5.0	5.03	5.8	5.8	6.2	Error	5.6	5.4
21	"	6.0	6.15	6.2	6.2	6.2	6.2	5.6	5.8

TABLE 6

RESULTS OBTAINED WITH THE DNV CORROSCAN

MINIMUM DEPTH MEASURED ON TEST SAMPLE

EQUIPMENT : CORROSCAN U/W

PROBE + SERIAL : MSEB4T

DEFECT TYPE : NOTCHES OF WIDTH W mms

DEFECT NO	W mms	DEPTH mms				
		NOMINAL	ACTUAL	RUN NO		
				24	25	24.5
4	1.0	3.0	3.05	*	*	*
10		4.0	4.04	*	*	*
16		5.0	5.08	*	*	*
22		6.0	5.97	*	*	*
5	2.0	3.0	3.08	4.2	4.2	3.6
11		4.0	4.14	4.8	4.8	5.2
17		5.0	4.98	5.8	5.8	5.8
23		6.0	6.22	6.6	6.6	6.8
6	3.0	3.0	3.33	4.2	4.2	3.8
12		4.0	4.19	4.8	4.2	4.4
18		5.0	5.13	Error	5.6	5.4
24		6.0	5.29	6.2	5.6	5.8

TABLE 7

RESULTS OBTAINED WITH THE PRIMSCAN SYSTEM

MINIMUM DEPTH MEASURED ON TEST SAMPLE

EQUIPMENT : PRIMSCAN

PROBE + SERIAL : MSEB4H (B)

DEFECT TYPE : FLAT BOTTOM HOLES OF DIAMETER ϕ mms

DEFECT NO	Ø mms	DEPTH mms			
		NOMINAL	ACTUAL	RUN NO	
				39.4	39.5
1	1.0	3.0	3.25	*	*
7	"	4.0	4.01	-	-
13	"	5.0	5.49	-	-
19	"	6.0	5.97	-	-
2	2.0	3.0	3.23	*	3.2
8	"	4.0	4.12	-	-
14	"	5.0	4.98	-	-
20	"	6.0	6.10	-	-
3	3.0	3.0	3.13	3.2	3.0
9	"	4.0	4.12	-	-
15	"	5.0	5.03	-	-
21	"	6.0	6.15	-	-

TABLE 8

RESULTS OBTAINED WITH THE PRIMSCAN SYSTEM

MINIMUM DEPTH MEASURED ON TEST SAMPLE

EQUIPMENT : PRIMSCAN

PROBE AND SERIAL : MSEB4T

DEFECT TYPE : FLAT BOTTOM HOLES OF DIAMETER Ø mms

DEFECT NO.	Ø mms	DEPTH mms			
		NOMINAL	ACTUAL	RUN NO.	
				18.3/18.6	
1	1.0	3.0	3.25	*	
7	1.0	4,9	4,91	-	
13	1.0	5.0	5.49	-	
19	1.0	6.0	5.97	+	
2	2.0	3.0	3.23	4.0	4.0
8	2.0	4.0	4.12	-	
14	2.0	5.0	4.98	-	
20	2.0	6.0	6.10	6.2	
3	3.0	3.0	3.13	3.5-4.1	3.7
9	3.0	4.0	4.12	-	
15	3.0	5.0	5.03	-	
21	3.0	6.0	6.15	6.2-6.4	

* Not detected

\- Not tested

\+ Detected but not sized

TABLE 9

RESULTS OBTAINED WITH THE PRIMSCAN SYSTEM

MINIMUM DEPTH MEASURED ON TEST SAMPLE

EQUIPMENT : PRIMSCAN

PROBE AND SERIAL : MSEB4T

DEFECT TYPE : NOTCHES OF WIDTH W mms

DEFECT NO.	W mm	DEPTH mms			
		NOMINAL	ACTUAL	RUN NO.	
				18.4/18.5	
4	1.0	3.0	3.05	4.0-4.4	
10	1.0	4.0	4.04	-	
16	1.0	5.0	5.08	-	
22	1.0	6.0	5.97	6.1-6.2	
5	2.0	3.0	3.08	3.5-3.9	
11	2.0	4.0	4.14	-	
17	2.0	5.0	4.98	-	
23	2.0	6.0	6.22	6.0-6.3	
6	3.0	3.0	3.33	3.3-3.5	
12	3.0	4.0	4.19	-	
18	3.0	5.0	5.13	-	
24	3.0	6.0	5.92	5.9-6.1	

- Test not performed

TABLE 10

RESULTS OBTAINED WITH THE PRIMSCAN SYSTEM

MINIMUM DEPTH MEASURED ON TEST SAMPLE

EQUIPMENT: PRIMSCAN

PROBE + SERIAL: SEB5KF3 (A)

DEFECT TYPE: Flat Bottom Holes of Diameter Ø mms

DEFECT NO	Ø mms	DEPTH mms		
		NOMINAL	ACTUAL	RUN NO 11.1 - 11.6
1	1.0	3.0	3.25	*
7	1.0	4.0	4.01	*
13	1.0	5.0	5.49	*
19	1.0	6.0	5.97	*
2	2.0	3.0	3.23	3.5
8	2.0	4.0	4.12	4.3
14	2.0	5.0	4.98	4.8
20	2.0	6.0	6.10	5.7
3	3.0	3.0	3.13	3.5
9	3.0	4.0	4.12	4.3
15	3.0	5.0	5.03	4.7
21	3.0	6.0	6.15	5.8

TABLE 11

RESULTS OBTAINED WITH THE PRIMSCAN SYSTEM

EQUIPMENT: PRIMSCAN

PROBE + SERIAL: SEB5KF3(A)

DEFECT TYPE: Notches of Width W mms

DEFECT NO	W mms	DEPTH mms		
		NOMINAL	ACTUAL	RUN NO 11.7 - 11.9
4	1.0	3.0	3.05	3.6
10		4.0	4.04	-
16		5.0	5.08	4.7
22		6.0	5.97	-
5	2.0	3.0	3.08	3.5
11		4.0	4.14	-
17		5.0	4.98	5.0
23		6.0	6.22	-
6	3.0	3.0	3.33	3.7
12		4.0	4.19	-
18		5.0	5.13	5.0
24		6.0	5.92	-

TABLE 12

RESULTS OBTAINED WITH THE P SCAN SYSTEM

MINIMUM DEPTH MEASURED ON TEST SAMPLE

EQUIPMENT: ABOVE WATER CORROSCAN

PROBE + SERIAL: MSEB4T No 1

DEFECT TYPE: FLAT BOTTOM HOLES OF DIAMETER Ø mms

DEFECT NO	Ø mms	DEPTH mms							
		NOMINAL	ACTUAL	RUN NO					
				1.2/1.3	1.4/1.5	14.0/14.1	1.0	1.1	Average
1	1.0	3.0	3.25	*	*	5.8	6.6	*	
7	"	4.0	4.01	*	*	*	*	*	
13	"	5.0	5.49	*	*	*	*	*	
19	"	6.0	5.97	*	Error	*	7.2	*	
2	2.0	3.0	3.23	4.2	4.4	4.4	4.4	4.4	4.36
8	2.0	4.0	4.12	4.8	4.8	4.4	5.4	5.2	4.92
14	"	5.0	4.98	5.4	5.4	4.4	5.8	5.8	5.36
20	"	6.0	6.10	6.4	Error	6.2	6.4	7.2	6.55
3	3.0	3.0	3.13	4.4	4.2	4.4	4.4	3.6	4.22
9	"	4.0	4.12	4.4	4.4	4.4	4.6	4.4	4.4
15	"	5.0	5.03	4.8	4.8	4.4	5.4	5.4	4.96
21	"	6.0	6.15	5.8	Error	5.4	7.2	6.2	6.15

TABLE 13

RESULTS OBTAINED WITH THE P SCAN SYSTEM

MINIMUM DEPTH MEASURED ON TEST SAMPLE

EQUIPMENT : AWS CORROSCAN

PROBE + SERIAL : MSEB4T No 1

DEFECT TYPE : NOTCHES OF WIDTH W mms

DEFECT NO	W mms	DEPTH mms							
		NOMINAL	ACTUAL	RUN NO					
				1.2/1.3	1.4/1.5	14.0/14.1	1.0	1.1	AVERAGE VALUES
4	1.0	3.0	3.05	5.2	4.8	4.4	5.2	5.4	
10		4.0	4.04	5.2	4.8	4.8	5.4	5.4	
16		5.0	5.08	5.8	5.8	4.8	6.2	6.2	
22		6.0	5.97	6.6	Error	5.6	7.2	7.2	
5	2.0	3.0	3.08	4.2	4.4	4.2	4.4	3.8	4.2
11		4.0	4.14	4.4	4.4	4.2	4.8	4.6	4.5
17		5.0	4.98	5.2	4.8	4.6	5.6	5.6	5.05
23		6.0	6.22	5.8	Error	5.4	6.6	6.4	6.05
6	3.0	3.0	3.33	4.2	4.2	4.4	4.4	3.6	4.15
12		4.0	4.19	4.2	4.4	4.4	4.8	4.4	4.5
18		5.0	5.13	4.8	4.4	4.4	5.4	5.2	5.0
24		6.0	5.92	5.4	Error	4.8	6.2	5.8	5.6

TABLE 14

RESULTS OBTAINED WITH THE PSCAN SYSTEM

MINIMUM DEPTH MEASURED ON TEST SAMPLE

EQUIPMENT: ABOVE WATER CORROSION

PROBE & SERIAL: SEB5KF3

DEFECT TYPE : FLAT BOTTOM HOLES OF DIAMETER ϕ mms

DEFECT NO	ϕ mms	DEPTH mms			
		NOMINAL	ACTUAL	RUN No 15.0	RUN No 16.0/16.1
1	1.0	3.0	3.25	*	4.4
7	"	4.0	4.01	*	5.4
13	"	5.0	5.49	*	*
19	"	6.0	5.97	*	*
2	2.0	3.0	3.23	4.4	4.4
8	"	4.0	4.12	5.4	4.4
14	"	5.0	4.98	6.6	4.4
20	"	6.0	6.10	8.6	5.4
3	3.0	3.0	3.13	4.4	4.2
9	"	4.0	4.12	4.8	4.4
15	"	5.0	5.03	5.8	4.4
21	"	6.0	6.15	6.8	5.2

TABLE 15

RESULTS OBTAINED WITH THE PSCAN SYSTEM

MINIMUM DEPTH MEASURED ON TEST SAMPLE

EQUIPMENT: AWS CORROSCAN

PROBE & SERIAL : SEB5KF3

DEFECT TYPE: NOTCHES OF WIDTH W mms

DEFECT NO.	W mms	DEPTH mms			
		NOMINAL	ACTUAL	RUN NO	
				15.0	16.0/16.1
4	1.0	3.0	3.05	4.4	4.2
10		4.0	4.04	5.6	4.4
16		5.0	5.08	6.2	4.6
22		6.0	5.97	8.2	6.4
5	2.0	3.0	3.08	4.4	4.2
11		4.0	4.14	4.8	4.4
17		5.0	4.98	6.2	4.4
23		6.0	6.22	7.2	5.4
6	3.0	3.0	3.33	4.4	4.4
12		4.0	4.19	4.8	4.4
18		5.0	5.13	5.4	4.4
24		6.0	5.92	6.2	4.6

TABLE 16 INFORMATION ON THE FOUR PIPE TEST SECTIONS TESTED

	Pipe 1	Pipe 2	Pipe 3	Pipe 4
Description:	Welded	Seamless	Welded	Electric welded
Nominal Diameter:	12 inches (30.48 cm)	12 inches (30.48 cm)	12 inches (30.48 cm)	12 inches (30.48 cm)
Wall Thickness:	0.265 inches (6.731 mm)	0.260 inches (6.604 mm)	0.405 inches (10.287)	0.250 inches (6.35 mm)
Length:	48 inches (121.92 cm)	48 inches (121.92 cm)	48 inches (121.92 cm)	48 inches (121.92 cm)
Testing Time:	200 hours	200 hours	12 months	96 hours
Macrohardness: (average)	114 BHN (67 RB)	143 BHN (78 RB)	N/A	N/A
Microhardness: (average)	147 VHN (140 BHN) (77.6 RB)	155 VHN (147.5 BHN) (80.2 RB)	N/A	N/A
AE Activity:	Concentrated	Sparse	Clustered	Concentrated
UT Method:	Manual	Manual	Computerised	Computerised
UT Indications:	Strong Agreement with AE	No Detected Defects	Initial Pipe Scan Acquired	Strong Agreement with AE
Metallography:	HIC Cracks Verified	No Cracks Detected	H.I.C. Cracks Verified	H.I.C. Cracks Verified
Microstructure:	Banded with NMI's	Banded and Clean	Banded	Banded

Chemical Analysis

Pipe Section

	C	S	P	Mn	Si	Cr	Cu	Nb	Ni
1	0.21	0.023	0.011	0.50	0.05	0.05	0.02	0.002	0.01
2	0.26	0.020	0.005	0.55	0.05	0.02	0.01	0.002	0.01
3	0.26	0.038	0.010	0.02	0.06	0.03	0.17	0.002	0.05
4	0.21	0.032	0.014	1.19	0.04	0.02	0.02	0.002	0.01

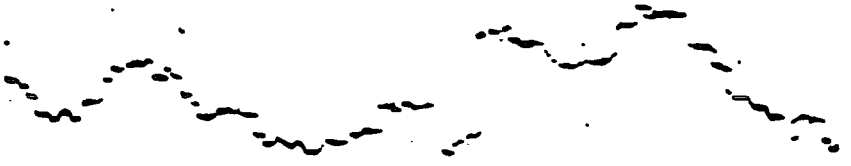

TYPICAL STEPWISE HIC FIG. 1

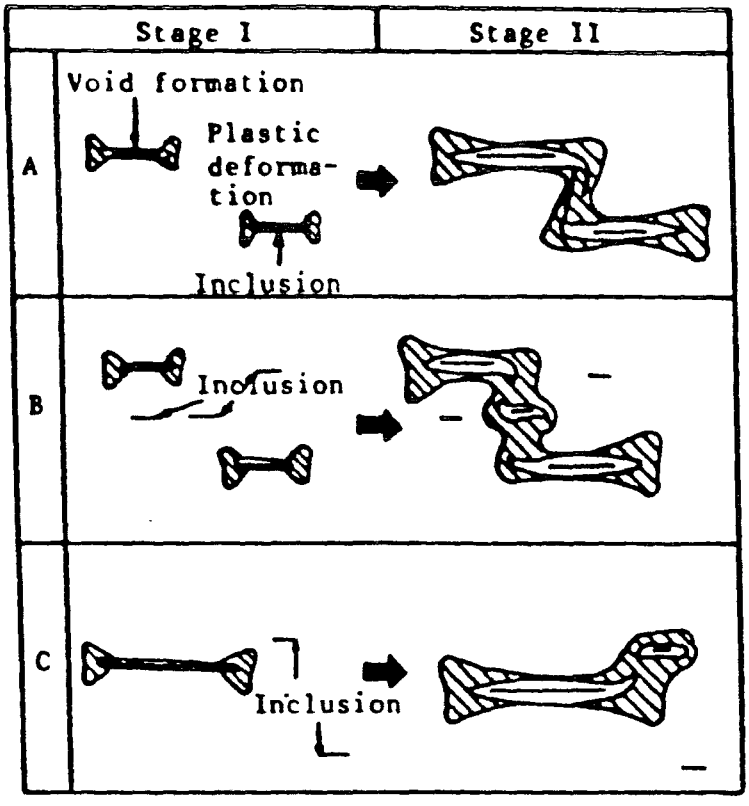

A The case of direct linkage between closely spaced crack sites.

B Creation of small cracks by the interaction of two main cracks. Joining between main crack and a small crack takes place by Mechanism A.

C Creation of small crack in front of main crack.

SCHEMATIC REPRESENTATION OF STEPWISE CRACKING PROCESS AFTER IKEDA ET AL

FIG. 2

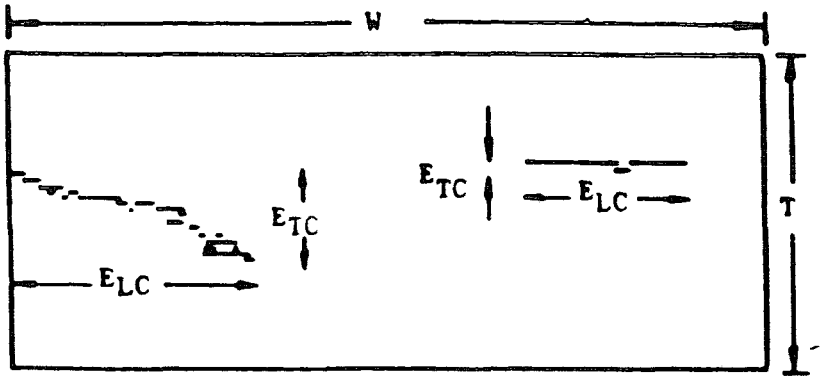

$$\text{Crack length ratio (CLR)} = \left[\frac{\Sigma E_{LC}}{W} \times 100\right] \%$$

$$\text{Crack thickness ratio (CTR)} = \left[\frac{\Sigma E_{TC}}{T} \times 100\right] \%$$

$$\text{Crack sensitivity ratio (CSR)} = \left[\frac{\Sigma\, E_{LC} \times E_{TC}}{W \times T} \times 100\right] \%$$

DEFINITION OF CRACK INDICES FIG. 3

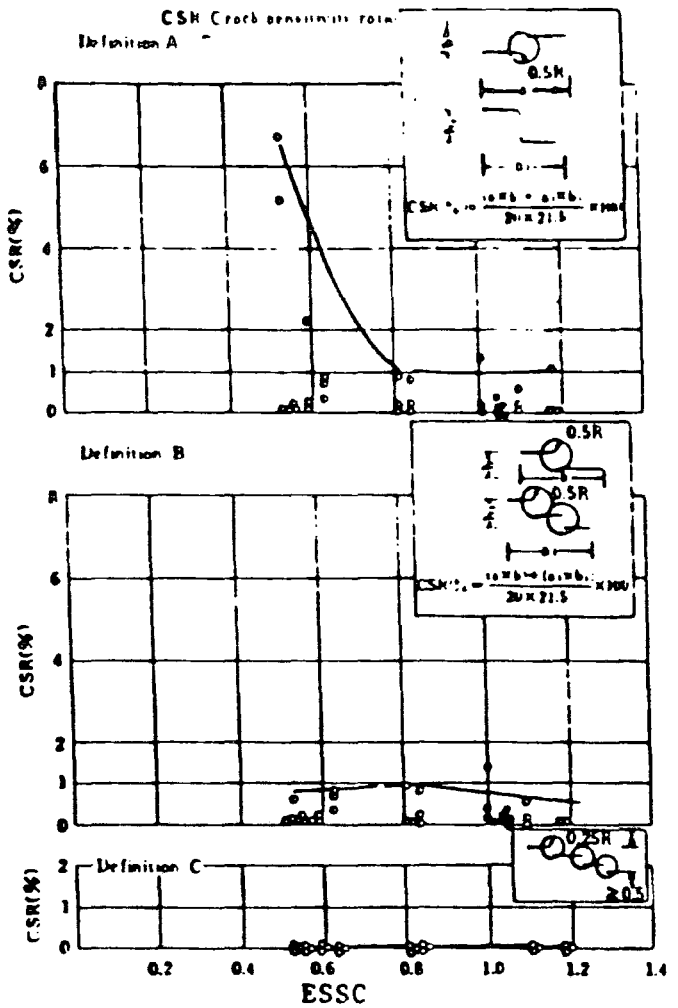

RELATION BETWEEN ESSC AND CSR DETERMINED BY DIFFERENT DEFINITIONS A, B AND C AFTER NSC [16]

FIG. 4

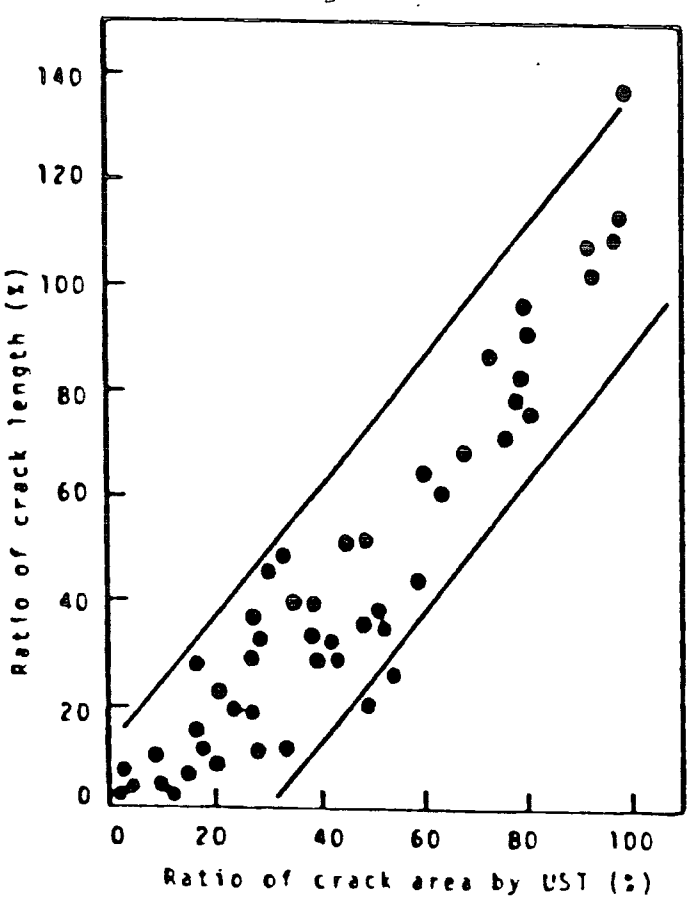

RELATIONSHIP BETWEEN RATIO OF CRACK LENGTH AND RATIO OF CRACK AREA BY UST
AFTER NAKAI ET AL [17]

FIG. 5

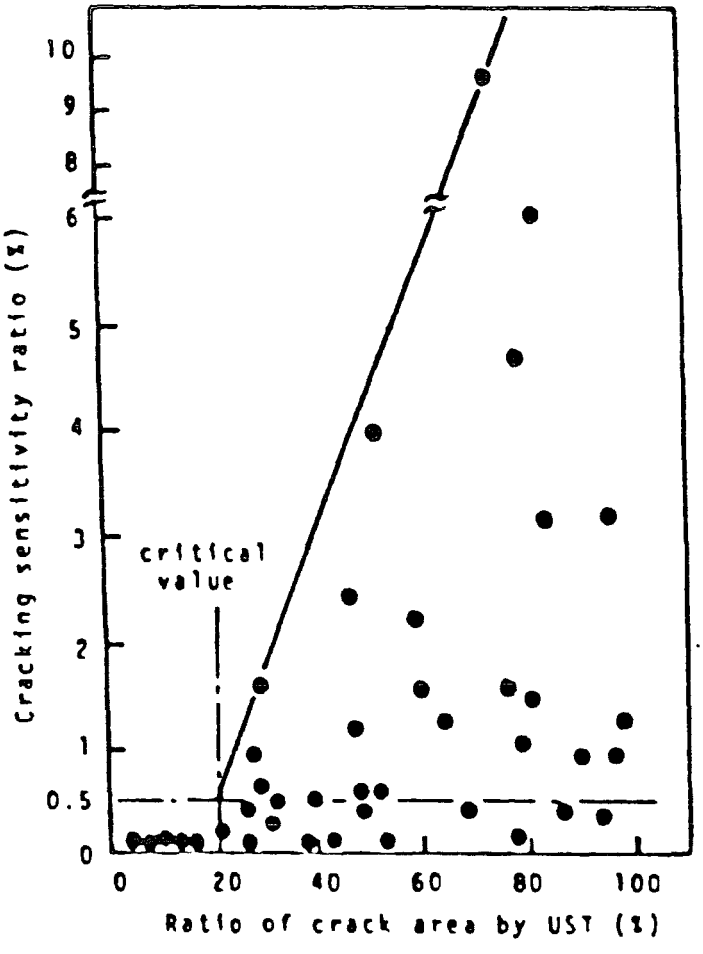

RELATIONSHIP BETWEEN CRACKING SENSITIVITY RATIO AND RATIO OF CRACK AREA BY UST AFTER NAKAI ET AL [17]

FIG. 6

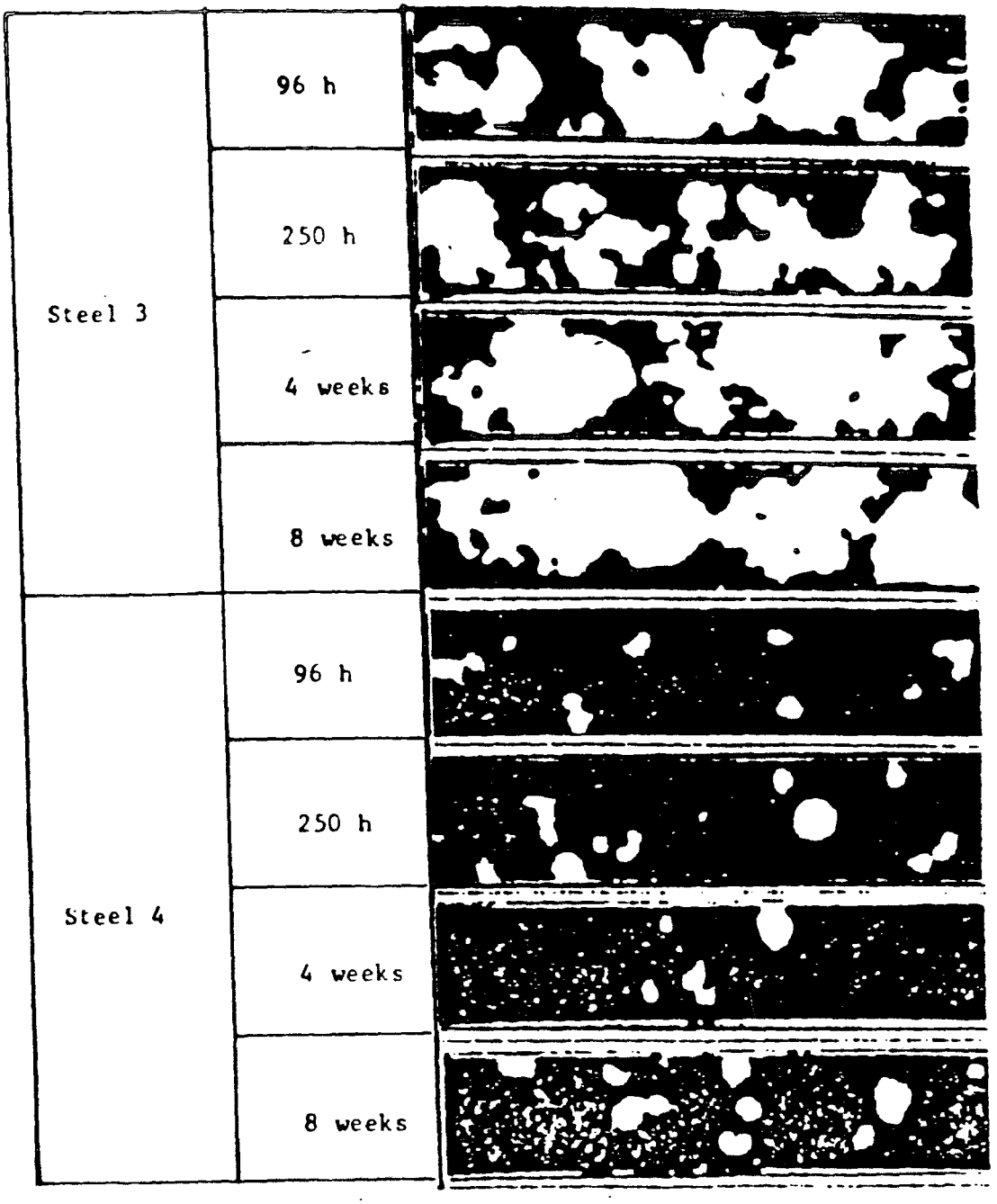

TYPICAL DISPLAY OBTAINED USING ULTRASONIC SCANNING FIG.7

AFTER TAIRA ET AL

Examination surfaces of Specimen X are x-y surfaces those of Specimen Y are x-z surfaces and those of Z are y-z surface

Specimen X is machined from the centre of plate thickness

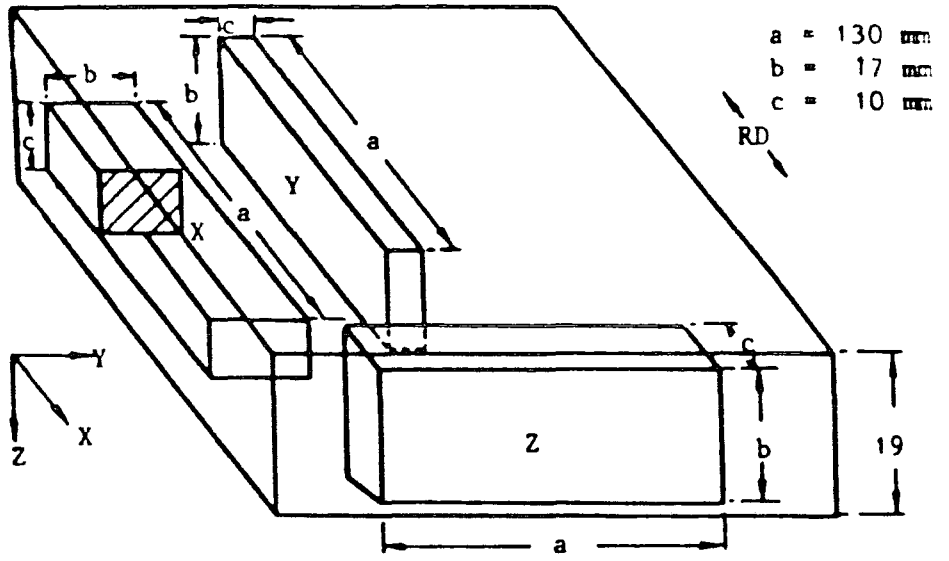

TEST SPECIMEN FOR THE EXAMINATION OF THE INFLUENCE OF SAMPLING METHOD ON HIC AFTER KOWAKA ET AL [19]

FIG. 8

C - Hydrogen content

Co - Hydrogen content at a corroded surface

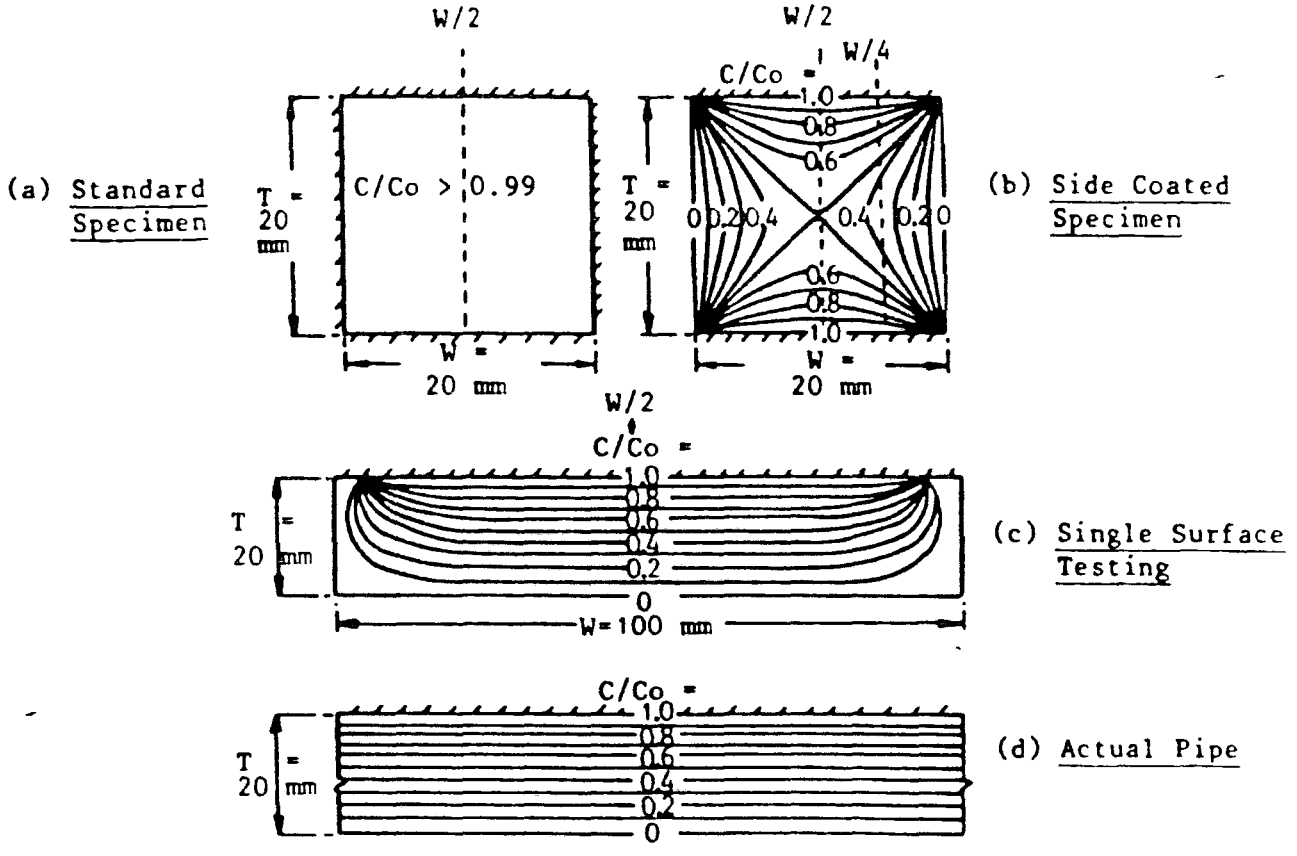

Assumed diffusion coefficient = 3.13×10^{-7} cm²/s
Test duration 96 h

ESTIMATED HYDROGEN DISTRIBUTION IN THE CROSS SECTION OF VARIOUS SPECIMEN CONFIGURATIONS AFTER TAIRA AND KOBAYASHI [20]

FIG. 9

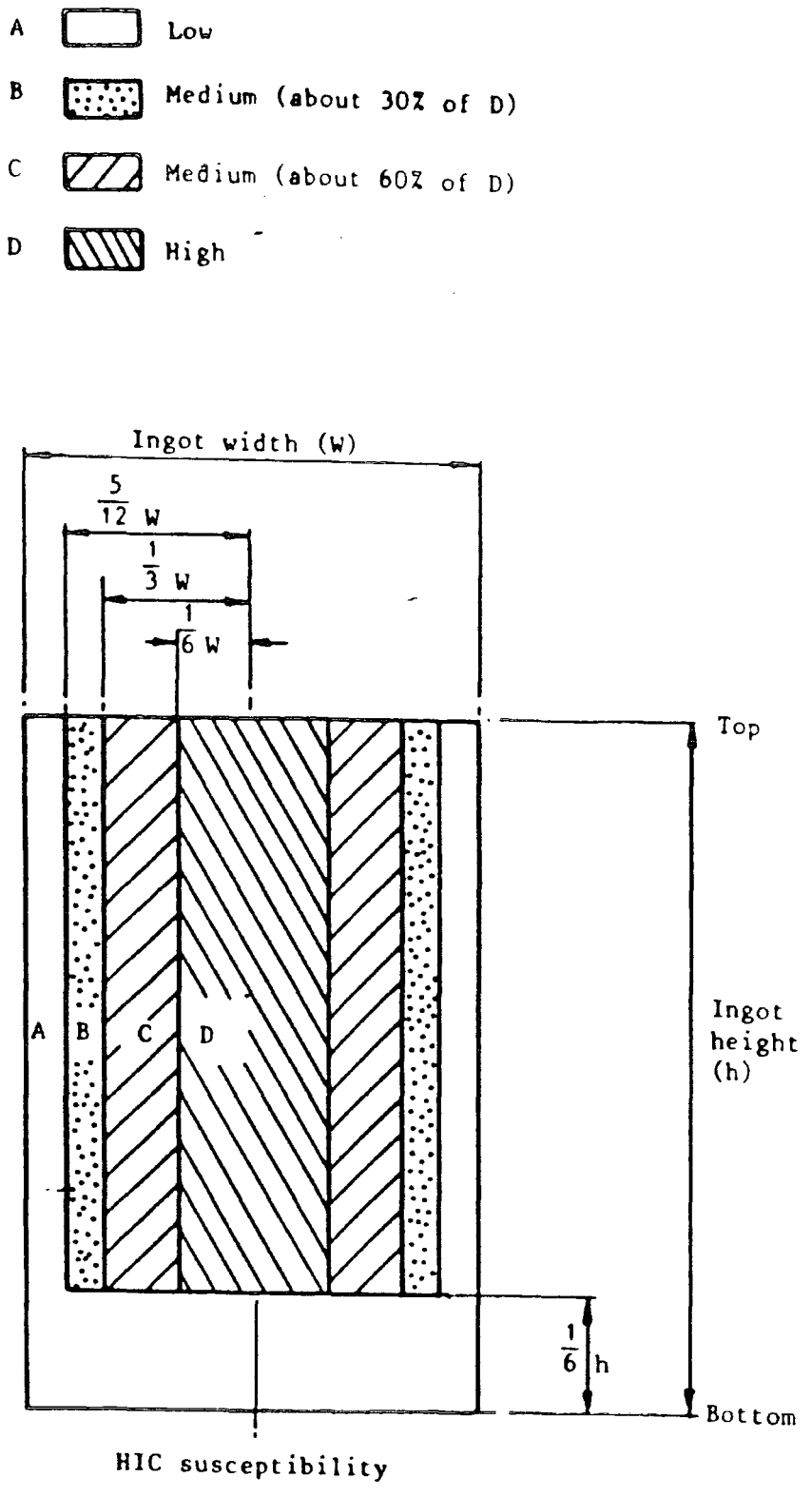

EFFECT OF INGOT LOCATION ON HIC SUSCEPTIBILITIES OF HOT ROLLED PRODUCTS AFTER IKEDA ET AL [23]

FIG. 10

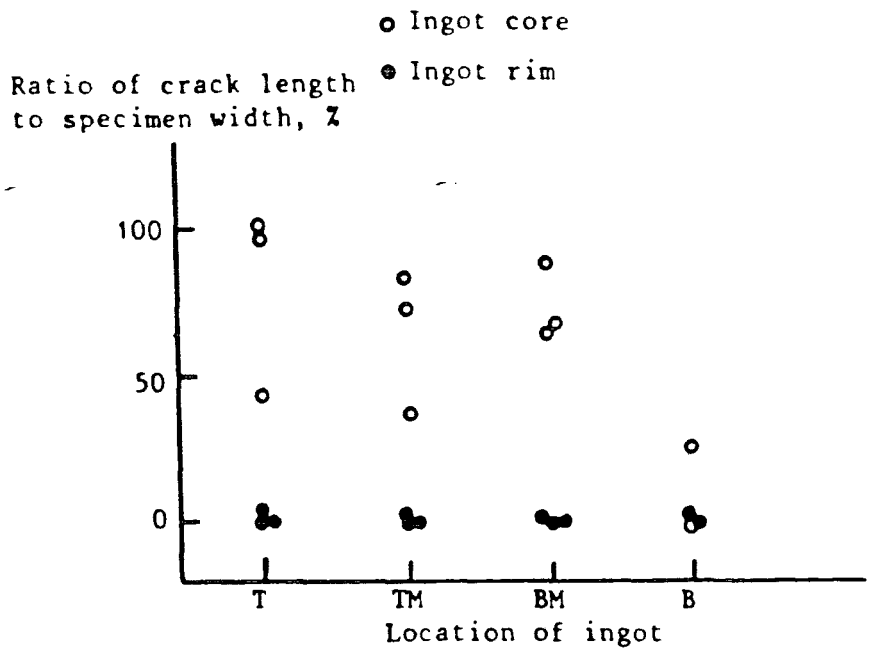

INFLUENCE OF SAMPLING LOCATION ALONG LENGTH OF INGOT ON HIC SUSCEPTIBILITY OF PLATE AFTER IKEDA ET AL [23]

FIG. 11

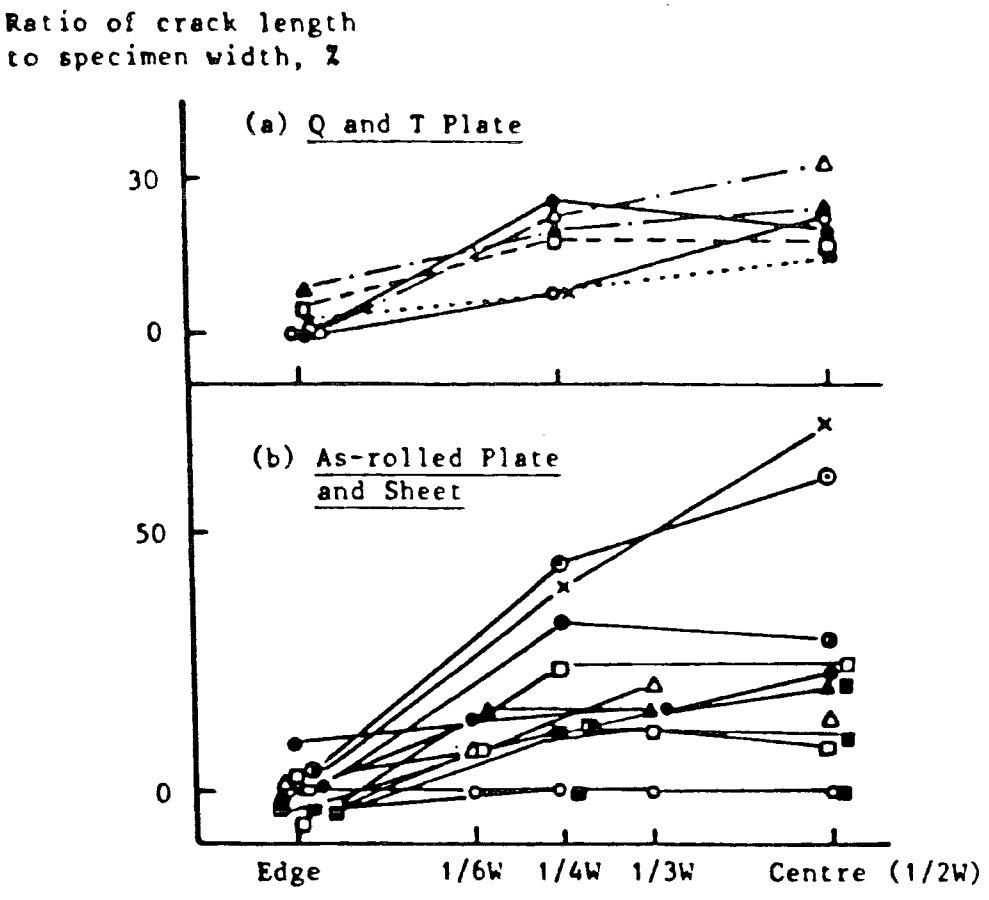

(Symbols refer to different steels)

INFLUENCE OF SAMPLING LOCATION ACROSS INGOT WIDTH ON HIC SUSCEPTIBILITY OF FLAT PRODUCTS AFTER IKEDA ET AL [23]

FIG. 12

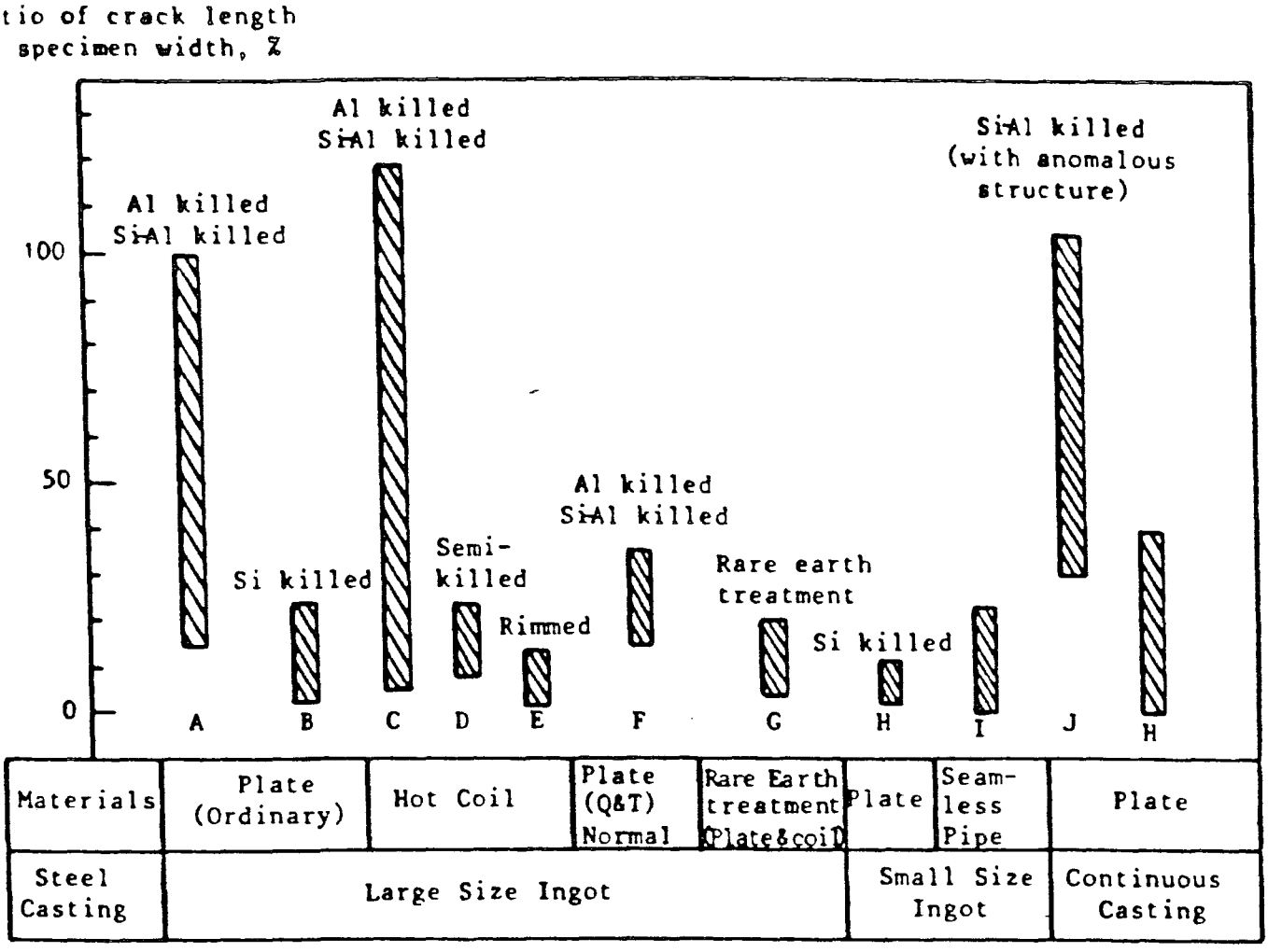

SUMMARY OF HIC SUSCEPTIBILITIES OF COMMERCIAL HOT ROLLED STEEL MATERIALS AFTER IKEDA ET AL 23

FIG.13

STEEL	C	Si	Mn	S	Cu	Ni	Cr	Mo	Nb	Al	INCLUSIONS
Al-killed steel	0.12	0.27	1.41	0.005	0.25	0.18	-	-	0.036	0.035	-Type II Mn S Al_2O_3
Si-Al-killed steel	0.17	0.26	1.23	0.011	-	-	0.15	0.041	-	0.008	-Type III Mn S Al_2O_3
Semi-killed steel	0.18	0.028	0.85	0.020	-	-	-	-	-	-	-Type I Mn S Silicates

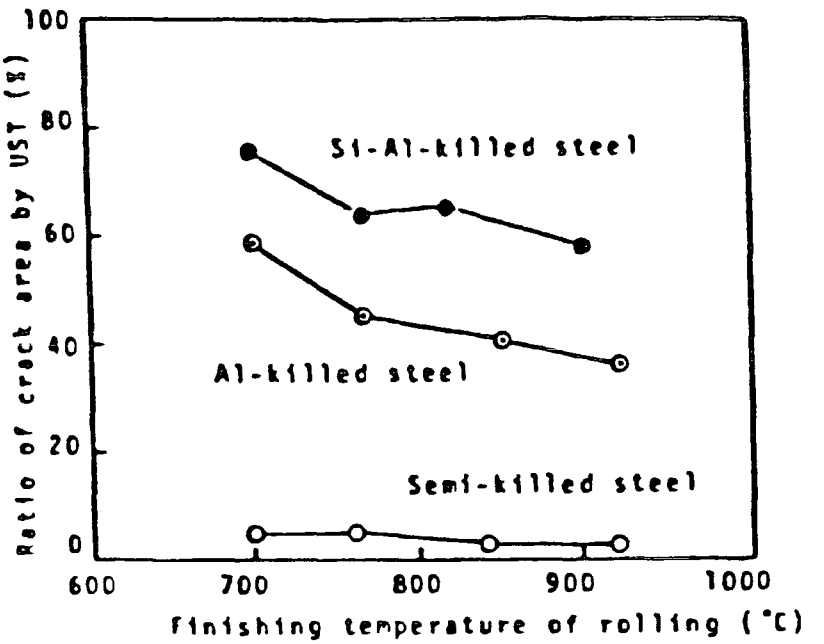

COMPARISON OF THE SUSCEPTIBILITY TO HIC BETWEEN SEMI-KILLED AND Al KILLED STEELS AFTER NAKAI ET AL.[17]

FIG. 14

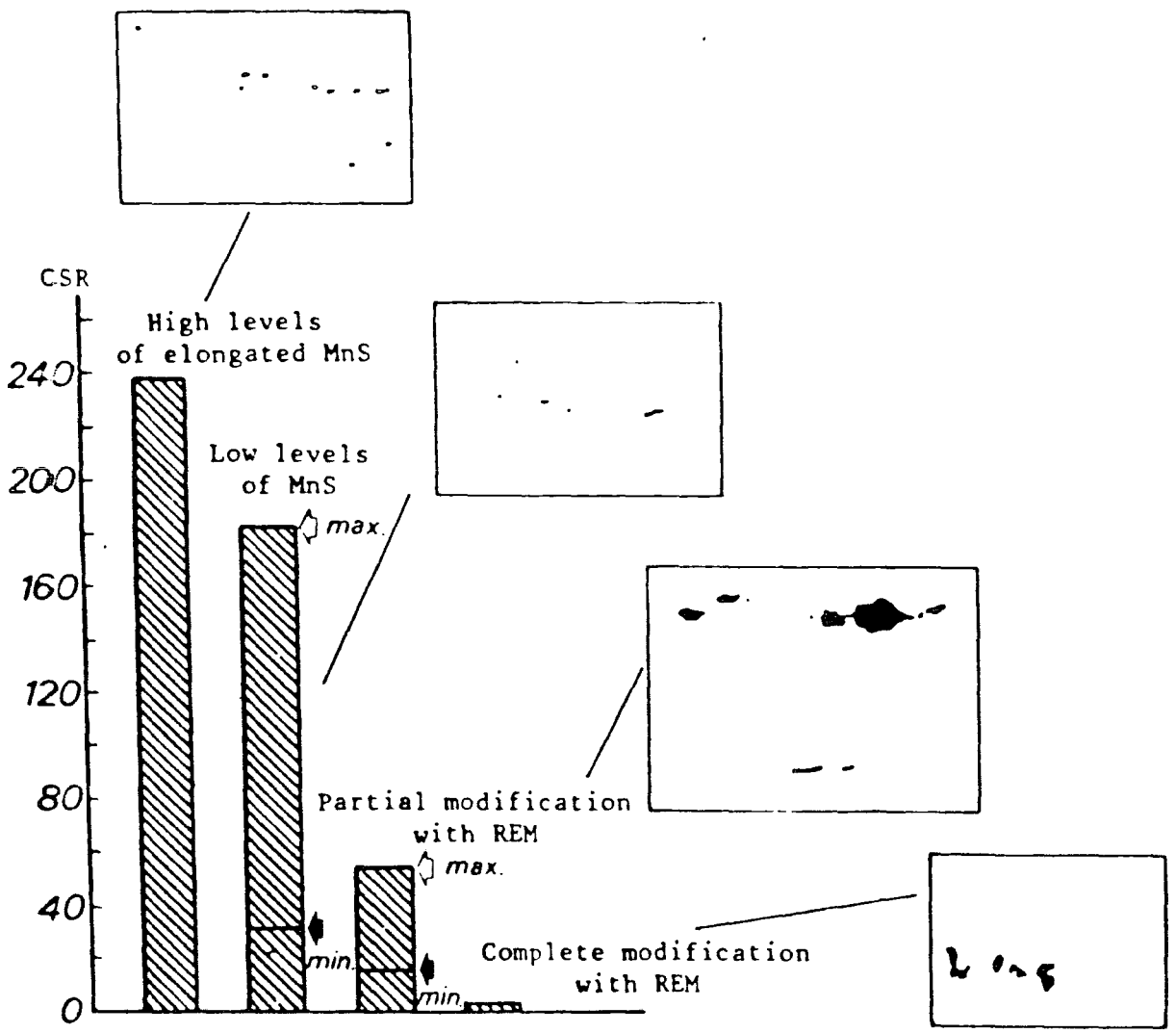

EFFECT OF SULPHIDE INCLUSION SHAPE ON CRACKING BEHAVIOUR FIG. 15

AFTER PARRINI AND De VITO[38]

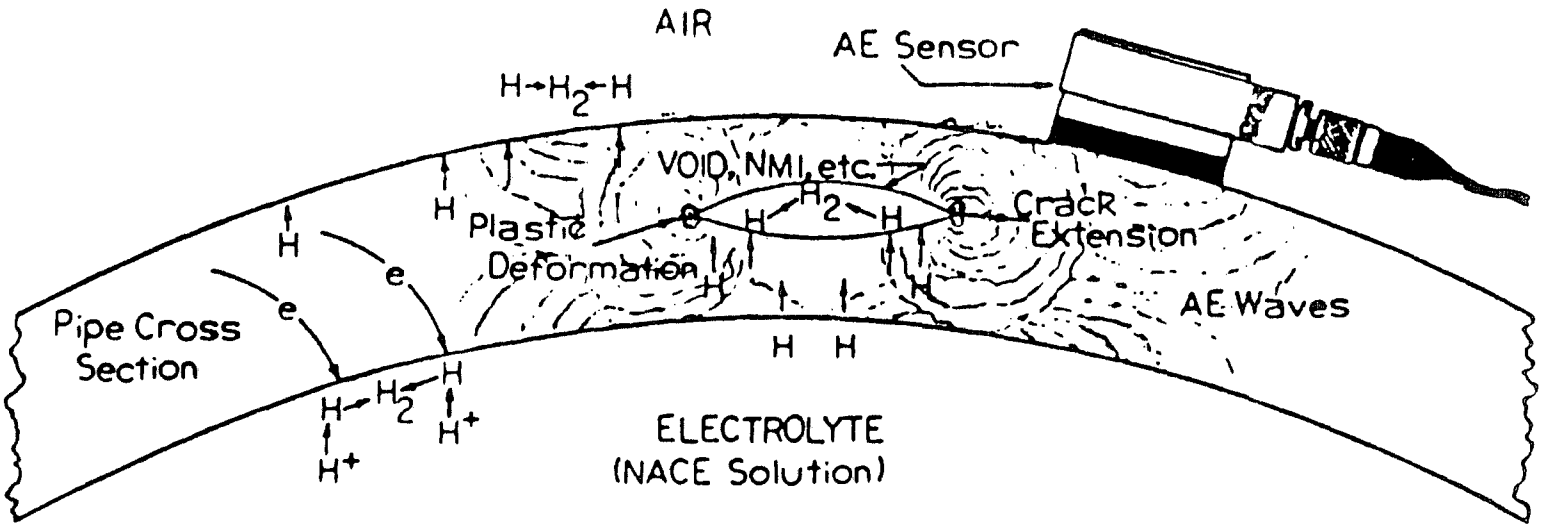

The Mechanism of Sulfide Corrosion Cracking (SCC):

(1) When there is an aqueous solution, H_2S is ionized in it.
$H_2S \rightarrow 2H^+ + S^{2-}$ (in aqueous solution)

(2) Fe in steel is ionized and dissolved in the solution (anodic reaction).
$Fe \rightarrow Fe^{2+} + 2e^-$ (into aqueous solution)

(3) H^+ ions combine with electrons and thus in atomized form the hydrogen migrates into the steel (cathodic reaction).
$H^+ + e^- \rightarrow H$ (actually a multi-stage process)

Figure 16 Representation of HIC Mechanism Showing an Acoustic Emission Sensor Attached to Test Piece for Observation.

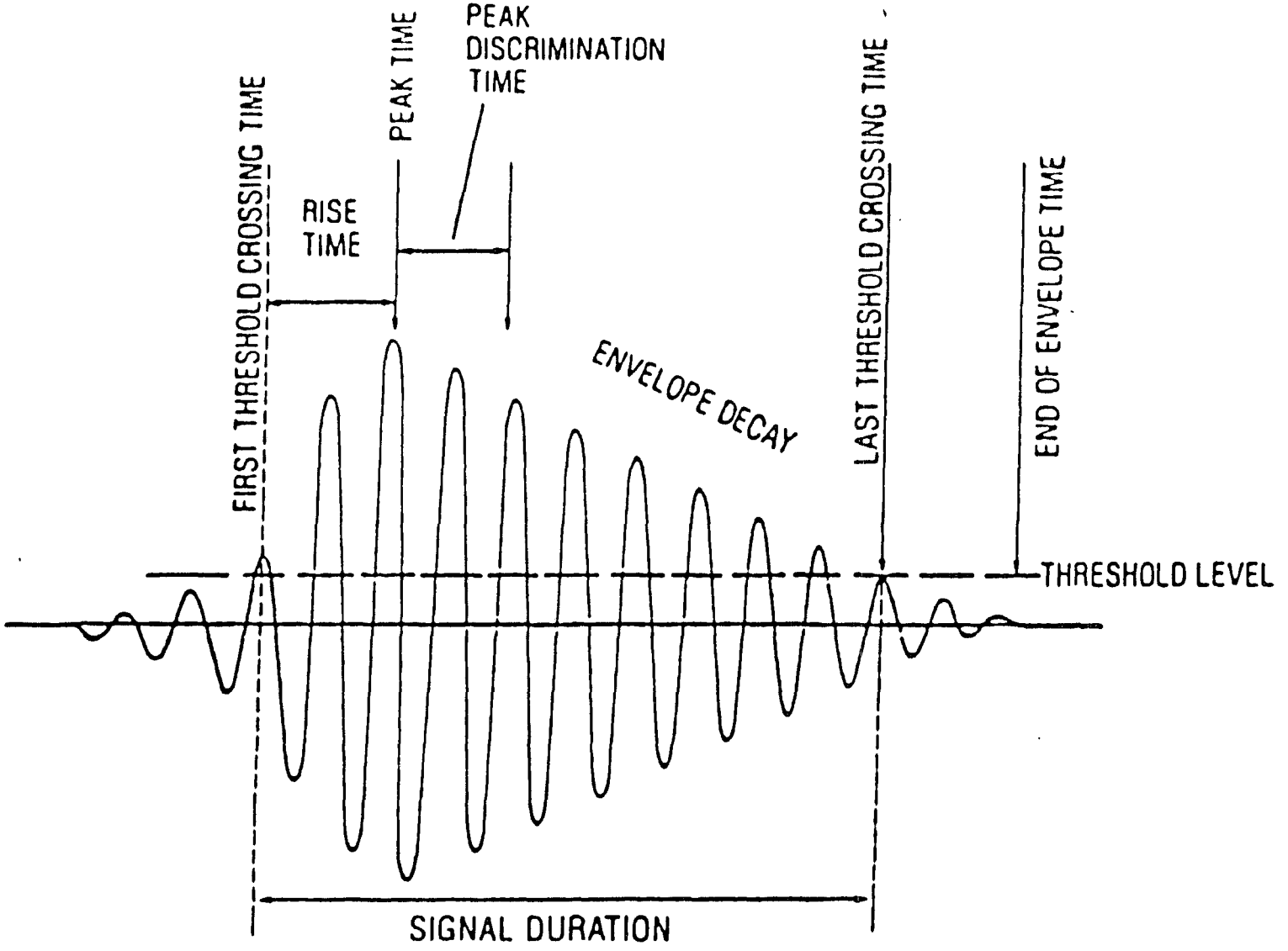

Figure 17 Analysis of Simple Waveform.

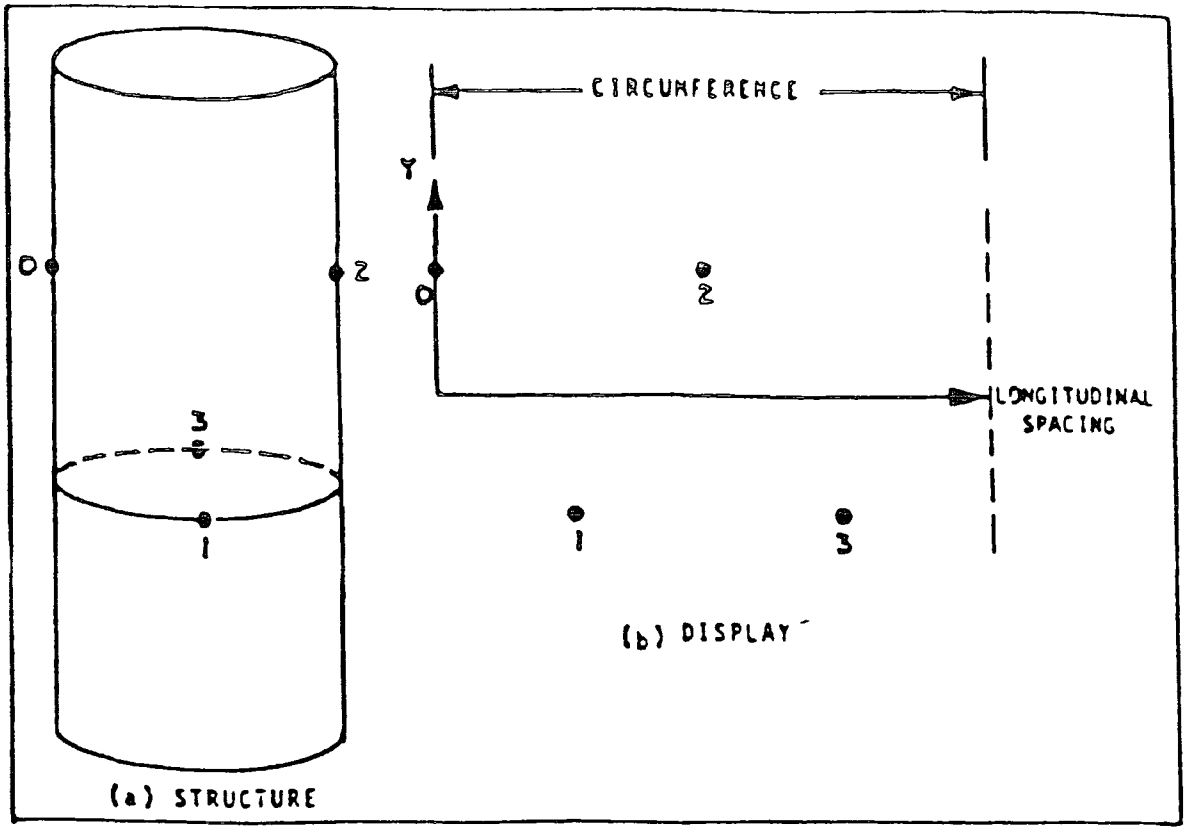

Cylindrical Array.

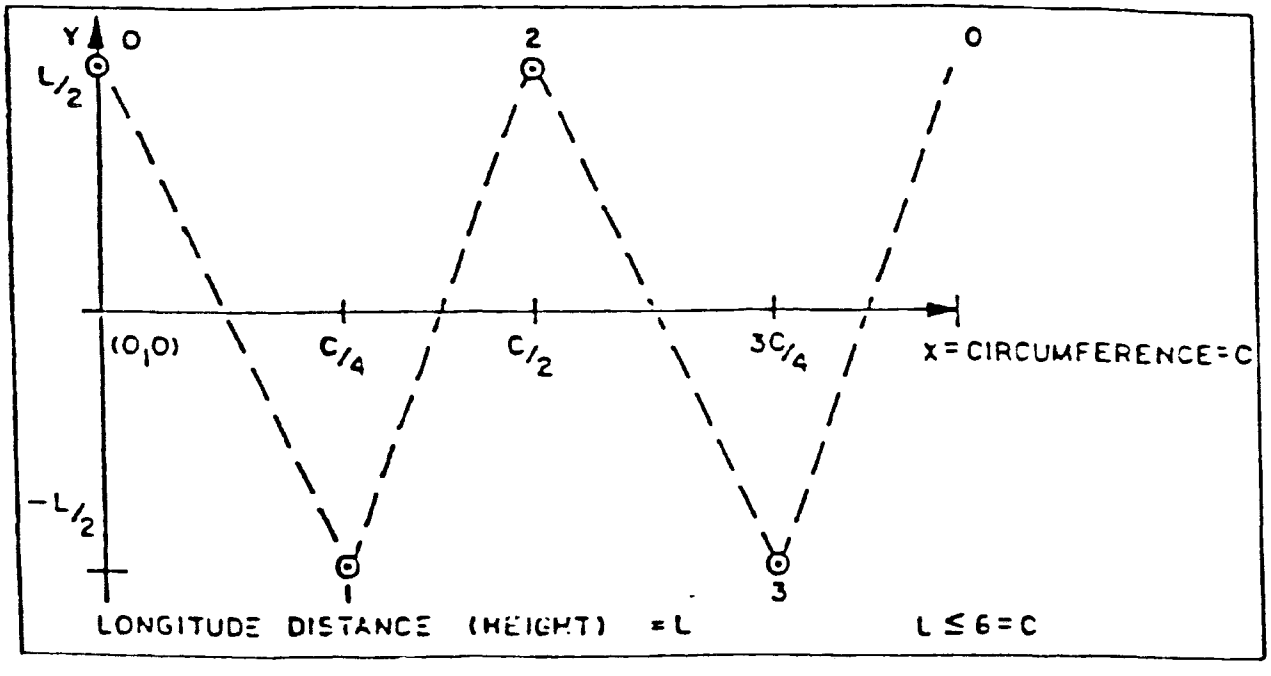

Figure 18 Cylindrical Array Unwrapped.

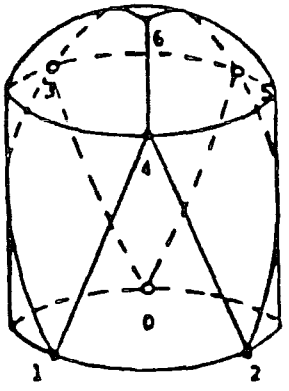

The structure with sensor locations. Circumference = 15', height = 5' to cap.

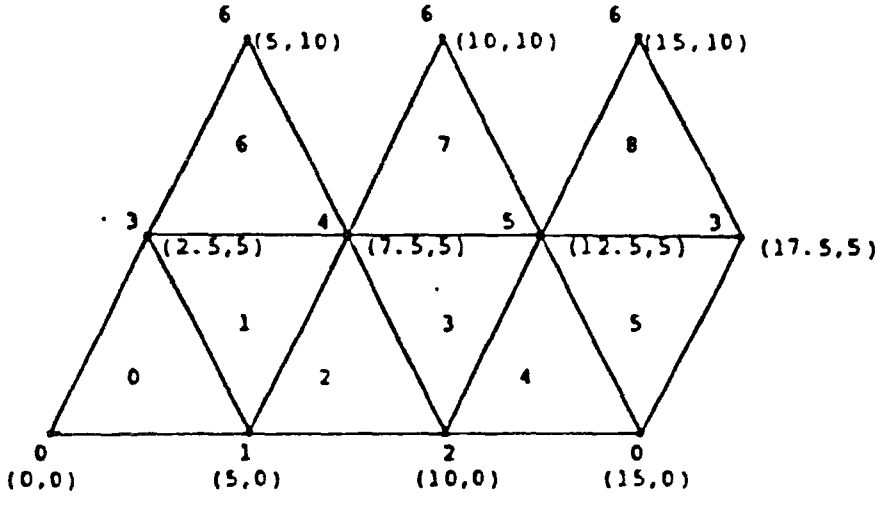

The display layout with array numbers, sensor numbers, and sensor coordinates. Note that the same sensor may appear at different locations in different arrays. Only the sensors and events will appear on location plots; there will be no lines or numbers.

Figure 19

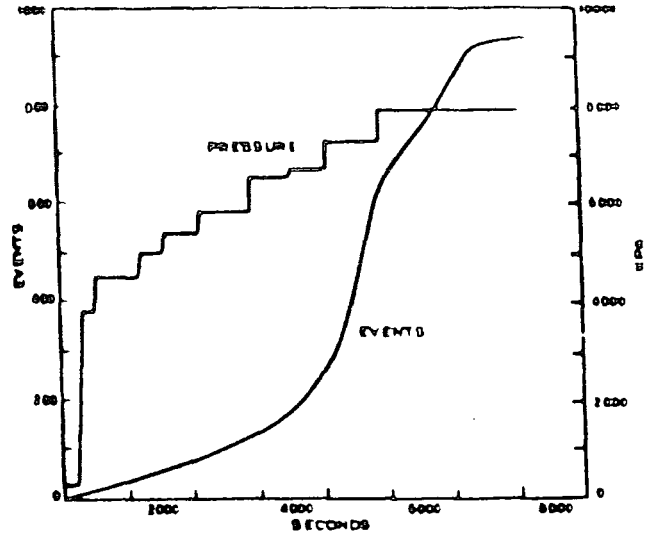

FIG. 20 *Event-pressure record for nozzle 2.*

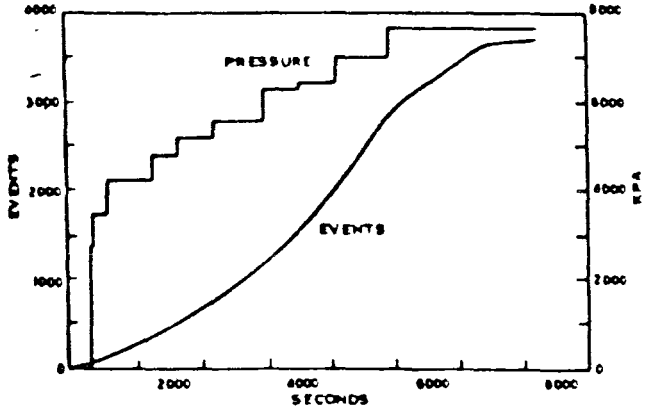

FIG. 20 *Event-pressure record for nozzle 3.*

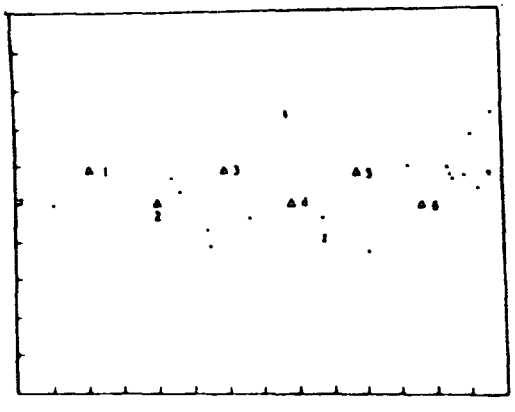

FIG. 21 *Source location map, nozzle 2.*

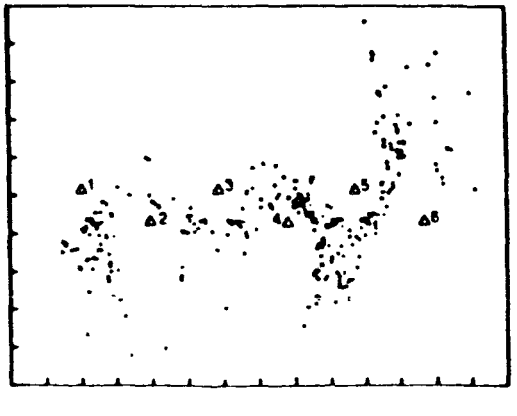

FIG. 21 *Source location map, nozzle 3.*

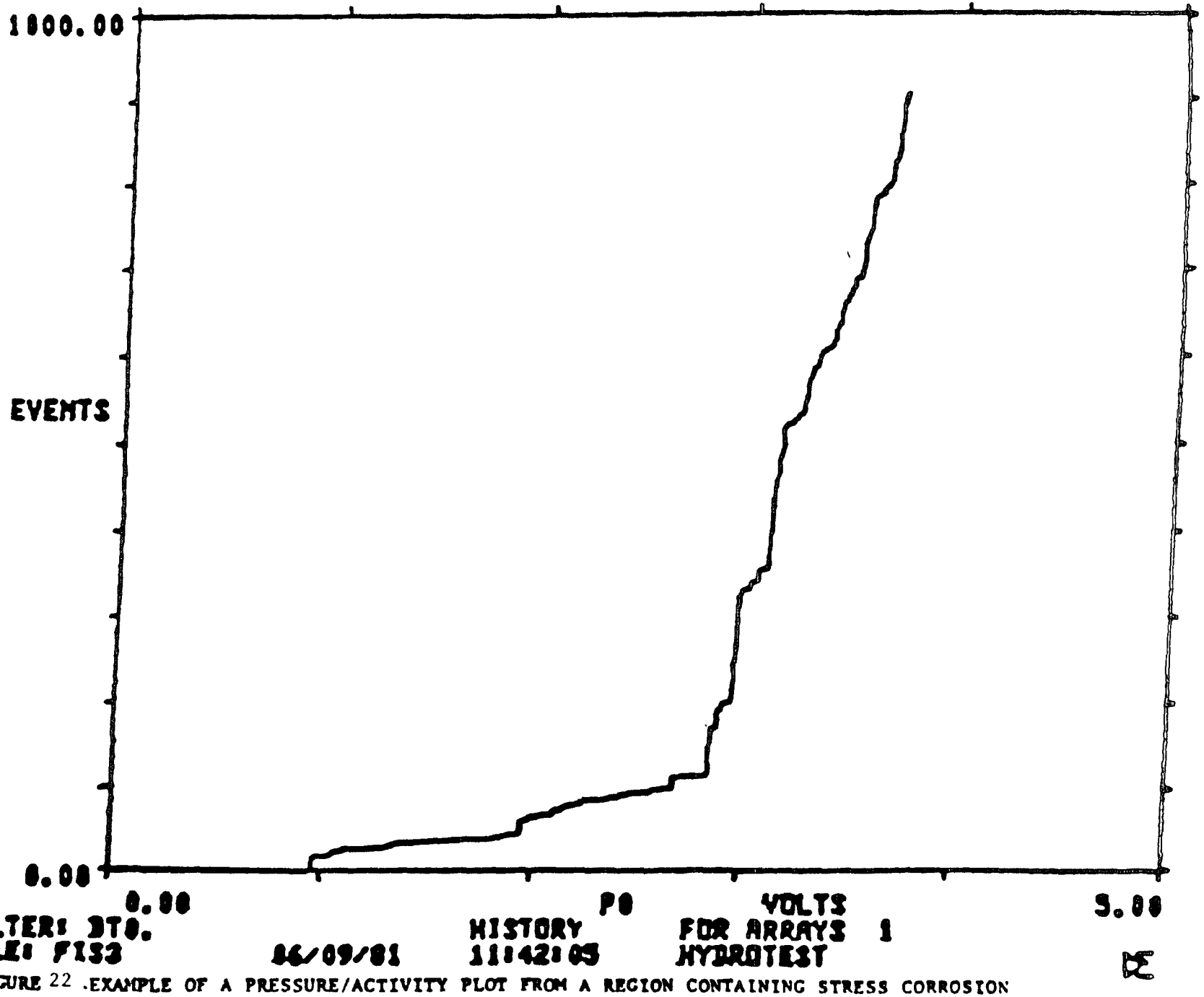

FIGURE 22 .EXAMPLE OF A PRESSURE/ACTIVITY PLOT FROM A REGION CONTAINING STRESS CORROSION CRACKS

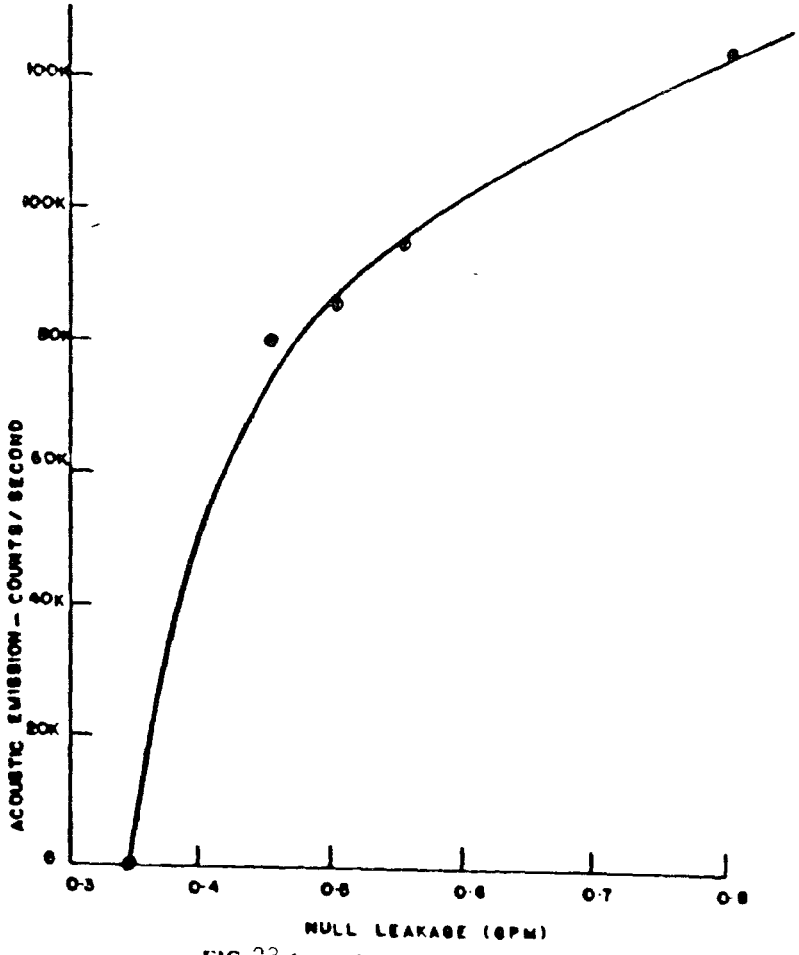

FIG. 23 *Acoustic emission versus leak rate.*

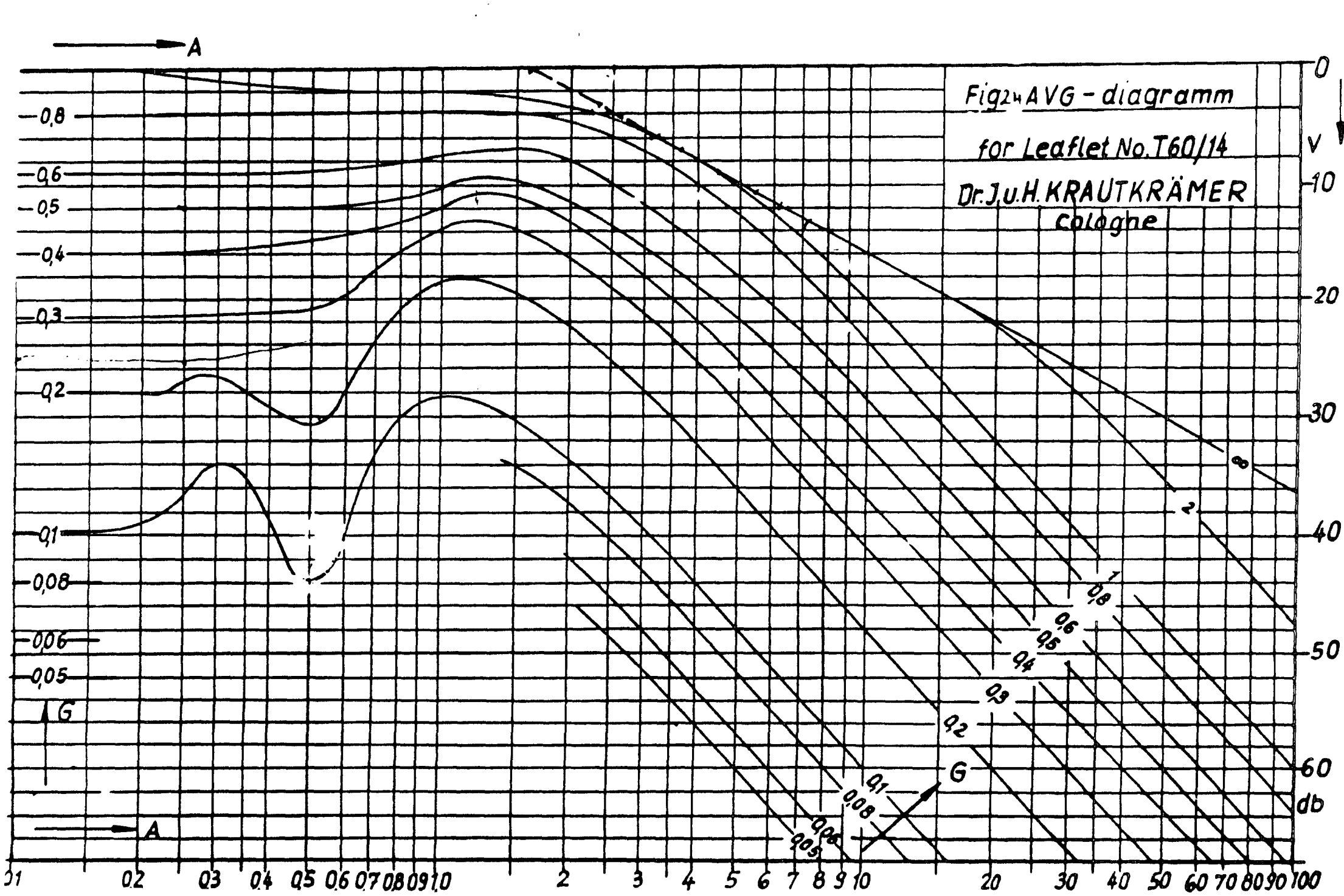
A
0,8
0,6
0,5
0,4
0,3
0,2
0,1
0,08
0,06
0,05
G
A
0
V
10
20
30
40
50
60
db
Fig24 AVG - diagramm
for Leaflet No. T60/14
Dr. J. u. H. KRAUTKRÄMER
Cologne
8
2
1
0,8
0,6
0,5
0,4
0,3
0,2
0,1
0,08
0,06
0,05
G
01 02 03 04 05 06 07 08 09 10 2 3 4 5 6 7 8 9 10 20 30 40 50 60 70 80 90 100

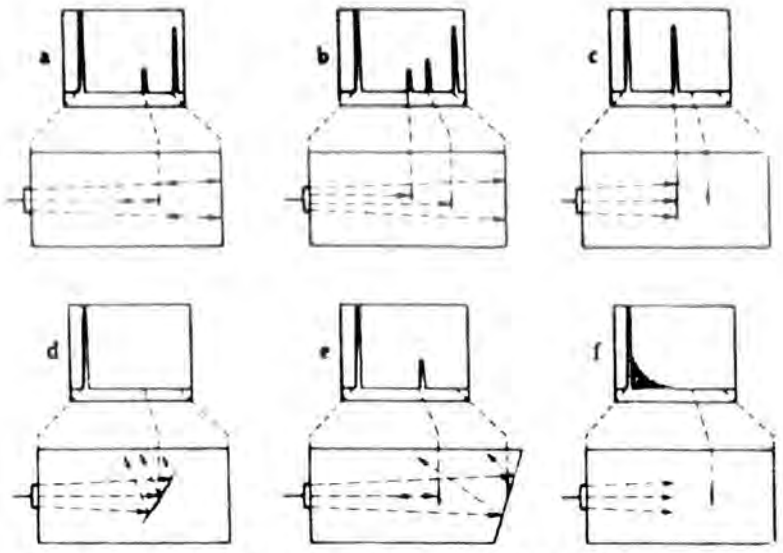

g Schematic screen pictures obtained by the pulse echo method. a) Small flaw in sound beam. b) two small flaws in sound beam. c) large flaw in sound beam, smaller second flaw and backwall masked. d) large, obliquely orientated flaw, backwall masked. e) small flaw but no backwall echo because the axis of the beam is not incident at right angles on back wall. f) strong attenuation of sound beam due to scattering, no echo from flaw or backwall, only grass

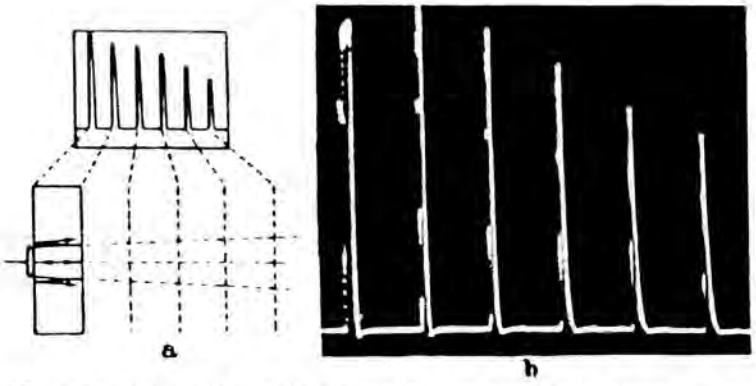

Fig. 25 Multiple echoes in a plate. a) Schematic, b) actual screen picture without time or thickness scale, steel plate 50 mm thick, frequency 4 MHz.

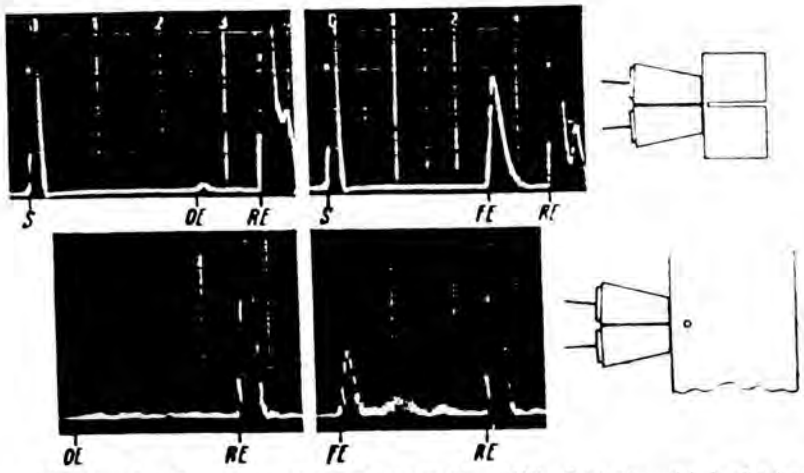

Fig. 26 Subsurface flaws as revealed by TR probe. Top: 4 MHz, flat-bottomed hole of 1.2 mm diameter, 2 mm below surface, aluminium 20 mm thick, *S* transmitting pulse, *OE* surface echo, *FE* flaw echo, *RE* backwall echo; bottom: 1 MHz, hole of 2 mm diameter parallel to surface and 5 mm below it, in grey cast iron (ASTM class 4) 100 mm thick, rough-cast surface, transmitting pulse shifted far to left, surface echo very weak. Screen traces on left side without, on right side with flaw indication.

QUARTZ 2S

FIG 27 CHARACTERISTIC CURVE FOR A 2 Mc/s QUARTZ PROBE

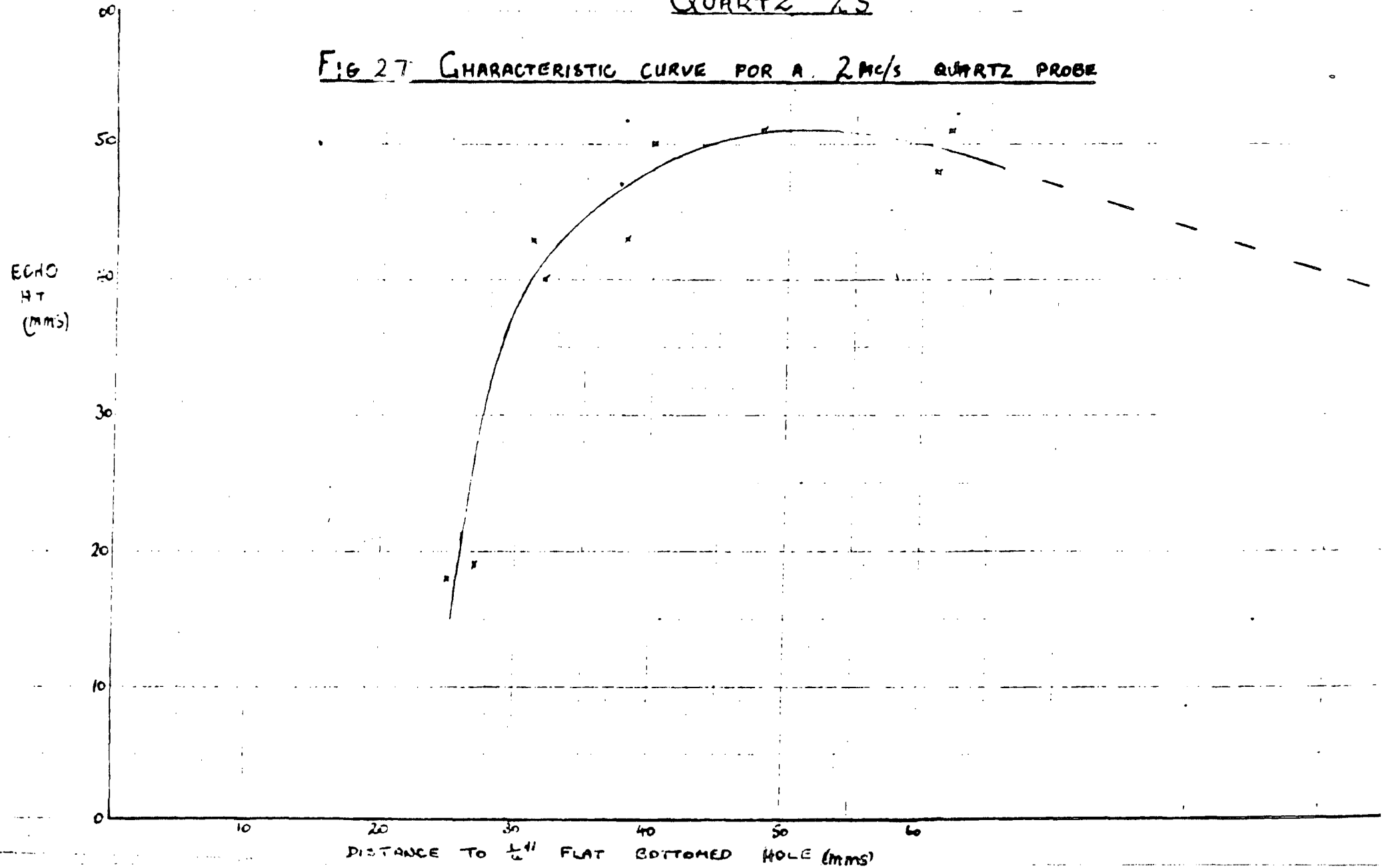

SEB 2T

FIG 28. CHARACTERISTIC CURVE FOR A 2mc/s TWIN CRYSTAL PROBE

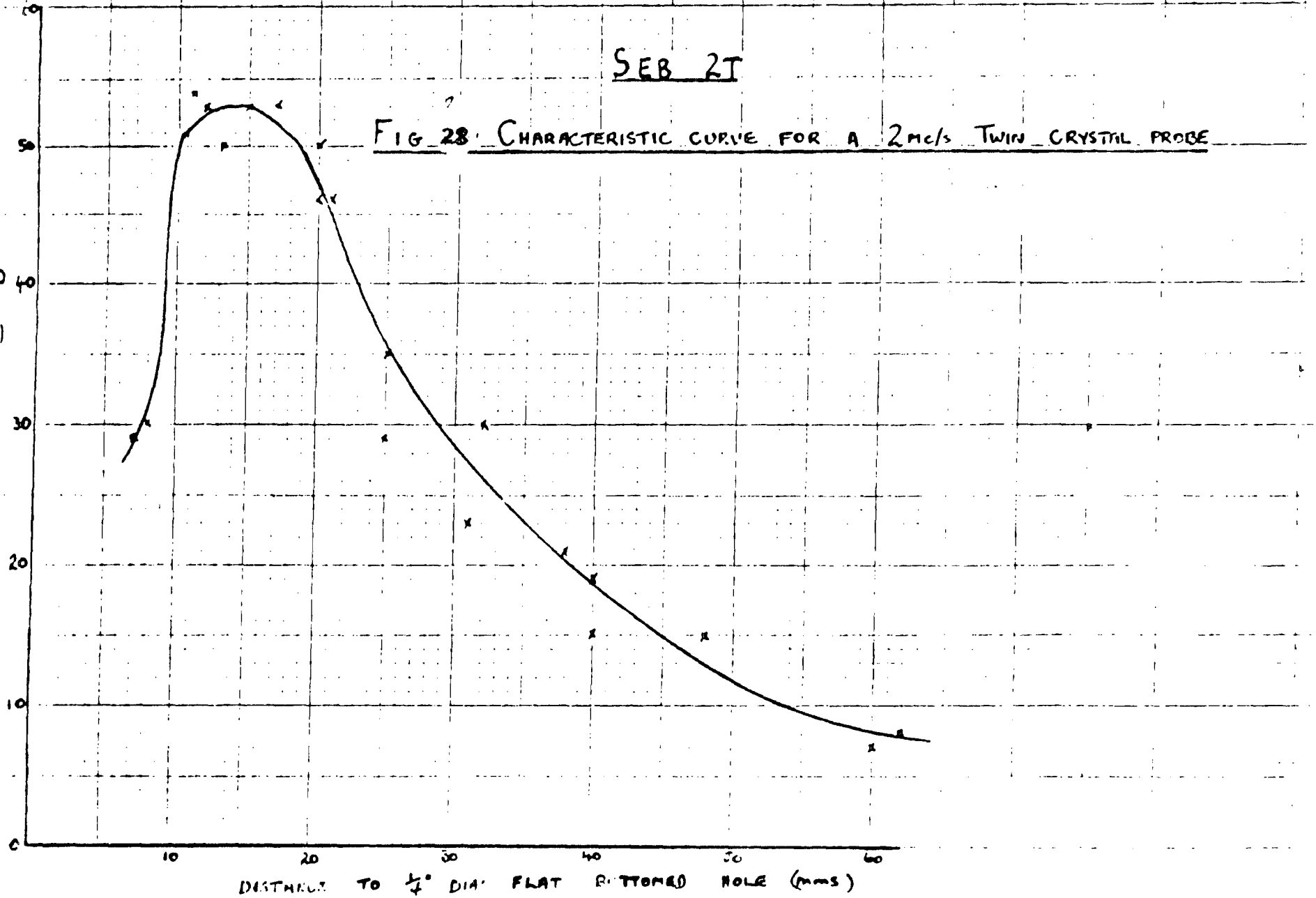

SEB 4T

FIG 29 CHARACTERISTIC CURVE FOR A 4 Mc/s TWIN CRYSTAL PROBE

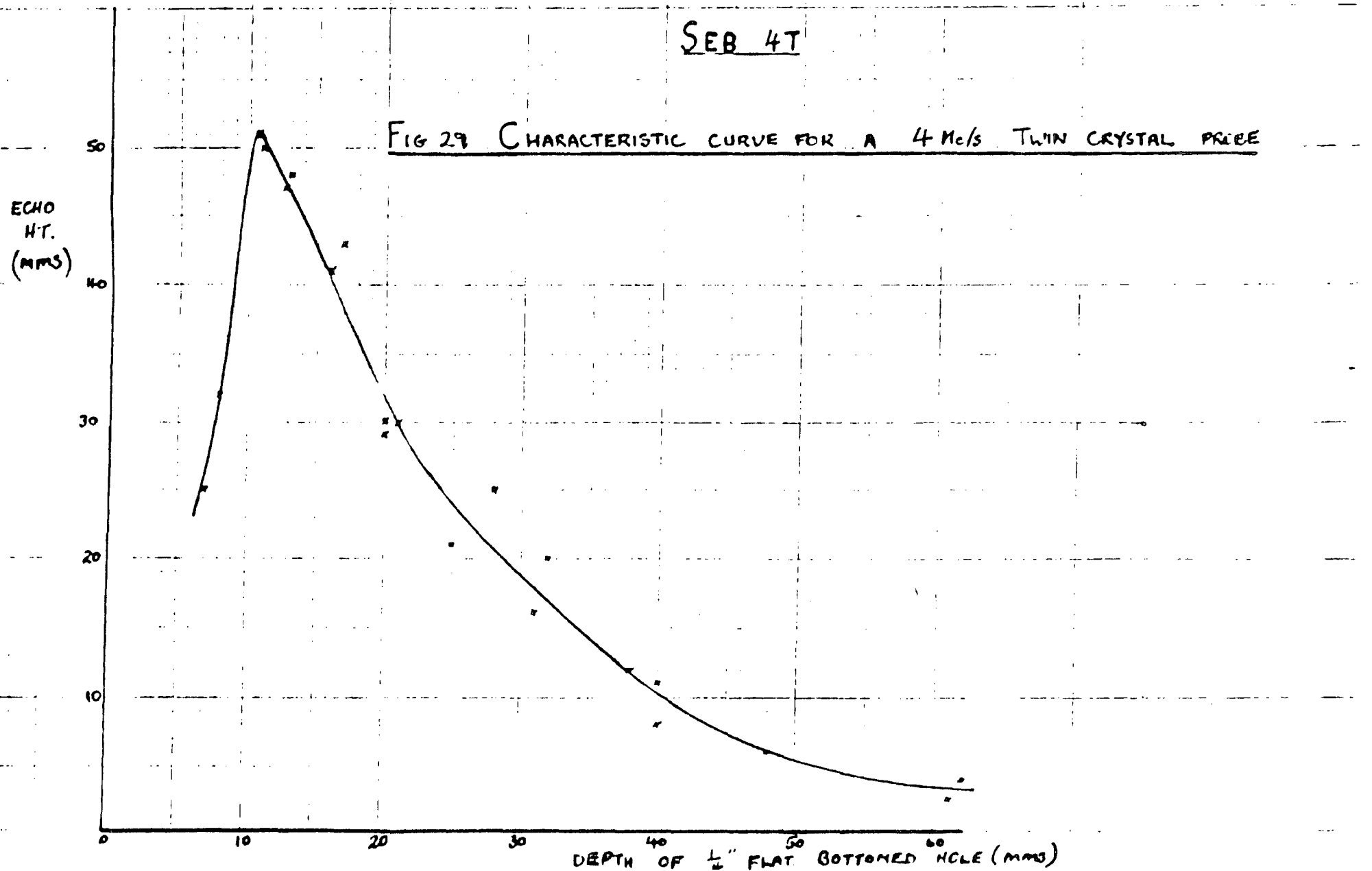

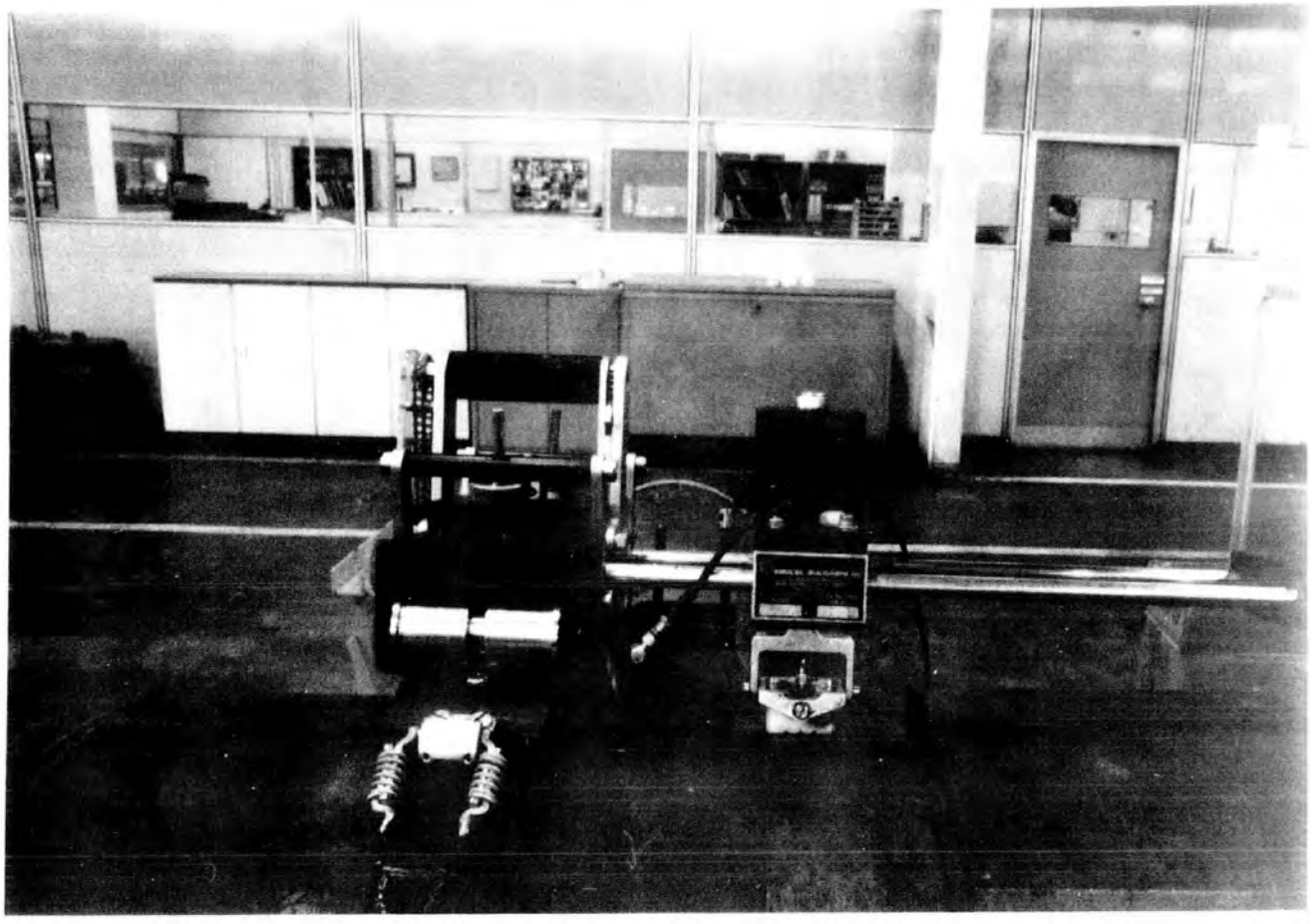

Figure 30
Ultra Image Manual Pipe Scanner

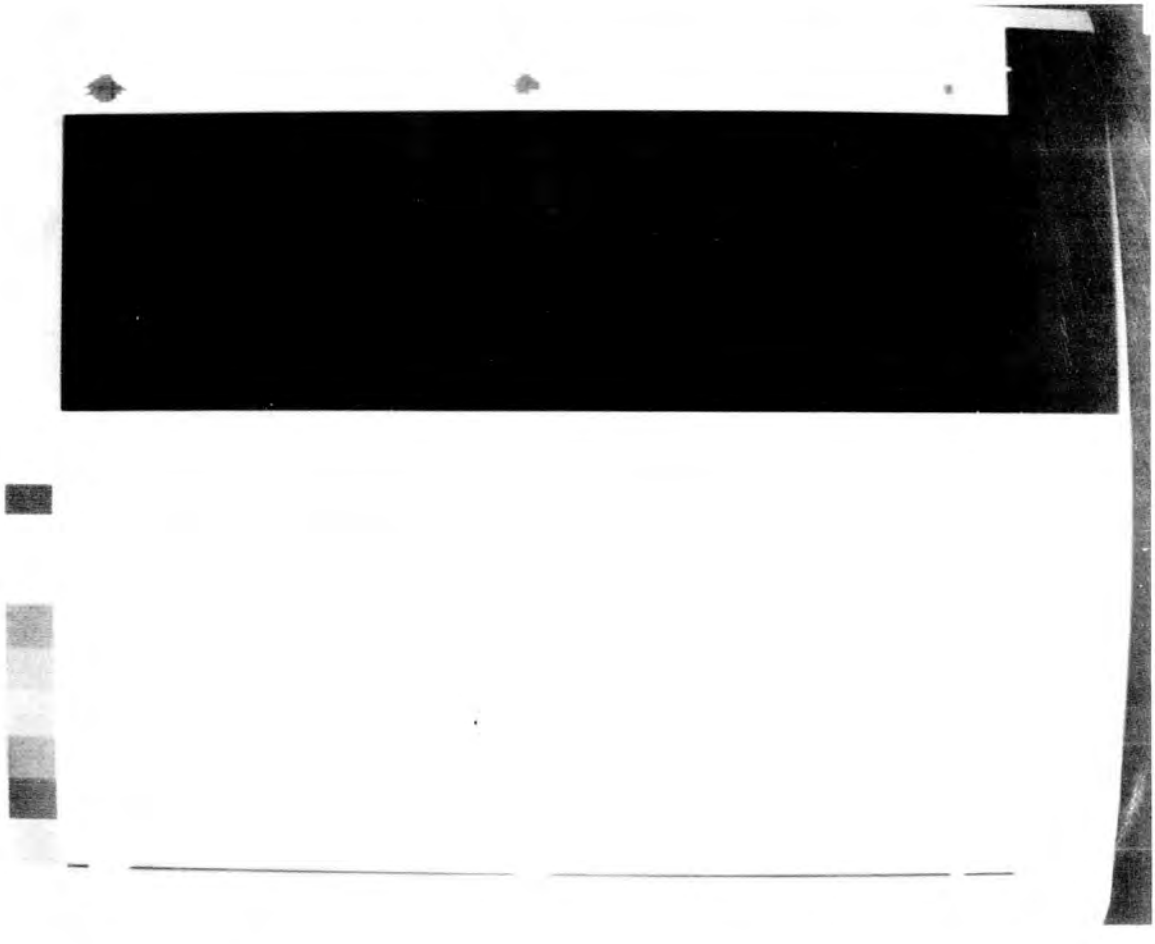

Figure 31
C-scan presentation of 1 mm, 2 mm and 3 mm flat bottomed holes produced by the Ultra Image Scanner.

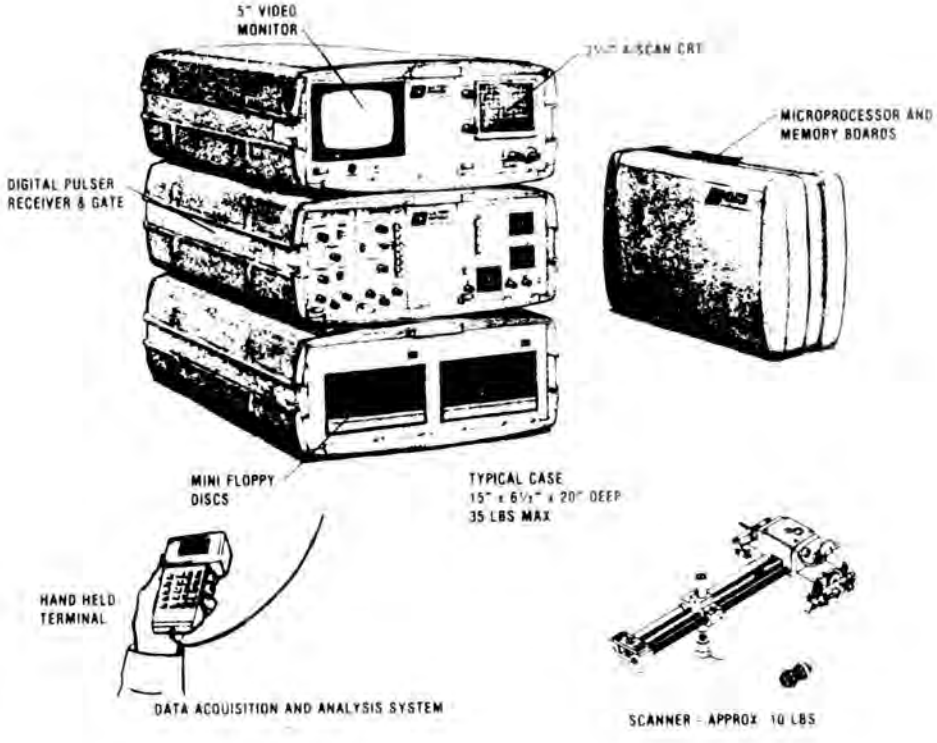

Figure 32
Ultra Image Mechanised Ultrasonic Scanning System.

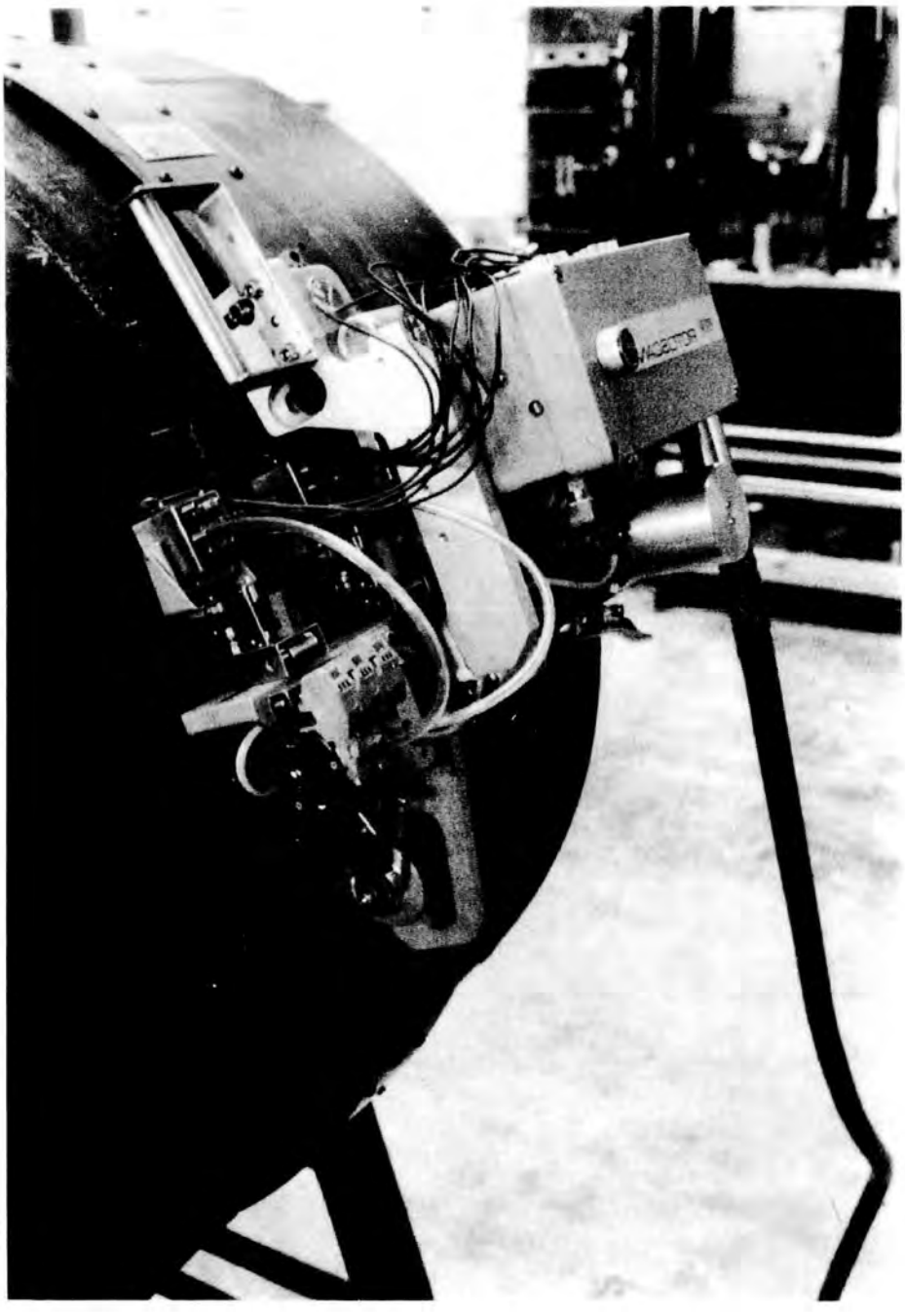

Figure 33
Primscan Automated Ultrasonic Probe Scanner.

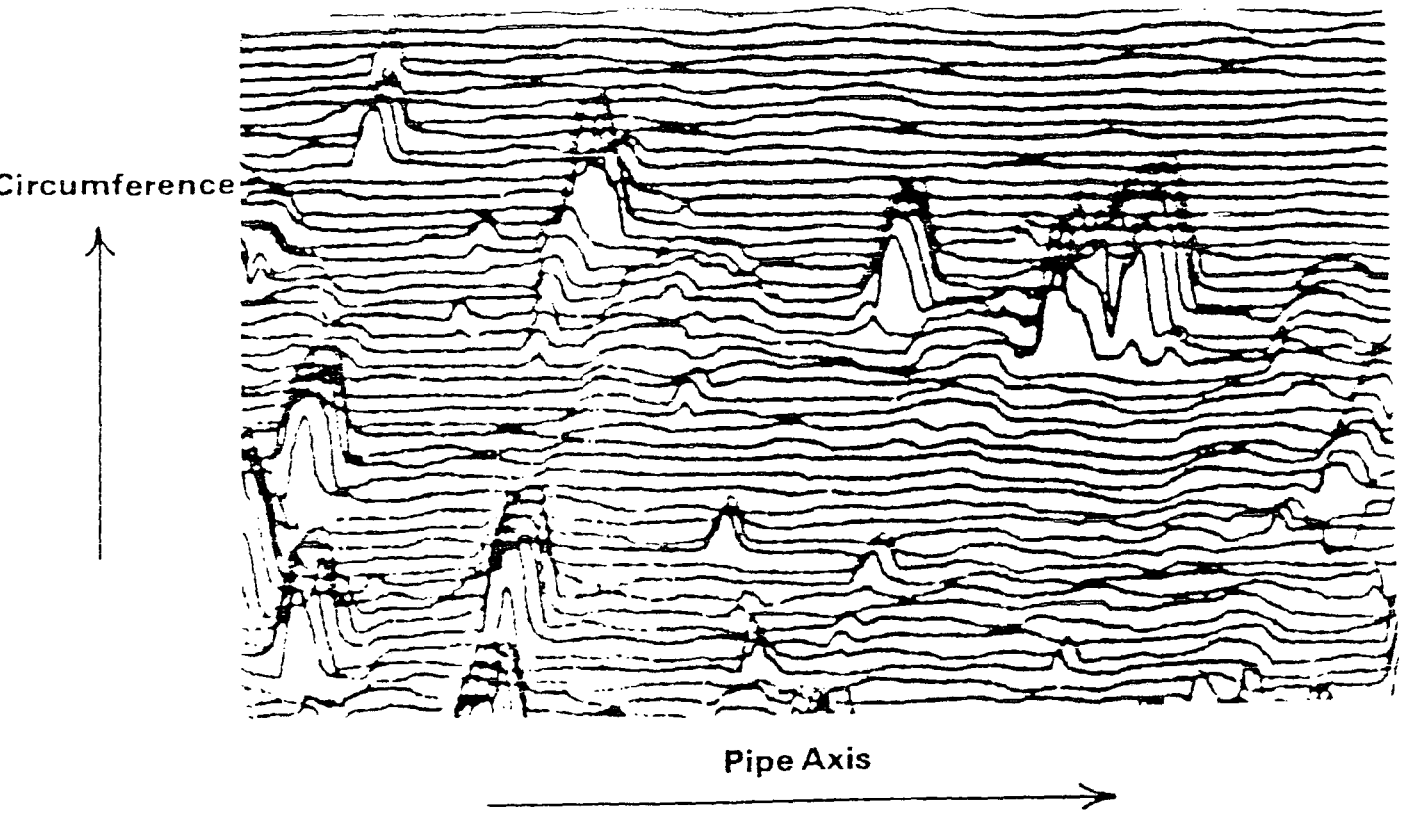

Figure 34

Pseudo 3D format produced from the Primscan mechanised ultrasonic system

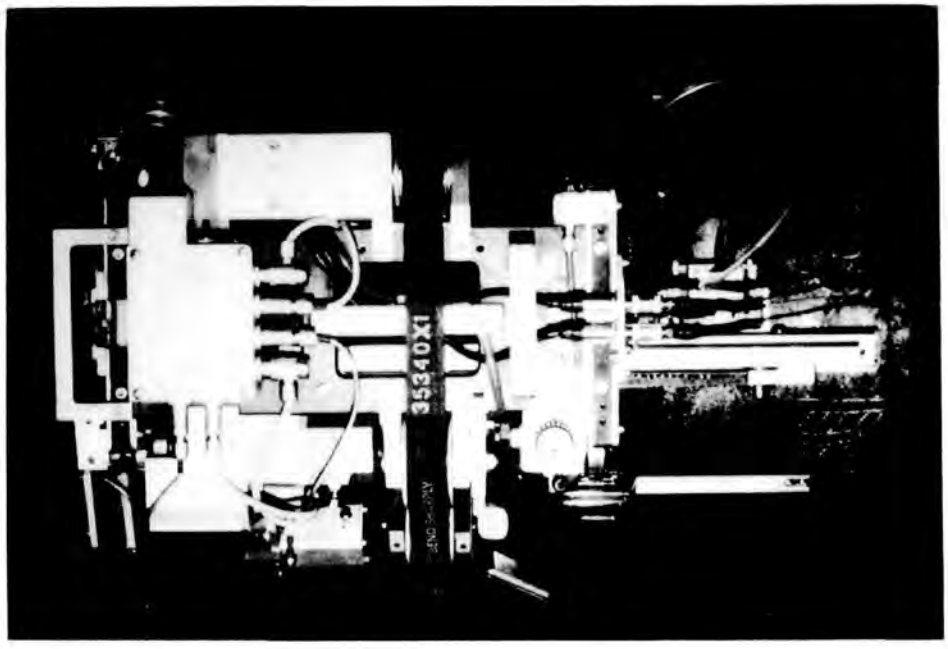

Figure 35
Plan view of the S.V.C. Mechanised Scanner.

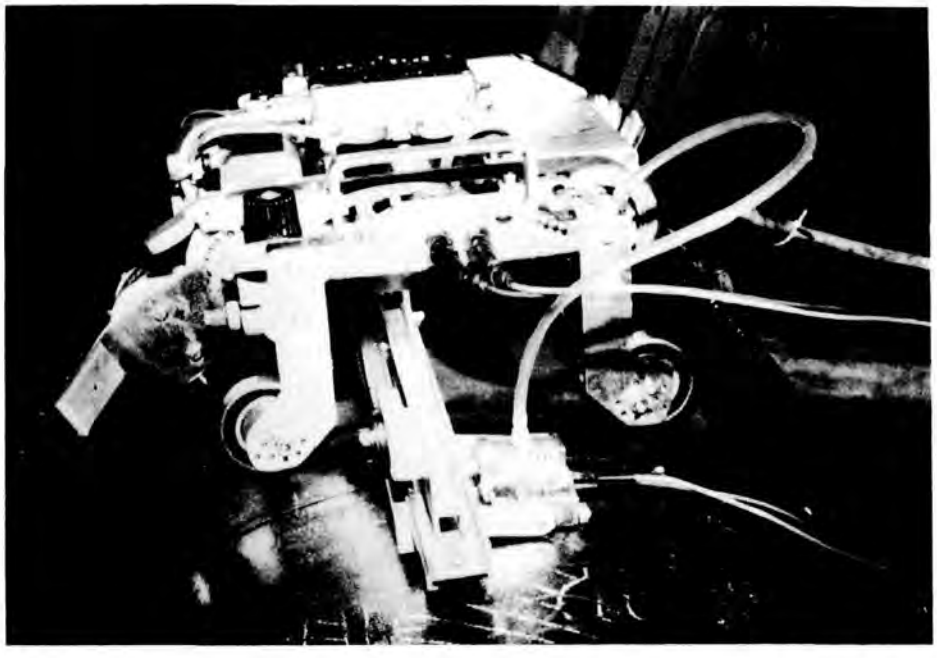

Figure 36
Side view of the S.V.C. Mechanised Scanner.

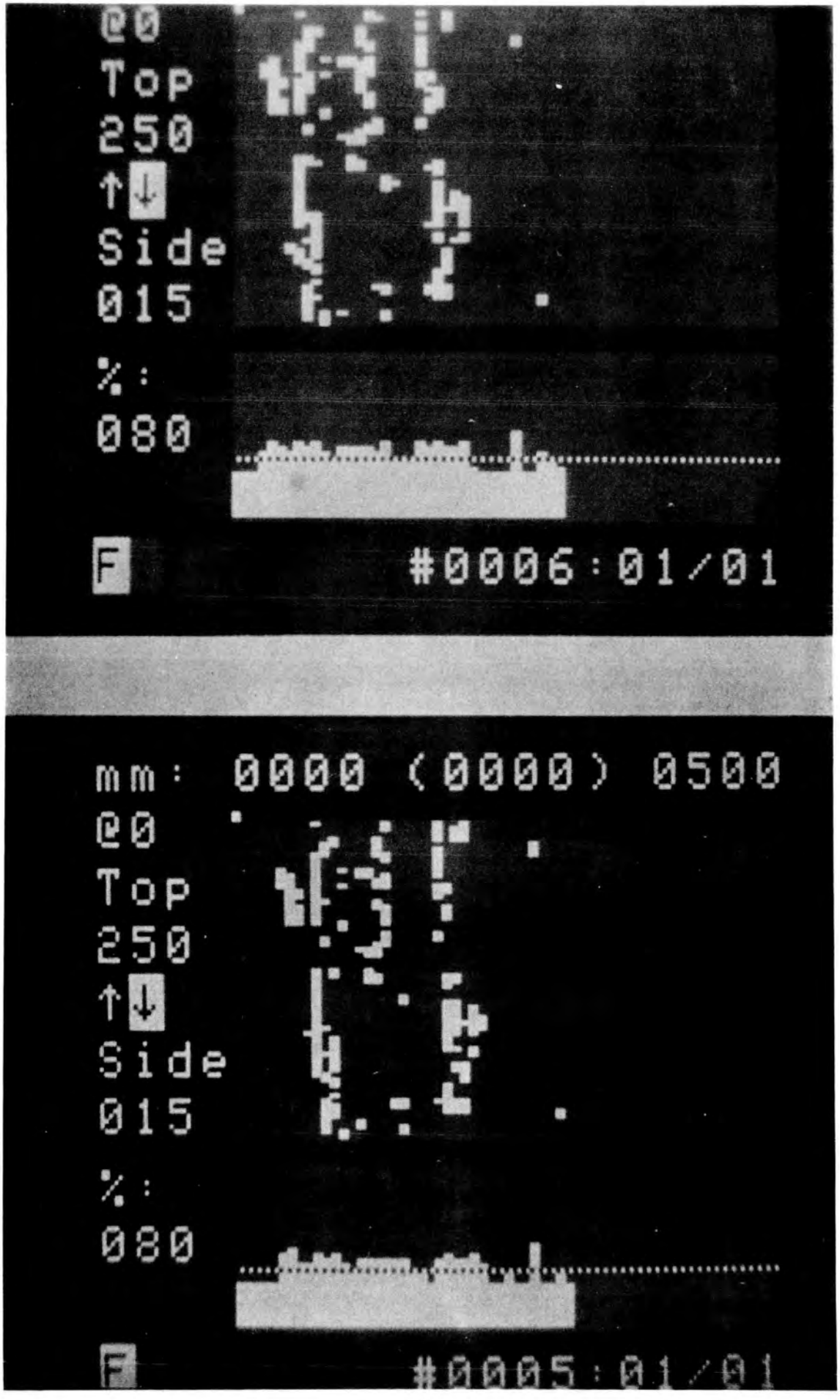

Figure 37
C-scan image produced by the S.V.C. P scan unit.

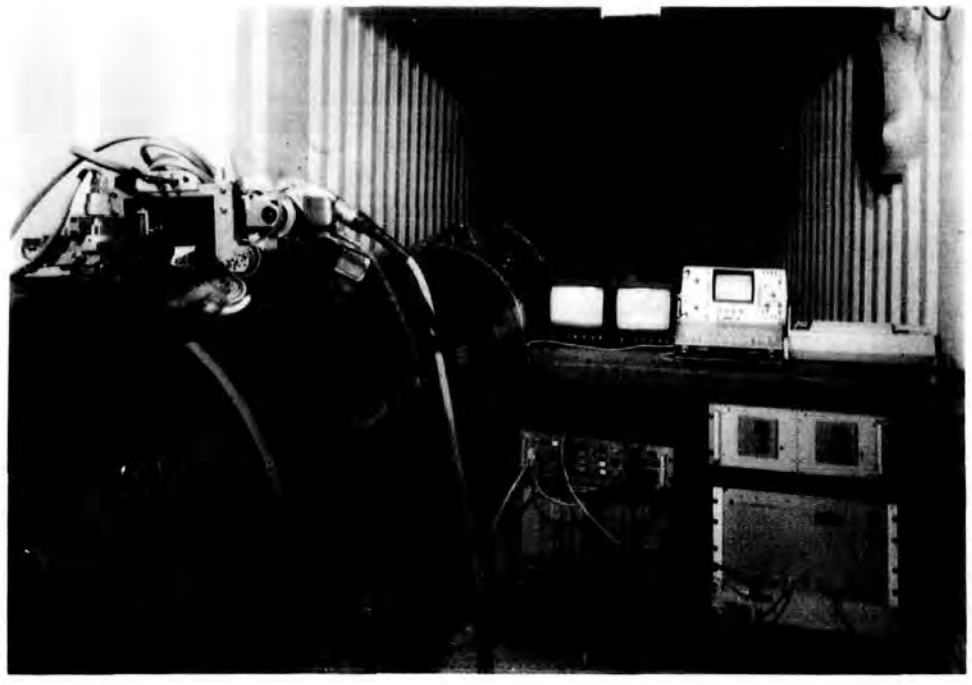

Figure 38
P scan system in operation

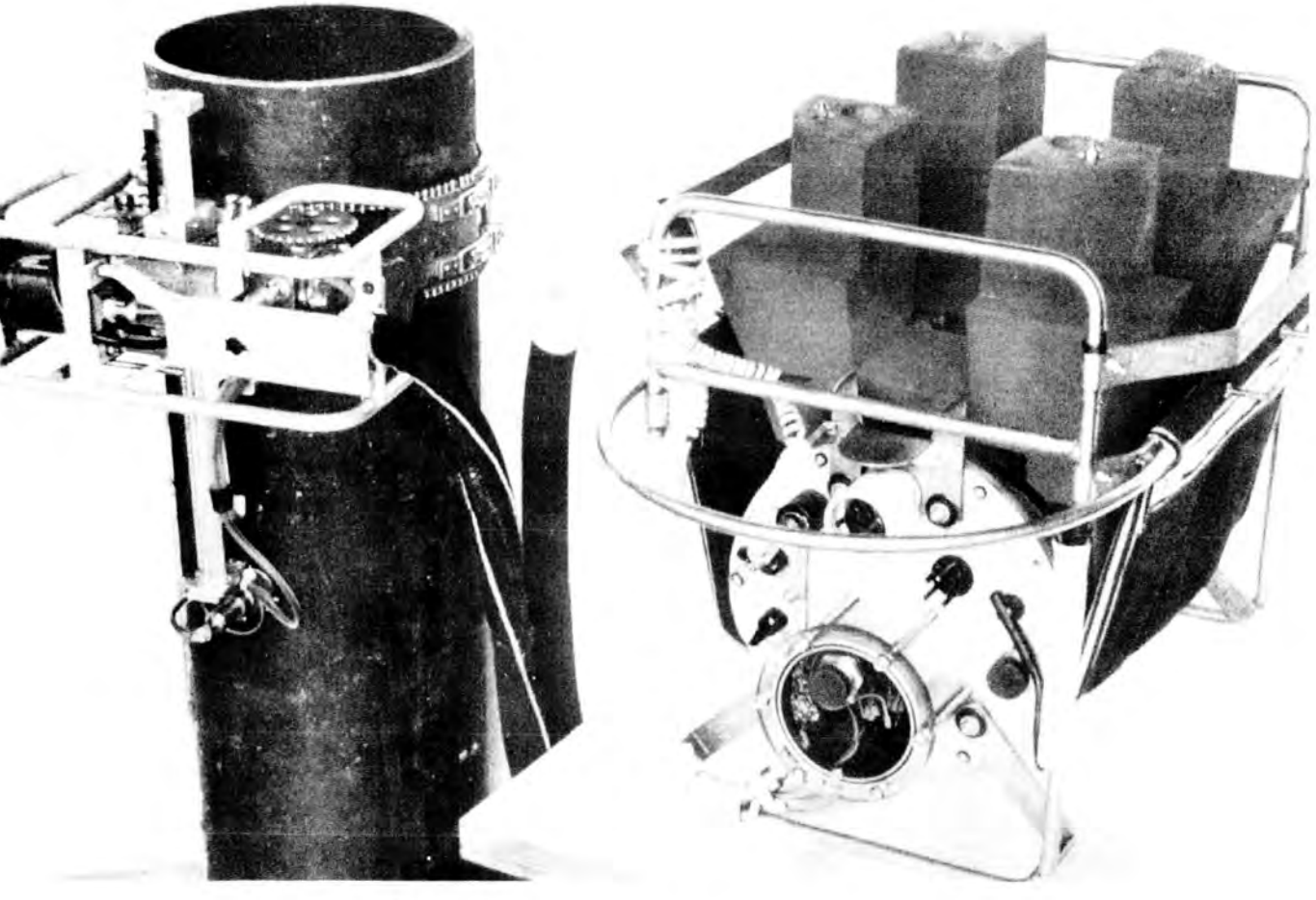

Figure 39
D.N.V. under water scanning system

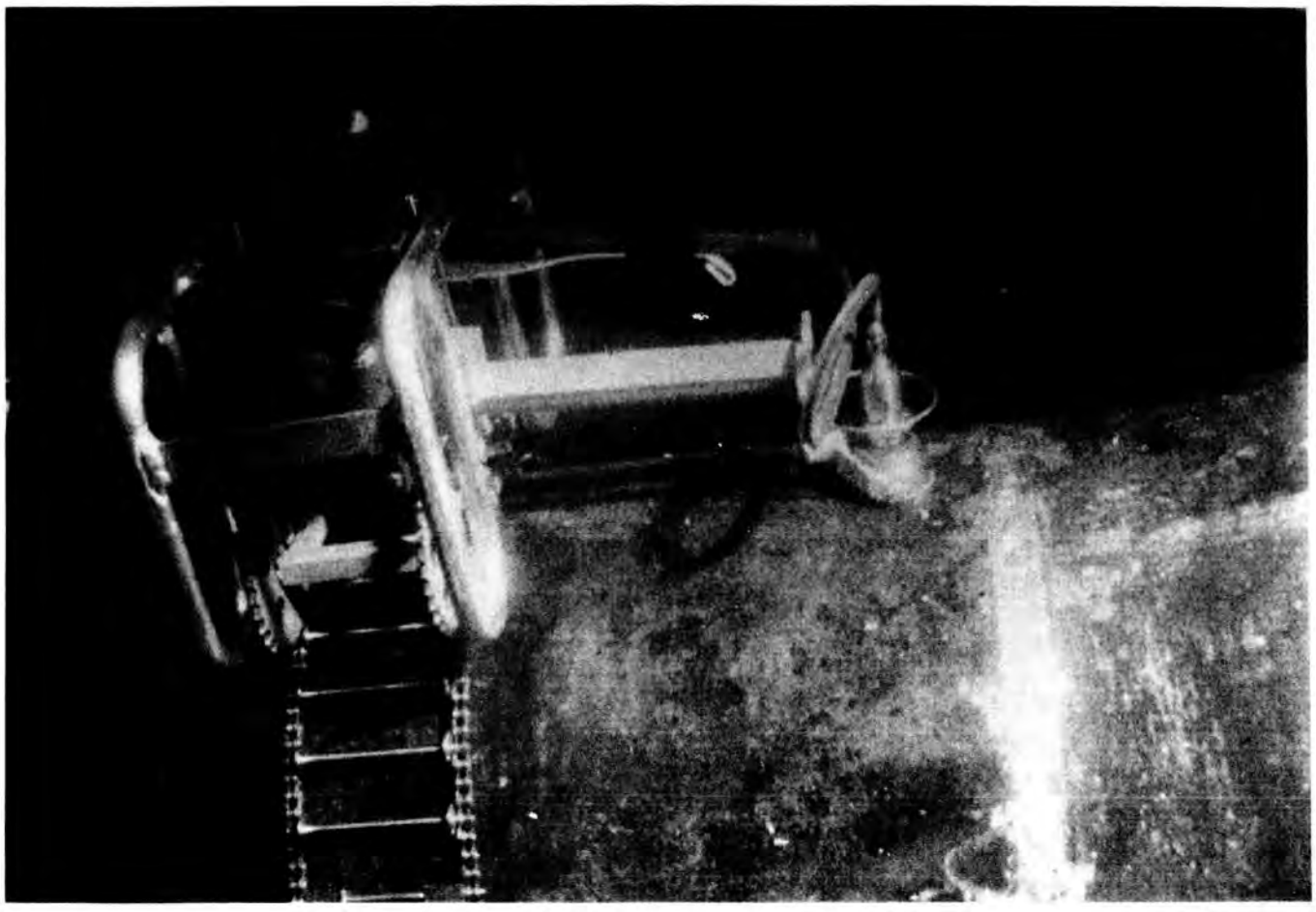

Figure 40
Scanning unit in use under water

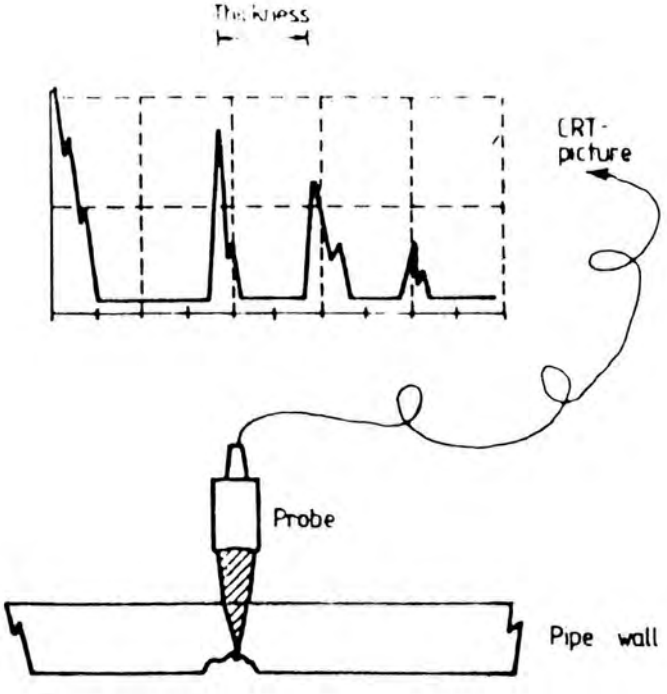

Figure 41
Schematic of focussed non contacting probe

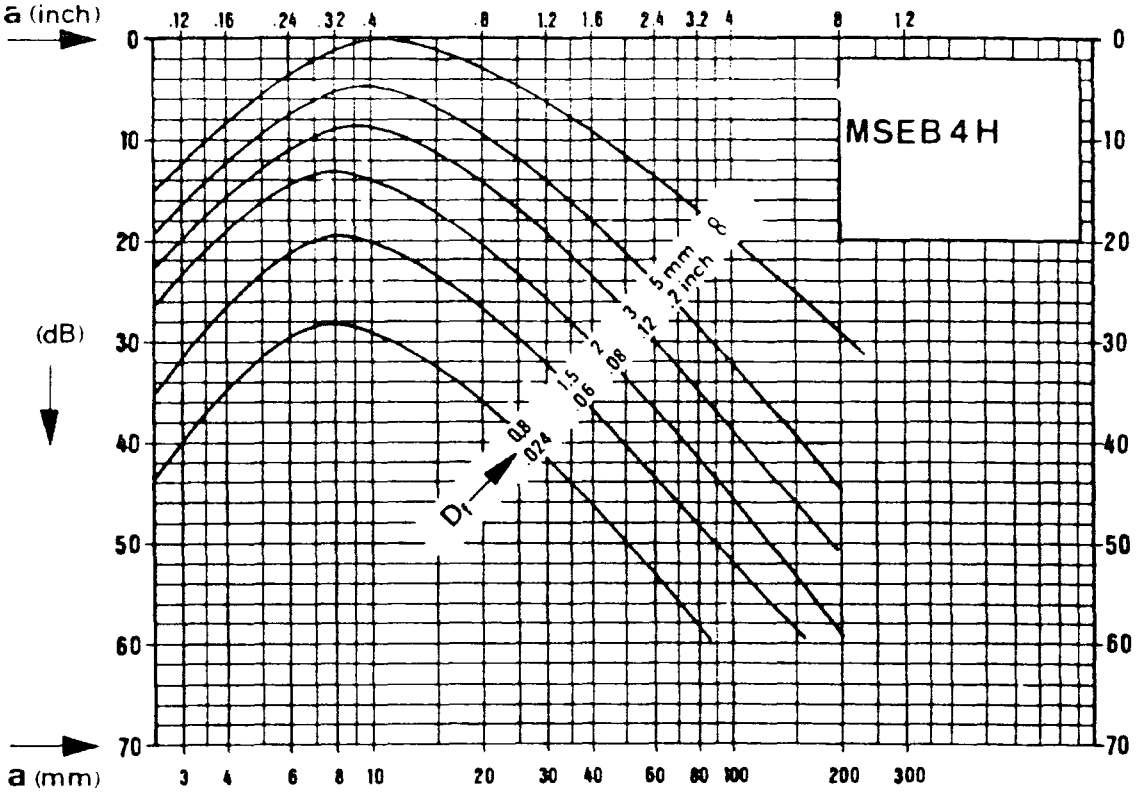

Figure 42

Distance gain sensitivity of the compression wave transducer MSEB 4H.

Df = diameter of equivalent flat bottom hole (mms)

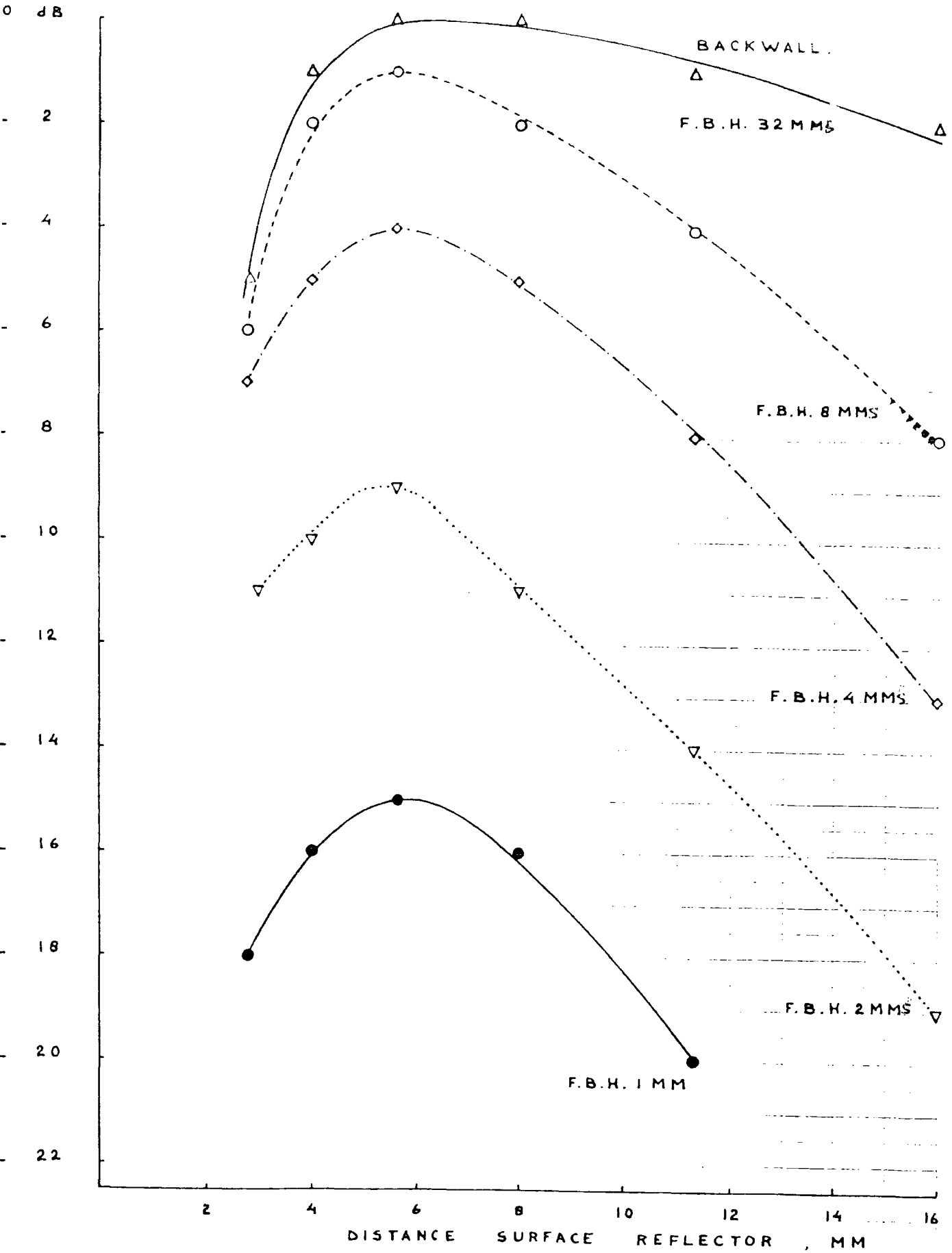

DISTANCE GAIN SENSITIVITY OF THE COMPRESSION WAVE TRANSDUCER MSEB 4T.

F.B.H. = Flat Bottom Hole of diameter "x" mms

Figure 43

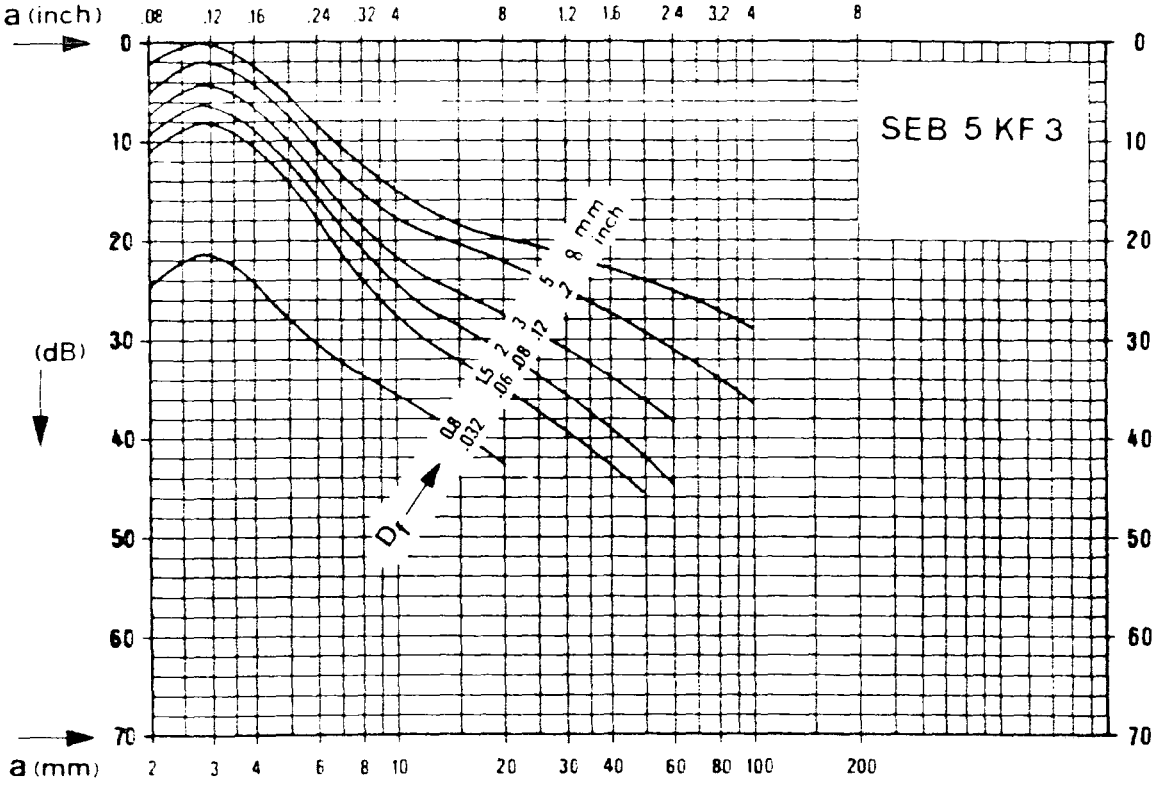

Figure 44

Distance gain sensitivity of the compression wave transducer SEB 5KF3.

Df = Equivalent flat bottom hole of diameter "x" mms.

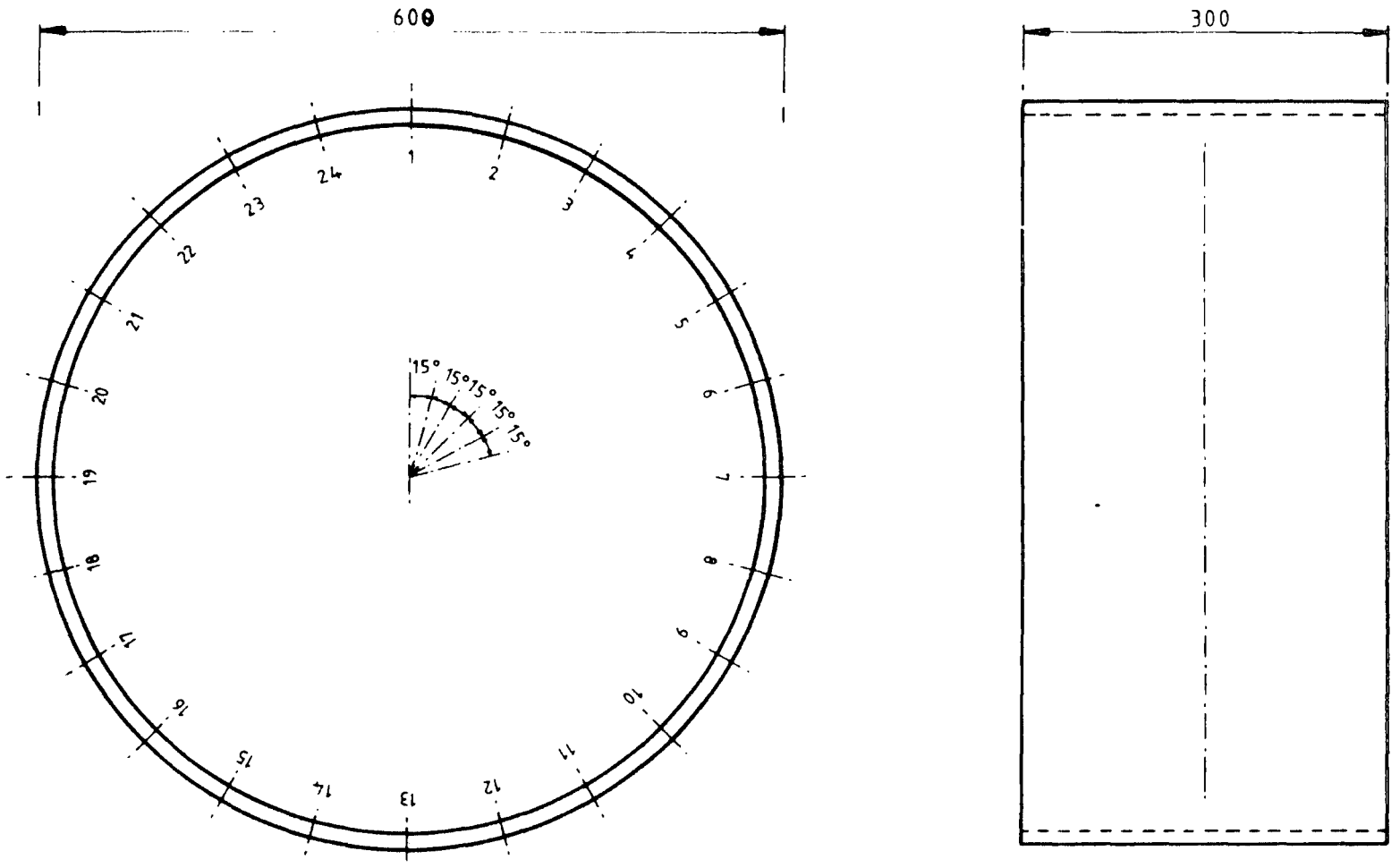

All Defects are Located at the Innerside and on the Centreline as Indicated

Dimensions in mm

Fig. 45 : Test Sample with Artificial Defects

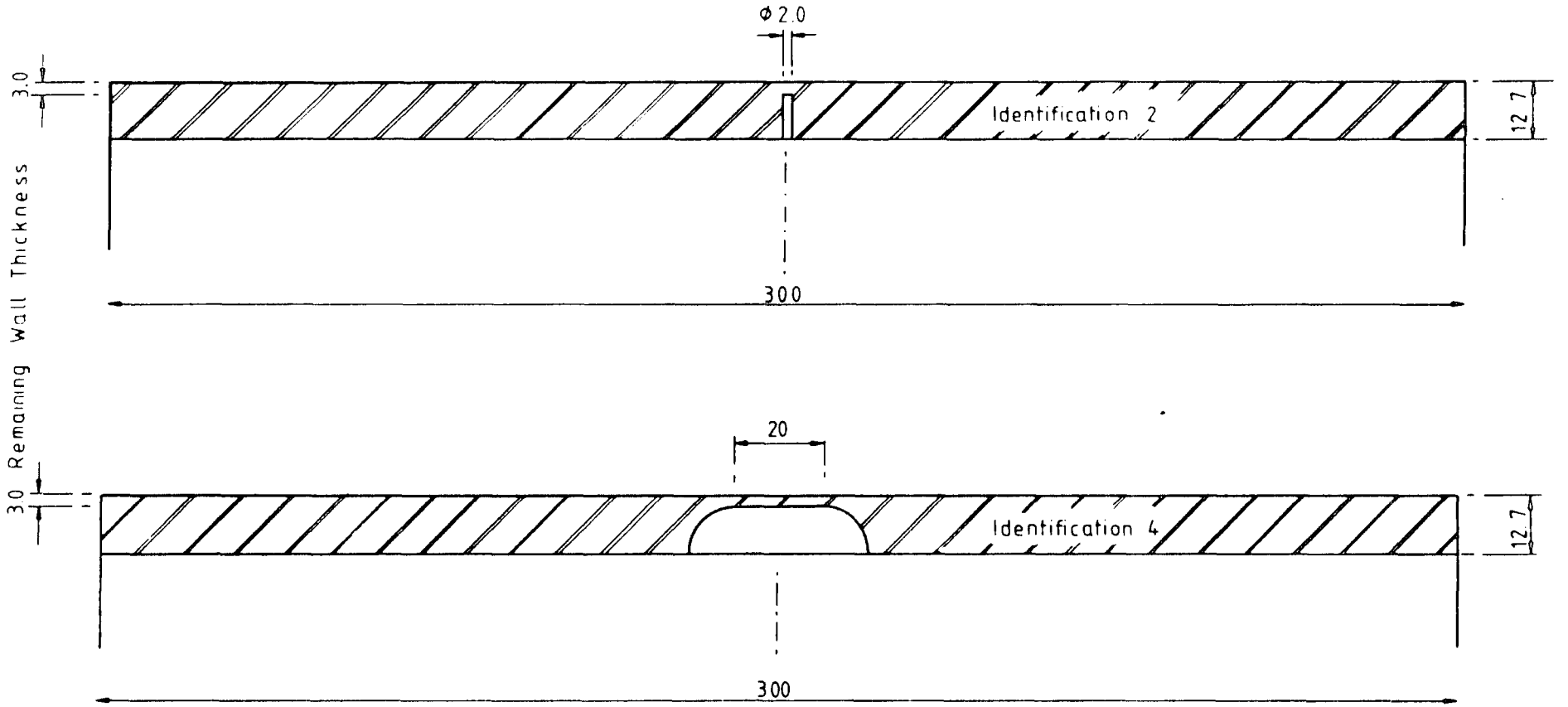

Fig. 46 : Details of a Flat Bottom Hole and an Axial Notch

Minimum Depths Measured on Testpipe

Ultra Image/0.25 * 8MHZ

Run 11-18

□ 1 mmØ
△ 2 mmØ
⊙ 3 mmØ

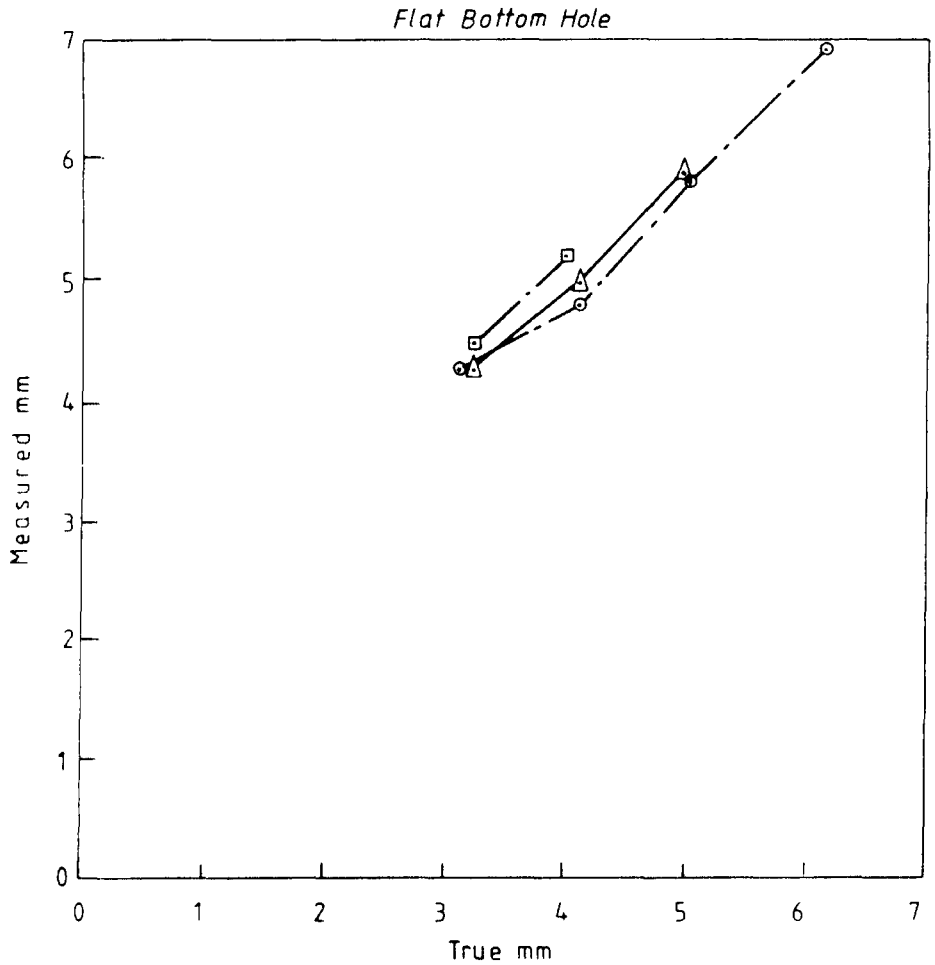

Fig. 47

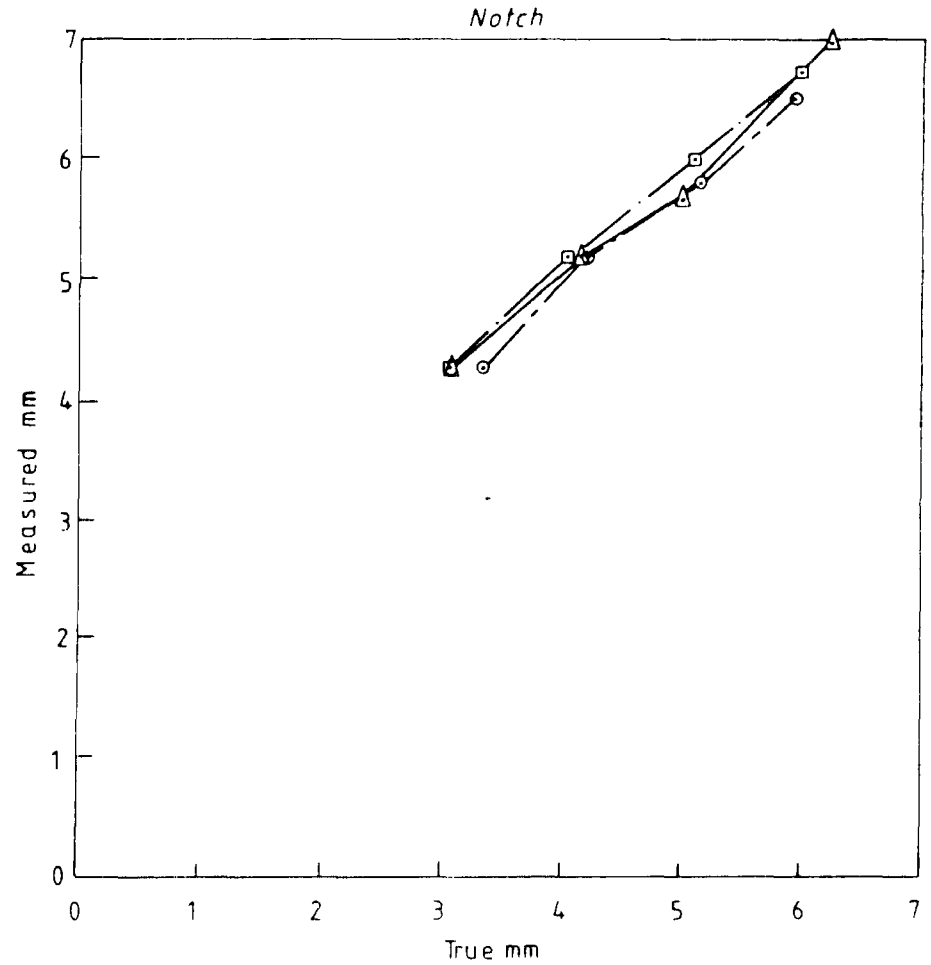

Fig. 48

Figs. 47 & 48 : Results Obtained with the Ultra Image Scanner

Minimum Depths Measured on Testpipe

Underwater Corroscan/MSEB4T

Run 24.5

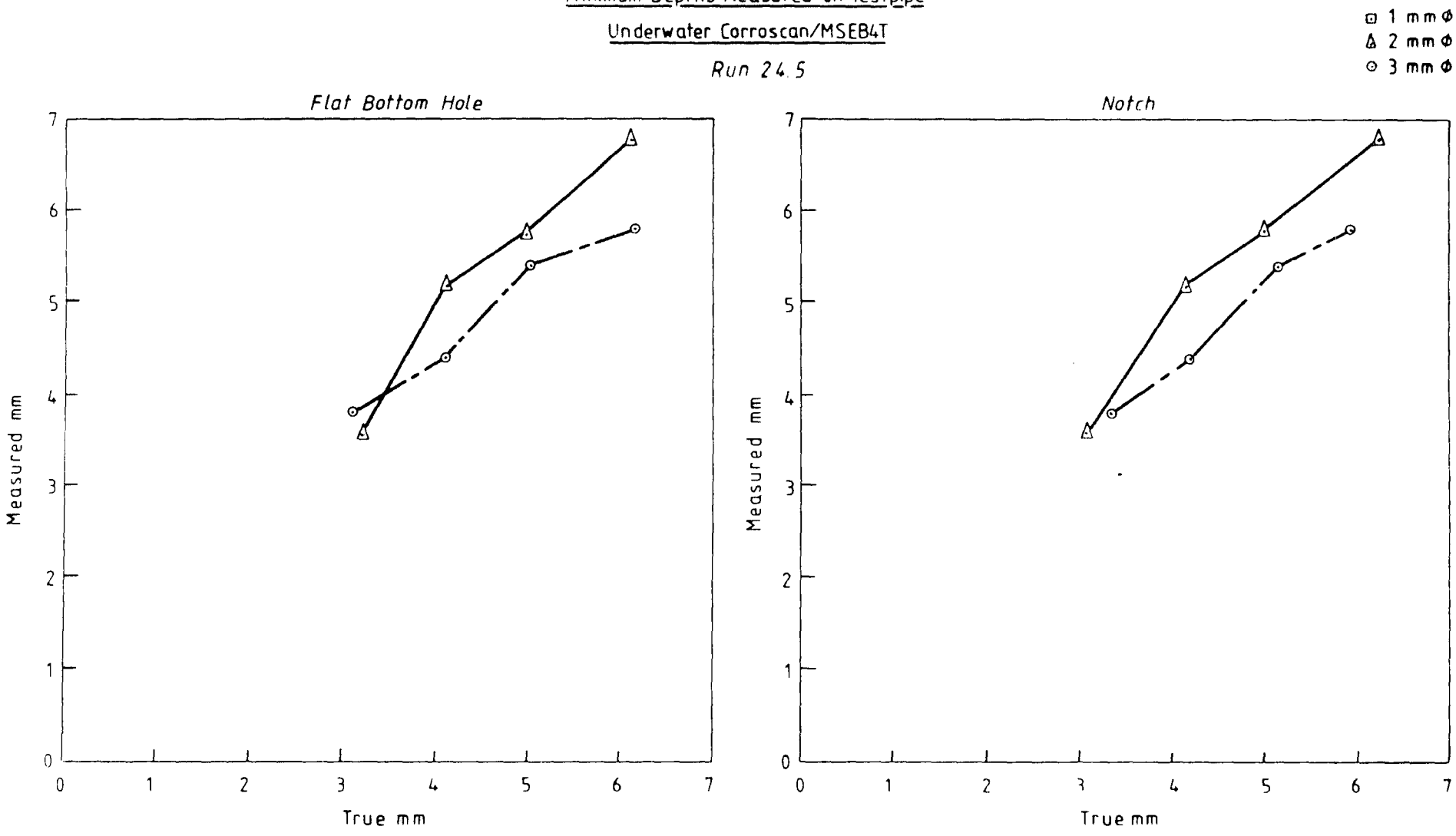

Fig. 49

Fig. 50

Figs. 49 & 50 : Results Obtained with the D.N.V. Corroscan

Minimum Depths Measured on Testpipe

PRIMSCAN /MSEB4H (B)

Run 39.4/5

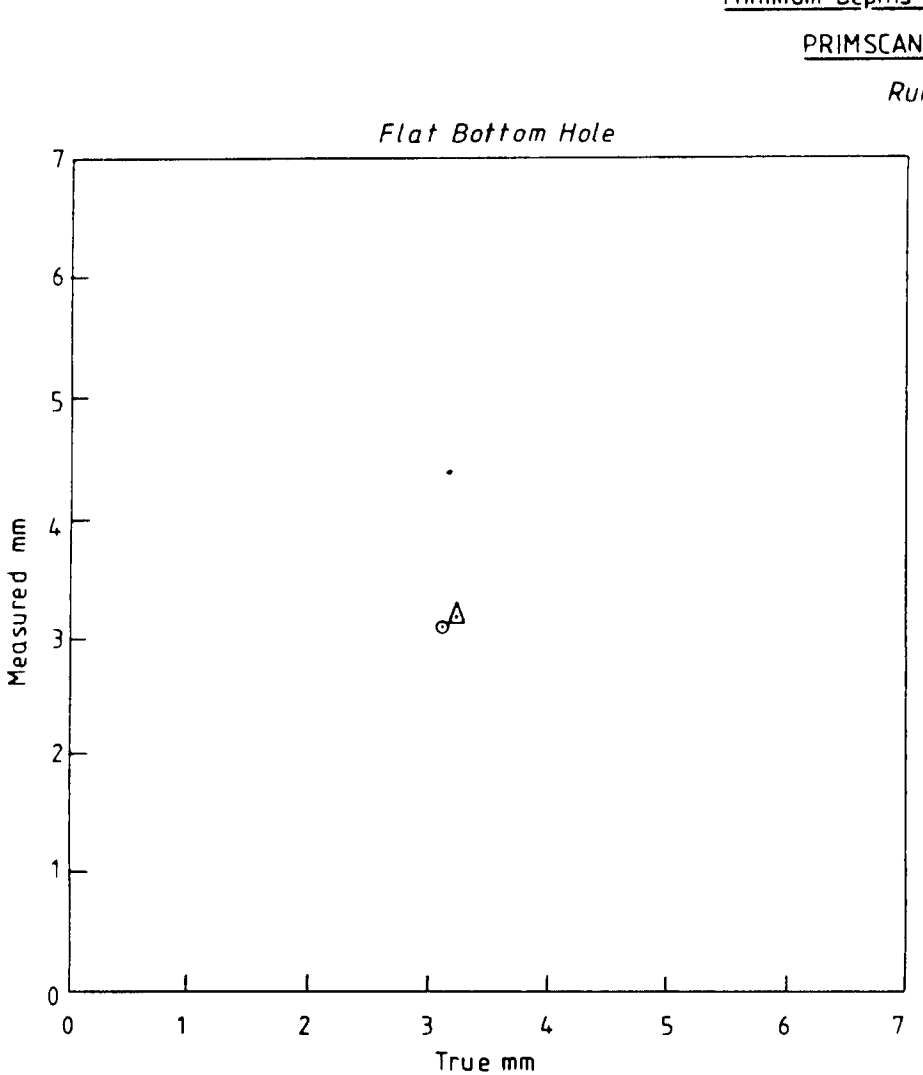

Fig. 51

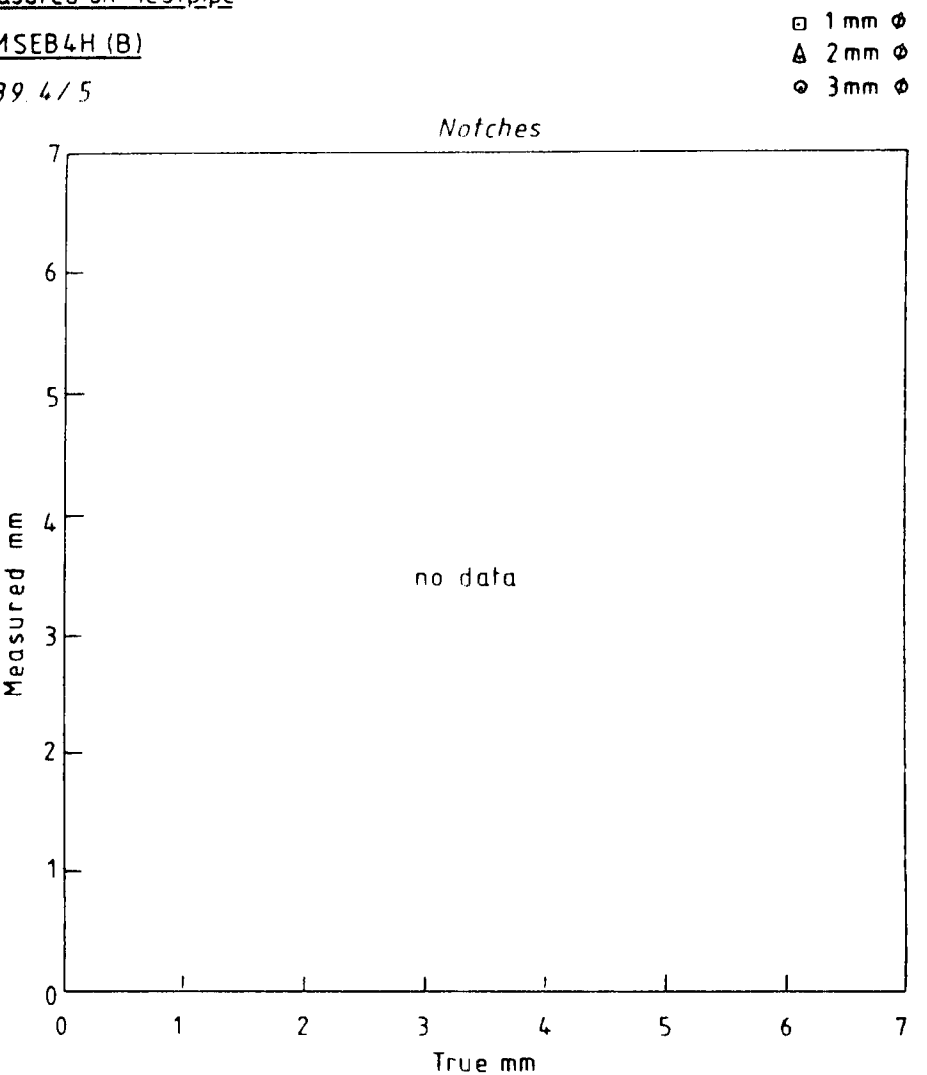

Fig. 52

Figs. 51 & 52 : Results Obtained with the Primscan

Minimum Depths Measured on Testpipe

Primscan / MSEB4T

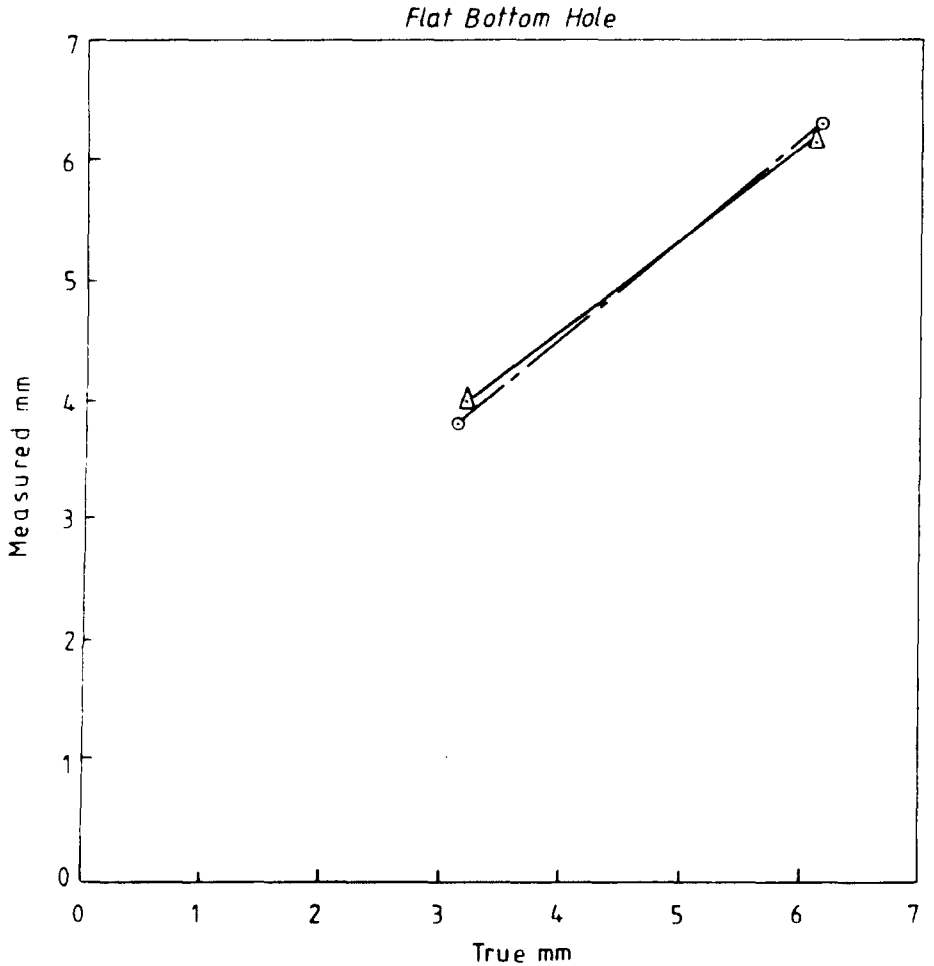

Fig. 53

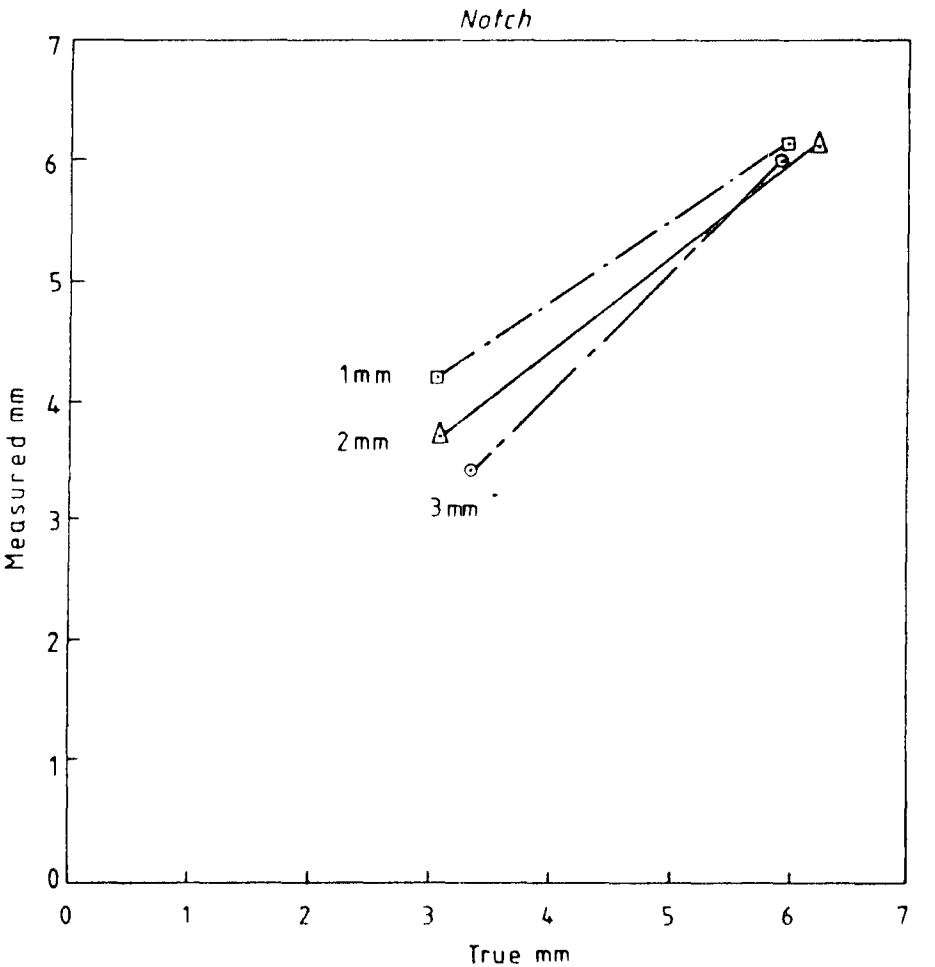

Fig. 54

Fig. 53 & 54 : Results Obtained with the Primscan

Minimum Depths Measured on Testpipe

PRIMSCAN/SEB5KF3(A)

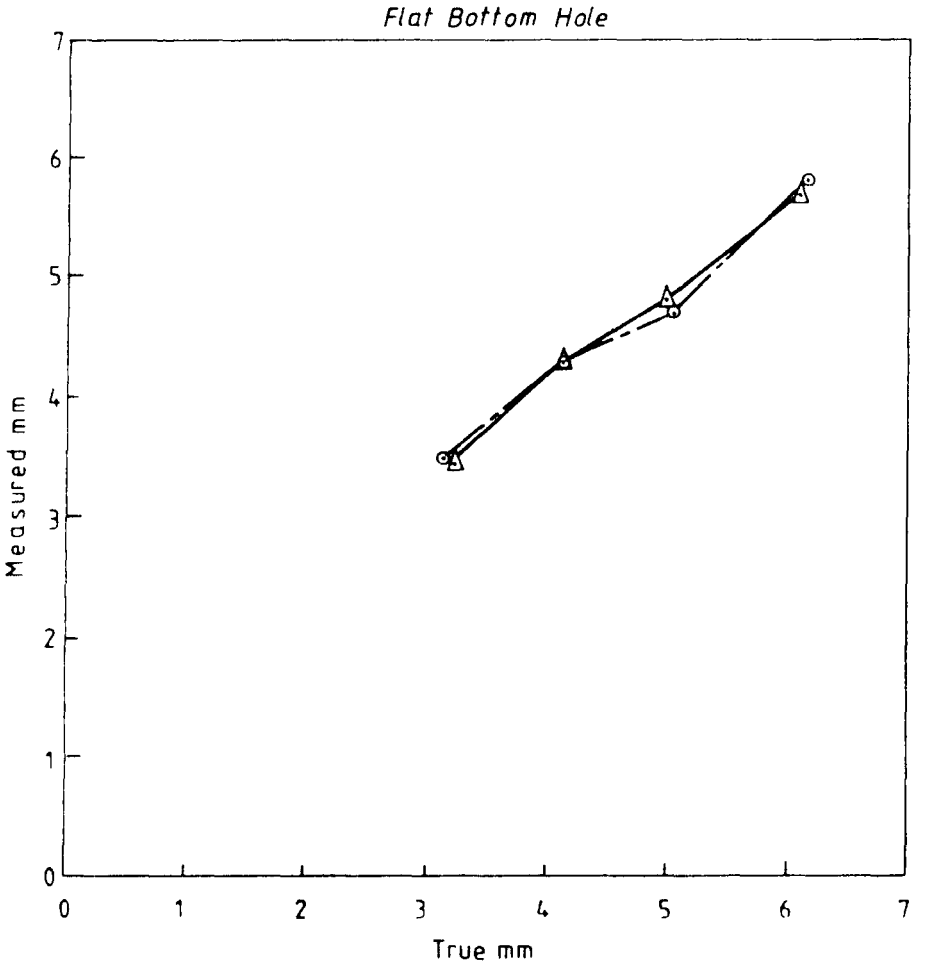

Fig.55

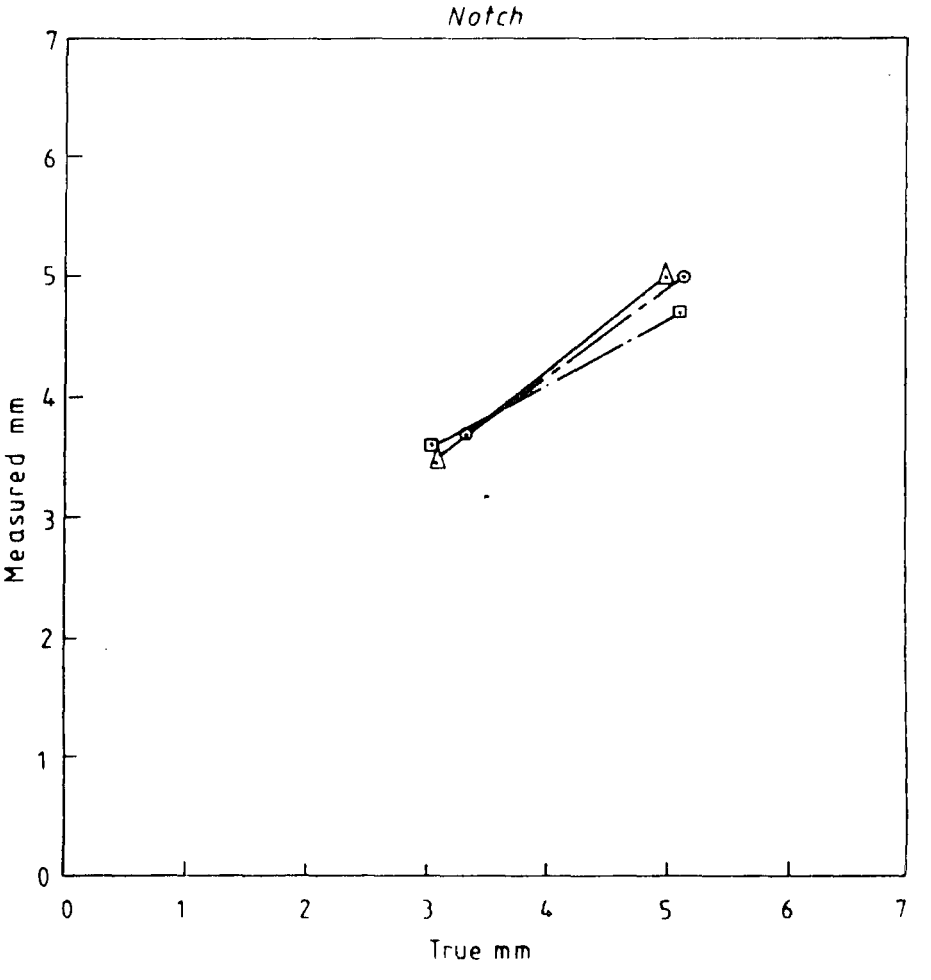

Fig.56

Figs. 55 & 56 : Results Obtained with the Primscan

Minimum Depths Measured on Testpipe
above Water Corroscan/MSEB4T
Run 1.0

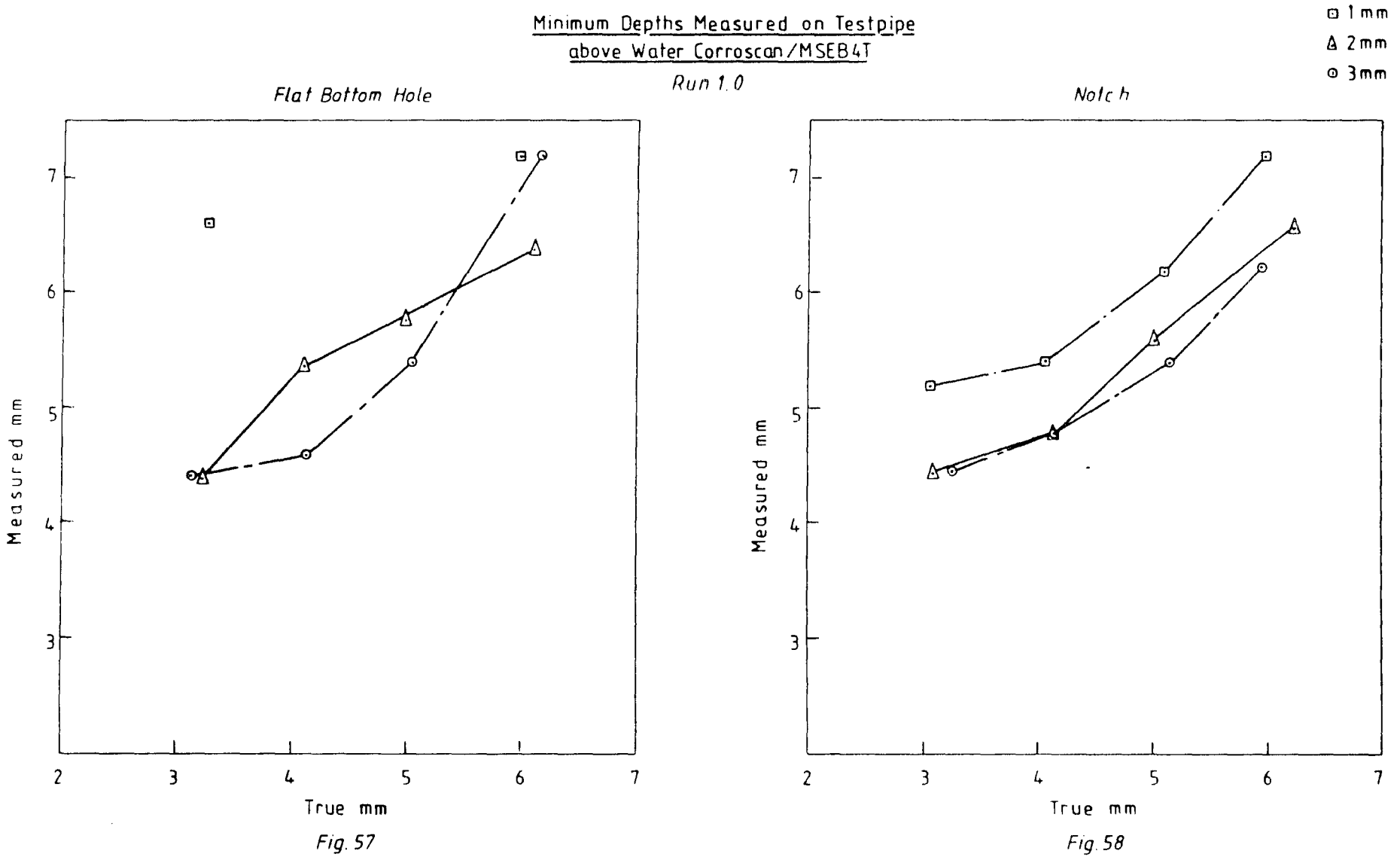

Fig. 57

Fig. 58

Figs. 57 & 58 : Results Obtained with the Above Water Corroscan - PScan

Minimum Depths Measured on Testpipe

above Water Corroscan/MSEB4T

Run 14.0/1

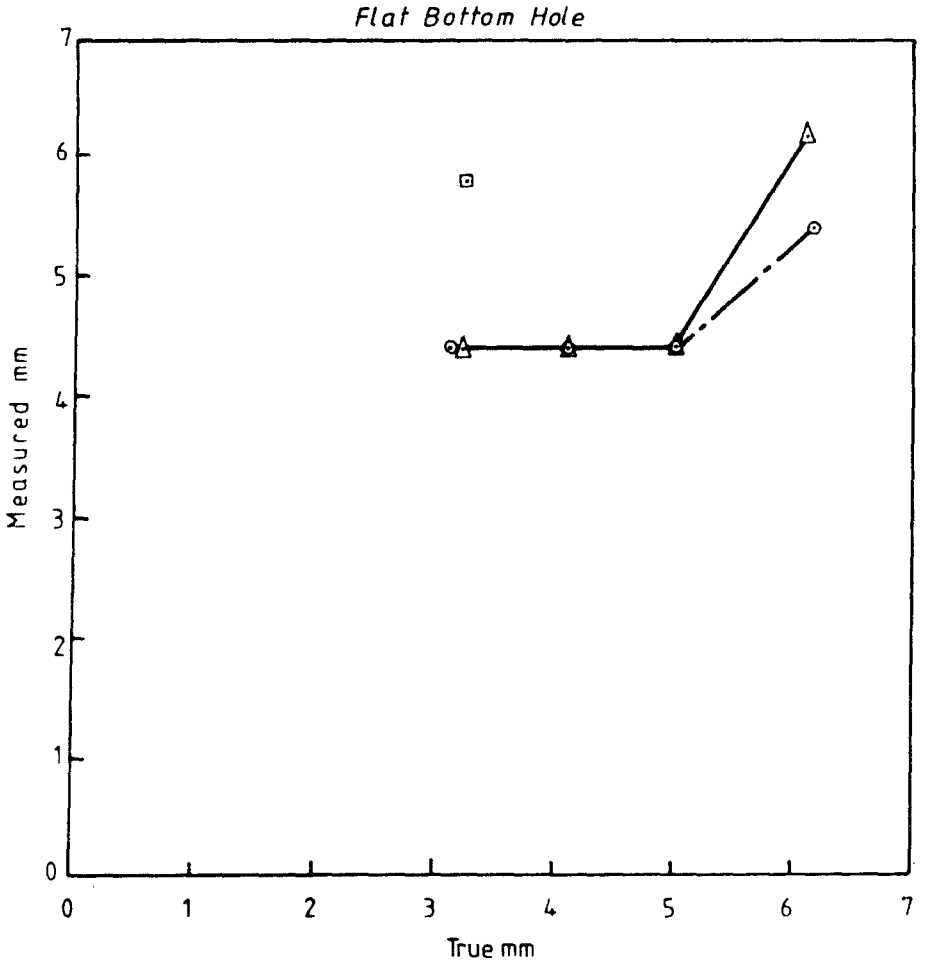

Fig. 59

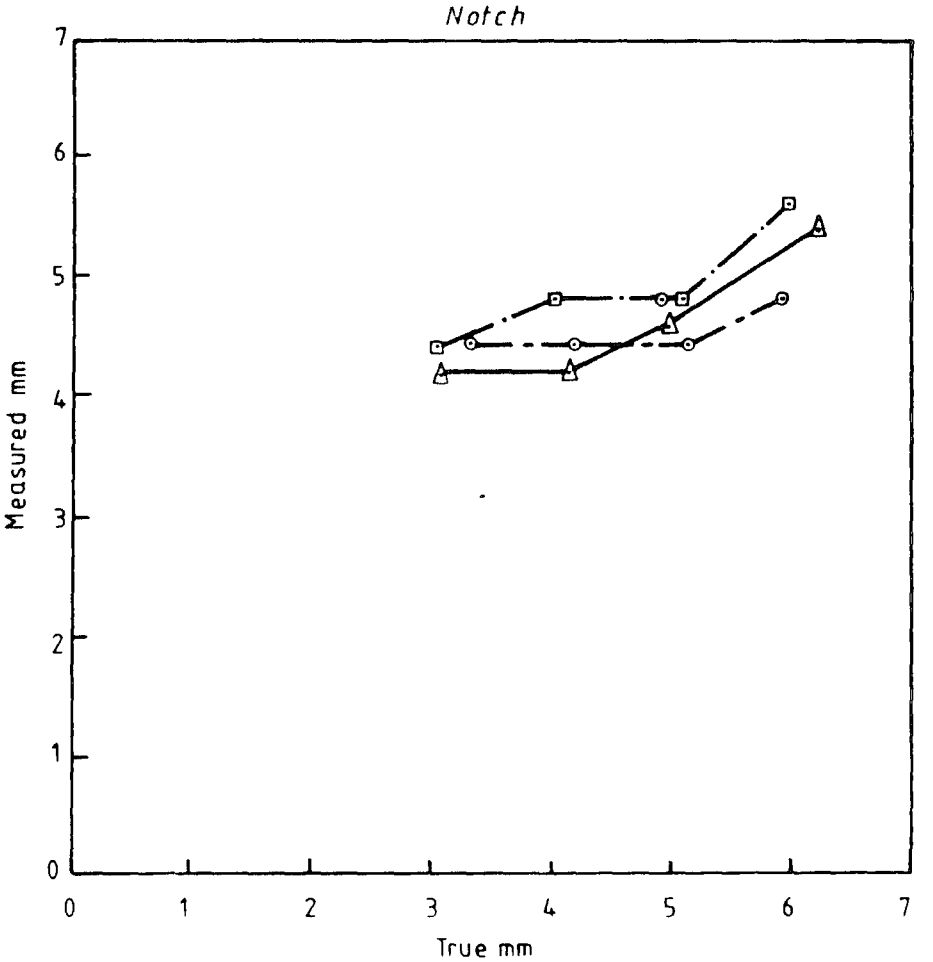

Fig. 60

Fig. 59 & 60 : Results Obtained with the Above Water Corroscan-P Scan

Average Depths Measured on Testpipe

Above Water Corroscan MSEB4T

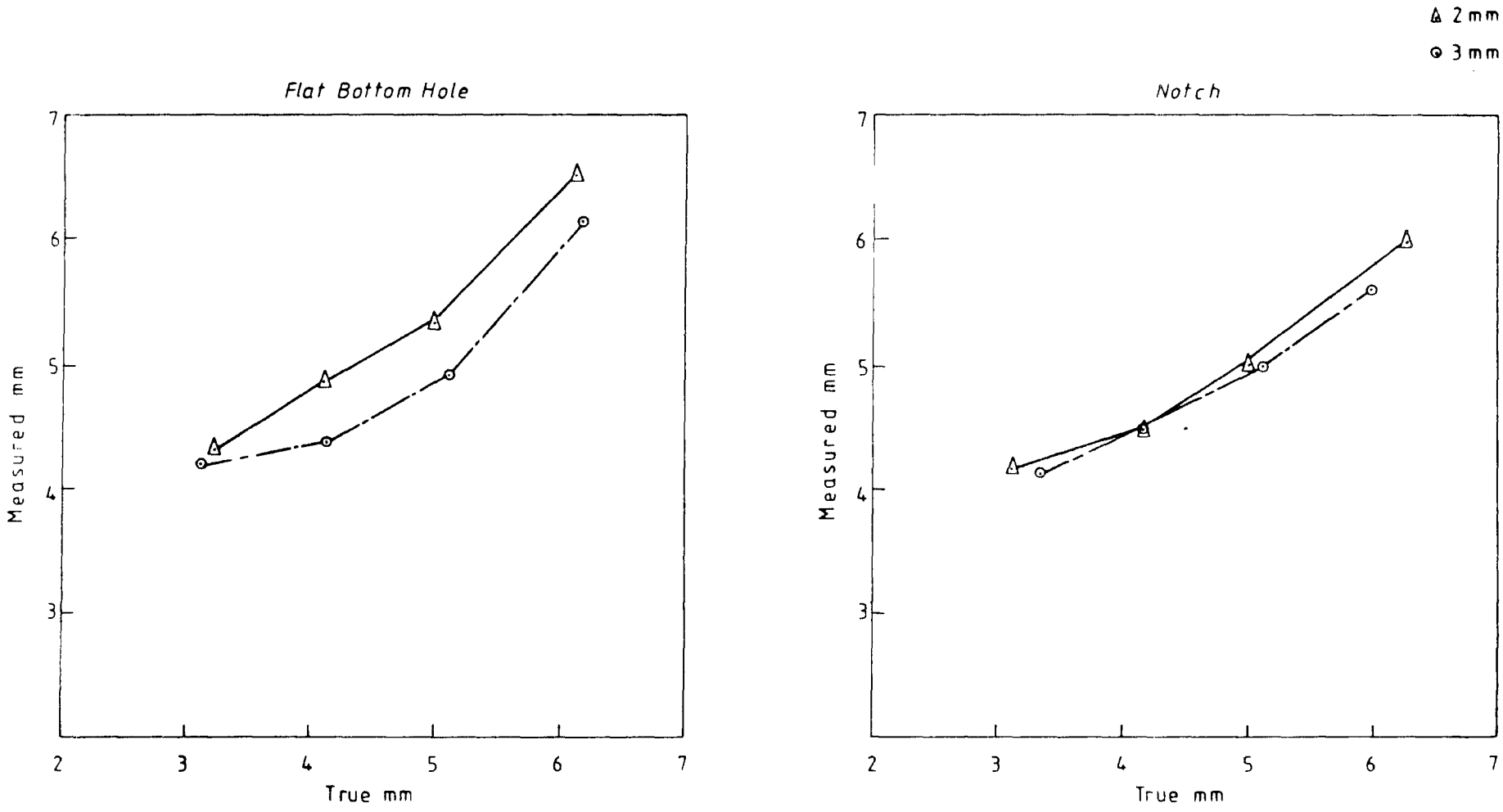

Fig. 61

Fig. 62

Figs. 61 & 62 : Average Depths Measured on the Testpipe from all Runs with the Above Water Corroscan P Scan

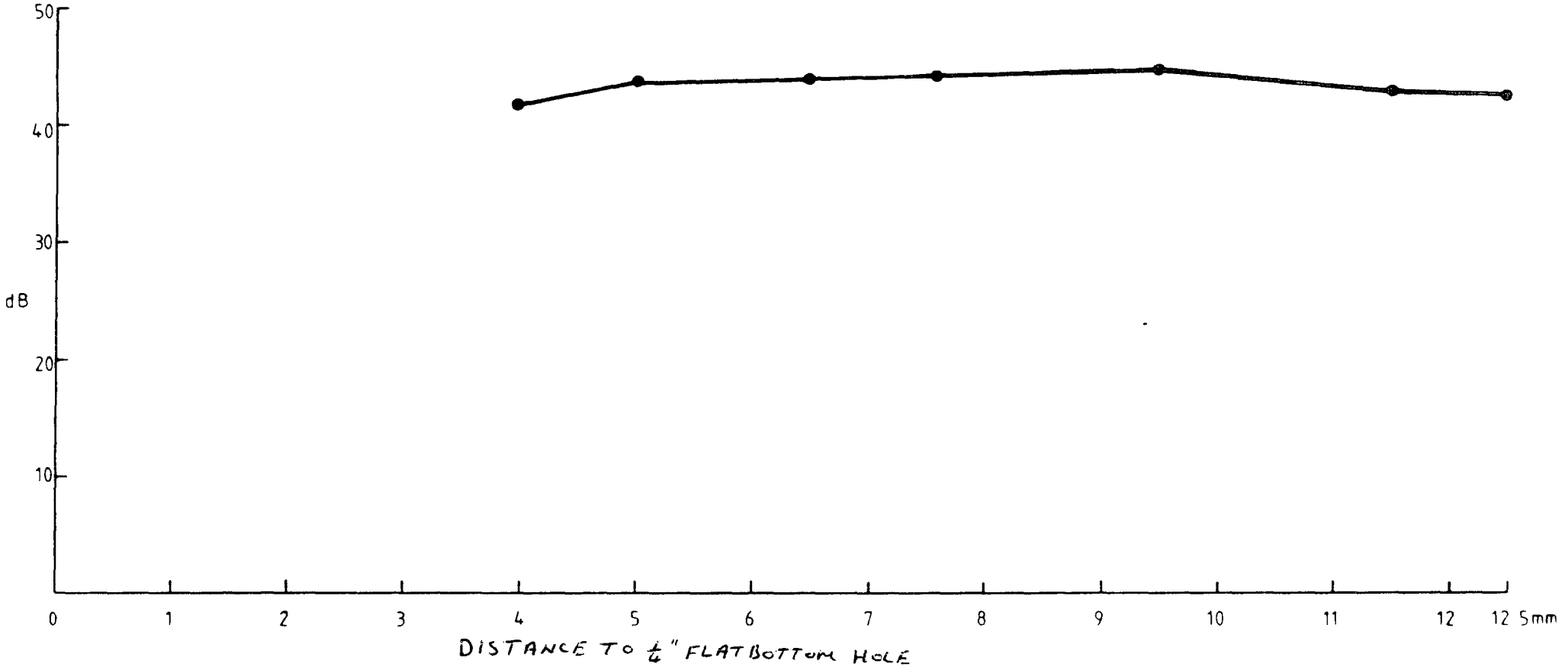

Fig. 63 : Characteristic Curve for the Ultra Image 0.25" Diameter 8MHz Transducer

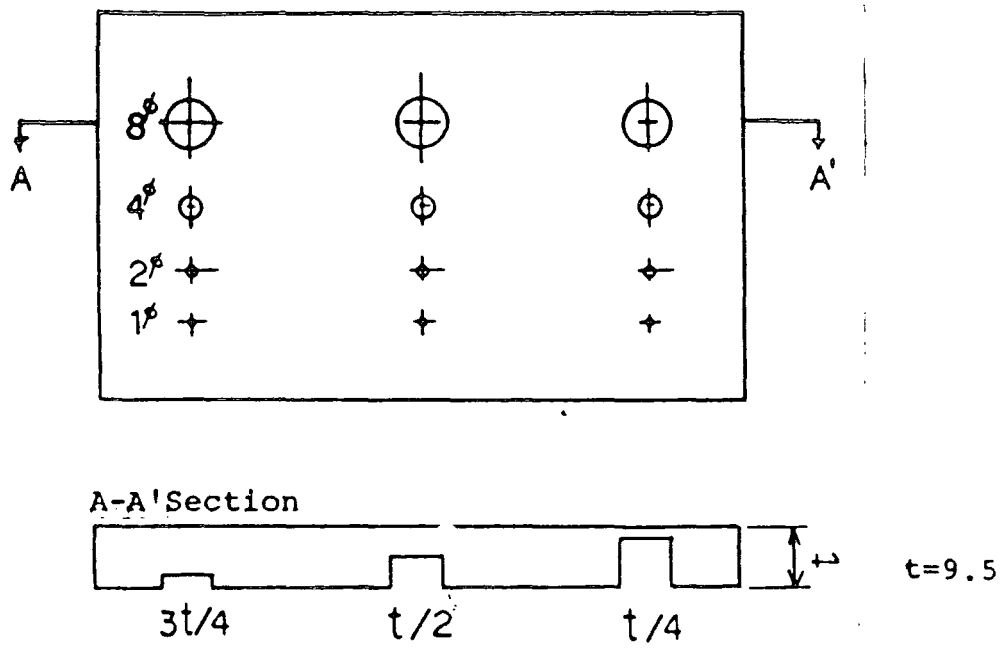

Figure 64 Reference Block for Ultrasonic Testing (Unit:mm)

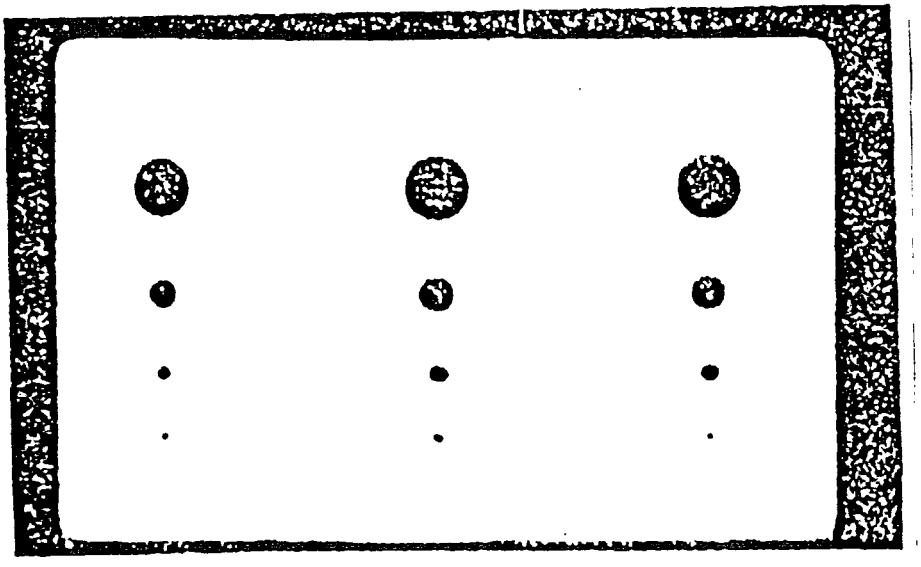

Figure 65 C-scan Image of Reference Block
(Transducer : 10MHz-1/4"D-1.5"F)

Figure 66 Pscan Results from a Reference Block as Shown in Figure 64

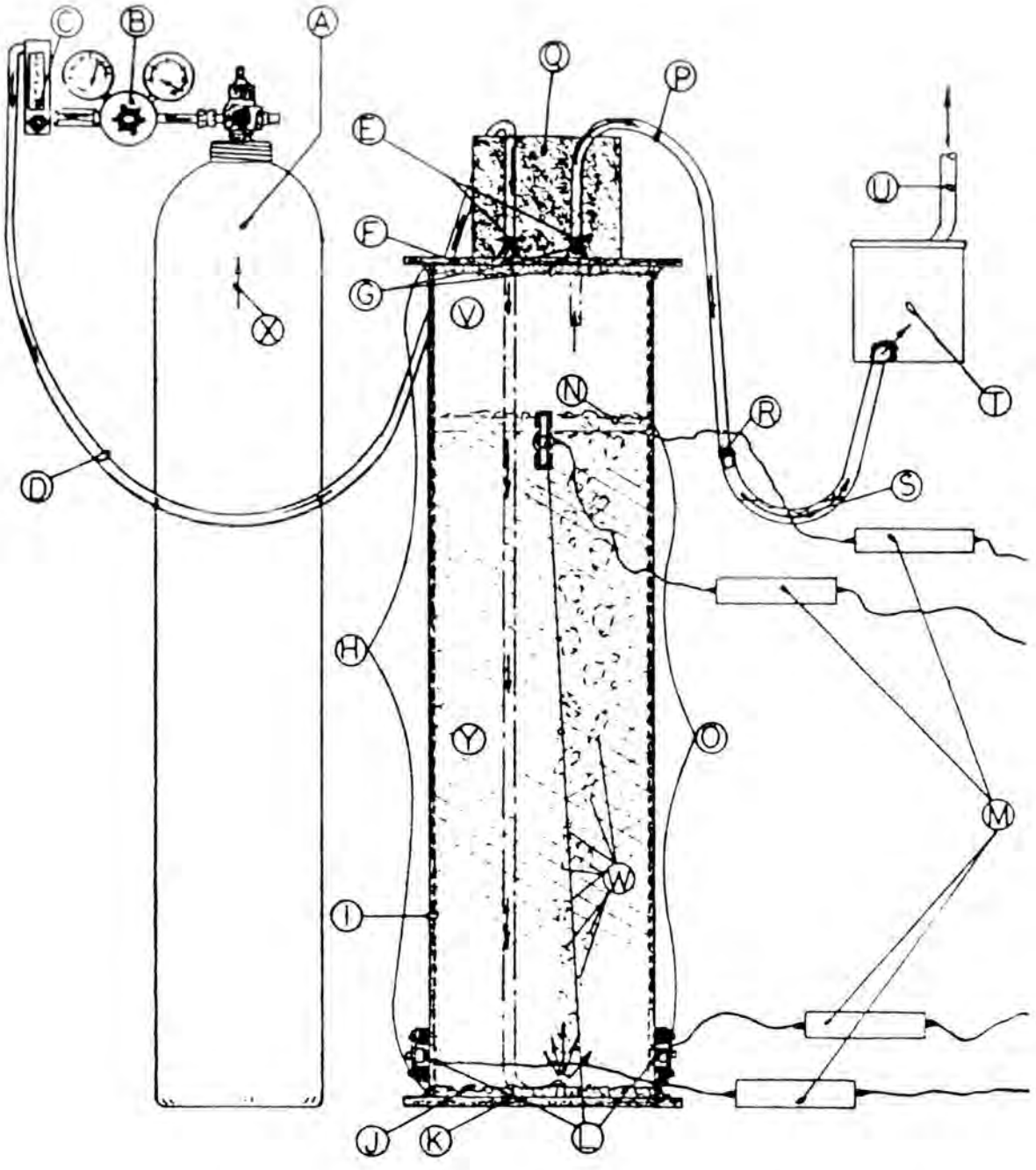

Figure 67 Schematic Representation of Testing Apparatus for HIC Under a Wet, Sour Environment (Scale 1:10). Legend of Labels Shown in the Figure Are Listed in the following Page.

Character	Identification
A	Hydrogen Sulfide (H_2S), Technical Grade UN 1053
B	Regulator
C	Flow Meter
D	Clear, Plastic Tubing for H_2S Tubing
E	Clamps for Hose and Fittings
F	Top End Plate
G	Top Rubber Seals
H	Pipe Test Section
I	Pipe Test Section Wall Thickness
J	Bottom Rubber Seal
K	Bottom End Plate
L	Magnetic AE Sensor Clamps (4 TYP), AE Sensors (4 TYP), & AE Sensor Lines (4 TYP)
M	Preamplifiers (4 TYP) & Coaxial Lines (Leading to Acoustic Emission Data Acquistion System) (4 TYP)
N	Solution Level
O	Area of Pipe Test Section Containing Wet, Sour Solution
P	H_2S Extraction Line
Q	Metal Block for Providing Rigid Seal
R	Break/Seal in Extraction Line for Maintaining Water Level
S	Water
T	Scrubber
U	Exhaust Line Leading to Vent Hood
V	Positive Pressure Maintained

Character	Identification
W	H_2S Bubbles
X	Gas Flow Direction
Y	Area Covered by Acoustic Emission

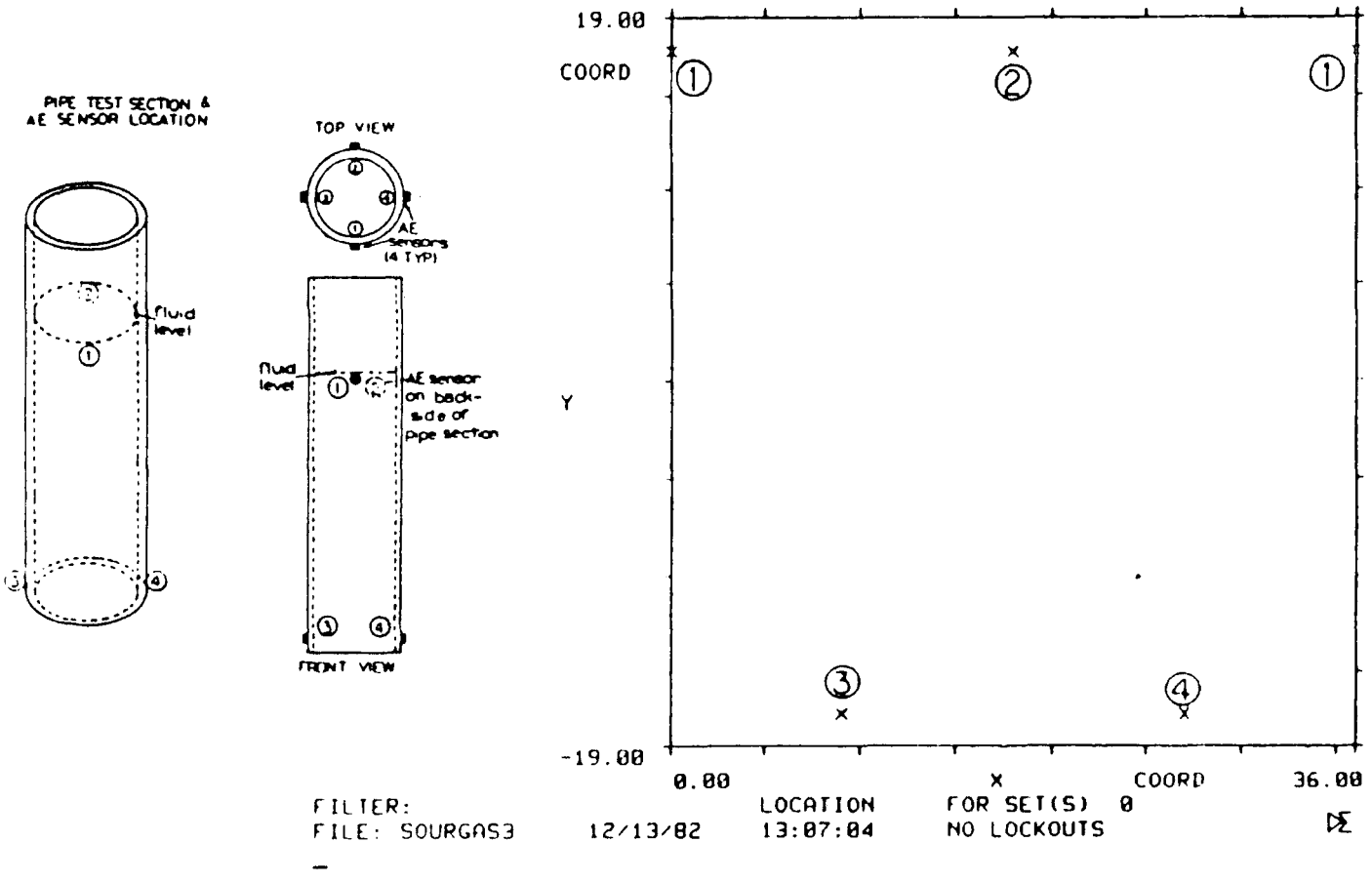

Figure 68 Sensor Location for Cylindrical Configuration (Dimensions: Inches).

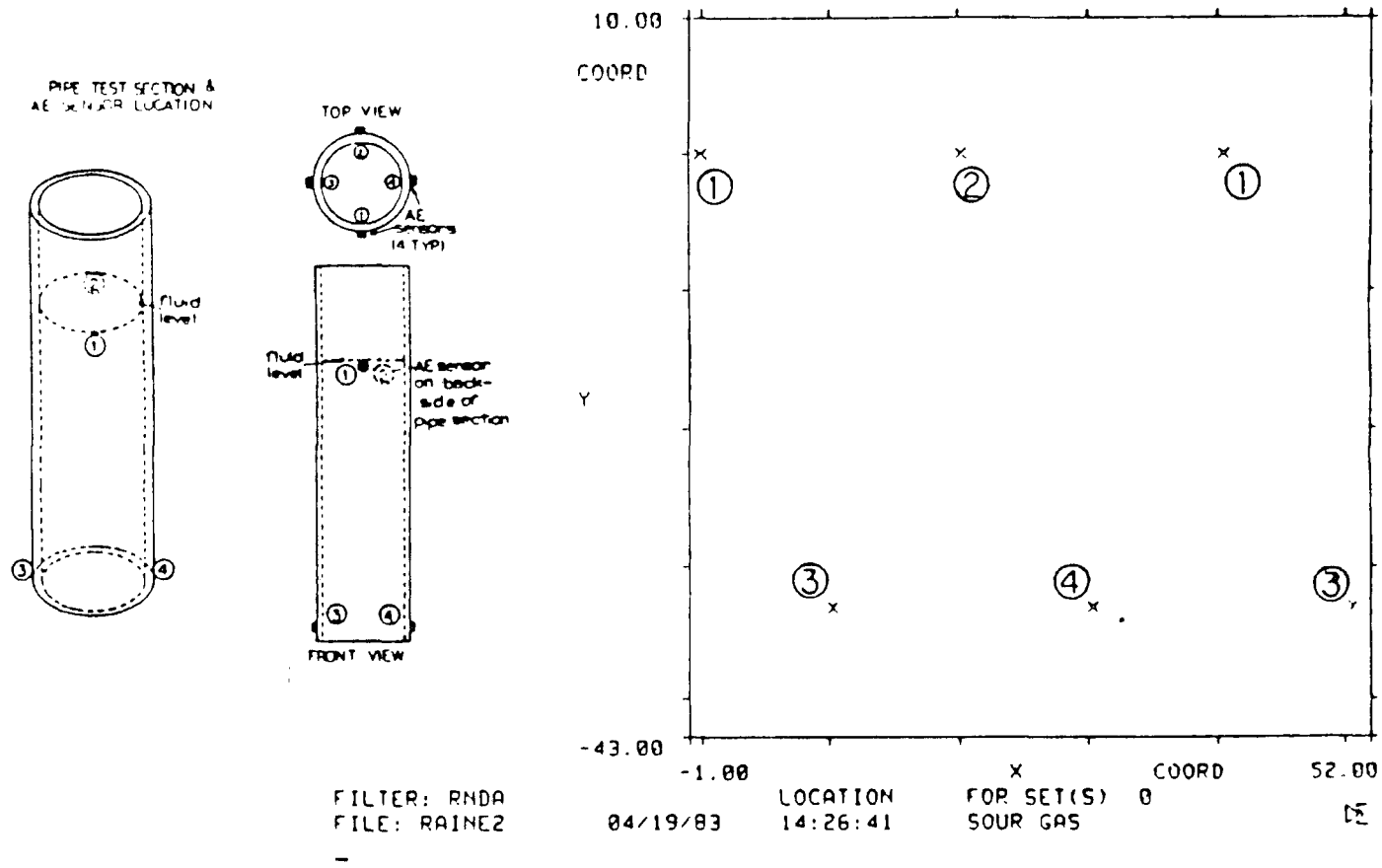

Figure 69 Sensor Location of Multi-Triplet Configuration (Dimensions: Inches).

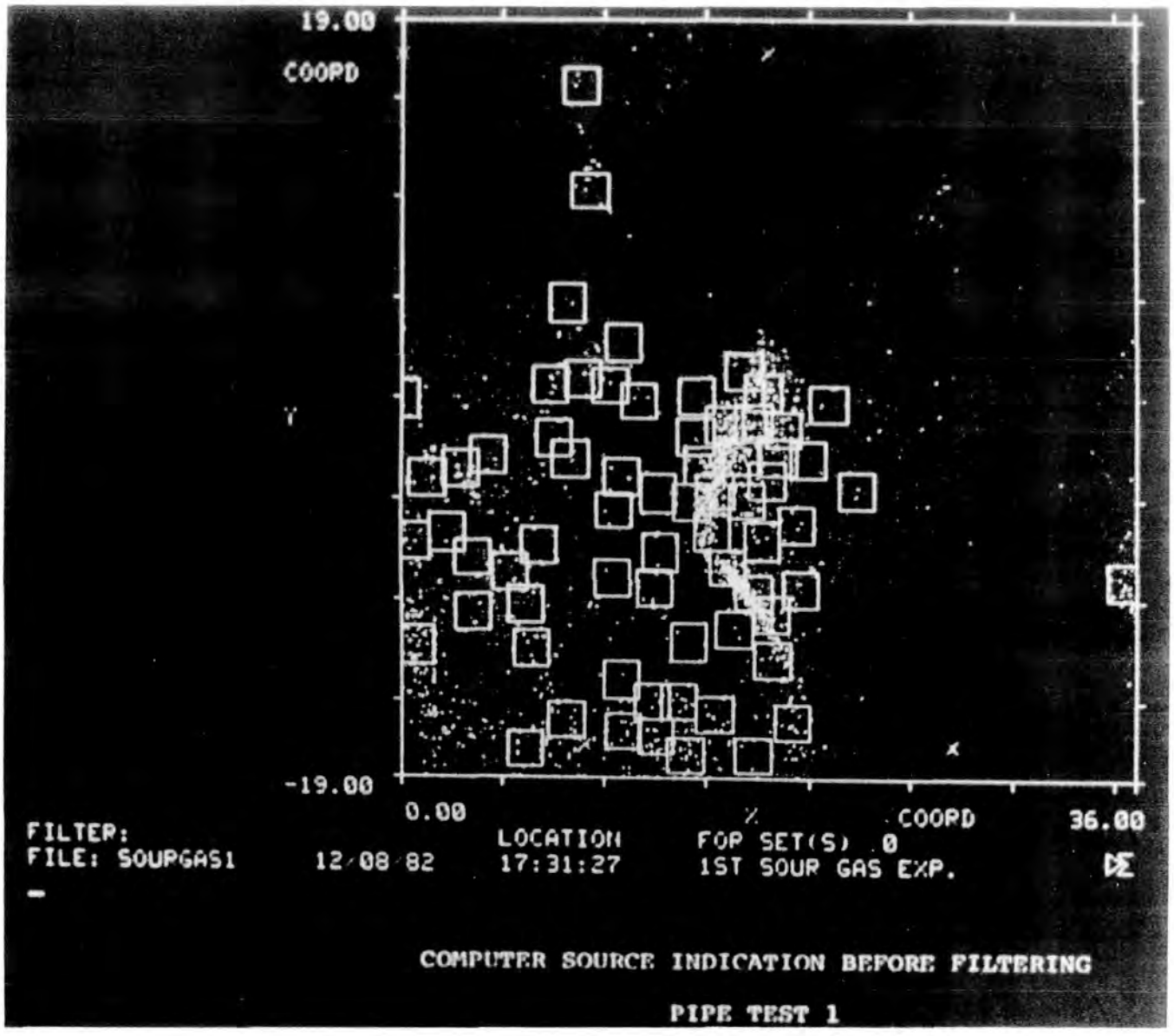

Figure 70
Computer source indication before filtering

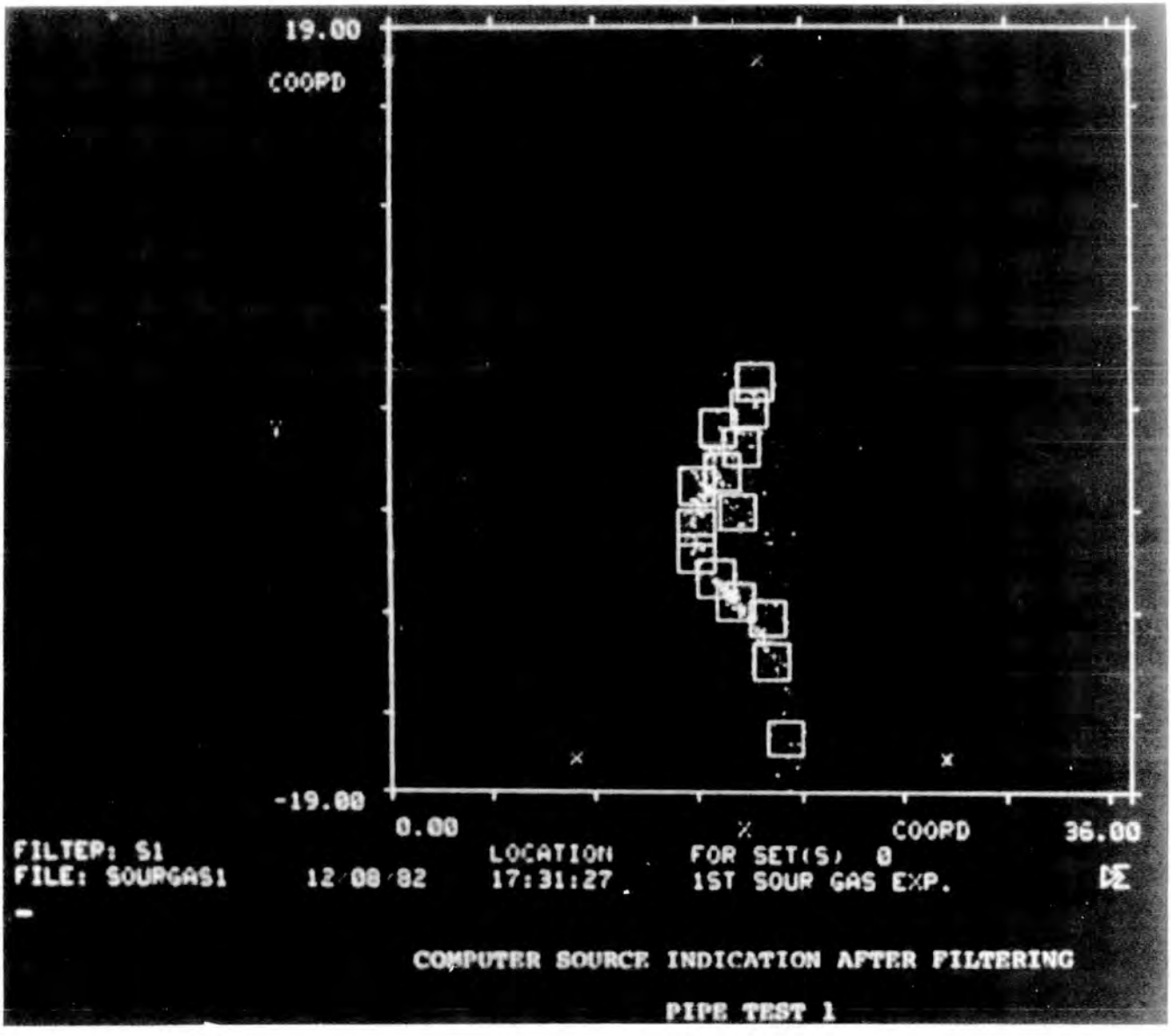

Figure 71
Computer source indication after filtering

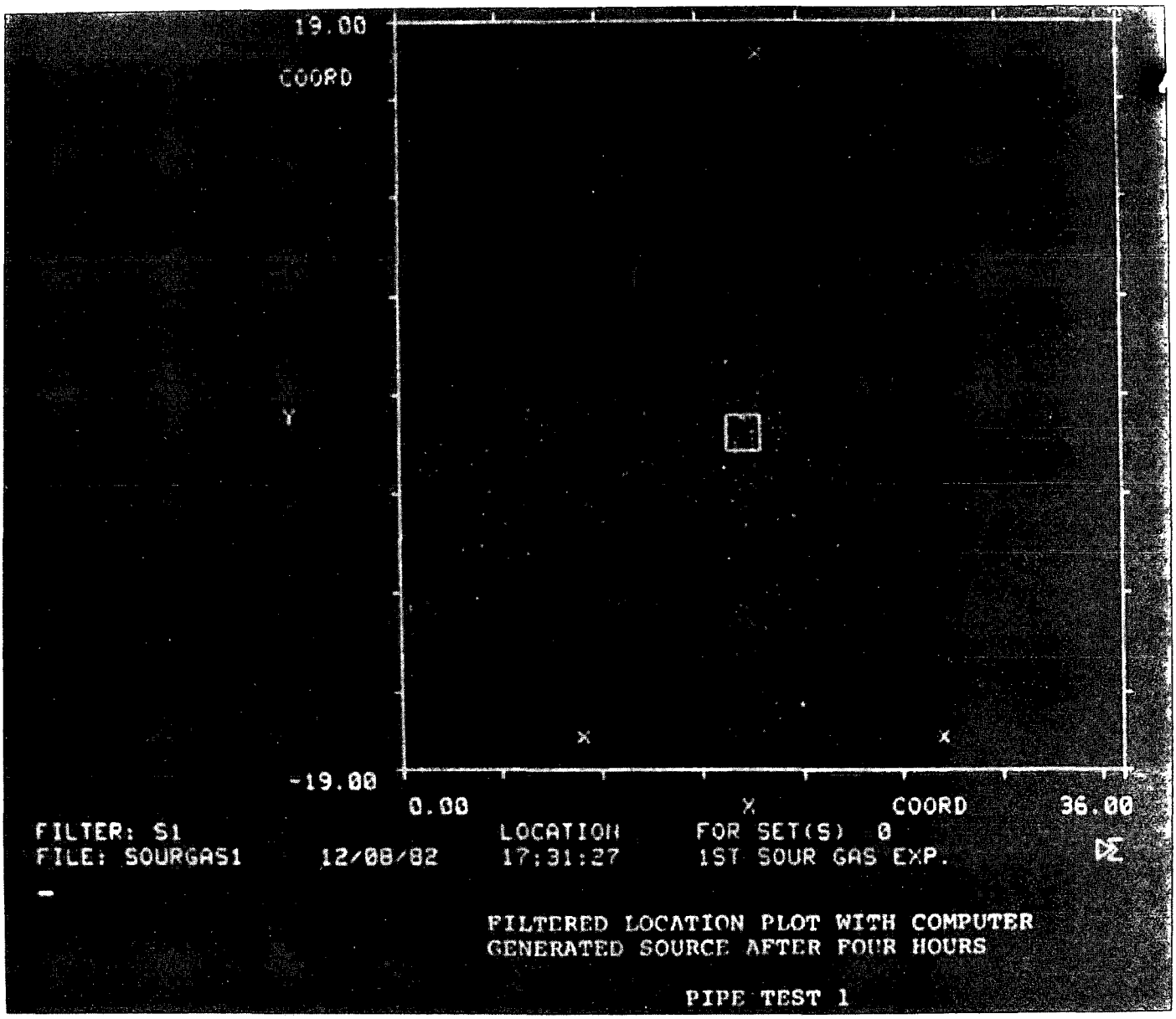

Figure 72
Location plot produced from a simulated source

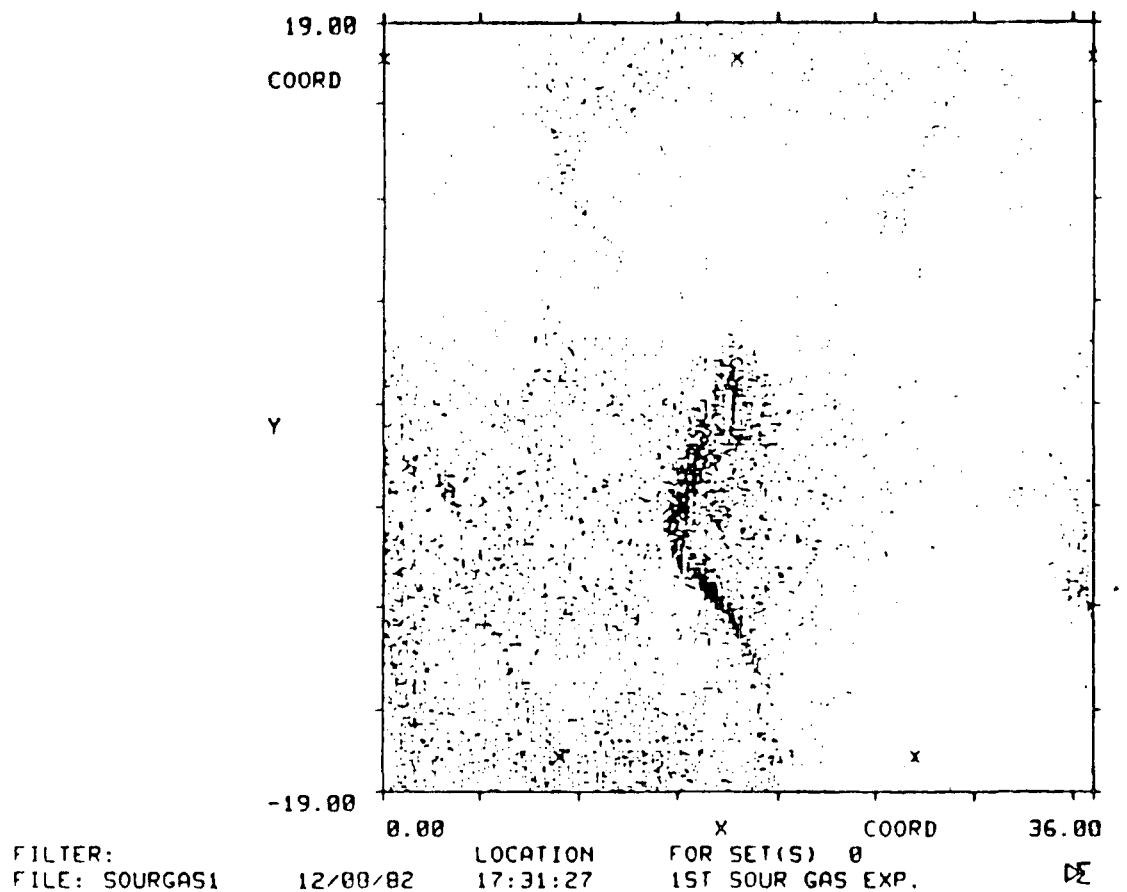

Figure 73 Unfiltered Cylindrical Location Plot of Pipe Test Section 1 (Dimensions: Inches).

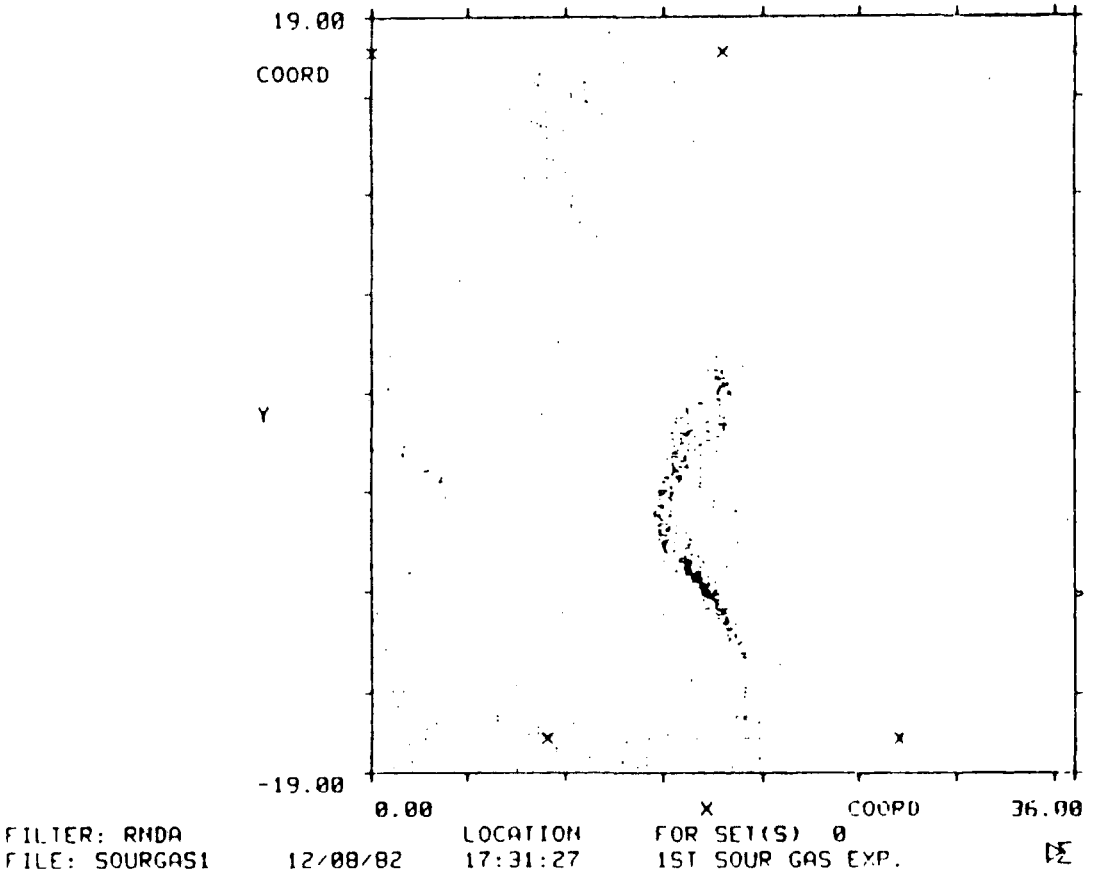

Figure 74 Cylindrical Location Plot of Pipe Test Section 1, Filtered, Disc 1 (Dimensions: Inches).

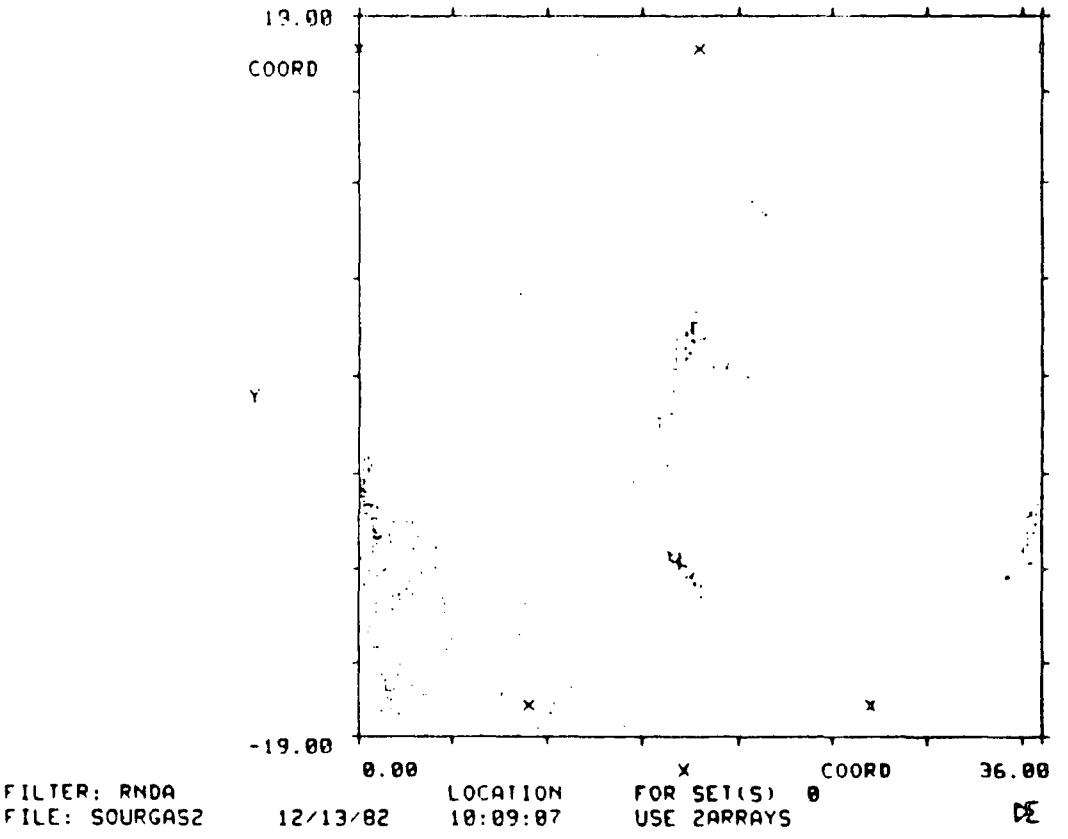

Figure 75 Cylindrical Location Plot of Pipe Test Section 1, Filtered, Disc 2 (Dimensions: Inches).

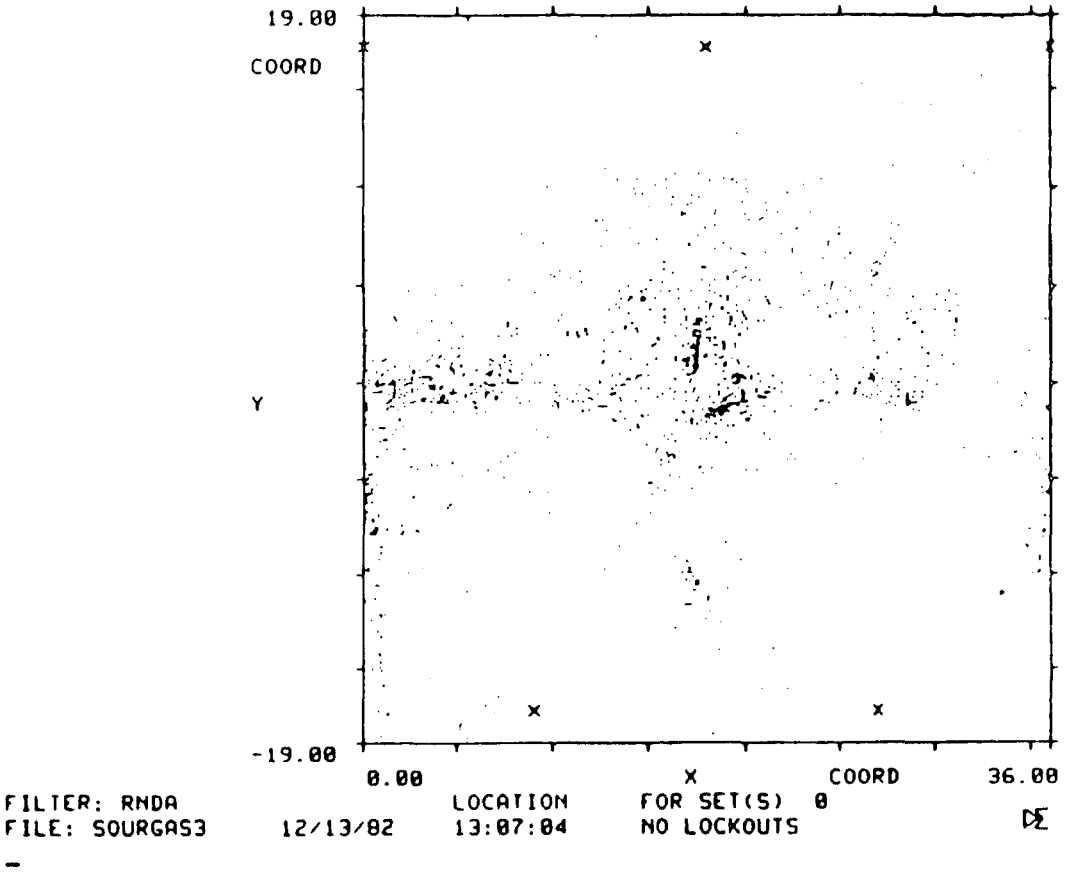

Figure 76 Cylindrical Location Plot of Pipe Test Section 1, Filtered, Disc 3 (Dimensions: Inches).

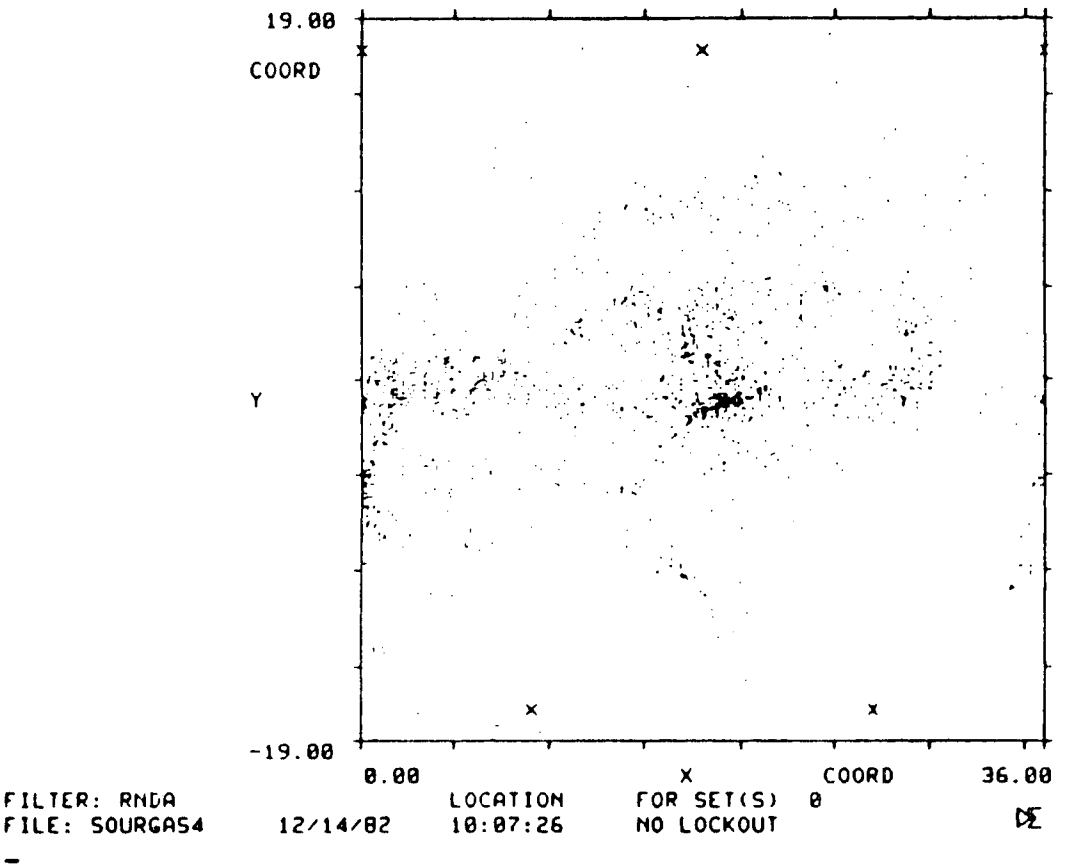

Figure 77 Cylindrical Location Plot of Pipe Test Section 1, Filtered, Disc 4 (Dimensions: Inches).

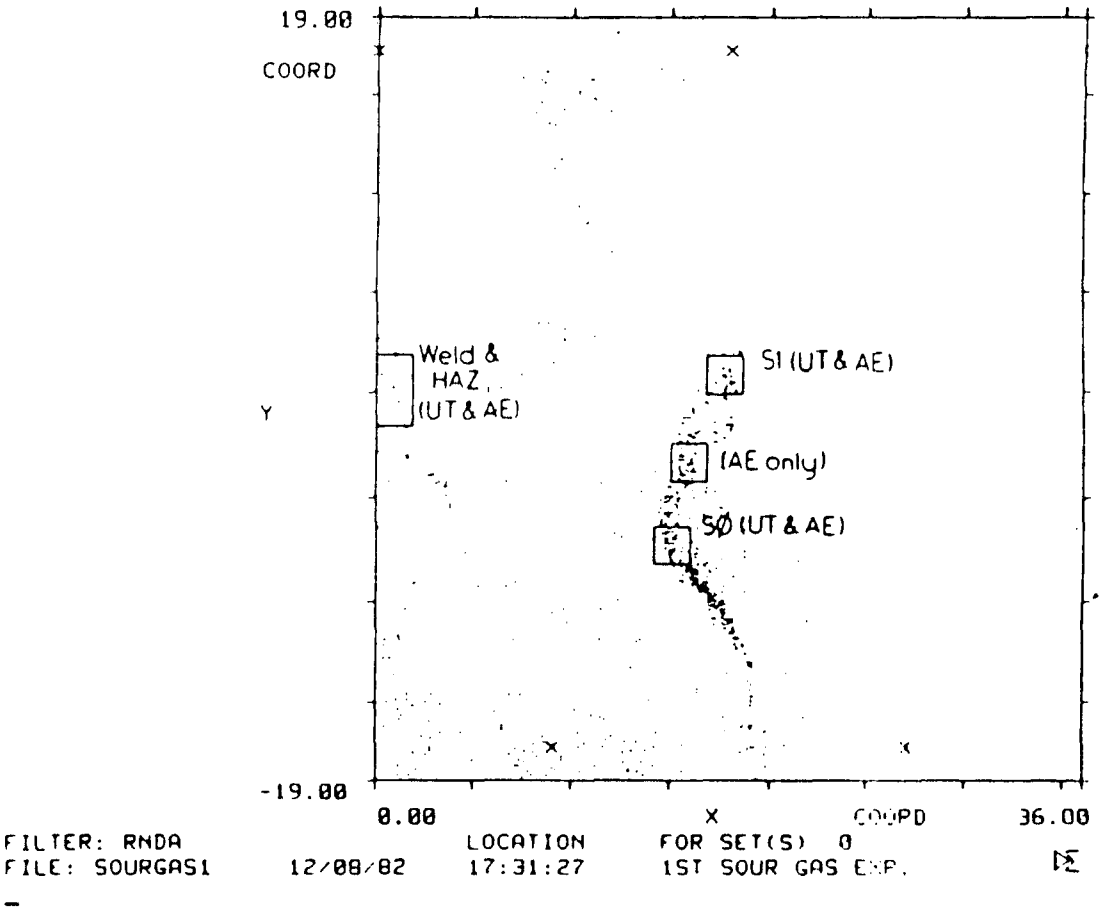

Figure 78 Cylindrical Location Plot of Pipe Test Section 1 Showing Areas of Ultrasonic Indications and Regions Removed for Metallographic Examination. (Dimensions: Inches)

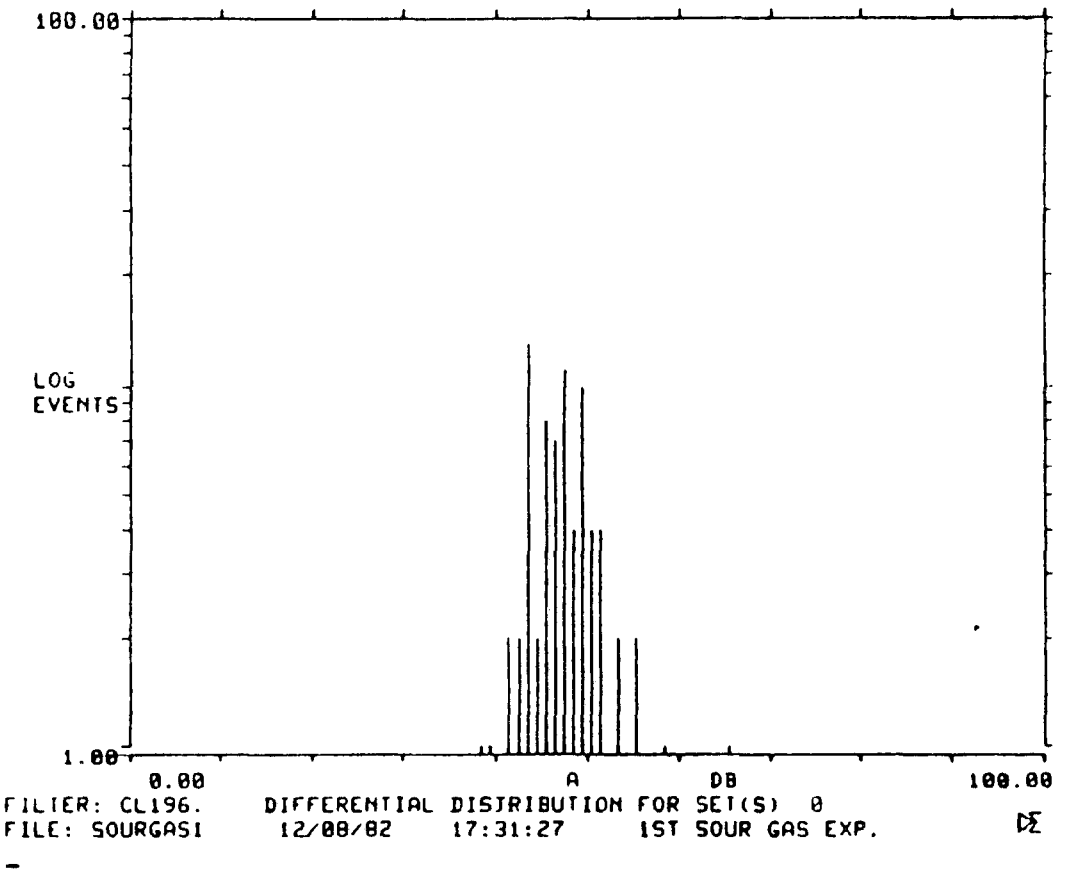

Figure 79. Amplitude Distribution Plot of Region SO Taken from Pipe Test Section 1.

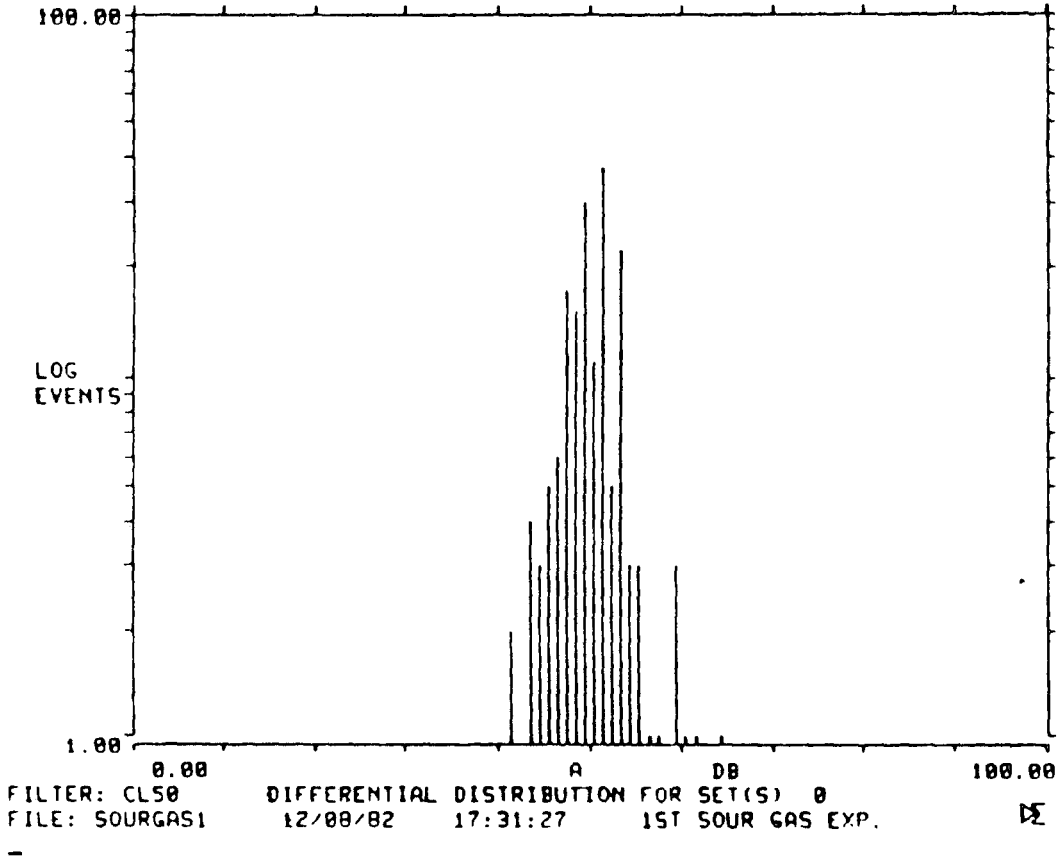

Figure 80 . Amplitude Distribution Plot of Region S1 Taken from Pipe Test Section 1.

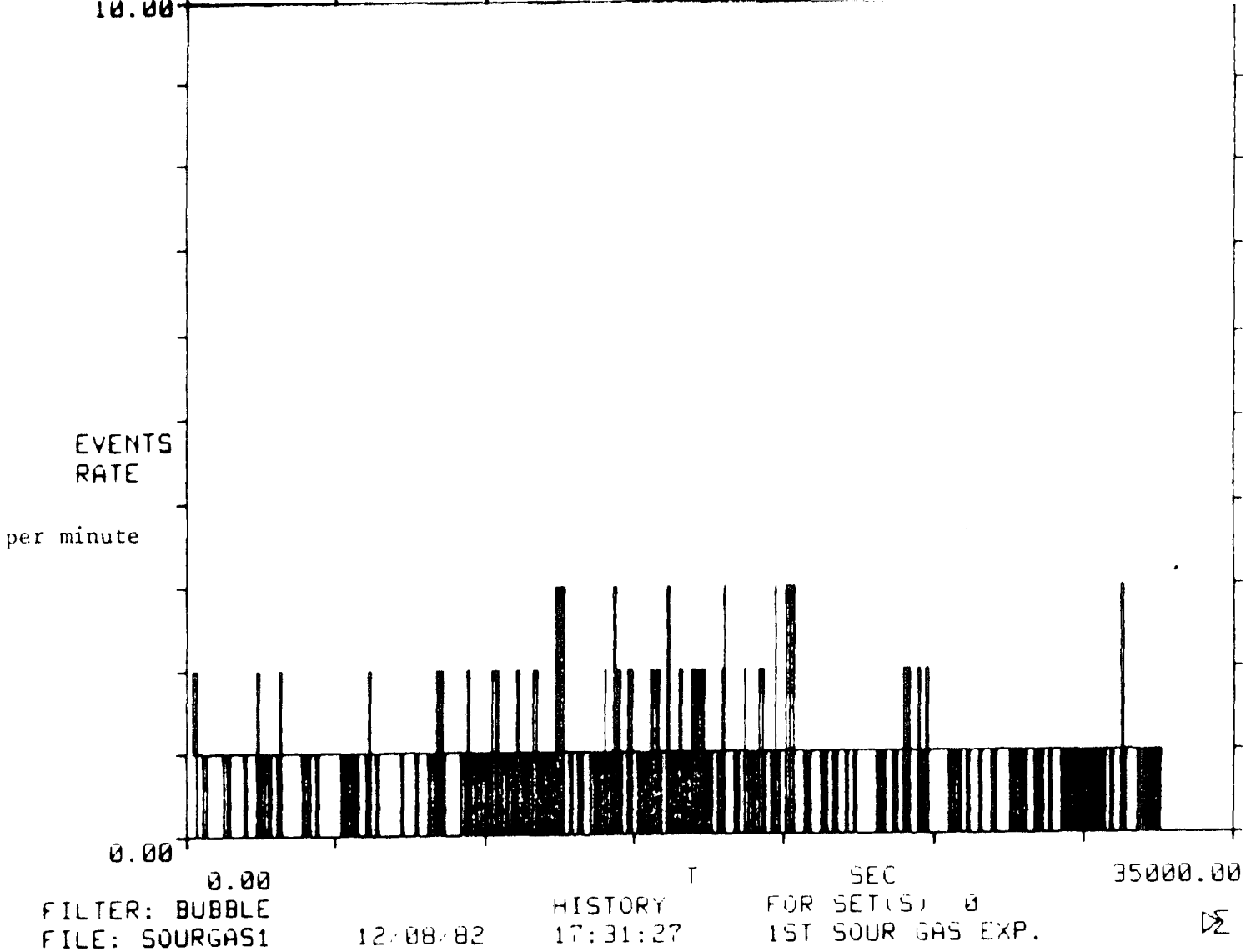

Figure 81 History Plot of Acoustic Emission Events over Ten Hours

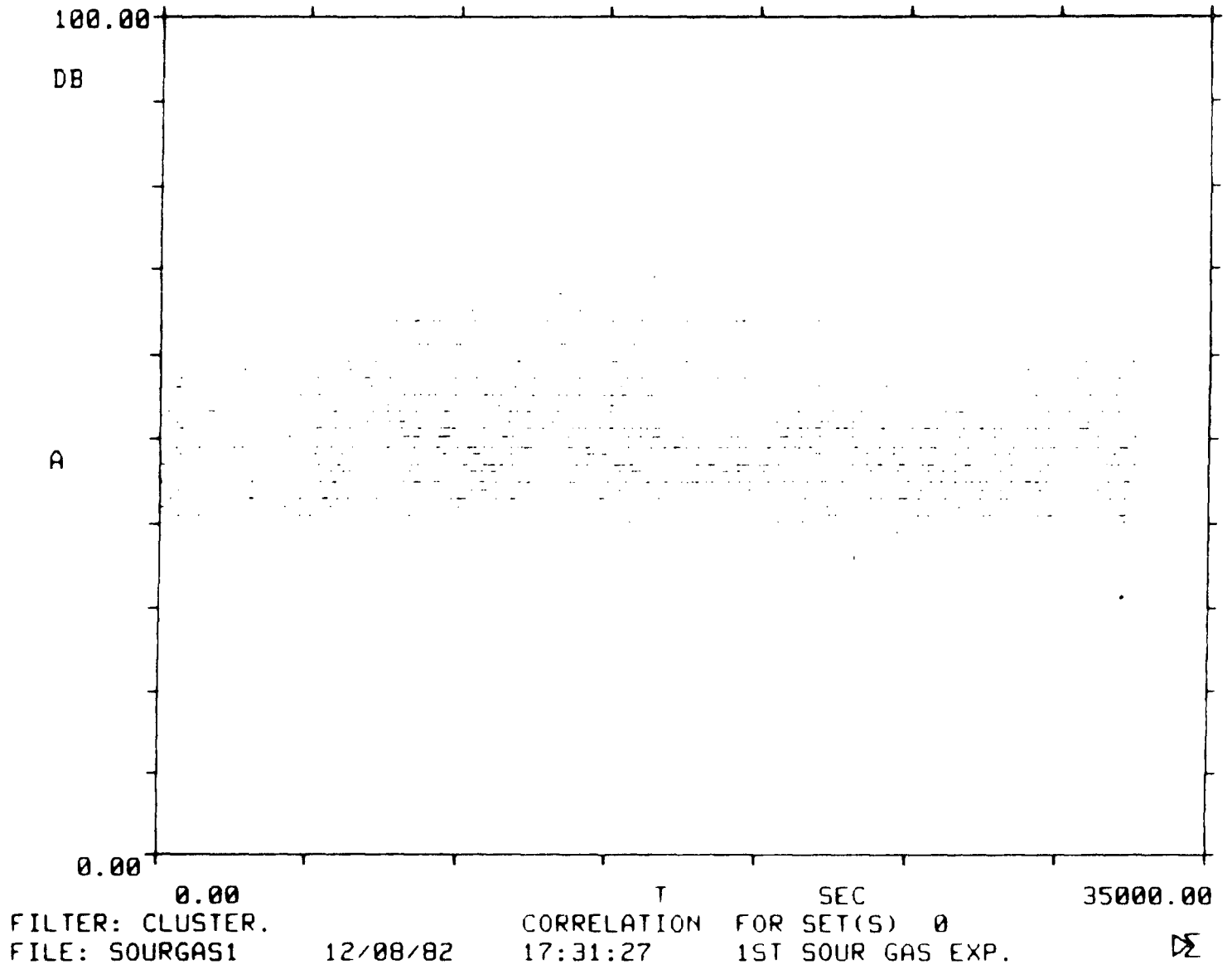

Figure 82 History of Amplitude Against Time

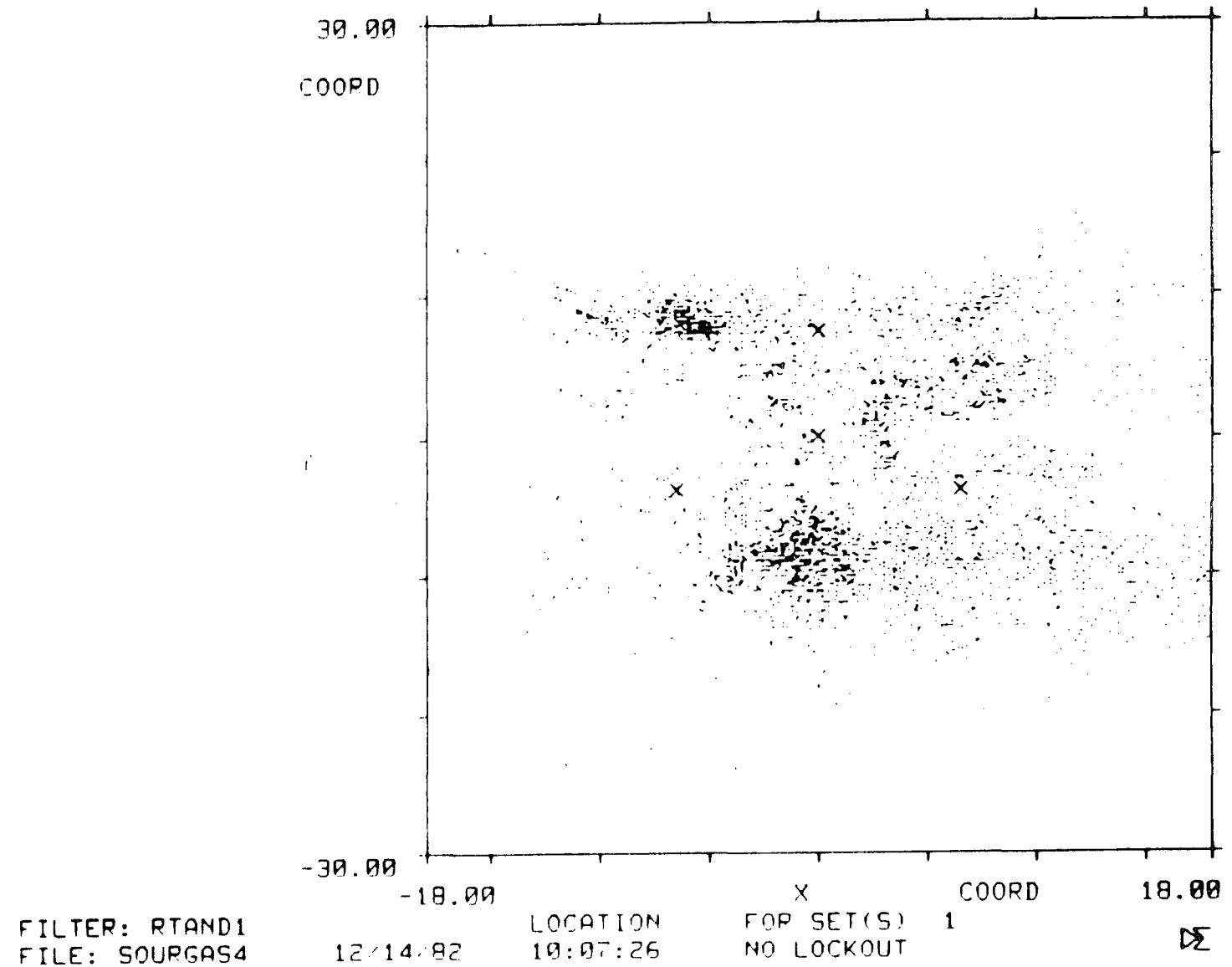

Figure 83 Location Plot for Array S1

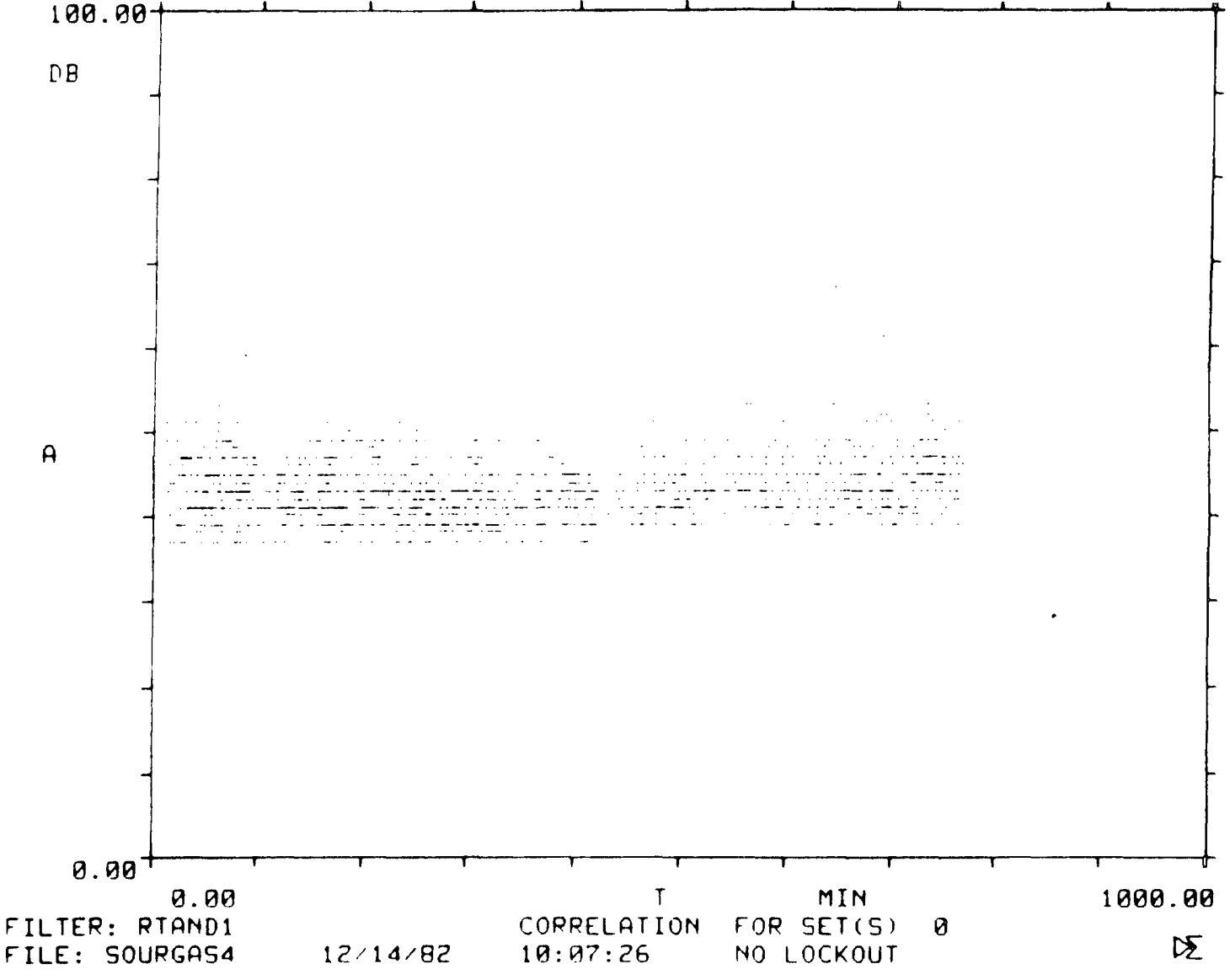

Figure 84 Amplitude history plot for array S0

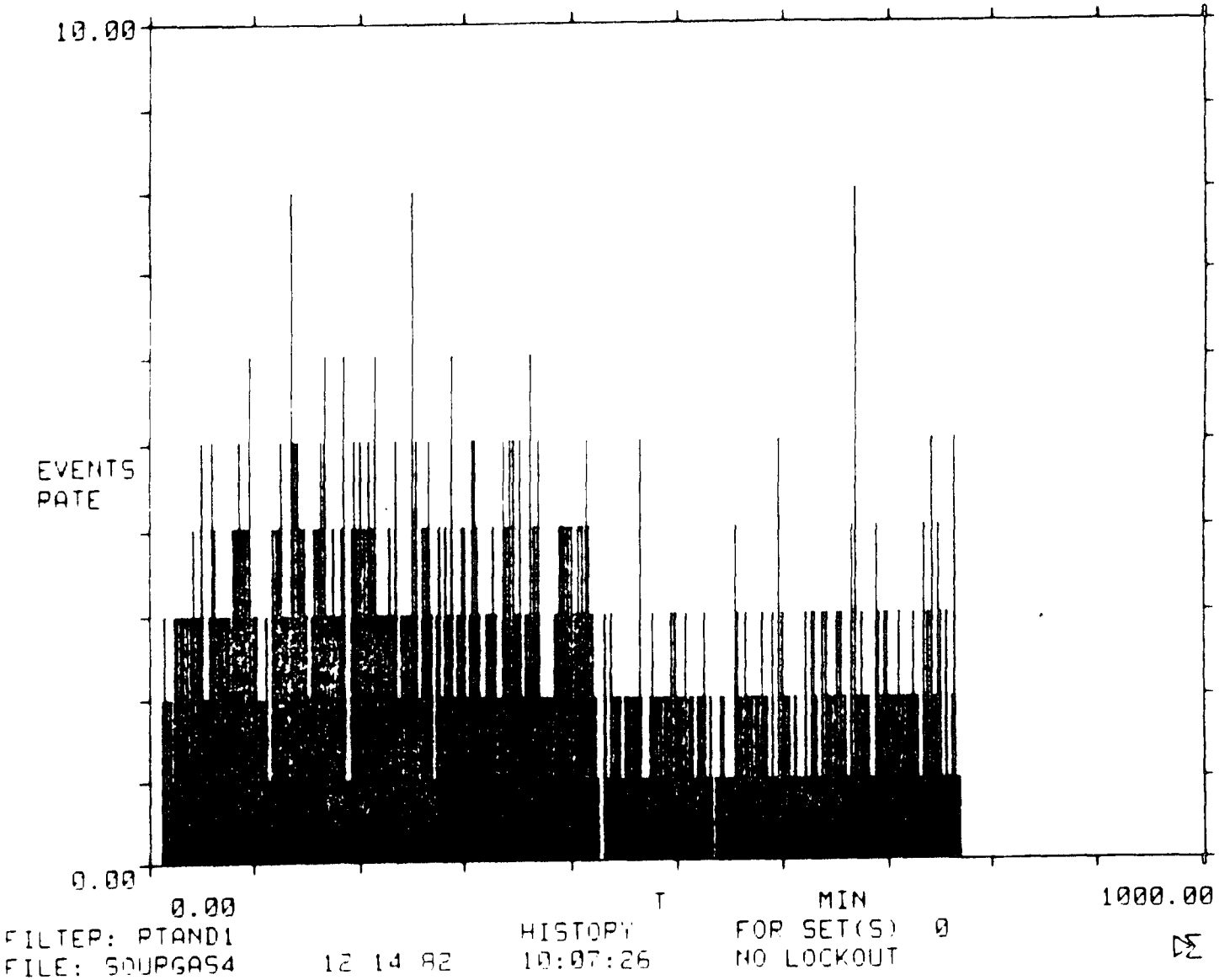

Figure 84(a) Event rate history plot for array SO

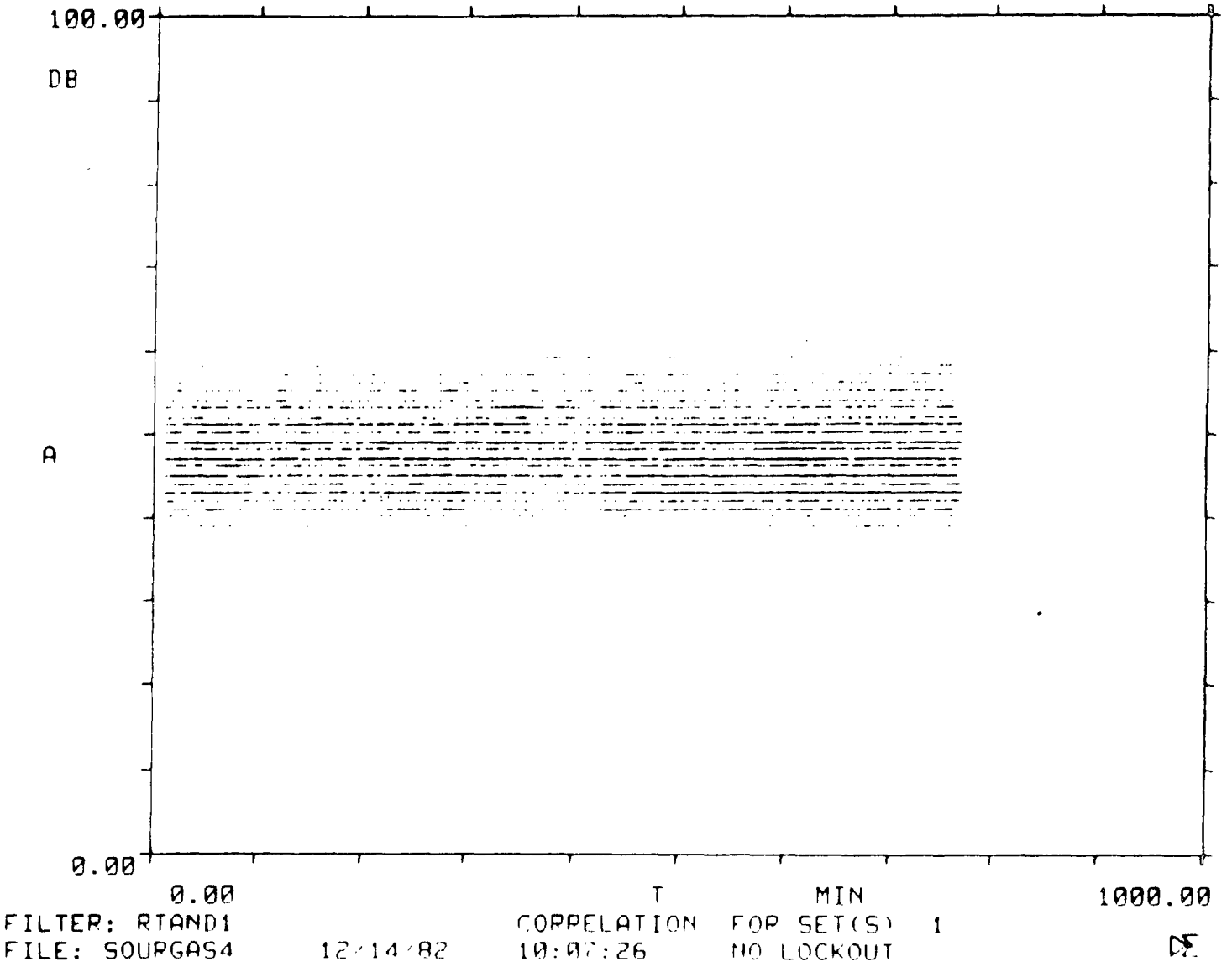

Figure 85 Amplitude history plot for array S1

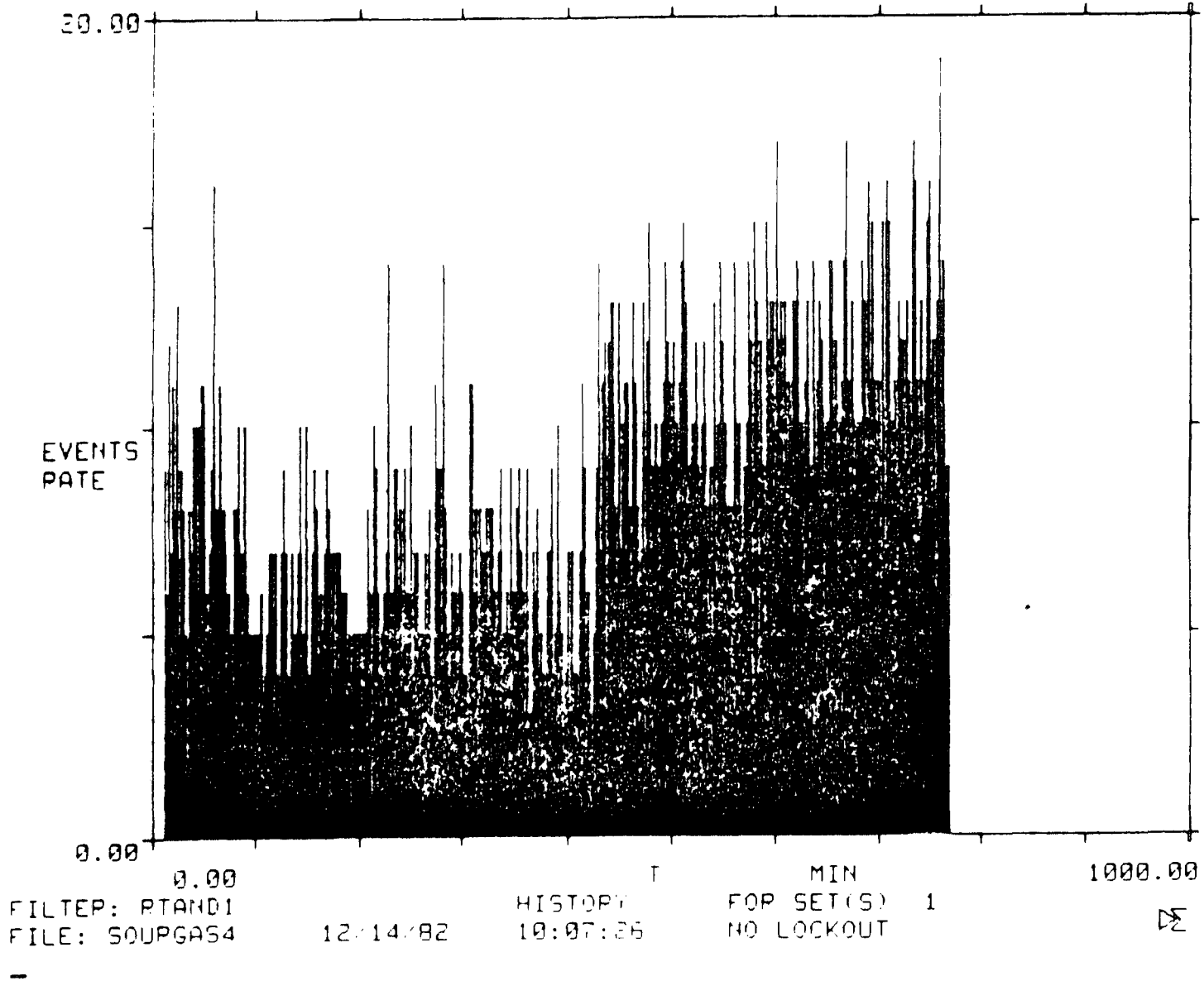

Figure 85(a) Event rate history plot for array S1

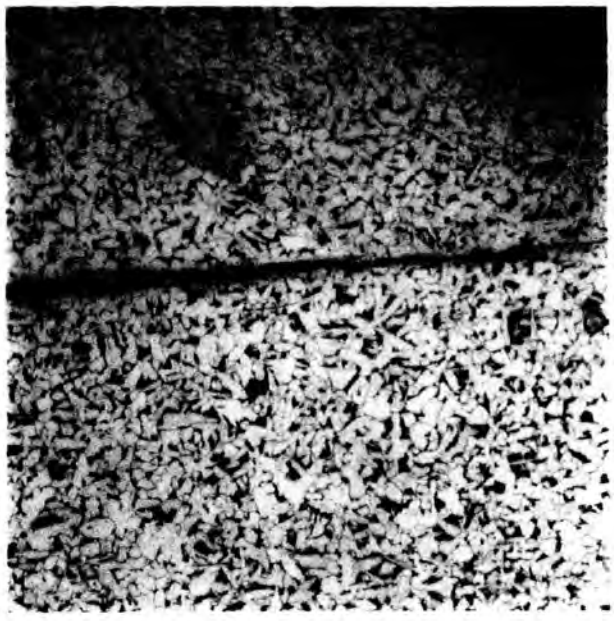

Figure 86
Laminar hydrogen induced crack detected in area S0 x 100

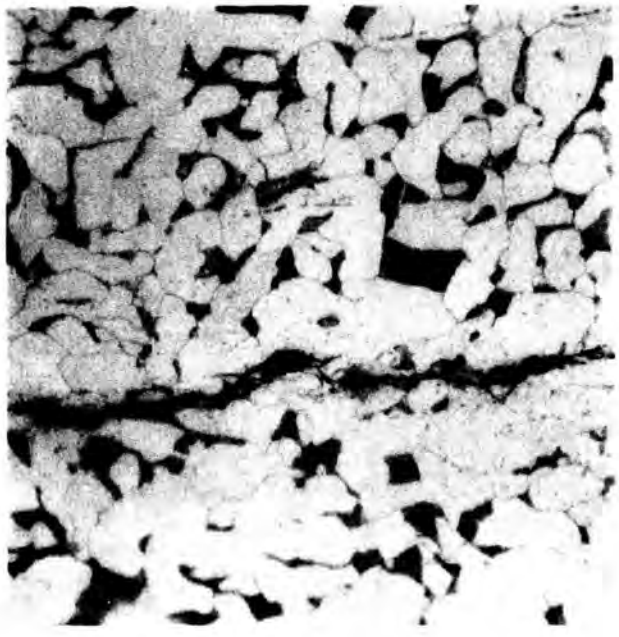

Figure 87
Non metallic inclusions associated with the crack x 400

Figure 88
Near surface crack located within 1 mm of the inner surface. x 10

Figure 89
Classical step wise hydrogen induced crack revealed near to the surface x 100 showing extreme banding.

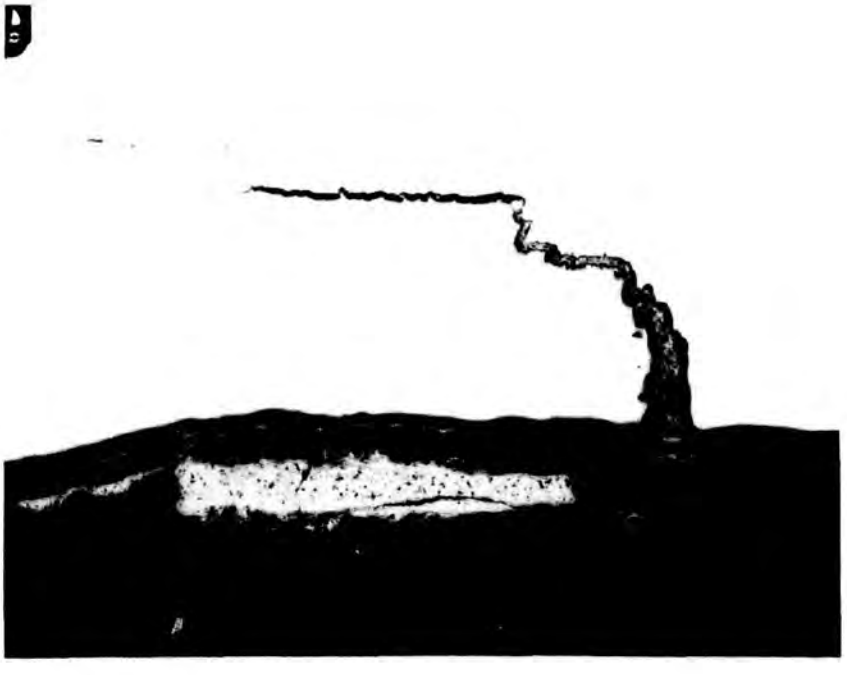

Figure 90
Hydrogen induced crack located in area S1 x 10

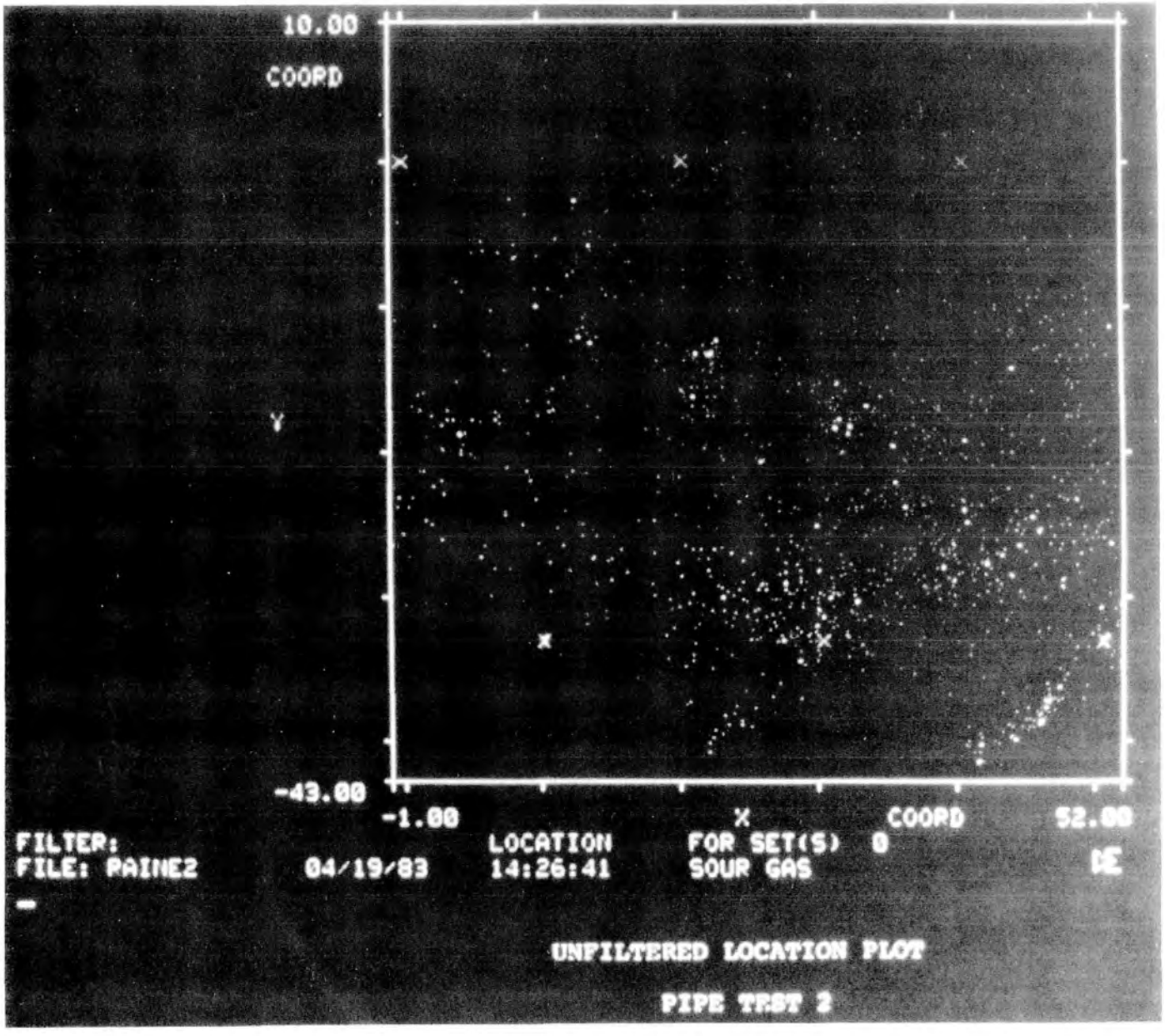

Figure 91
Multi Triplet Location Plot of Pipe Section 2,
Unfiltered

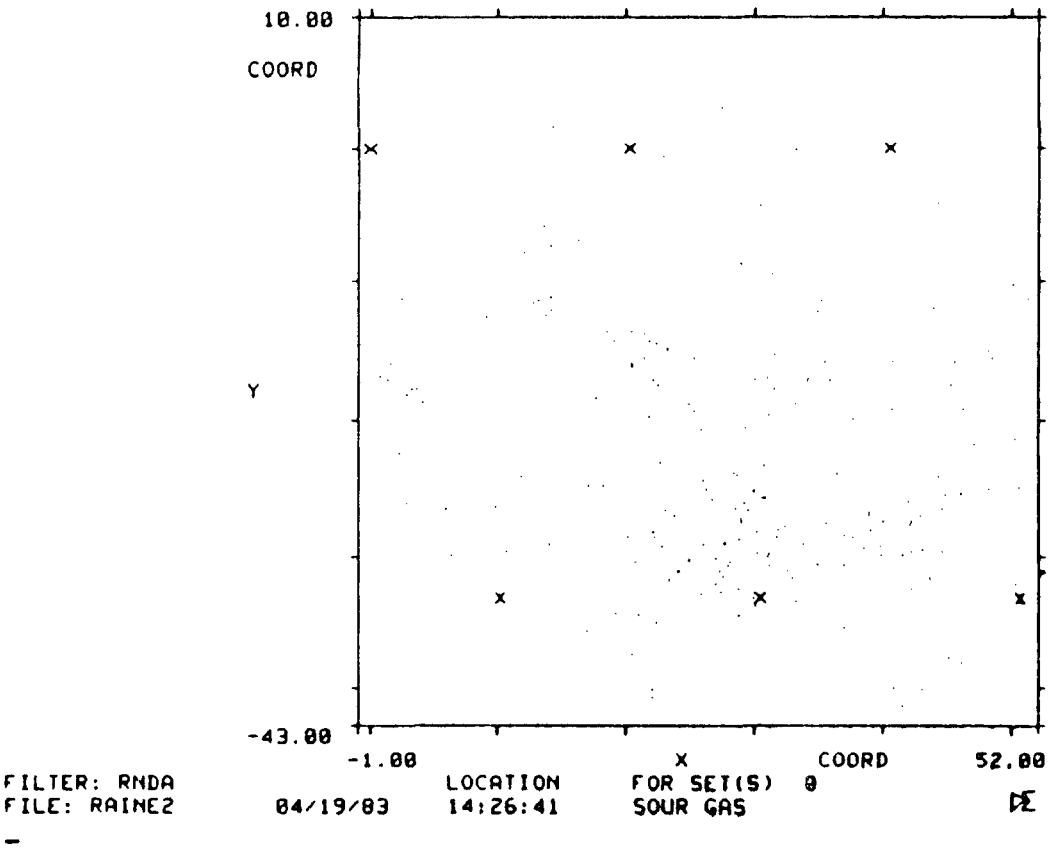

Figure 92 Multi-Triplet Location Plot of Pipe Section 2, Filtered. (Dimensions: Inches)

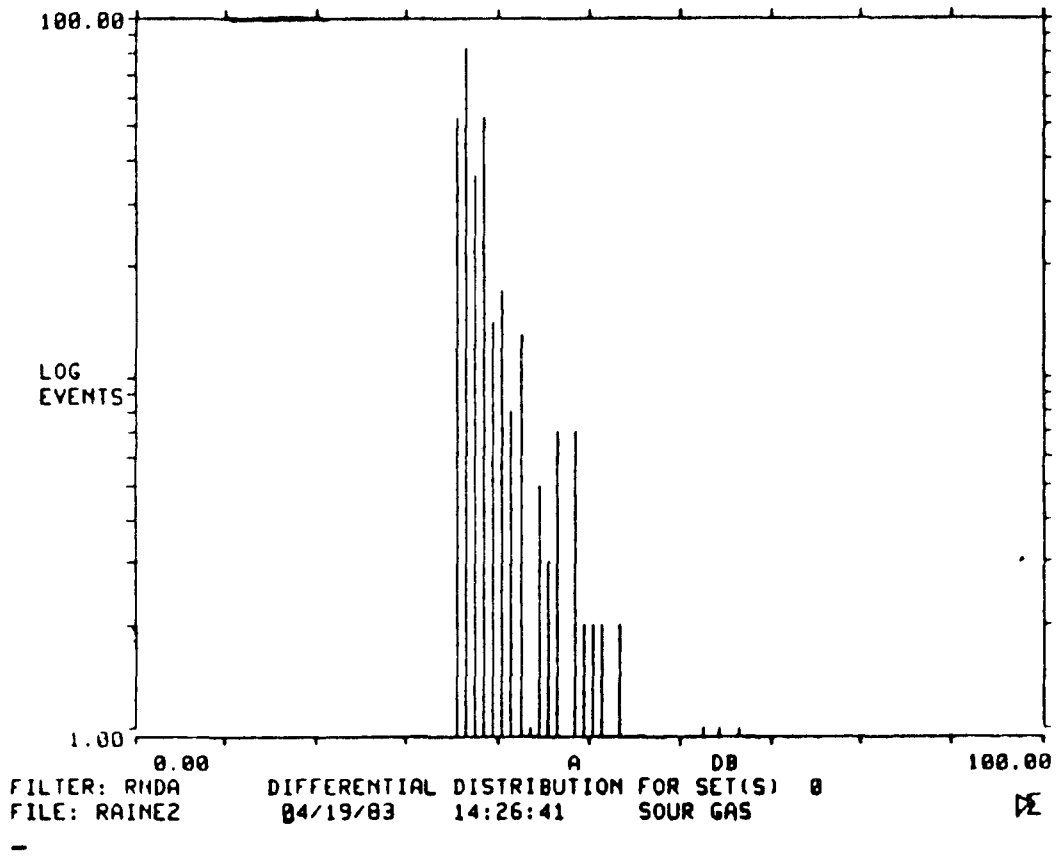

Figure 93 Amplitude Distribution Plot of Pipe Test Section 2.

Figure 94 Microphotograph of Banded Microstructure as Seen in Pipe Test Section 1.
150x, 2% Nital.

Figure 95 Microphotograph of Banded Microstructure Present in Pipe Test Section 2. Although the Banded Microstructure Was Present, the Elongated, Stringer-Like Inclusions Were Not
150x, 2% Nital.

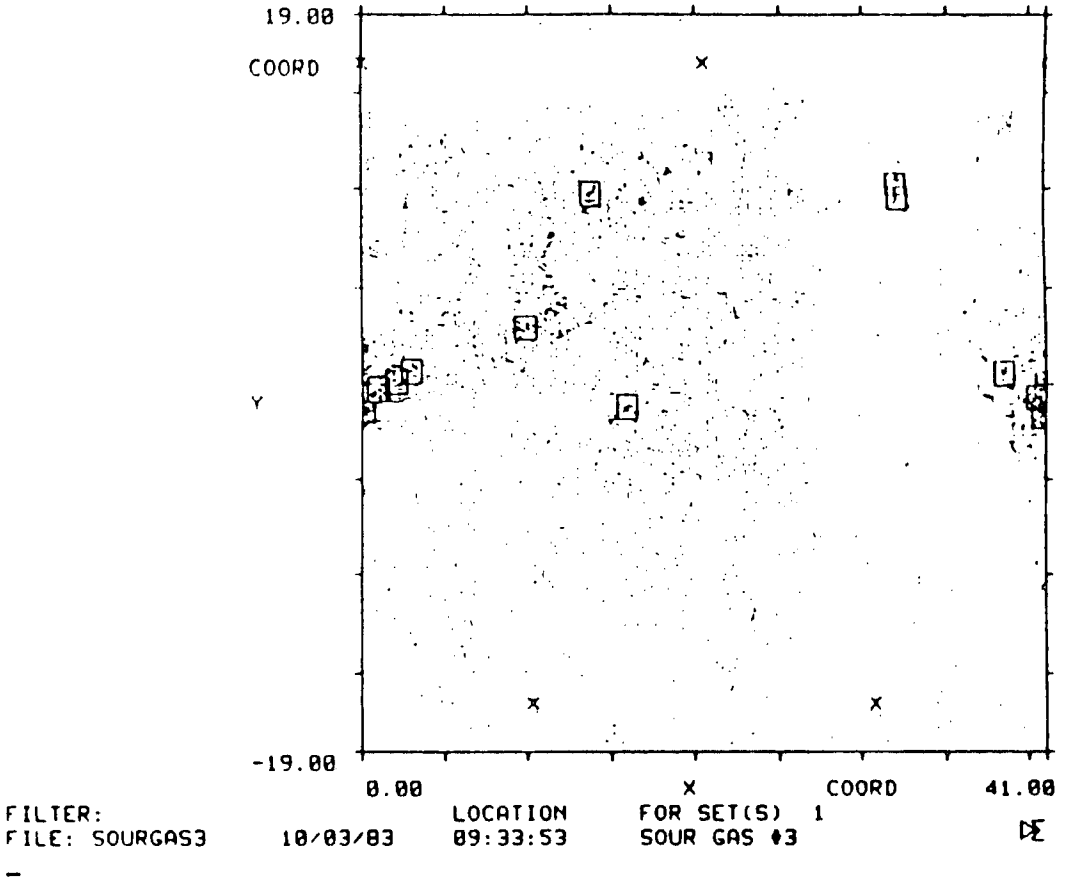

Figure 96 Cylindrical Location Plot of Pipe Test Section 3, Unfiltered. (Dimensions: Inches)

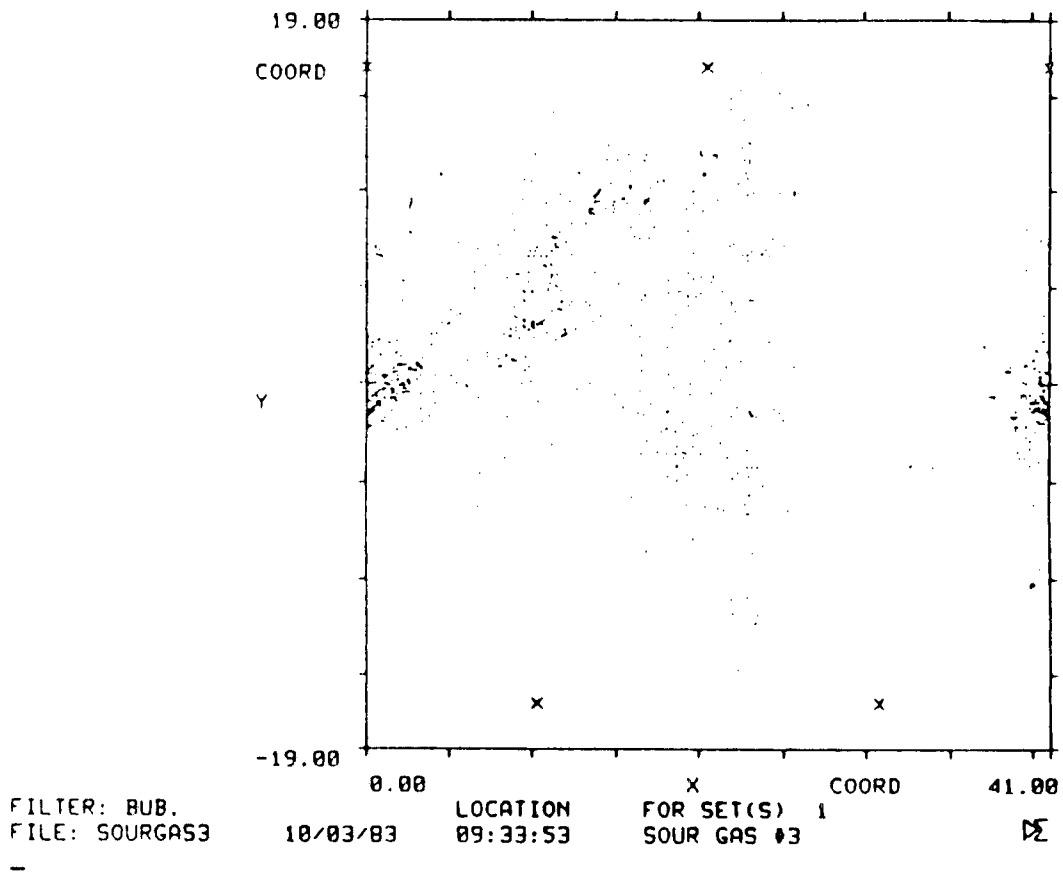

Figure 97 Cylindrical Location Plot of Pipe Test Section 3, Filtered. (Dimensions: Inches)

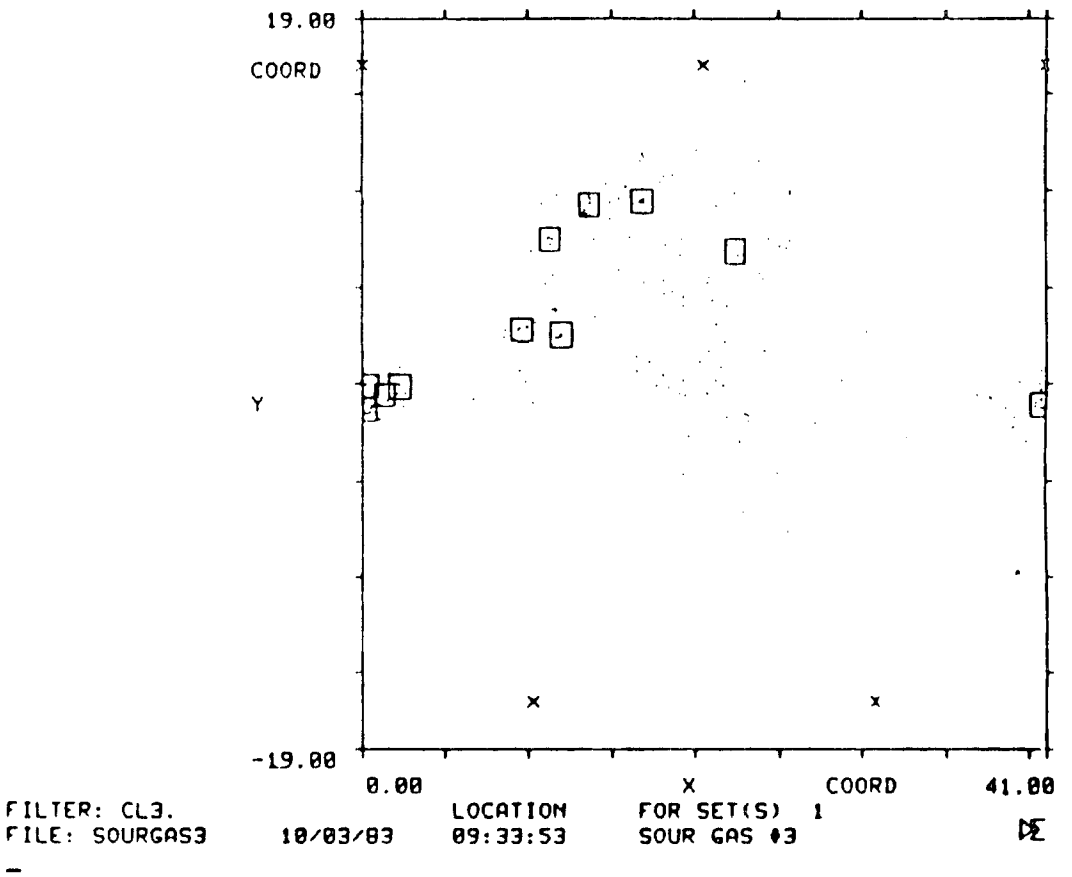

Figure 98 Cylindrical Location Plot of Pipe Test Section 3, Filtered. (Dimensions: Inches).

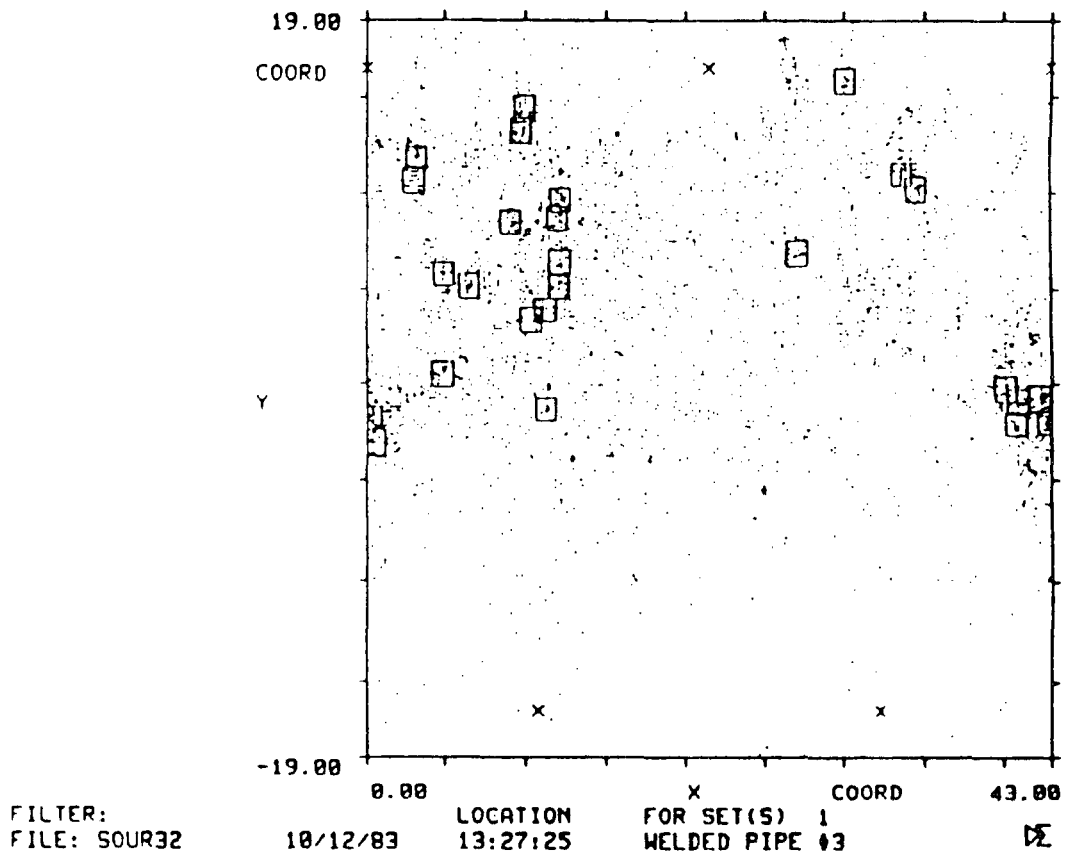

Figure 99 Cylindrical Location Plot of Pipe Test Section 3, Unfiltered. (Dimensions: Inches)

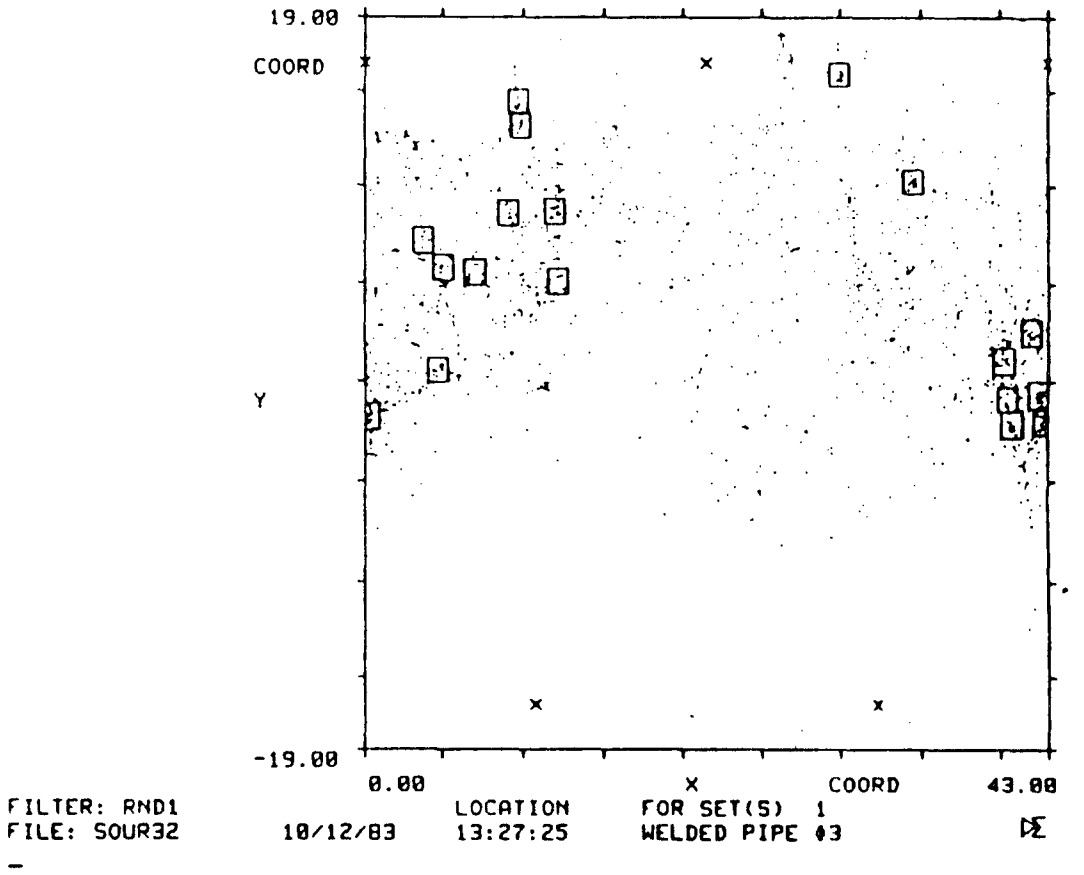

Figure 100 Cylindrical Location Plot of Pipe Test Section 3, Filtered. (Dimensions: Inches)

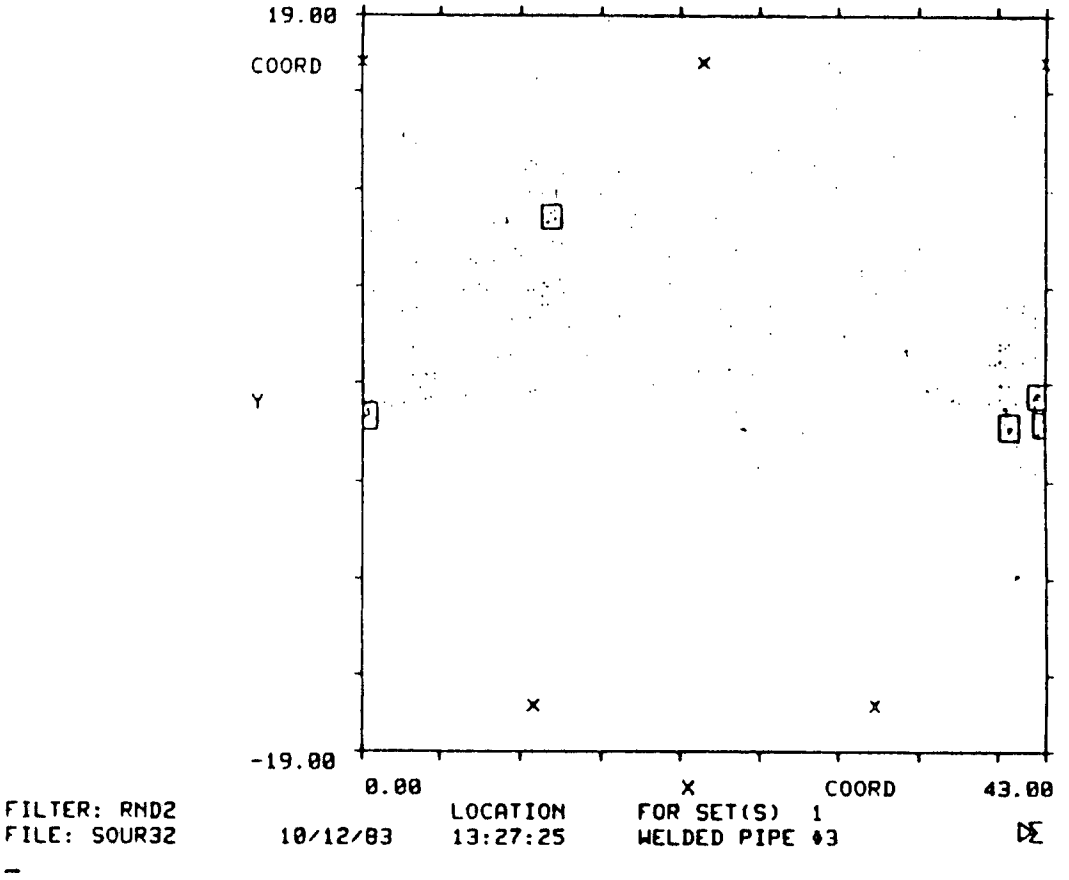

Figure 101 Cylindrical Location Plot of Pipe Test Section 3, Filtered. (Dimensions: Inches)

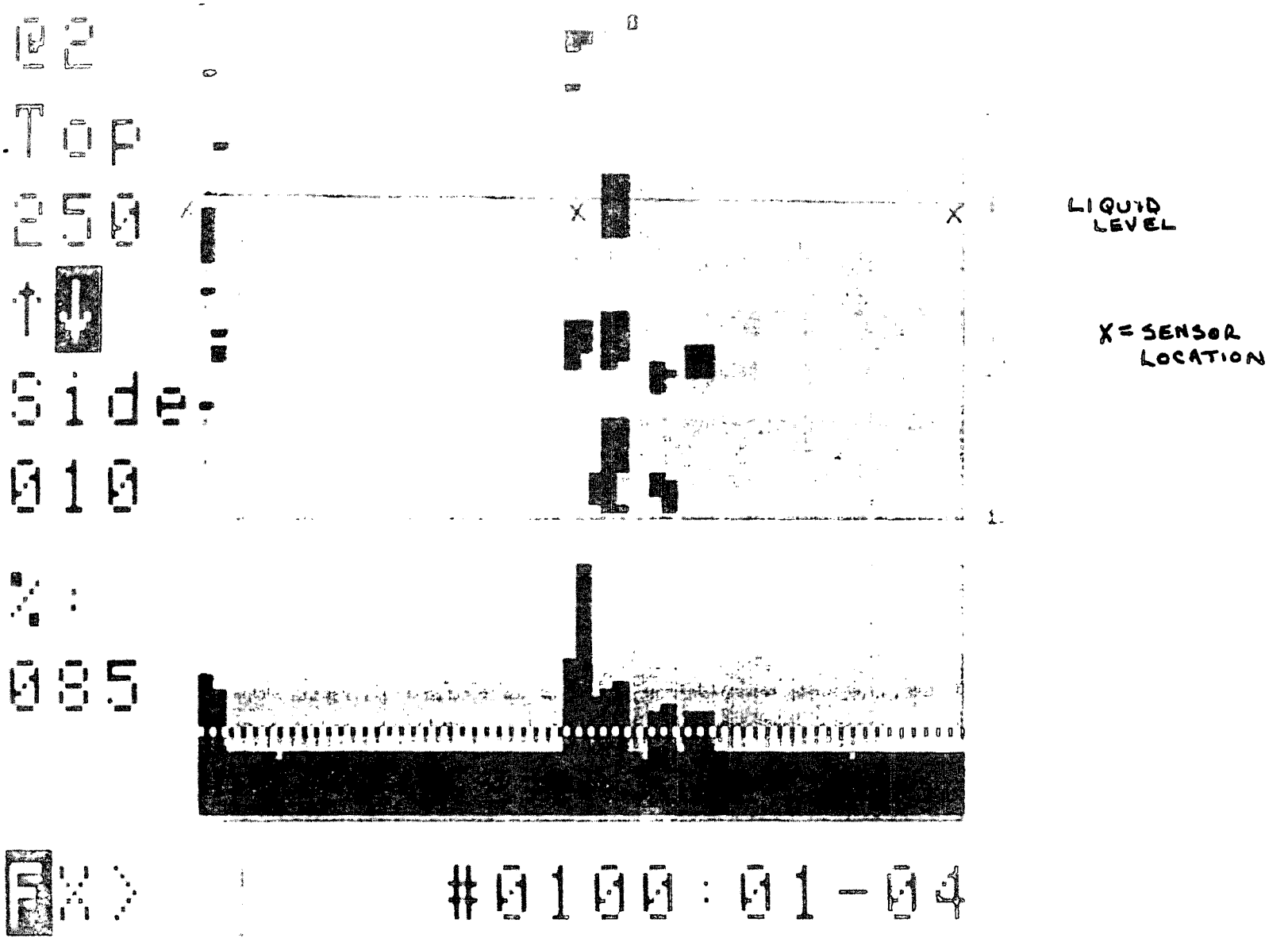

Figure 102 Ultrasonic scan of top area of pipe section 3

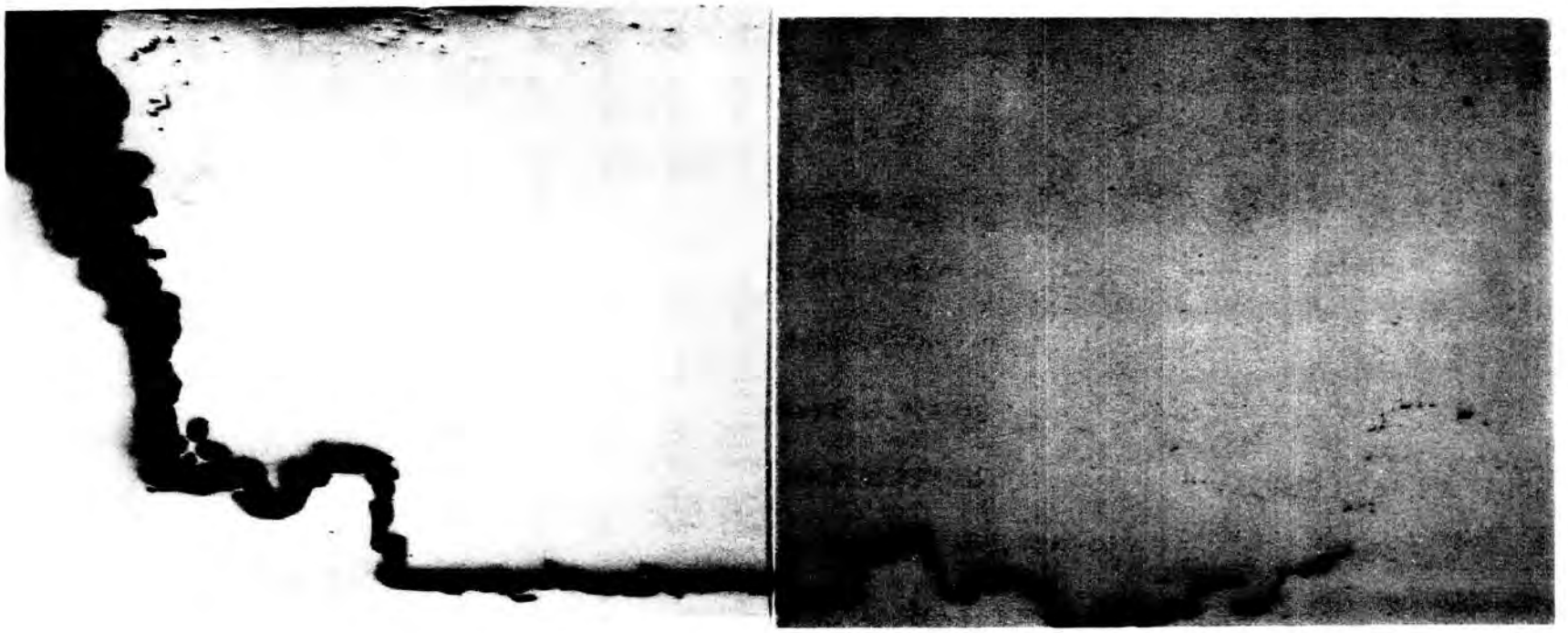

Figure 103
Micrograph of near surface defect located near to the inner wall of the pipe x 100.

Figure 104
Non metallic inclusions associated with the step wise section of the crack x 200.

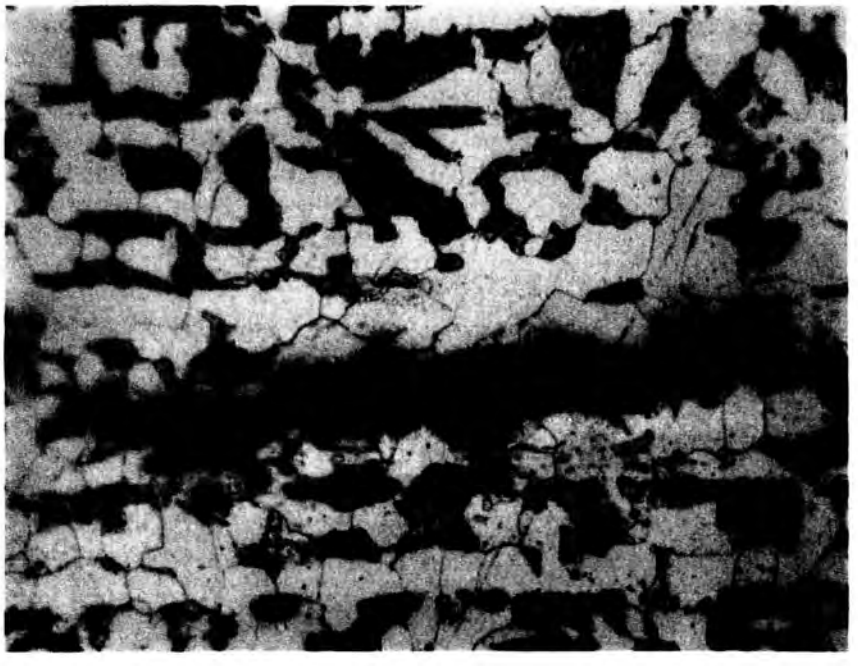

Figure 105
Fine cracking revealed of the extremity of the crack x 500

Figure 106
Metallographic section of pipe section 3 showing extent of banding x 200

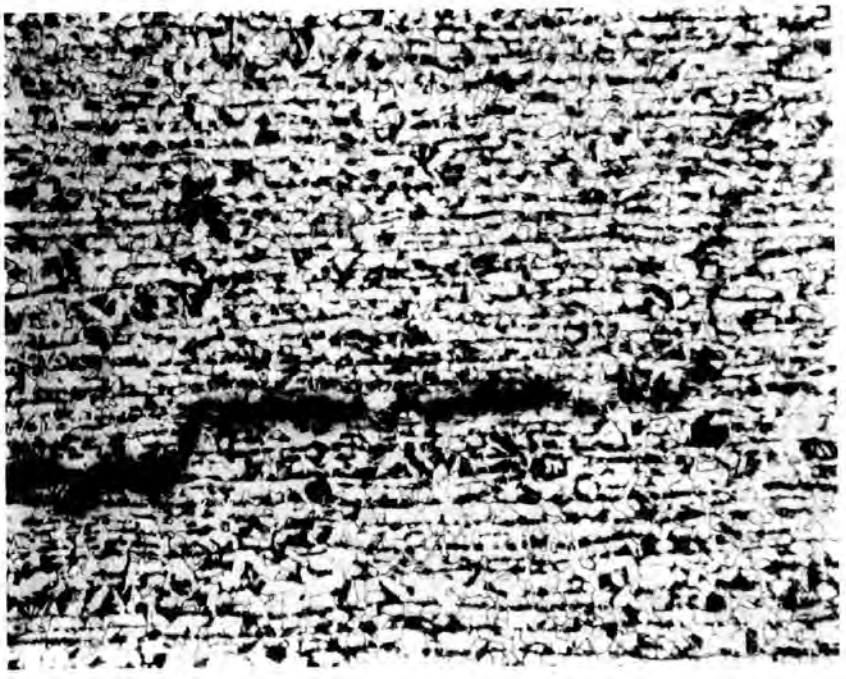

Figure 107
Metallographic section of pipe section 3 showing the extent of the banding x 100

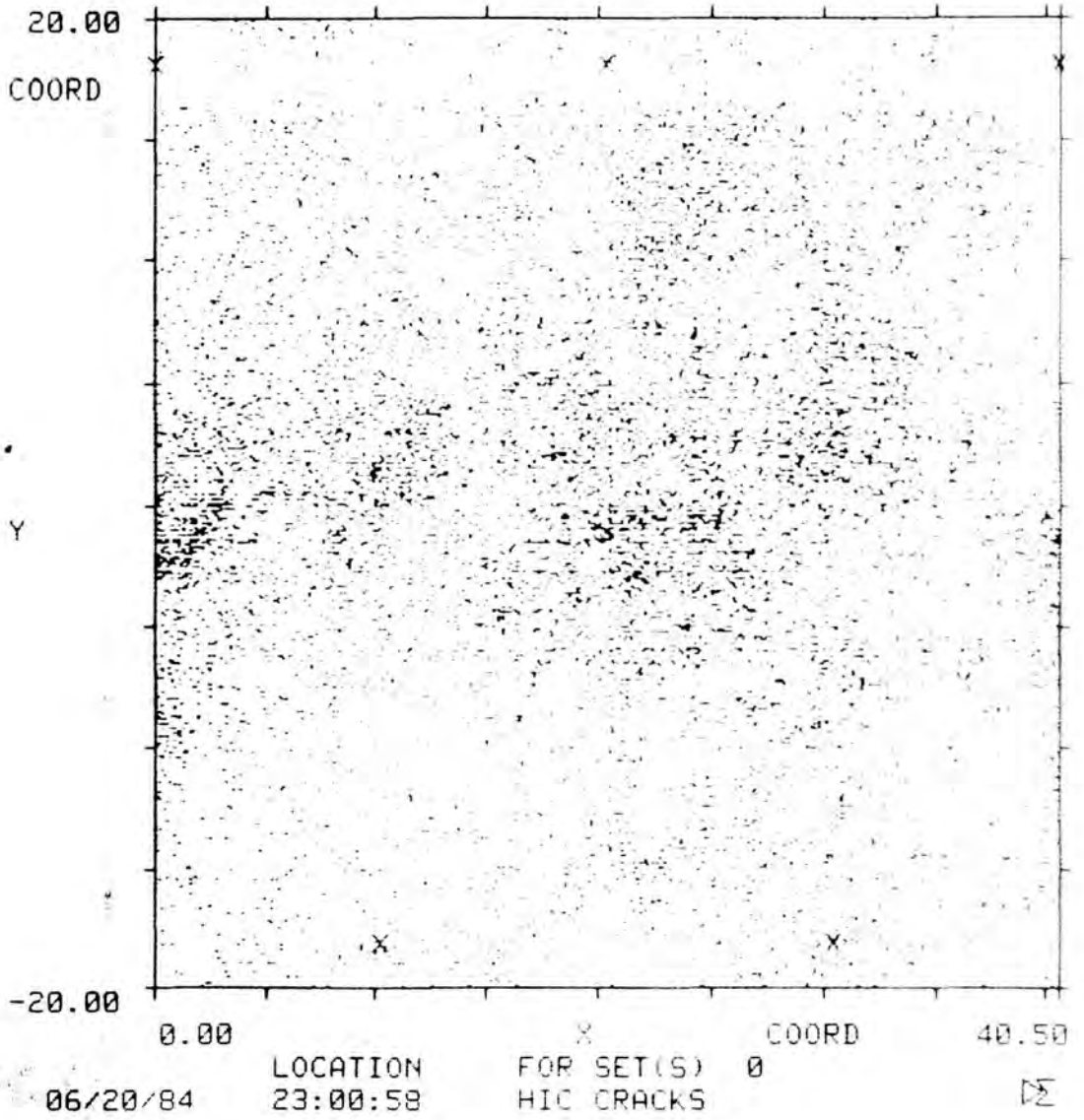

Figure 108 Disc One Pipe 4 No Filtering

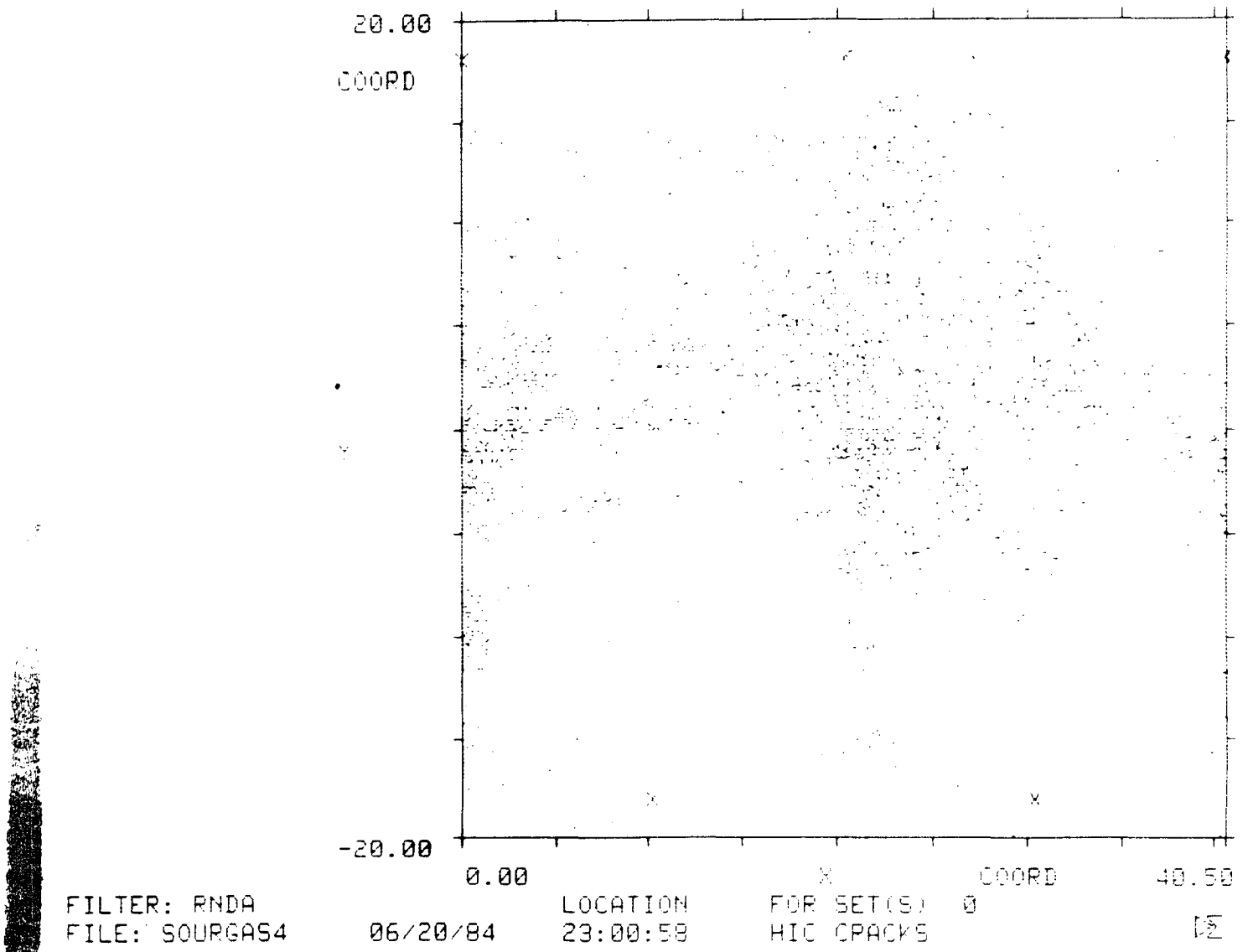

Figure 109 Disc One Pipe 4 Intermediate Filtering

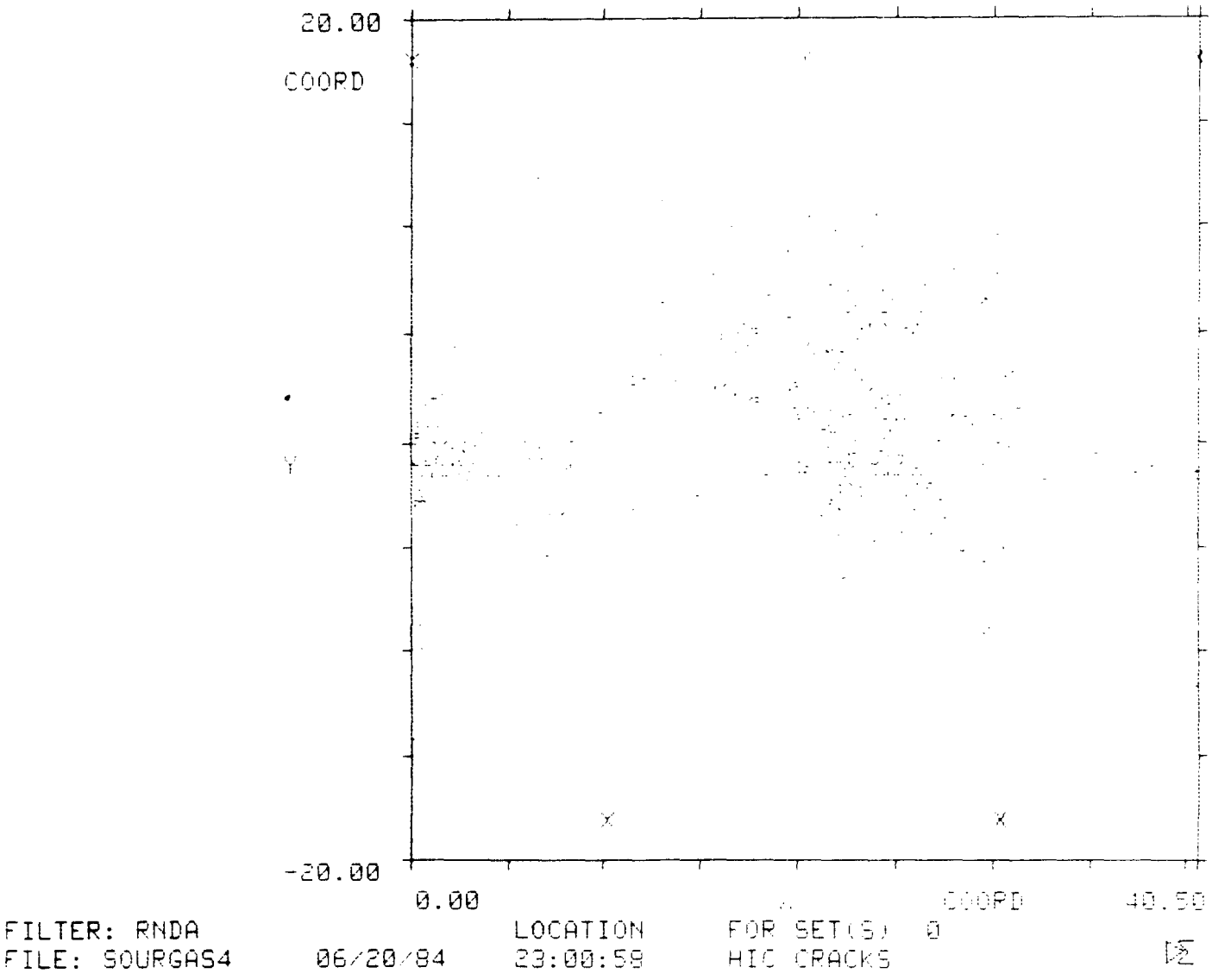

Figure 110 Disc One Pipe 4 Final Filter

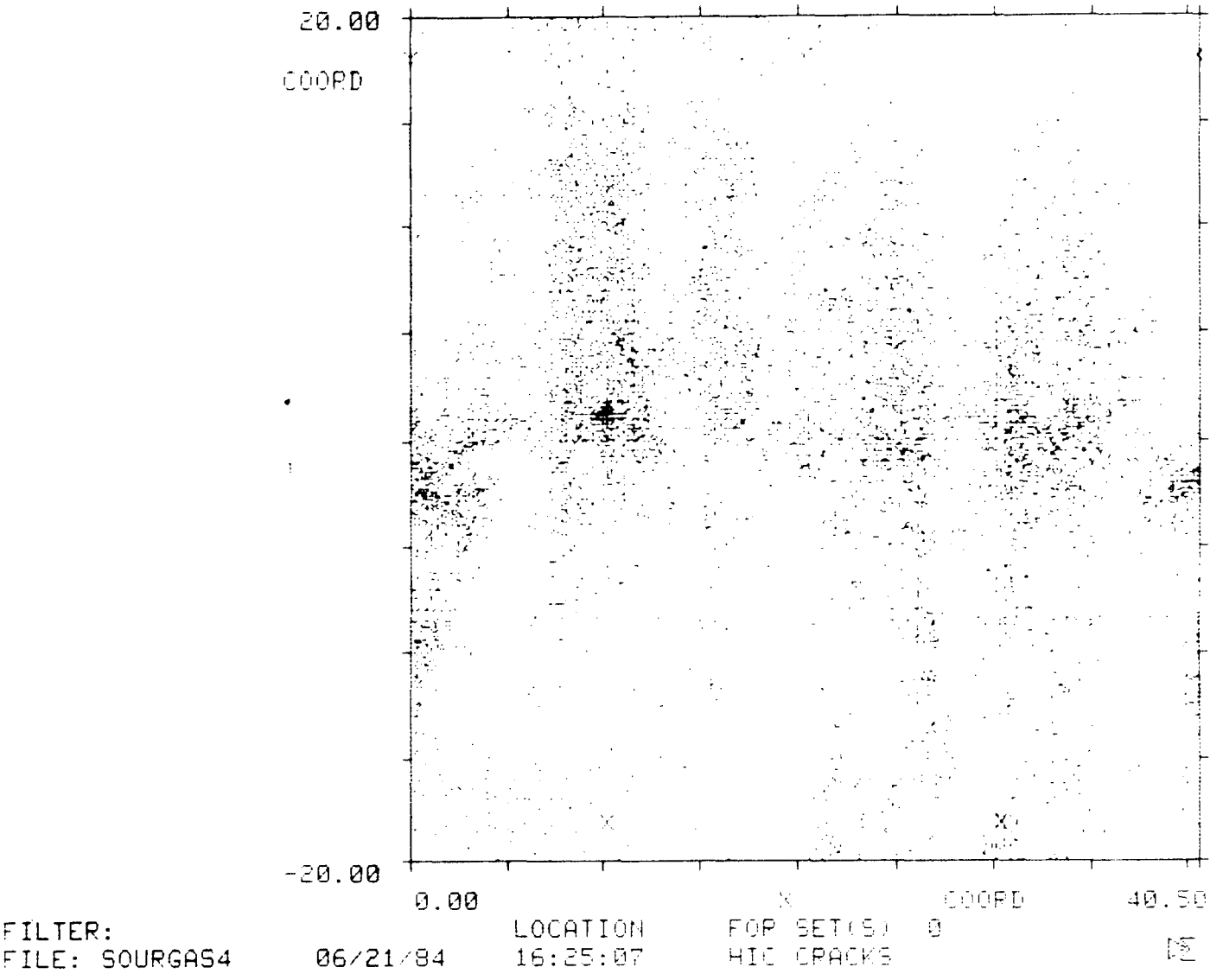

Figure 111 Disc 2 Pipe 4 No Filtering

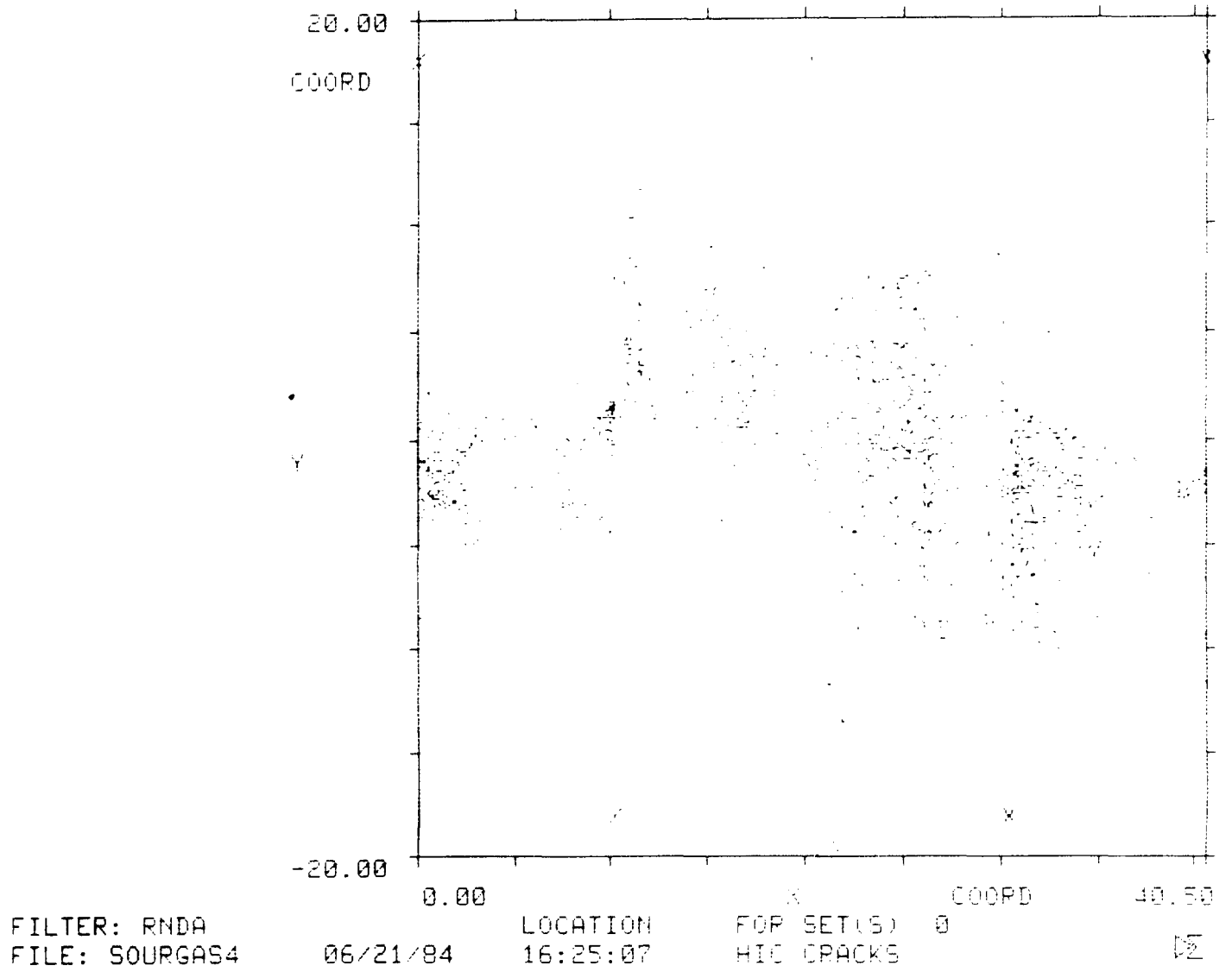

Figure 112 Disc 2 Pipe 4 Intermediate Filtering

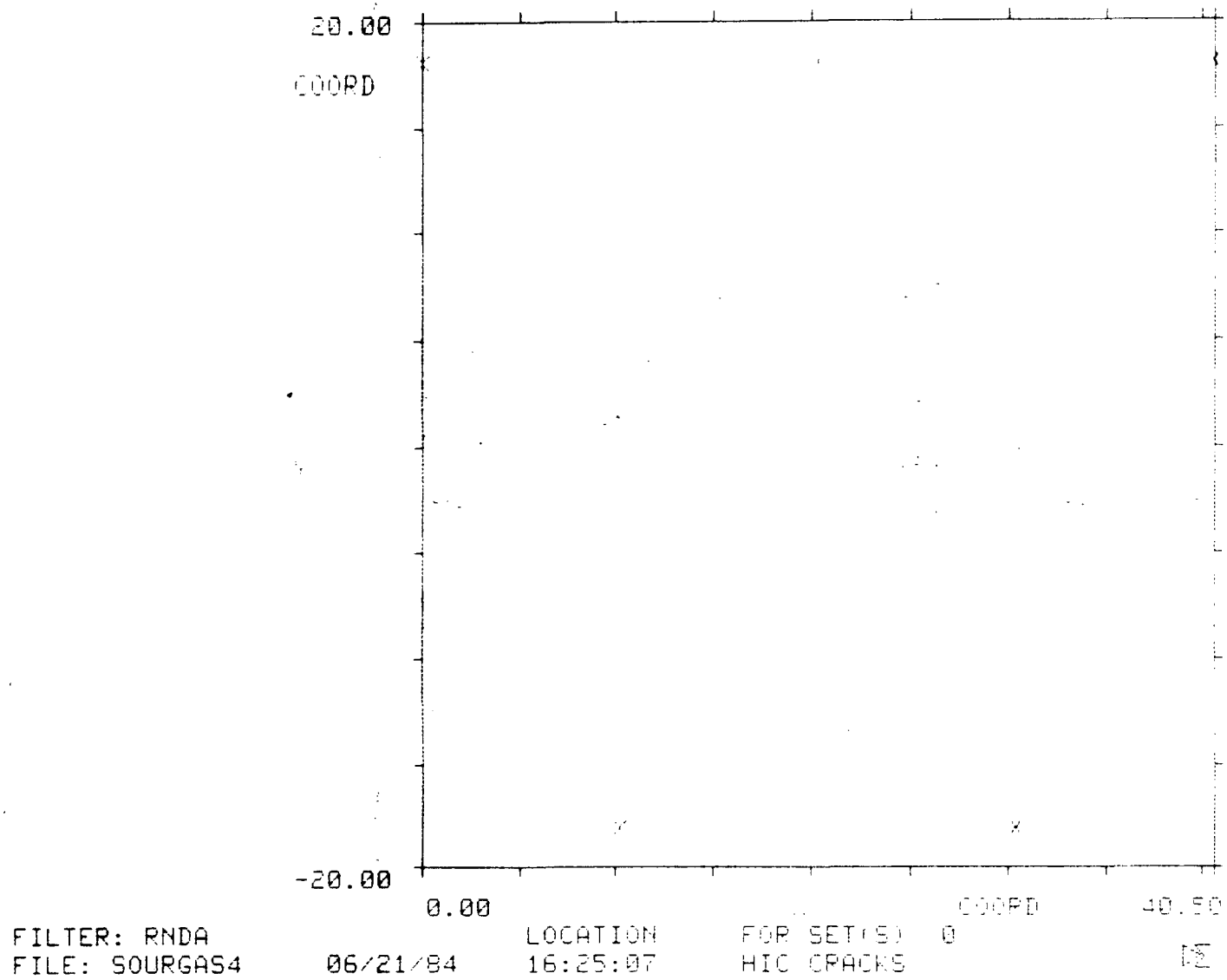

Figure 113 Disc 2 Pipe 4 Final Filter

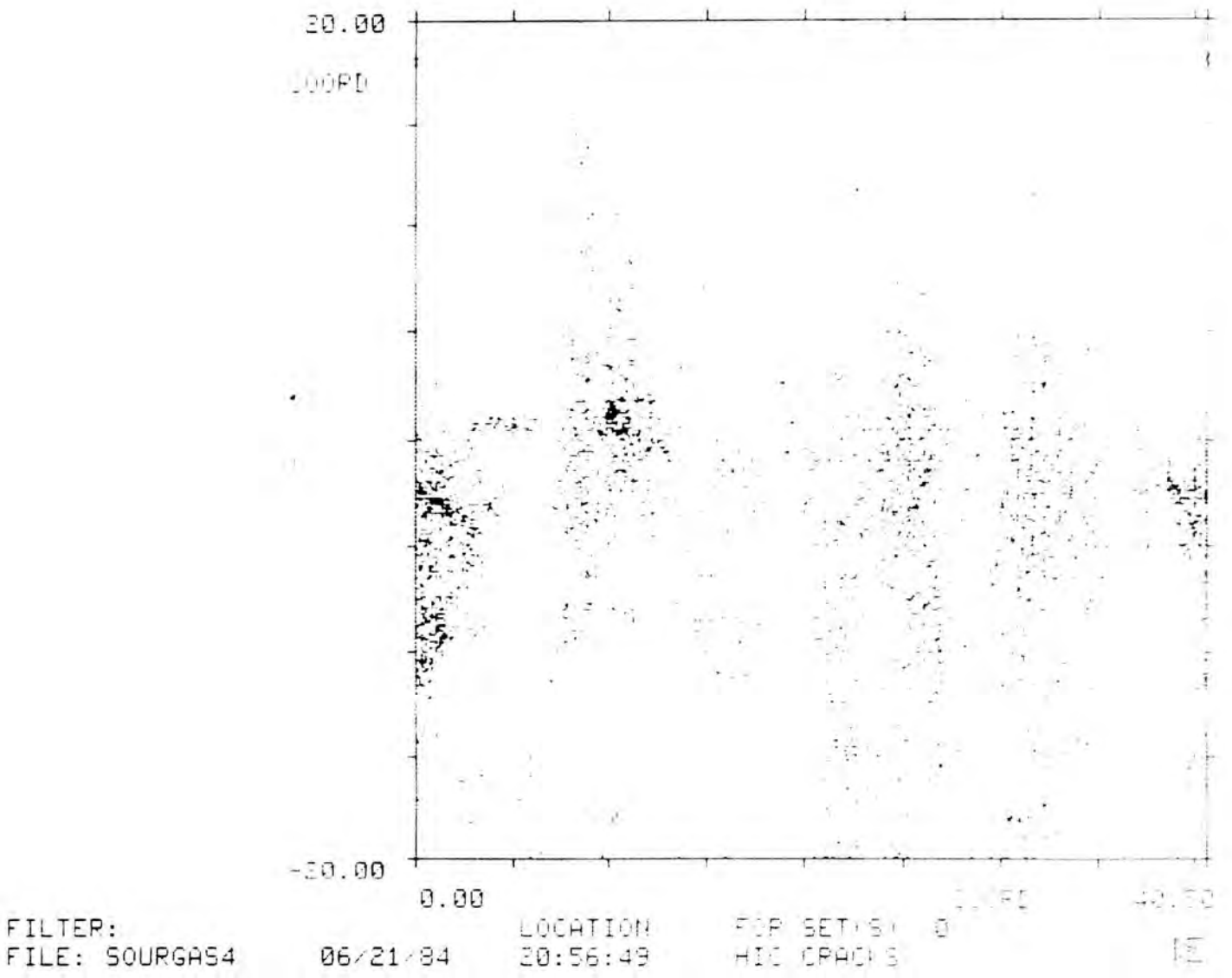

Figure 114 Disc 3 Pipe 4 No Filter

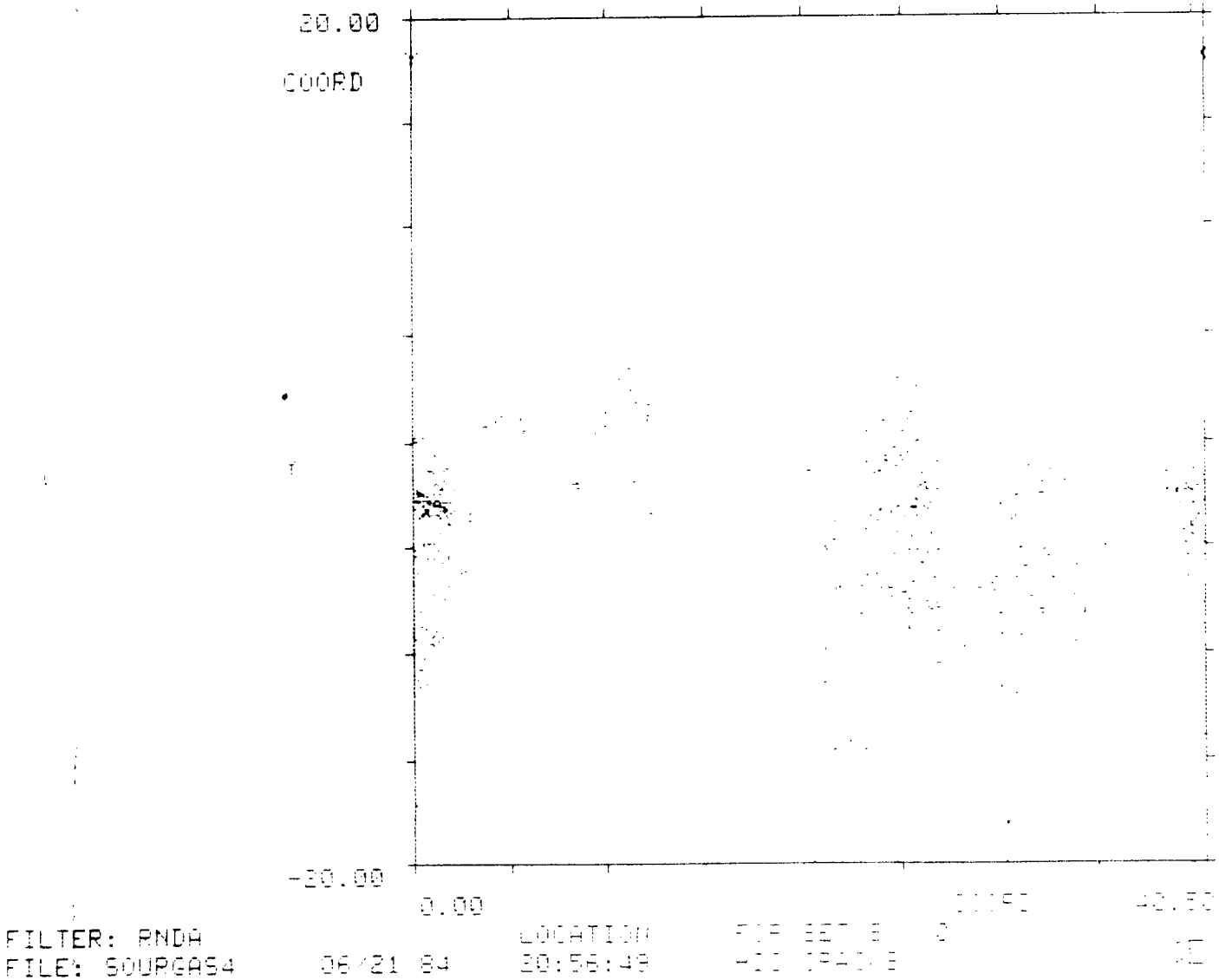

Figure 115 Disc 3 Pipe 4 Final Filter

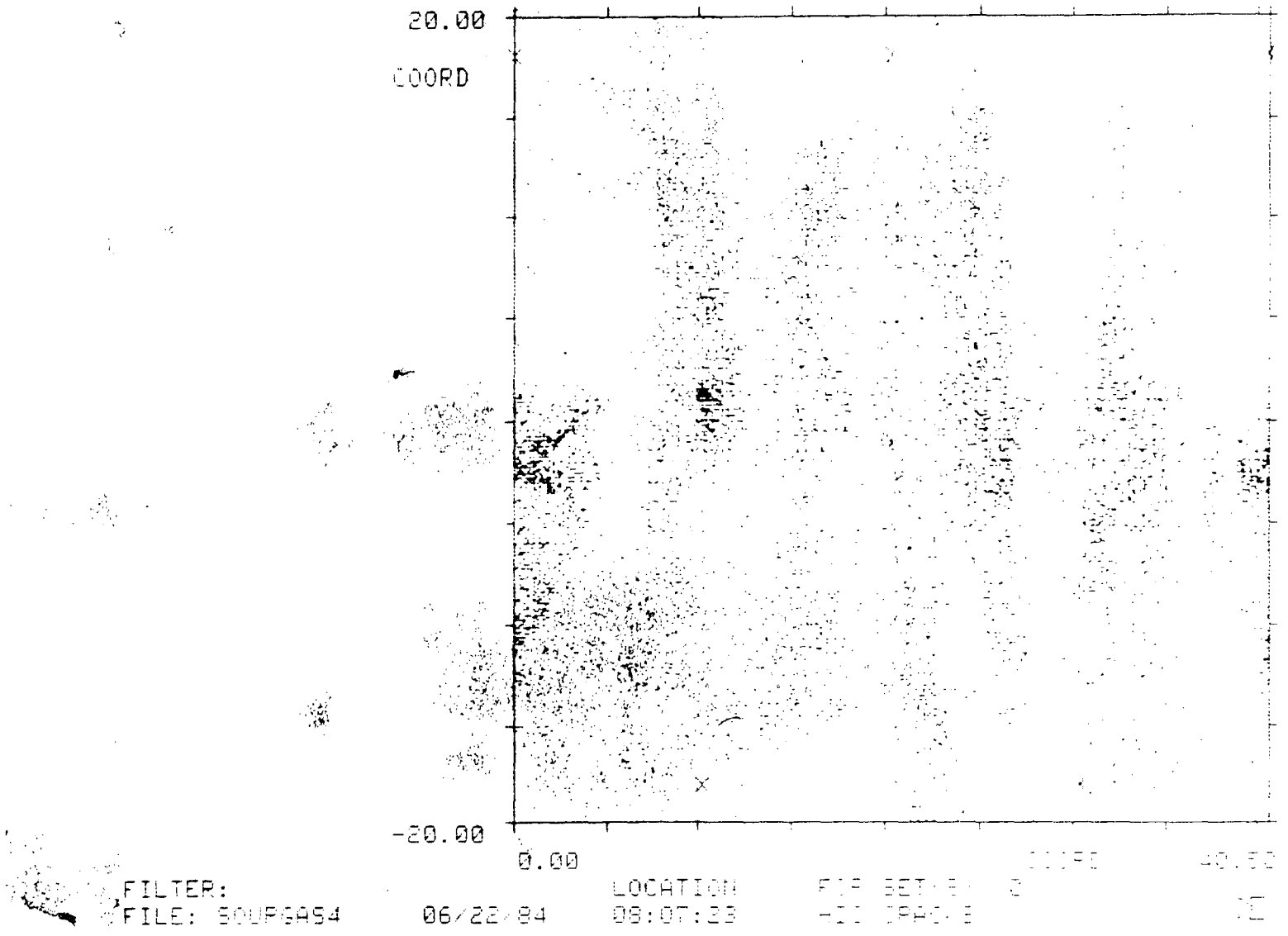

Figure 116 Disc 4 Pipe 4 No Filter

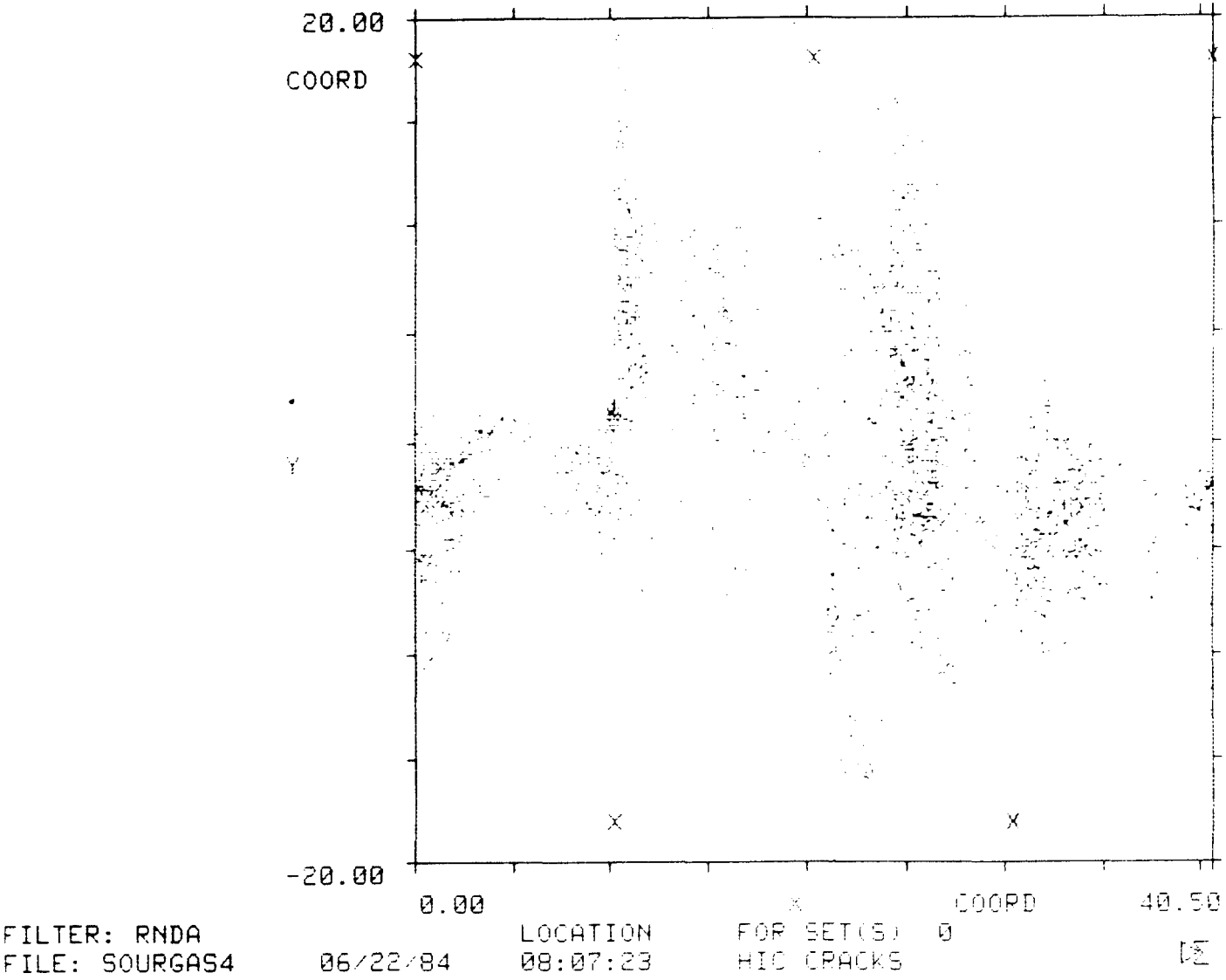

Figure 117 Disc 4 Pipe 4 Final Filter

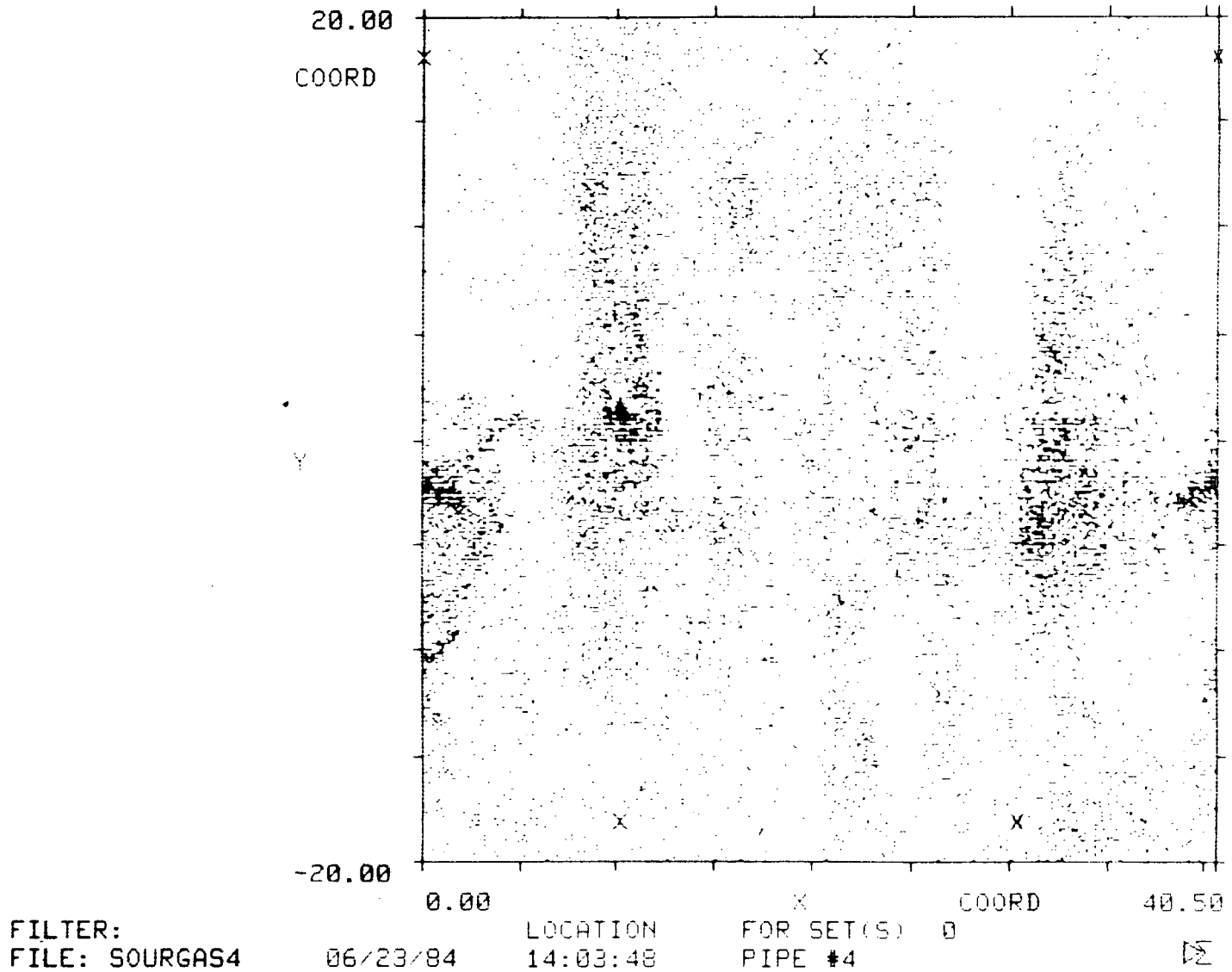

Figure 118 Disc 5 Pipe 4 No Filter

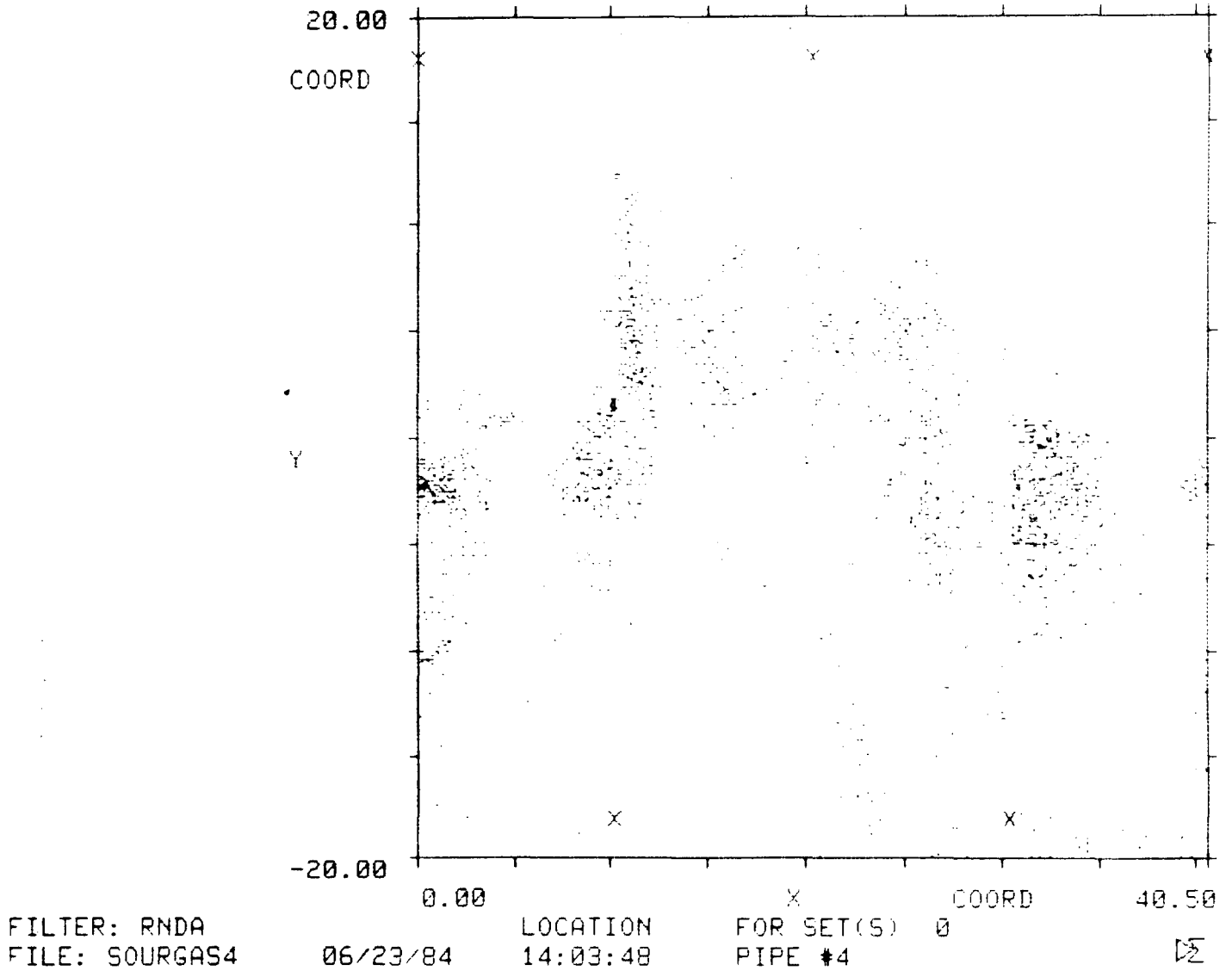

Figure 119 Disc 5 Pipe 4 Final Filter

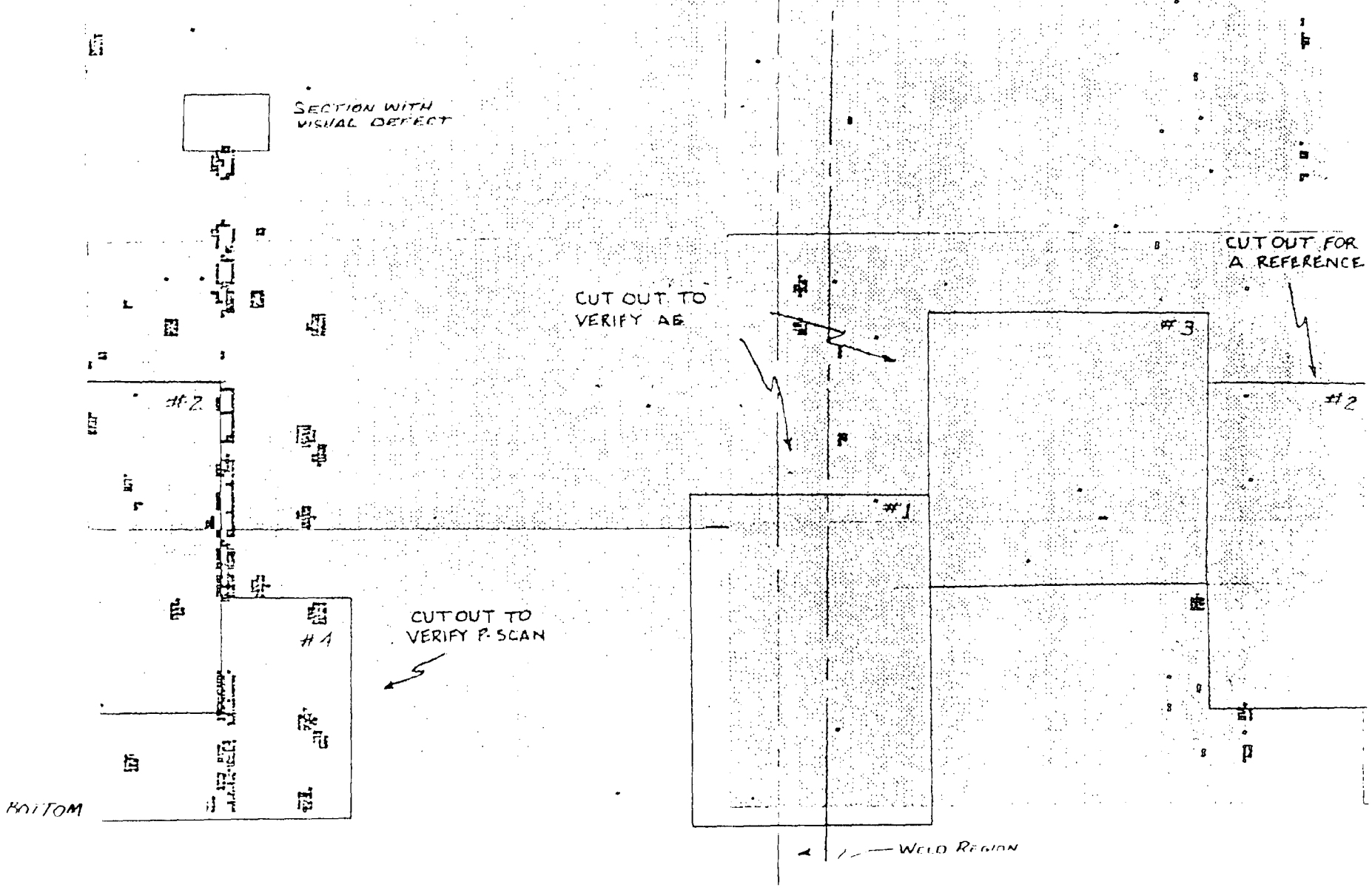

Figure 120 Ultrasonic Scan of Pipe 4

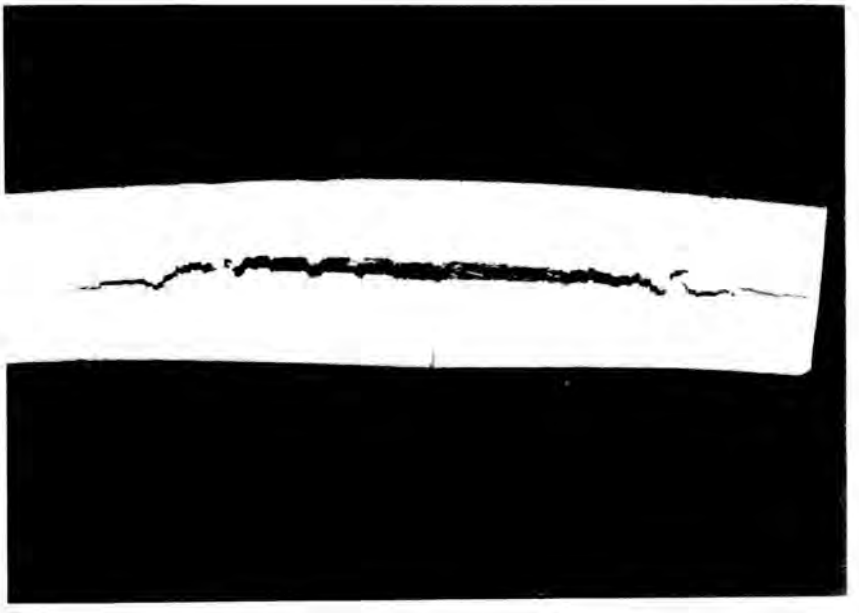

Figure 121
Delamination of the pipe wall and stress corrosion cracking detected in the pipe section 4.